Synthesis, Structure-Activity Relationship and Solubility Improvement Studies of Potential Antimalarial and Antischistosomal Pyrido[1,2-*a*]benzimidazoles

Kelly Chisanga

Supervisor

Professor **Kelly Chibale**

University of Cape Town,

Department of Chemistry and Institute of Infectious Disease and Molecular Medicine

Rondebosch, 7700

Dissertation Presented for the Thesis towards the Award of the Master of Science (MSc)

Degree by Dissertation

November 2018

Blank Page

DECLARATION

I, **Kelly Chisanga**, hereby:

a) grant the University of Cape Town free license to reproduce the thesis, in whole or in part, for the purpose of research;

b) acknowledge that I fully understand the meaning and the adverse consequences of plagiarism.

c) declare that this thesis is my own single-handed work, both in concept and execution, and that apart from the normal guidance of my supervisor; I have received no assistance apart from that acknowledged; and that neither the substance nor any part of the thesis has been submitted in the past, or is to be submitted for a Degree at this University or any other University.

Signed: Signed by candidate Date: 23rd November 2018

THESIS DEDICATION

TO MY LOVELY WIFE ETHEL LUNGU CHISANGA, MY ADORABLE SON MUTALE CHISANGA AND MY PRECIOUS DAUGHTER MARY MULENGA CHISANGA AS A GESTURE OF MY AFFECTIONATE GRATITUDE FOR YOUR PATIENCE, PERSEVERANCE AND ENDURANCE DURING THE TOUGH TIMES I WAS NOT WITH YOU WHILE I WAS STUDYING THOUSANDS OF MILES AWAY.

TO YOU ALL I SAY THIS IS THE START OF OUR LITTLE STORY, THE PART WHERE YOUR PAGE MEETS MINE NO MATTER WHERE THE TALE TAKES US TOMORROW, OUR STORY WILL ALWAYS BE READ.

LOTS OF LOVE!

BASHI MUTALE.

Conferences and Seminars

June 2018 – Poster Presentation:

Synthesis, Structure-Activity Relationship and Solubility Improvement Studies of Potential Antimalarial and Antischistosomal Pyrido[1,2-a]benzimidazoles at the **Gordon Research Seminar (GRS) on Biology of the host-parasite interactions**, 9 – 10 June 2018, Salve Regina University, Newport, Rhode Island, United States of America (USA).

June 2018 – Poster Presentation:

Synthesis, Structure-Activity Relationship and Solubility Improvement Studies of Potential Antimalarial and Antischistosomal Pyrido[1,2-a]benzimidazoles at the **Gordon Research Conference (GRC) on Biology of the host-parasite interactions**, 10 - 15 June 2018, Salve Regina University, Newport, Rhode Island, United States of America (USA).

August 2018 – Poster Presentation:

Synthesis, Structure-Activity Relationship and Solubility Improvement Studies of Potential Antimalarial and Antischistosomal Pyrido[1,2-a]benzimidazoles at the **Southern African Malaria Research Conference**, 29 July – 1 August 2018, Centre for infectious disease research, Johannesburg, Republic of South Africa.

ACKNOWLEDGEMENTS

Foremost, I acknowledge the sovereignty of God the Almighty and His grace upon my life, the life of my beloved ones, friends and the financial sponsors of this research program.

Secondly, I would like to acknowledge my supervisor, Professor Kelly Chibale for the guidance he provided during this program. You have greatly inspired me in an uncountable number of ways. I am grateful to you for the strides you have made in developing my science career, for the opportunity you gave me to work in your laboratories and for opening my eyes to have a glimpse of the medicinal chemistry research world. It has been a great and motivating experience that will go a long way in my career.

May I also thank the administrative team, Ms Elaine Rutherfoord-Jones and Saroja Naicker for their steady-fast and timeous provision of the research materials. May I also thank Deidre Van-Rooyen for the logistics and facilitation of sample analysis. May God bless you all!

I am grateful to all members of the KC Medicinal Chemistry and H3D research groups for the support you rendered to me materially, emotionally and technically which all together facilitated the smooth flow of my research. May I also gratefully acknowledge Peter Mubanga Cheuka (PhD-Student) for his selflessness in the sharing of knowledge and skills. Most importantly, I want to thank him for sharing his limited and precious time to proof-read my chapters. A lot of thanks go to Godfrey Mayoka (PhD-Student) for the role he played in my research as a mentor and to Dr Aloysius Nchinda (H3D staff member) for helping me organizing and managing my work.

My cordial gratitude and a lot of thanks to Dr Taylor Dale for maintaining a big heart of tolerance during the stressful moment when the transmission and provision of antiplasmodium assays were required. My heartfelt gratitude also goes to Professor Jennifer Keiser (University of Basel, Switzerland) for the endless support in the provision of antischistosomal assays and her technical input in the unfolding of this research. Many thanks also go to Pete Roberts for the spectroscopic evaluation of my data.

Further gratitude goes to my family members for their constant engagement in prayers for me and my work, for your constant encouragement and your trust in me. May God bless you too!

Finally, thanks to Novartis Research Foundation and the Department of Chemistry of the university of Cape Town for their generous financial support to facilitate my research.

Abstract

In 2016, 216 million malaria cases with 445,000 associated deaths were recorded according to the World Health Organization (WHO). Schistosomiasis also remains a public health issue with 207 million cases recorded globally and 280,000 deaths in the same year. Widespread emergence of parasite resistance to once-effective antimalarial options has rendered currently used drugs ineffective. Moreover, the current WHO-recommended first-line antimalarial drugs in clinical use, the artemisinin combination therapies (ACTs) are faced with the challenges of limited availability, unaffordable cost, and undesirable adverse effects. On the other hand, the treatment of schistosomiasis is severely limited to one treatment regimen, praziquantel (PQZ) which, unfortunately, has recently shown low curing rates in some parts of West Africa. Furthermore, this treatment option is far from ideal because its activity is limited to only adult schistosomes while displaying no activity towards young stages of the liver flukes. These challenges collectively provide a justification for stepping up drug discovery and development efforts aimed at identifying novel, safe and efficacious antimalarial and antischistosomal agents.

Whereas, the pyrido[1,2-*a*]benzimidazole (PBI) scaffold is found in many pharmacologically relevant molecules including Rifaximin, an approved gastrointestinal antibacterial drug, medicinal chemistry explorations around the PBI nucleus have recently identified analogues as novel antimalarial and antischistosomal agents. Additionally, while promising antimalarial efficacy has been demonstrated in animal studies, preliminary *in vitro* studies of the PBI class of compounds have also demonstrated good activity against Schistosoma parasites. Recently, Mayoka reported the impressive dual antiparasitic potency of the lead compound **GMP-19** (figure 1) against Plasmodium and Schistosoma parasites *in vitro* (IC_{50} = 0.430 μM, drug-sensitive strain (NF54) and IC_{50} = 0.210 μM, adult *S. mansoni*, (unpublished data)). However, **GMP-19** and other PBI analogues in this series of compounds, have been beset by poor solubility.

Towards addressing solubility issues while retaining and improving antiparasitic activity, in this MSc dissertation, the design, synthesis, structure-activity relationship (SAR) and solubility improvement studies of PBI analogues based on the **GMP-19** template are reported. In this regard, chemical modification approaches such as disruption of molecular planarity, increasing saturation, incorporating water solubilizing groups such as the polar-ionizable and the neutral-polar functionalities around the PBI nucleus were adopted. Consequently, we obtained SAR 1

analogues after substituting the 4-(trifluoromethoxy)phenyl (4-OCF_3Ph) moiety of **GMP-19** with assorted α-methyl benzylamines. In addition, the phenyl ring on the left-hand side of the core scaffold was substituted with electron withdrawing groups such as the chloro and fluoro atoms (SAR 1.1 – 1.4), (figure 1). Although some analogues demonstrated a significant loss of antiparasitic activity (> 6.00 µM), strong submicromolar antiparasitic activity was observed with most analogues (IC_{50} = 0.022 -0.940 µM, *Pf*NF54 and 30 - 69% inhibitory effect at 0.370 µM, against young forms of *S. mansoni*). Moreover, some analogues demonstrated poor solubility as low as < 10 µM while others showed highly improved solubility as good as 80 µM.

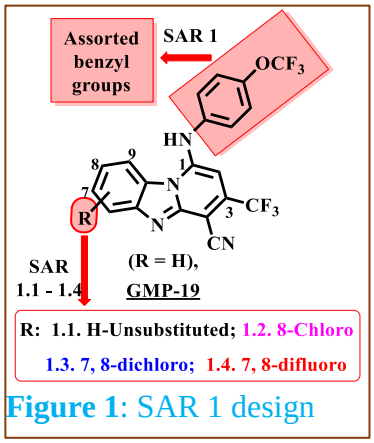

Figure 1: SAR 1 design

In SAR 2.1 – 2.2, the 4-OCF_3Ph and the trifluoromethyl (CF_3) on the right-hand side (RHS) of the scaffold were fixed while introducing amino moieties (**R**) on the lipophilic phenyl ring on the left-hand side (LHS) of the PBI core (figure 2). Upon identifying the moiety with the best balance of solubility and biological activity, the 4-OCF_3Ph was replaced with various acyclic amino (SAR 2.3) while the CF_3 was maintained on C-3 of the core scaffold. Finally, the CF_3 was replaced with the 4-CF_3Ph (SAR 2.4 and 2.5) while keeping fixed the optimal basic amine and the acyclic amino moieties on the LHS, respectively. Interestingly, the pursued structural modifications delivered analogues with a wide diversity of pharmacological and physicochemical properties. While some analogues demonstrated significant loss of pharmacological activity, others exhibited potent submicromolar antiparasitic activity (IC_{50} < 0.012 – 0.990 µM, *Pf*NF54 and 0.360 – 0.850 µM, adult *S. mansoni*). Similarly, some analogues demonstrated poor solubility as low as < 10 µM while others demonstrated improved solubility as good as 180 µM.

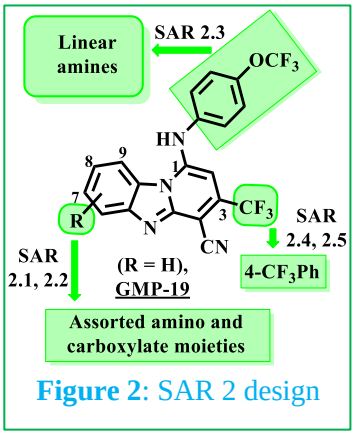

Figure 2: SAR 2 design

LIST OF ABBREVIATIONS AND SYMBOLS

ACT	Artemisinin Combination Therapy
APCI	Atmospheric Pressure Chemical Ionization
ASU	Asymmetric Unit
Å	Angström
ºC	Degrees Celsius
µL	Microlitre
µM	Micromolar
µm	Micrometer
ADMET	Absorption, Distribution, Metabolism, Excretion and Toxicology
$CDCl_3$-*d*	Deuterated Chloroform
CD_3OD-d_4	Deuterated Methanol
cLogP	Calculated logarithm of n-octanol/water partition coefficient
CYP	Cytochrome P450
DCM	Dichloromethane
DFT	Density Functional Theory
DMF	*N*,*N*-Dimethylformamide
DMPK	Drug Metabolism and Pharmacokinetics
DMSO-d_6	Deuterated Dimethyl Sulfoxide
ESI	Electron Spray Ionization
EtOAc	Ethyl Acetate
GMP	Godfrey Mayoka's Project
HCl	Hydrochloric Acid
HPLC	High-Performance Liquid Chromatography
Hz	Hertz
IC_{50}	Inhibitory Concentration required to inhibit the growth of 50 % of the organism
ip	intraperitoneal
PBI	Pyrido[1,2-*a]*benzimidazole
PQZ	Praziquantel
WHO	World Health Organization

Table of Contents:

Table of Figures

1.0 INTRODUCTION AND LITERATURE REVIEW

1.1 Malaria

1.1.1 History, introduction and aetiology

The word "malaria" was derived from two Italian words "mal" (bad) and "aria'' (air). The malaria parasites were first detected in a patient's blood by the French army officer Charles Louis Alphonse Laveran in 1880. Before then, malaria had been associated with marshy areas whose foul air was assumed responsible for its causation.[1] In the year 1897, the parasites' blood sexual stages and the elucidation of the transmission cycle in culicine mosquitoes and birds infected with *Plasmodium relictum* were respectively discovered by William McCallum and Ronald Ross.[1,2] These discoveries laid a landmark in understanding the cause and transmission of malaria and thus, paved the way to the conclusive evidence by an Italian malariologist Giovanni Battista Grassi in 1898,[1] that human malaria was transmitted by various species of female *Anopheles* mosquitoes.[1–3] The consequent discovery of the development of malaria parasites in the liver before entry into the bloodstream by Henry Shortt and Cyril Garnham in 1948 facilitated the ultimate discovery of the presence of dormant stages of the parasite in the liver as was proved by Wojciech Krotoski in 1982.[2]

Malaria is caused by over 100 known single-celled protozoan parasite species of the genus *Plasmodium* of which, *P. falciparum*, *P. vivax, P. malariae*, *P. ovale* and *P. knowlesi* are the main five (5) species known to infect humans.[4] *P. falciparum* is the highest in disease transmission, most lethal and is responsible for the world's most acute cases of sickness, organ dysfunction and deaths.[3,5] Although *P. vivax* and *P. ovale* only cause a milder form of the disease and aren't as life-threatening as *P. falciparum*, they are associated with relapses due to the persistence of dormant hypnozoite forms in the liver.[3,6,7] *P. malariae* is usually associated with infections of a chronic nature and can persist in blood asymptomatically for long periods of time.[8] A fifth species, zoonotic *P. knowlesi* that was only known to infect macaques has surprisingly been traced to cause human malaria in some parts of South-East Asia.[3,9]

Malaria has continued to pose devastating effects on human health and the economy worldwide due to vector resistance to commonly used insecticides,[10] unavailability of an effective malaria vaccine,[7,11,12] excessive cost, toxicity and severe adverse effects of existing antimalarials besides parasite resistance to these therapeutic agents.[13–16]

1.1.2 Epidemiology

Malaria is a public health problem whose endemicity spans more than 91 countries worldwide affecting more than 40% of the global population. The highest rates of infection and transmission are confined within the tropical and sub-tropical regions, Amazon and the temperate zones of the world. The highest disease cases and deaths are contributed by sub-Saharan Africa, Amazonia and South-East Asia.[17,18] Factors contributing to a huge malaria burden in these regions include their auspicious tropical climatic conditions conducive for mosquito breeding and political instability in some resource-poor economies which limit investment in malaria prevention strategies.[19] Although only dealing with the challenges of imported malaria due to international travels and some consequent occasional secondary transmission, regions such as Australia, Europe, North America and some parts of Southern and Northern Africa (figure 1.1) have been classified as non-malaria endemic.[1,20–23]

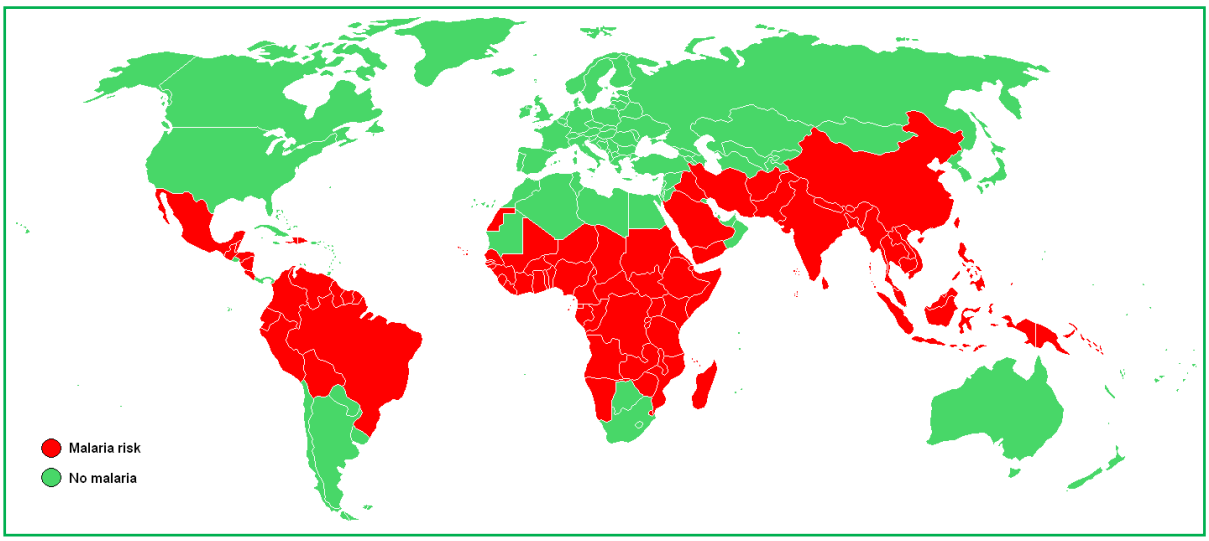

Figure 1.1: World malaria map.[24]

The 2017 World Health Organization (WHO) malaria report revealed that about 216 million people were infected and roughly, 445 000 malaria-related deaths were recorded globally of which 90% and 91% of the infections and deaths, respectively, occurred in tropical regions of sub-Saharan Africa in 2016.[18,25,26] In the same region, about 125 million pregnant women have been reported to be at risk of infection and over 200,000 maternal-infant deaths occur each year, translating into a worrisome statistic that one child dies of malaria every two minutes. Records also show that 13 out of the 32 most endemic countries of sub-Saharan Africa account for about 76% and 75% annual global malaria cases and deaths, respectively.[27,28]

1.1.3 Malaria parasite life cycle

Although there are some minor variations, four-major malaria-causing parasites (*P. falciparum, P. vivax, P. malariae and P. ovale*) exhibit similar development steps and life cycle which completes in two phases including the human and mosquito phases. The human phase of *Plasmodium's* life cycle starts with an exoerythrocytic asymptomatic stage lasting between 9 and 16 days inside the host's liver.[1] The cycle inception involves a female *Anopheles* mosquito that inoculates salivary *sporozoites* into the host's punctured dermis during its blood meal (figure 1.2).[1,3] The *sporozoites* enter hepatocytes and form a parasitophorous vacuole (PV) where they undergo development and maturate into liver *schizonts* each of which contains tens of thousands of the first generation *merozoites*.[29,38] In the case of *P. vivax* and *P. ovale* infection, some exoerythrocytic *schizonts* undergo a dormant period known as the *hypnozoite stage* (which may result in relapses months or even years after the first infection).[17,32] As infected hepatocytes rapture, free *merozoites* invade circulatory erythrocytes to begin the erythrocytic infection stage. At this stage, a *schizont* is formed which, upon maturation, bursts open to release even more *merozoites* that are infectious to new erythrocytes and the cycle continues until death of, or parasites get cleared from the host by chemotherapy.[33] It is at this blood stage infection that malaria symptoms such as intermittent fever attacks, convulsions and vomiting among others, are manifested. These symptoms arise from the simultaneous rupture of the infected erythrocytes and the associated release of antigens and waste products into the blood.[4] The mosquito phase of *Plasmodium* parasite life cycle commences with the intraerythrocytic differentiation of *merozoites* to male and female *gametocytes*.[34] These sexual forms of the parasite are ingested by a healthy mosquito taking a blood meal. Once in the mosquito's gut, *gametocytes* undergo exflagellation to form *microgametes*, which fuse and undergo fertilization to yield a *zygote*. The *zygote* then develops into an *ookinete*, which penetrates the midgut epithelial cells of the carrier mosquito and develops into an *oocyst* that further undergoes sporogony to produce *sporozoites.*[35] The resulting *sporozoites* lodge in the vector's salivary glands, which can be injected into the human host to continue the cycle.

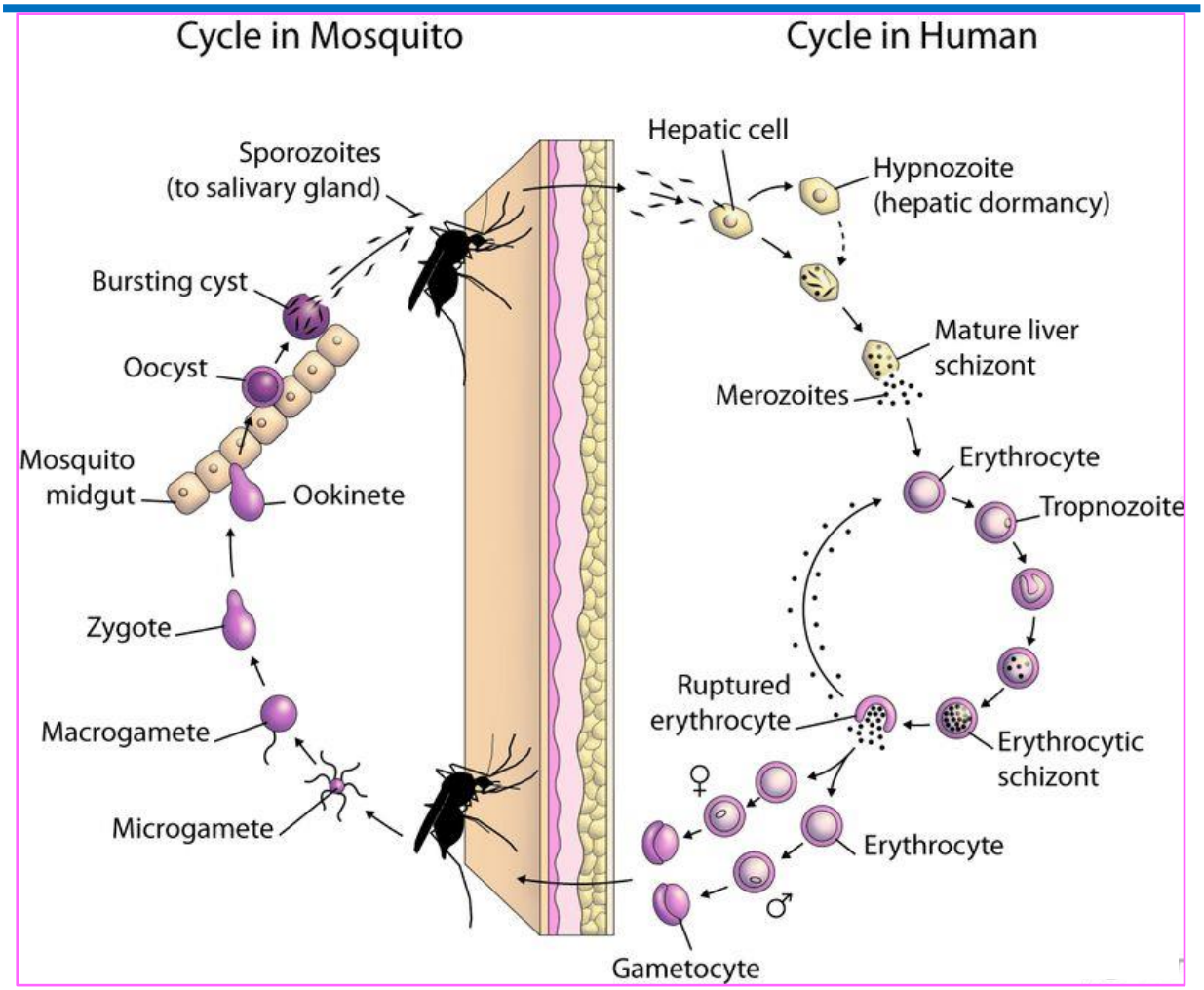

Figure 1.2: Life cycle of the *Plasmodium* parasite.[36]

1.1.4 Control, prevention and treatment of malaria

A combination of malaria control strategies such as sleeping under insecticide-treated bed nets (ITNs), indoor residual spraying (IRS),[10] use of repellents and the intermittent preventive therapy for pregnant women (IPTp) have significantly mitigated maternal illnesses and prevented infected vector contacts within the high-malaria-risk groups.[1,17,38] In addition, filling or draining stagnant water pools (mosquito breeding sites), as a mean of vector control, has supplemented efforts toward preventing the spread of malaria.[39,40] The awareness campaigns and provision of chemoprophylaxis to travellers to high-risk malaria infested areas ensure informed decision making on disease prevention and management in case of infection. In the case of infection, there is a need for the deployment of appropriate chemotherapies.

In 2005, the WHO issued malaria treatment guidelines and recommended synergistic artemisinin combination therapies (ACTs) as first-line regimens for uncomplicated *P. falciparum* malaria.[37,41] ACTs are formed by combining a rapid but short-acting artemisinin or a synthetic derivative with a slowly-eliminated but longer-acting partner drug. Such

combinations were envisaged to mitigate parasite resistance to the artemisinin component, facilitate dosing convenience and reduce treatment duration from 7 to 3 days. The artemisinin components of ACTs include artemisinin (**1**) itself and its synthetic derivatives; dihydroartemisinin (DHA) (**2**), artemether (**3**), arteether (**4**), artesunic acid (**5**) and artelinic acid (**6**) (figure 1.3). When administered to patients, the derivatives **3** – **6** are rapidly biotransformed to the active metabolite DHA (**2**). Apart from its ability to rapidly kill other blood stage forms of the parasite, DHA is also parasiticidal to the sexual forms of the parasite thereby blocking human-to-vector parasite transmission.[38,42]

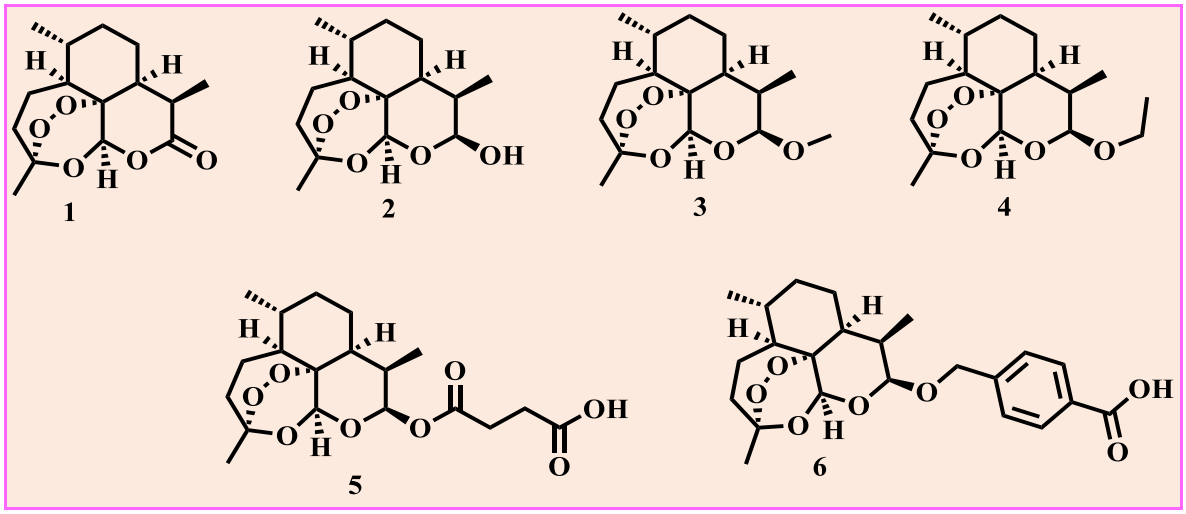

Figure 1.3: Chemical structures of artemisinin (**1**) and its derivatives- DHA (**2**), Artemether (**3**), Arteether (**4**), Artesunic acid (**5**) and Artelinic acid (**6**).

The use of a combination of any one of the fast-acting artemisinins (figure 1.3) with a long-acting schizonticide such as lumefantrine (figure 1.4) is known to minimise chances of recrudescence after clearance of initial parasitaemia and/or mitigate emergence of parasite resistance to partner drugs in ACTs.[43] A typical example of such an ACT is coartem, a combination of artemether and lumefantrine (AL)[44] which was developed by Novartis Pharmaceuticals in collaboration with Medicines for Malaria Venture (MMV) in 2009.[45,46] A further formulation of coartem into the "child-size" and sweet-tasting therapeutic doses, among other malaria control measures, led to significant decline in the global malaria morbidity and mortality in the period 2010 - 2016;[10,47] compared to the yesteryears. Other examples of ACTs include artesunate-amodiaquine, artesunate-mefloquine, DHA-piperaquine. For pregnant women, the pyrimethamine (**8**) and sulphadoxine (**11**) combination (SP) (figure 1.4**)** has been recommended.[48]

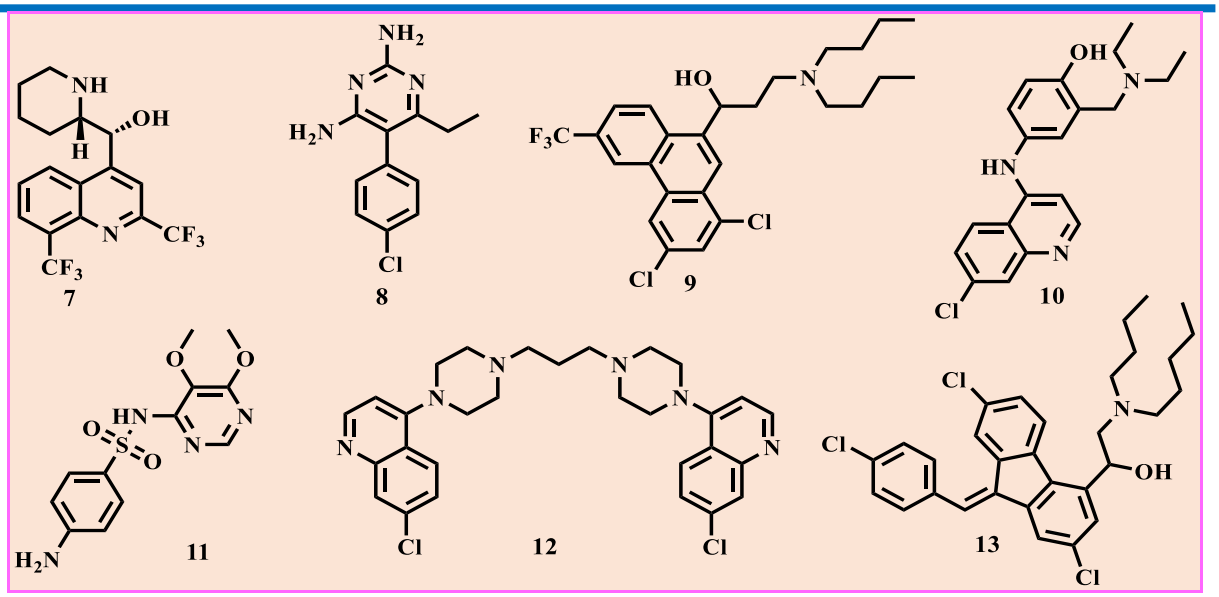

Figure 1.4: Chemical structures of partner drugs used in ACTs: Mefloquine (**7**), pyrimethamine (**8**), halofantrine (**9**), amodiaquine (**10**), sulfadoxine (**11**), piperaquine (**12**) and lumefantrine (**13**).

The second line options for treatment of complicated *P. falciparum* malaria generally consists of either individual components of ACTs such as artemether (**3**), artesunate (**5**) etc which are administered as monotherapies or, quinine (**14**), atovaquone (**15**) and proguanil (**16**) that are administered in combination with an appropriate antibiotic partner drug, which mainly includes clindamycin (**17**), doxycycline (**18**) and tetracycline (**19**) shown in figure 1.5. Additionally, a combination of **15** and **16** has been established for therapeutic application as well as prophylaxis of malaria.[49,50] Primaquine (**20**) remains the only antimalarial known to deliver a radical cure by targeting the liver stage hypnozoites of *P. vivax* and *P. ovale*. It also targets the sexual forms of the malaria parasites thereby blocking transmission into the mosquito vector.[3,51–53] Regrettably, it is not recommended for pregnant women and individuals with glucose-6-phosphate dehydrogenase (G6PD) deficiency because it causes severe haemolysis in such patients. Thus the requirement that G6PD status of patients is known before initiation of primaquine therapy[54] makes it an obvious limitation in malaria treatment in resource-limited African countries. Lastly, chloroquine (**21**), the oldest, once effective and cheapest antimalarial (figure 1.5) has experienced widespread resistance, and has been withdrawn from clinics and markets in areas of endemic *P. falciparum* malaria.[55,56]

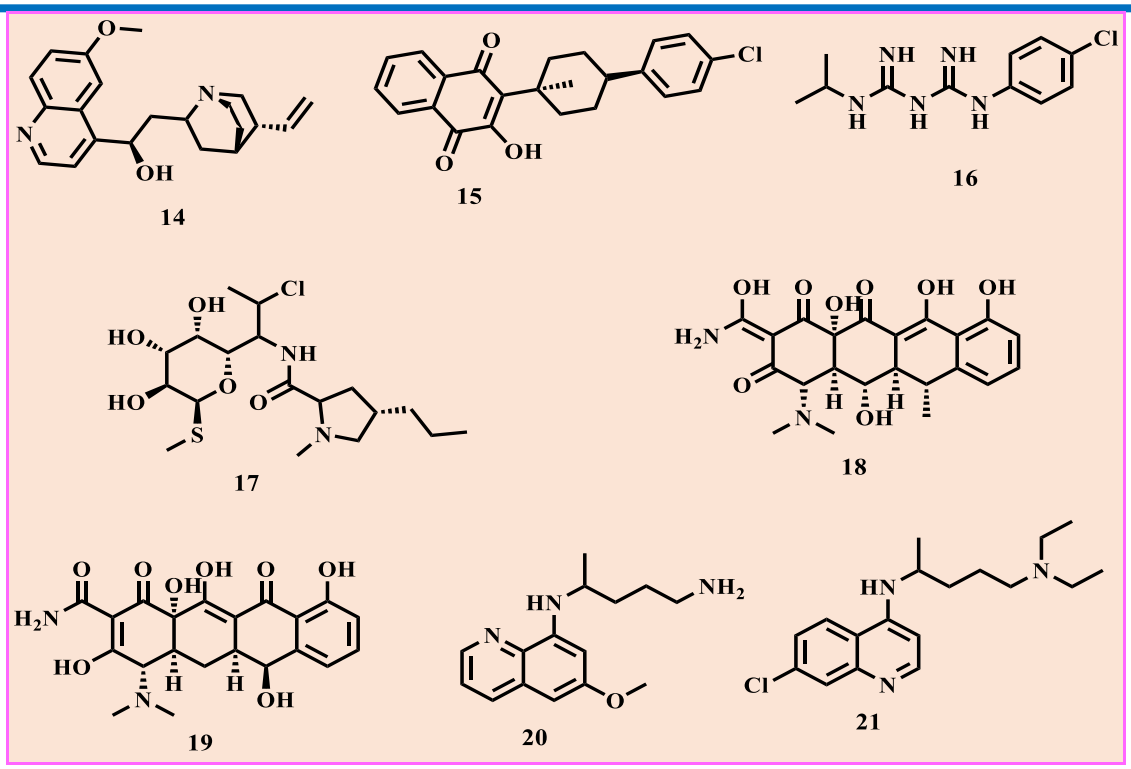

Figure 1.5: Chemical structures of selected second line antimalarial drugs and the antibiotics–quinine (**14**), atovaquone (**15**) proguanil (**16**), clindamycin (**17**), doxycycline (**18**) and tetracycline (**19**), primaquine (**20**) and chloroquine (**21**).

Malaria treatment is currently challenged with the spread of resistance to artemisinin-based antimalarial drugs in both Cambodia and Africa.[57] The emerging resistance, especially in Cambodia and its bordering areas of Vietnam, Laos, Thailand and the Myanmar-Indian border, is threatening to reduce the efficacy of all ACTs.[16,47,58,59] The issues of limited use of ACTs,[41,60] patient's poor adherence to previously prescribed long doses (7 days)[61] or under-dosing, low efficacy, poor safety (counterfeit drugs) and unaffordable cost of malaria treatment, have contributed to the emergence of resistance.[62,63] Parasite resistance to artemisinins has been manifested in the phenomenon of delayed parasite clearance following exposure to the fast-acting artemisinin component in ACTs.[57,59,64] This incomplete parasite clearance is thought to increase the chances that some parasites will spontaneously develop genetic resistance to long-acting ACT partner drugs as well.

While estimates of disease burden have been reduced in between the years 2010 and 2014, the impact of resistance in areas of endemic malaria has resulted in an increase in both statistical malaria cases (figure 1.6) and deaths (figure 1.7) between the years 2013 and 2016.

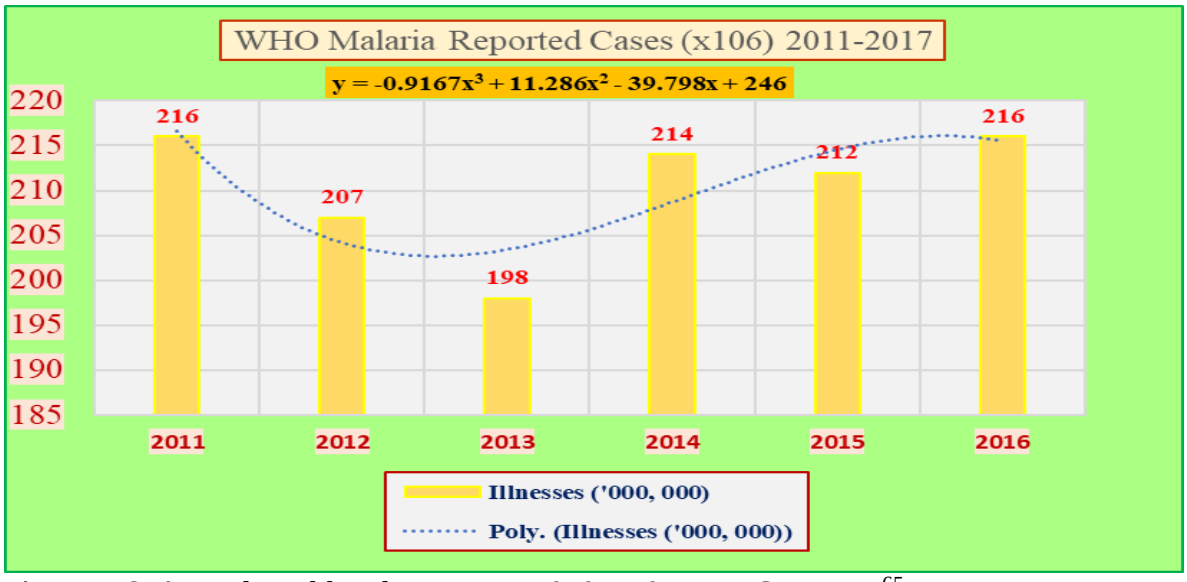

Figure 1.6: Annual world malaria cases- 2010 – 2017 WHO reports.[65]

The confirmed reports of spreading resistance and the resulting increase in malaria cases pose a significant threat to the strides made in the control and eradication of malaria so far as can be exemplified by the latest statistics in which 212 million malaria cases and 429 000 deaths reported in the year 2015, increased to 216 million cases and 445, 000 deaths in 2016.[57] This translates into 4 million new malaria cases (figure 1.6) and about 16 000 additional malaria-related deaths (Figure 1.7).

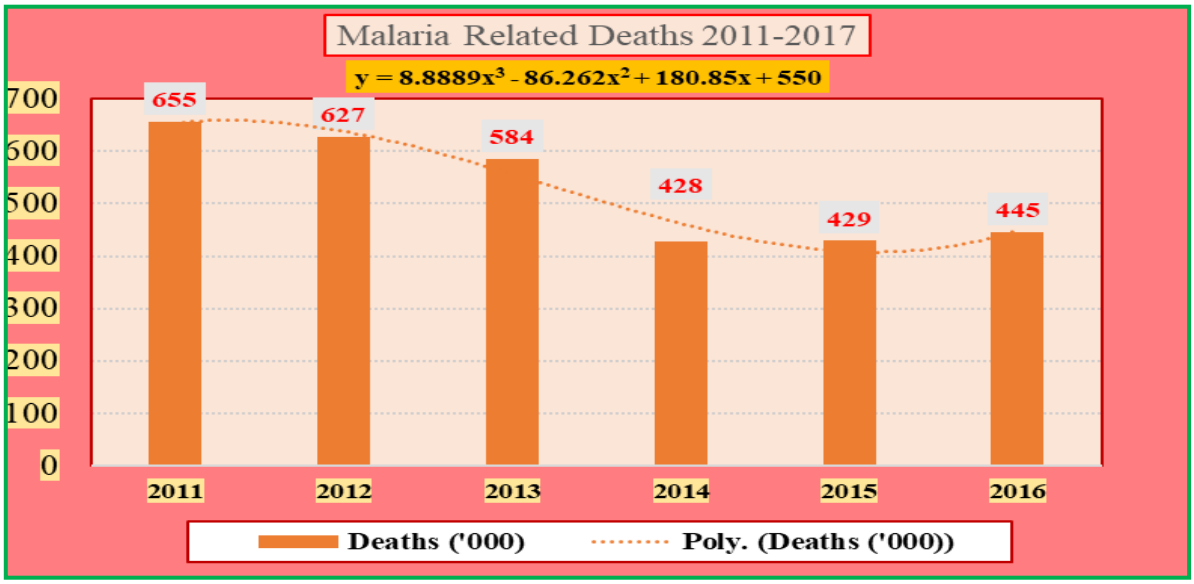

Figure 1.7: Annual world malaria deaths- 2010 – 2017 WHO reports.[65]

The devastating global morbidity and mortality record, with one child dying of malaria every two minutes, and drug resistance collectively provide justification for stepping up global efforts in antimalarial drug discovery and development research. Intensive efforts should be aimed at

developing new, safer, affordable and effective antimalarial drugs with alternative mechanisms of action so as to impede resistance,[66] roll-back malaria, mitigate morbidity and mortalities while improving the economic livelihoods and wellbeing of the world's poor majority.

1.1.5 Current antimalarials in clinical development

To combat the increasing malaria illnesses, deaths and parasite resistance to chemotherapy, research and development have been instituted globally to develop malaria vaccines and drugs, which are meant to backup current antimalarials. Currently, a total of fourteen (14) MMV-supported antimalarial candidates, among others, have been developed and are in preclinical and clinical development. It is noteworthy that nine (9) of these drug candidates provide entirely novel mechanisms of action compared with partner drugs used in ACTs.[67] In addition to these chemotherapeutic candidates, a vaccine candidate (**RTS, S/AS01**) has been developed and discovered to offer immunity against malaria. Its potential to prevent *P. falciparum* malaria infection has been assessed and proven in infants aged 6–12 weeks and children aged 5–17 months in a phase (III) clinical trial. The clinical trial conducted between 2009 and 2014 proved the concept and revealed that **RTS, S/AS01** exhibited at least 50% protection against malaria infections.[68]

Among the newer antimalarial candidates which have advanced into clinical development includes **OZ439** (**22**),[69] **KAE609** (**23**),[70] **KAF156** (**24**),[71] **DSM265** (**25**),[72] **AQ-13** (**26**)[73] and **MMV390048** also known as **MMV048** (**27**),[74] whose structures have been summarised in figure 1.8 below. In addition to their unique modes of action, these antimalarial candidates have been studied and found potent with favourable properties such as multiple stage activity, parasite transmission blocking and chemo-protection.[50] A newly discovered artefenomel-based antimalarial candidate **OZ439** has been evaluated and found to be a fast-acting schizonticidal agent in addition to its activity at the symptomatic stage of *P. falciparum* malaria. Moreover, **OZ439** has been assessed and found to have a good safety profile and is well-tolerated in healthy volunteers.[69]

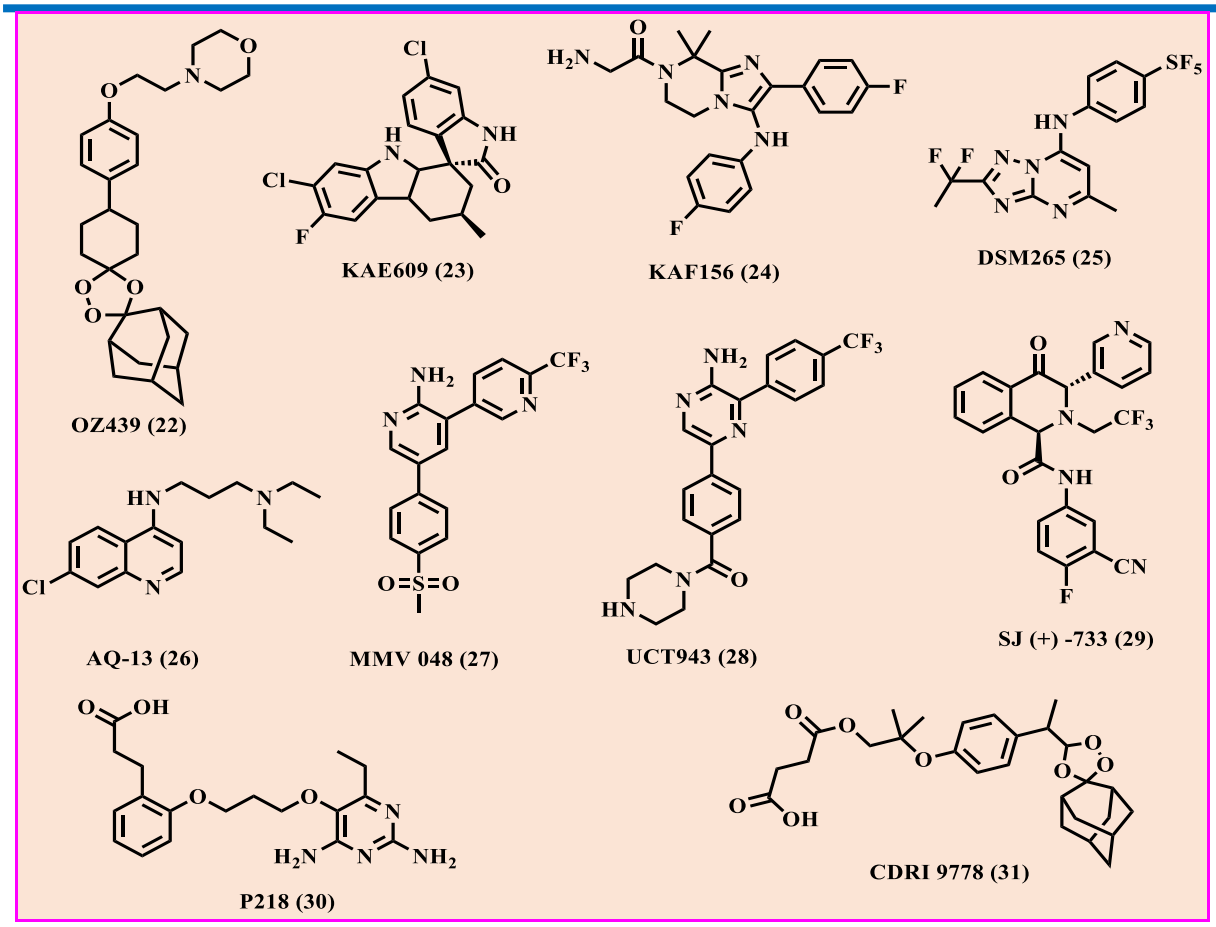

Figure 1.8: Chemical structures of selected clinical and pre-clinical antimalarial candidates

On the other hand, a spirotetrahydro-β-carboline (spiroindolone) based antimalarial candidate, **KAE609** has been studied and shown to target the parasite plasma membrane Na-ATPase and inhibit plasma membrane Na^+ efflux pump (P*f*ATP4) leading to the ultimate disruption of the parasite's sodium homeostasis.[77] Most favourable properties of **KAE609** include its activity against the asexual and sexual stages of parasite development and its ability to provide parasite to vector transmission blocking. Conversely, an imidazolopiperazine based antimalarial, **KAF156** has shown potent antiplasmodium activity by inhibiting gametocytogenesis. Due to its multistage activity; at pre-erythrocytic liver stages as well as asexual and sexual blood stages of parasite development, **KAF156** provides parasite-to-vector transmission blocking and chemoprotection which makes it a suitable chemotherapy for the malaria eradication agenda.[70,71] Further in clinical development, is a novel antimalarial candidate **DSM265** which provides a totally different mode of action. The compound targets the pyrimidine biosynthesis pathway where, has been shown to inhibit plasmodial dihydroorotate dehydrogenase (*Pf* DHODH).[72] In addition, it has also been shown to be active against the asexual stage of *P. falciparum* development as well as provide chemoprotection. The 4-aminoquinoline-based antimalarial candidate **AQ-13** (**26**) showed activity against both chloroquine susceptible and

resistant *P. falciparum* parasite strains with a good safety profile in human volunteers and thus has been progressed to the clinical development stage.[73] Finally, amongst the antimalarial candidates in clinical development is **MMV390048** (**27**). Except for hypnozoites, compound **27** was found active against all *Plasmodium* parasite lifecycle stages thus, possessing both transmission blocking and chemo-protection properties.[74,76] This novel aminopyridine-based antimalarial candidate was identified from a phenotypic whole cell high-throughput screening of commercially available SoftFocus kinase library followed by medicinal chemistry optimization.[74] Moreover, compound **27** has been shown to exert its antimalarial activity by inhibiting *Plasmodium falciparum* phosphatidylinositol 4-kinase (*Pf*PI4K) which also represents a novel mechanism of action in antimalarial drug research.[25,75,76] However, compound **27** was found to have low solubility in biorelevant media resulting in variable pharmacokinetic profiles in healthy volunteers and prompting time-consuming formulation studies. As a result, further research at the University of Cape Town (UCT) led to the identification of a back-up candidate, **UCT943** (**28**) (figure 1.8**)** which was developed with an improved solubility profile.[78]

If successfully developed, compounds **27** and **28** would not only be part of the first new antimalarial drugs in many years to provide a completely new mode of action and treatment option but also, they will be the first-ever antimalarial drugs to be discovered by an African-led international team.

In addition to the above mentioned antimalarials candidates, other compounds which have entered the drug development portfolio with unique modes of actions include (+)-**SJ733 (29)**,[79] **P218 (30)**[80] and **CDRI 9778 (31)**[81]. These compounds have been assessed in animal models and healthy human volunteers and found to be well tolerated with good safety margins and oral bioavailability. As such, the dihydroisoquinolone-based antimalarial candidate, **29** has been identified with properties that are likely to effect radical cure and prophylaxis in a single exposure. Moreover, the drug candidate has been studied and observed to be well-tolerated and exhibited good oral bioavailability in multiple species.[79] On the other hand, the dihydrofolate reductase (P*f*DHFR) inhibitor drug candidate, **30** has been identified with excellent ADME-PK profile while exhibiting full activity against the pyrimethamine-resistant parasite strains.[80] The trioxane peroxide based antimalarial candidate **31** is among the inhibitors of plasmodial phospholipid metabolism and is highly efficacious against multidrug-resistant *P. falciparum* strains.[81] In addition to the drug candidates discussed above, various drugs in the antimalarial development portfolio are summarised in figure 1.9 below:

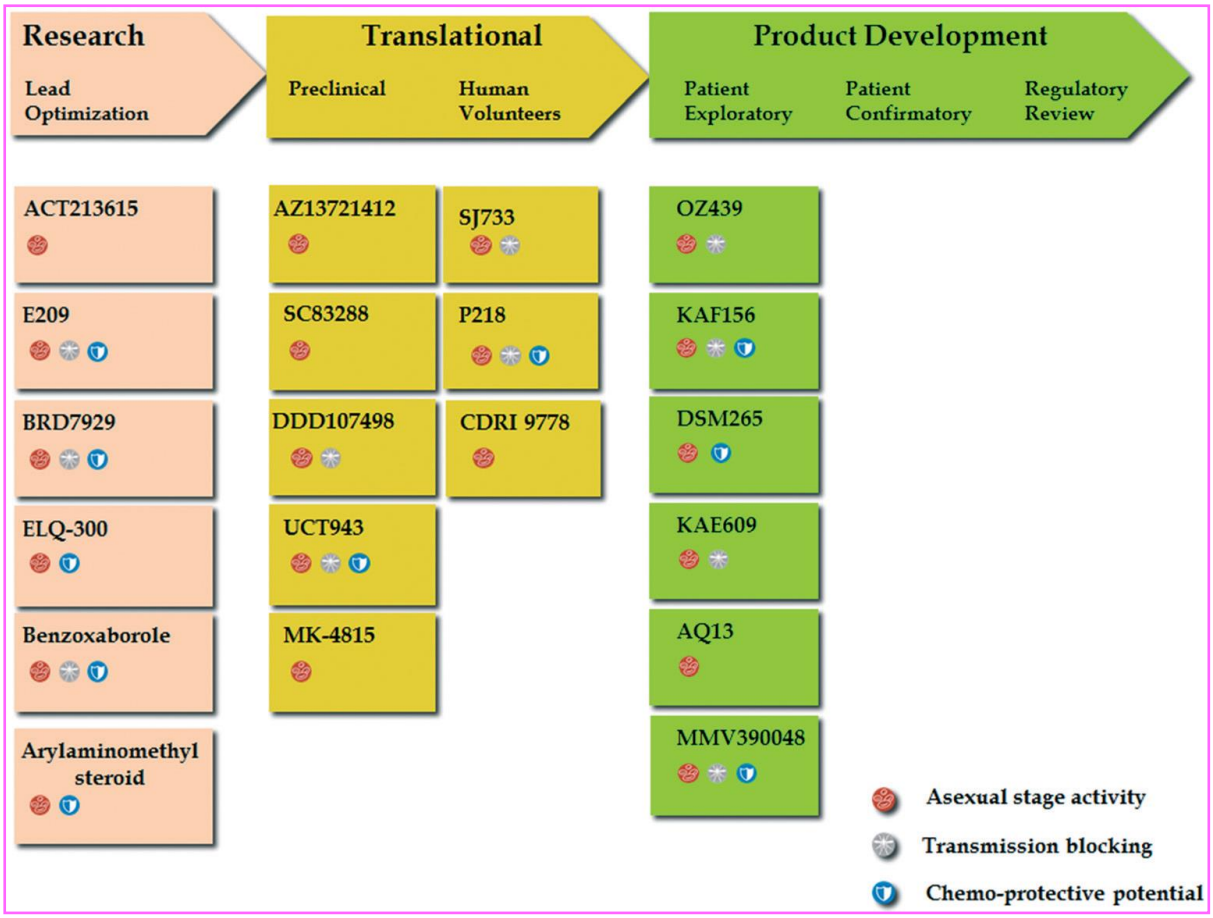

Figure 1.9: Medicines for Malaria Venture antimalarial drug pipeline-2018.[76,82]

1.2 Schistosomiasis

1.2.1 History, introduction and aetiology

Schistosomiasis, commonly known as bilharzia, is caused by the bisexual blood flukes of the genus *Schistosoma*,[83,84] which are transmitted by various species of gastropod molluscs (snails). Snails and schistosomes have a coevolutionary relationship spanning more than 200 million years.[85] The predominant pathogenic species of human schistosomiasis, however, were only discovered in the middle of the 18th century and include, in chronological order of detection, *S. haematobium* (1852), *S. japonicum* (1904), *S. mansoni* (1907), *S. intercalatum* (1934) and *S. mekongi* (1978).[85–87] However, the three trematode species that are most prevalently associated with human infections include *S. mansoni*, *S. haematobium* and *S. japonicum*. The respective vectors include Biomphalaria, Bulinus and Oncomelania snails.[84,88]

Schistosomiasis is an important, highly prevalent (figure 1.10) and infectious disease that is ranked second to malaria in causing long-term chronic human morbidity in many parts of the world.[51] Since its discovery, schistosomiasis has adversely impacted human health and socio-economic development. It has affected mainly both the growth and intellectual development of children, increased women exposure to HIV and other sexually transmitted infections (STIs) and compromised women's reproductive health leading to infertility.[90] Additionally, it has decreased the production and working capacity of adults leading to poor economies and poverty in areas of endemicity.[88–90] Despite the severe and devastating effects of schistosomiasis on both human health and the economy, no new drug nor vaccine to date has been developed to treat or prevent the infections and transmission of the disease, besides Praziquantel (PQZ), the only chemotherapy of choice.

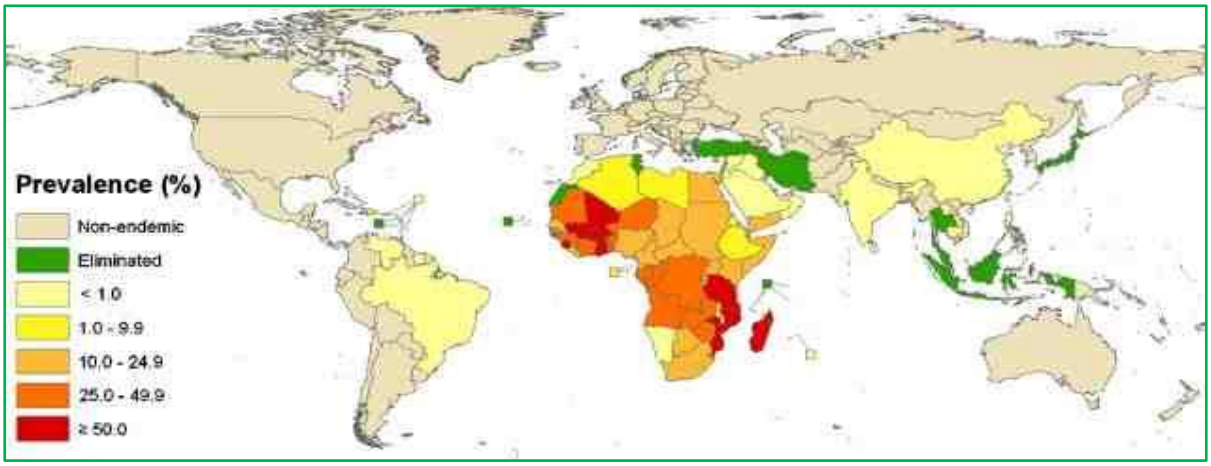

Figure 1.10: World schistosomiasis distribution.[91]

Schistosomiasis is mostly predominant in the tropical regions of the world with sub-Saharan Africa accounting for over 90% of the world's disease burden (figure 1.10).

1.2.2 Epidemiology

Approximately 779 million and about 207 million people are at risk of, and infected with schistosomiasis respectively, leading to about 280,000 annual deaths globally. In the year 2003, sub-Saharan Africa accounted for 90% of the total cases of the disease.[92] However, reduction in the number of disease cases has been observed and reported in 2017 WHO report on schistosomiasis. According to this report, approximately 95.2 million people are at risk of infection while 90 million others are infected, leading to about 41,000 annual deaths globally in the year 2016. In the same report, the number of treated cases increased from ~66.5 to ~90 million people in between the years 2015[93] and 2016,[90] of which 70.9 million were school-aged children and 18.3 million people were adults.[90]

1.2.3 Responsible parasite species and life cycle

Schistosomes are parasitic, with a life cycle alternating between a snail and the vertebral host as shown in figure 1.11. The three most prevalent schistosome species associated with human infections (*S. mansoni*, *S. haematobium* and *S. japonicum*) share a common life cycle and development stages. Adult schistosome worms living in the blood venules of a human host lay about 300 eggs per day,[94] some of which become trapped in the tissues while others are released through faeces or urine, depending on the schistosome species. Upon contact with freshwater, the eggs hatch into free-swimming *miracidia*, which seek and infect specific species of snails. The intramolluscan development takes about 4–6 weeks. Within the snail, the *miracidia* transform into mother *sporocysts* that undergo asexual replication to produce daughter *sporocysts*. Each daughter *sporocyst* undergoes further replication, ultimately yielding *cercariae* – a second free-swimming form of the parasite, which is infective to humans. *Cercariae* lose their tails during penetration of the host's dermis and become *schistosomulae*. These migrate via the blood circulation to the portal veins of the liver where they differentiate and mature into adult worms. Adult male and female worms pair up, mate, and then migrate to the mesenteric venules of the bowel and rectum or the venous plexus of the bladder to complete the life cycle (figure 1.11). It takes about 6–8 weeks from *cercariae* penetration to the maturation of worms and laying of eggs.[94–96]

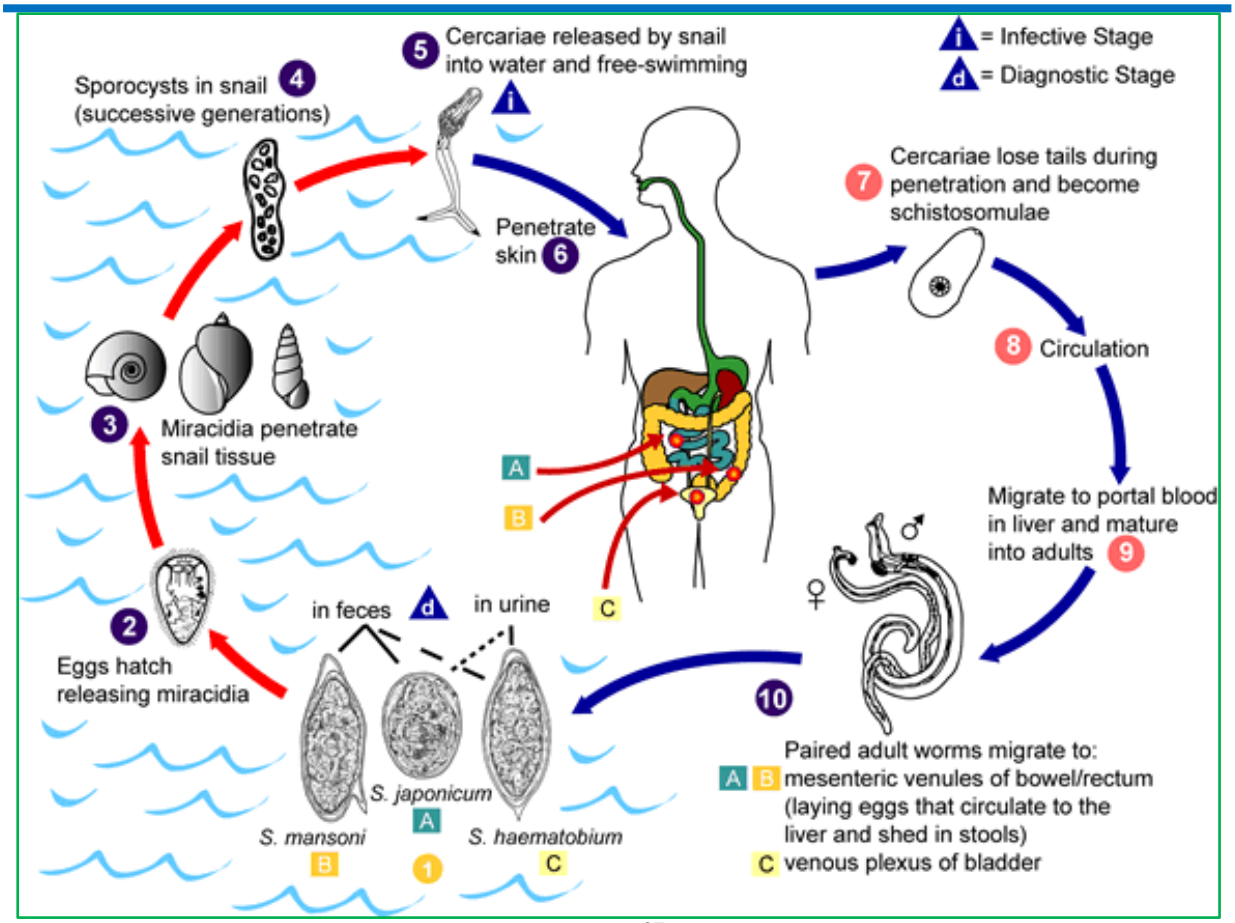

Figure 1.11: Life cycle of schistosome parasites.[97]

1.2.4 Control, prevention and treatment

Between 1930 and 1985, control of schistosomiasis was based on chemical molluscicides (niclosamide or copper sulphate) for snail control. In 2015, the WHO recommended mass drug administration (MDA) alongside various preventive measures, which include improved sanitation as has been demonstrated by using modern bio-composting toilets, which have effectively killed parasite eggs. Additionally, draining marshes and swamps is another recommended strategy for vector control and prevention of parasite transmission. Public education campaigns which highlight the risk of employing irrigation methods that involve long-standing still waters have been launched. Furthermore, awareness talks are given to visitors going to schistosome-infested areas about dangers of immersing in potentially contaminated waters. In addition to preventive and control measures, most schistosomiasis affected countries have adopted curative methods in mitigating schistosomiasis.[98]

PQZ (**32**) (figure 1.12) has been the only readily available drug for treatment of schistosomiasis in about five decades and is characterised by broad spectrum activity against the prevalent three schistosome species while providing good therapeutic efficacy and safety.[99] The drug has shown curative effects at the adult stage of the liver fluke. Antimonium tartaratum (**33**), the

antique drug used to treat *S. haematobium* infections dating back to 1918 was terminated and withdrawn from the market for safety reasons, that mainly involved the bioaccumulation of antimony in the body.[100] In the 1960s and 1970s, furapromidum (**34**), metrifonate (**35**) and oxamniquine (**36**), which were active against *S. japonicum, S. haematobium* and *S. mansoni*, respectively, entered WHO's model list of essential drugs until the late 1990s.[44] Since then, these drugs (see figure 1.12) are no longer available commercially.[101]

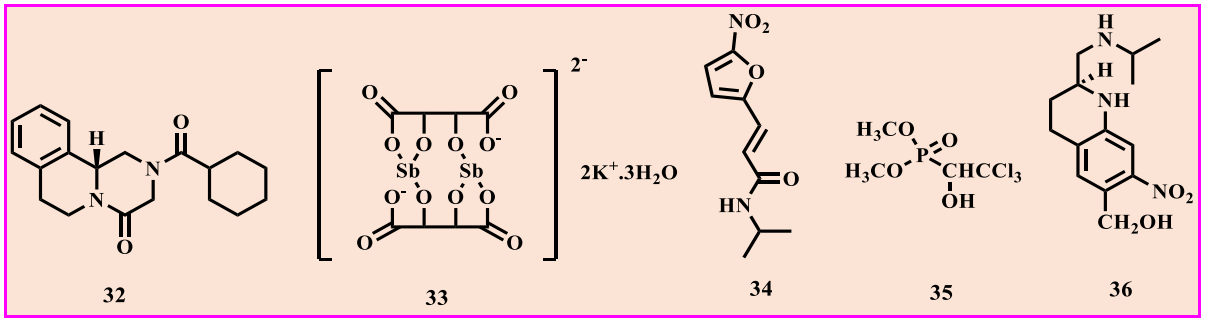

Figure 1.12: Chemical structures of selected antischistosomal drugs- PQZ (**32**), Antimonium tartaratum, (**33**) Furapromidum (**34**), Metrifonate **(35**) and Oxamniquine (**36**).[101,102]

However, PQZ has exhibited a number of challenges that include its bitter taste,[44] high production costs as the drug is produced as a racemic mixture of dextrorotatory [D(-)] and laevorotatory (L(-)] of which only the L(-) isomer has schistosomicidal activity.[44,101–103] In addition, the drug has a limited activity to only adult schistosomes and has shown no activity towards young stages of the liver flukes,[44,104] thus posing risks of relapse of the disease after treatment. Moreover, slow curing rates have recently been noted in some parts of West Africa, thus, posing a risk of the emergence of resistance.[105]

1.2.5 Antischistosomal drug pipeline

Schistosomiasis is one of the most neglected infectious tropical diseases to which, little to no attention has been paid in terms of research and development of new chemotherapeutic agents in about five decades. Several lead compounds including artemisinin (**1**) artemether (**2**), artesunate (**3**), mefloquine (**7**) (figures 1.3 – 1.4), the ozonides (1,2,4-trioxolanes; **OZ288** (**37**) and **OZ418** (**38**)),[106] trioxaquine (the aminoquinoline linked 1,2,4-trioxane; **PA-1259** (**39**)) and aryl hydantoins (**Ro 11-3128** (**40**) and **Ro 13-3978** (**41**))[44,100](figure 1.13), have been shown to possess antischistosomal properties. Although most of these lead compounds were pursued as antimalarials, they were discovered to have good activity at various stages of the schistosomal liver flukes.[44] Nevertheless, none are currently being actively pursued for further antischistosomal drug development due to lack of funds, prospects of poor investment return

from the product and the widespread belief that PQZ is a sufficient curative control for schistosomiasis.[107]

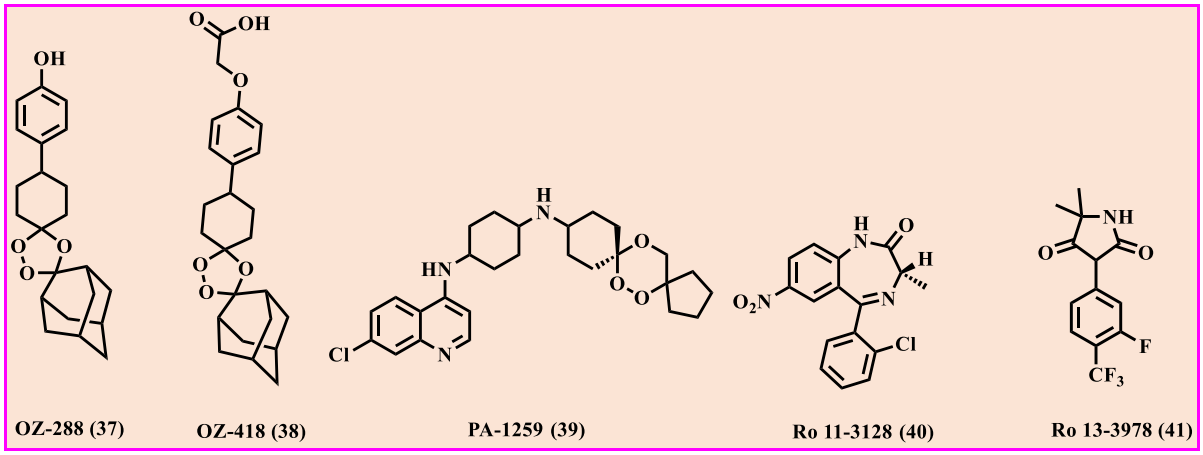

Figure 1.13: Structures of antischistosomal lead compounds

There is a need to speed up research and development activities to develop new more affordable and effective antischistosomals to serve as alternatives to PZQ, and which would potentially prevent devastating effects of total resistance to the only available treatment option.

1.3 Approaches to antimalarial and antischistosomal drug discovery

The duration, high labour intensity and the huge cost associated with the development of a drug from scratch is an enormous challenge. Cutting down on such costs requires the strategic adoption of some drug candidates which might have gone through various developmental stages hence, whose pharmacokinetic parameters, formulation and safety or potential toxicity profiles are documented.[108,109] Two cost reduction drug discovery approaches namely, drug repurposing and drug repositioning become useful choices. Drug repurposing involves discovering a new therapeutic application of an existing drug that has been approved by the regulatory body for use in a specified medical indication. Upon identification of the therapeutic effect on a totally different medical condition, the next step in development may only involve optimising the dosing regimen for the new application. On the other hand, drug repositioning involves the use of a dispensary or candidate drug as the scaffold for the development of other drug derivatives that possess a therapeutic effect for a totally different medical indication. Drug repurposing and repositioning approaches have been, in the past, effectively exploited in antimalarial, antischistosomal and antitubercular drug discovery and development.[110] For instance, sulfa-based drugs for malaria, and fluoroquinolones for tuberculosis (TB) were initially developed for the treatment of non-malaria and non-TB diseases. In principle, a clear

identification of the drug's target enzyme and understanding of the mode of action of the drug may allow for treatment of two or more different parasites using one drug.

This dissertation research will take advantage of the findings that *Schistosoma spp.*, have the same blood-feeding characteristics as *Plasmodium* parasites and coherently share the same haem degradation mechanisms.[111–114] In this mechanism, the parasite digests host haemoglobin as a major source of amino acids they need to supplement nutritional requirements and complete their sexual development. Toxic free-heme (ferriprotoporphyrin IX) is released in the process, which can produce oxygen radicals or damage cell membranes and parasite proteins. To avoid the toxic effects, *Schistosoma* and *Plasmodium* parasites bio-crystallise heme molecules into inert and insoluble hemozoin.[111–114]

The postulate that the antimalarial drug candidates could positively effect a similar pharmacological response toward both the blood-digesting liver flukes and *Plasmodium spp.* is deemed logical, since their mechanism of action shares a common pathway.[44] Recently, clinically useful antimalarial drugs and drug candidates have been discovered and found with antischistosomal properties upon tests in rodents.[44] Such drugs include mefloquine,[115] artemisinin and its semi-synthetic derivatives such as artemether and artesunate.[44,84,116,117] Additionally, the ozonide class of compounds (1,2,4-trioxolanes: **OZ288** (**37**) and **OZ418** (**38**)),[106,118] and trioxaquines (**PA-1259** (**39**)),[119,120] (figure 1.13), are some of the other antimalarial drug candidates discovered to possess antischistosomal properties as well. These antischistosomal lead compounds were developed in antimalarial research programs and were at various stages of drug development.[44]

1.4 Solubility in drug design and development: importance and strategies for improvement

In the context of medicinal chemistry, solubility can be defined as the property of a drug molecule to dissolve in an aqueous solvent to form a homogeneous solution at a specified temperature and pH.[121] Solubility is a significant physicochemical property in drug discovery that impacts a drug's pharmacokinetics and how it is used in the clinic.[121,122] With the exception of the first-pass metabolism in the liver, oral bioavailability is highly dependent on intestinal absorption, which is a function of the compound's solubility and permeability.[123] Thus, an orally ingested drug with optimal solubility and dissolution rate is most likely absorbed, and permeated which brings about a desired pharmacological response. Conversely, a sub-optimally soluble drug is frequently associated with formulation challenges, limited and variable absorption, poor permeation and bioavailability (in oral administration), and is likely to precipitate if administered intravenously leading to poor tissue distribution and metabolism.[124] Such a drug may further present inconsistencies in clinical response due to the drug's suboptimal pharmacological effect and is likely to result in adverse and side effects.[125]

1.5 Strategies to improve solubility

Various techniques to enhance the solubility of poorly soluble drug candidates are principally based on physical[126] and chemical modifications.[127] The choice of the solubility-improving method to apply depends on the drug property, site of absorption and required dosage form characteristics.[121] Although a drug's solubility can be improved upon by physical means and formulation efforts, these approaches have limitations and are expensive. Therefore, it is important that the drug's sub-optimal solubility is addressed early in the discovery phases using chemical modification approaches.[121,128] These methods are discussed in greater detail in the following section.

1.5.1 Chemical methods

Although arduous, chemical structure modification is a key factor in influencing intrinsic solubility properties of a drug candidate.[129] Substituent groups bonded to the drug scaffold determine overall lipophilicity, size and ionisability of the final drug molecule. Approaches that are frequently employed by synthetic medicinal chemists in improving aqueous solubility mainly involve modifying the drug core by incorporating hydrogen-bond donors and acceptors, introducing polar-ionisable or neutral polar groups, salt formation, saturation (increasing sp^3 character) and disruption of planarity. [127,129–131]

1.5.1.1 Introducing hydrogen-bonding groups

The hydrogen-bond donors and acceptors such as amino, carbonyl and hydroxyl substituents play a significant role in enhancing aqueous solubility due to their strong hydrophilic aqueous interactions.[78,130] In this regard, and as an example, Le Manach *et al*., have reported improved aqueous solubility by incorporating a water solubilizing hydrogen bonding group to afford a potential clinical candidate **UCT943** (figure 1.14A).[78] Molecules containing such functional groups can donate and accept hydrogen bonds, are basic in nature, and thus, have influence on the p*K*a of a compound and can exist in ionized forms at a suitable pH. These substituents are thus important and useful groups that have found widespread application in improving aqueous solubility and frequently given primary consideration in the medicinal chemistry optimization programs.[78,129–132] Scheme 1.14A – 1.14D in figure 1.14 summarizes this and other solubility enhancing approaches discussed in this subsection.

1.5.1.2 Polar ionisable and neutral-polar groups

The amino, amide and carboxylic acid functional groups have strong solubilizing potential due to their polar functionality. Improving solubility through the incorporation of such molecular features has found application in different therapeutic areas including antimalarial drug discovery. For instance, artemisinin derivatives containing a carboxylic acid and its corresponding salts (figure 1.14B) are more water soluble than the parent artemisinin.[133] Furthermore, the presence of acidic and basic functionalities in the candidate drug provides opportunities for further manipulations such as formulations that may result from the salt formation,[134] (figure 1.14B) leading to significant improvement of the drug's solubility. Many other drug discovery programmes have employed this strategy.[108–110]

1.5.1.3 Reducing aromaticity by introducing saturation

Increasing saturation by reducing the aromatic character of the analogue is a modification that has also been used in improving the oral aqueous solubility of various drug molecules as has been exemplified in figure 1.14C.[131] This approach involves increasing the fraction of sp^3-hybridized (Fsp^3) carbons which in turn, leads to the reduced structural planarity and less crystal-stacking capability of the drug analogue. Ultimately, the melting point of the saturated final analogue is reduced, thus, leading to improved drug solubility.[131]

1.5.1.4 Disrupting molecular planarity

Approaches to improve drug solubility may also focus on disrupting planarity of the drug molecule by incorporating substituents which may twist the scaffold out of the plane as has been exemplified in figure 1.14D. In this approach, introducing either chirality on suitable

positions of the scaffold or an electron-rich mono or polyatomic group on *ortho* positions of a bi-aryl system, includes some of the frequently used approaches to disrupt planarity. The resulting increased dihedral angle makes the drug molecules unsuitable for π-stacking and crystal packing thus, leading to low melting point and improved solubility.[127,128,132]

1.5.1.5 Pro-drug approach

A pro-drug may be defined as a poorly active or inactive compound, which upon undergoing an *in vivo* biotransformation, either through chemical or enzymatic cleavage, releases the active molecule at efficacious levels at the active site.[135] Pro-moieties such as acyl, carbamate, ether, phosphate, ester, among others, are some commonly used bio-reversible derivatives associated with enzymatic hydrolysis to release the active parent drug *in vivo* (figure 1.14E).[136] These groups are associated with ideal water solubilizing potential, good absorptivity and permeation properties to bring about improved overall drug efficacy.

In general, pro-drugs have achieved superior physicochemical properties compared to parent drugs. Thus, based on prodrug approach, Zimmermann *et al.*, have successfully improved the solubility and bioavailability of a broad spectrum anthelmintic and anticancer drug (mebendazole) by > 10, 000 and 2-fold, respectively.[136]

1.5.1.6 Reducing lipophilicity

Phenyl-polycyclic aromatic analogues are lipophilic and tend to form hydrophobic crystals because of intermolecular π-π interactions.[127,128,132] By so doing, molecules tend to form crystals, which have reduced surface area for aqueous interactions and thus, making drug molecules hydrophobic. Approaches such as substituting the lipophilic phenyl rings with pyridyl or pyrimidinyl rings have been studied and observed to reduce lipophilicity leading to improved solubility.[128]

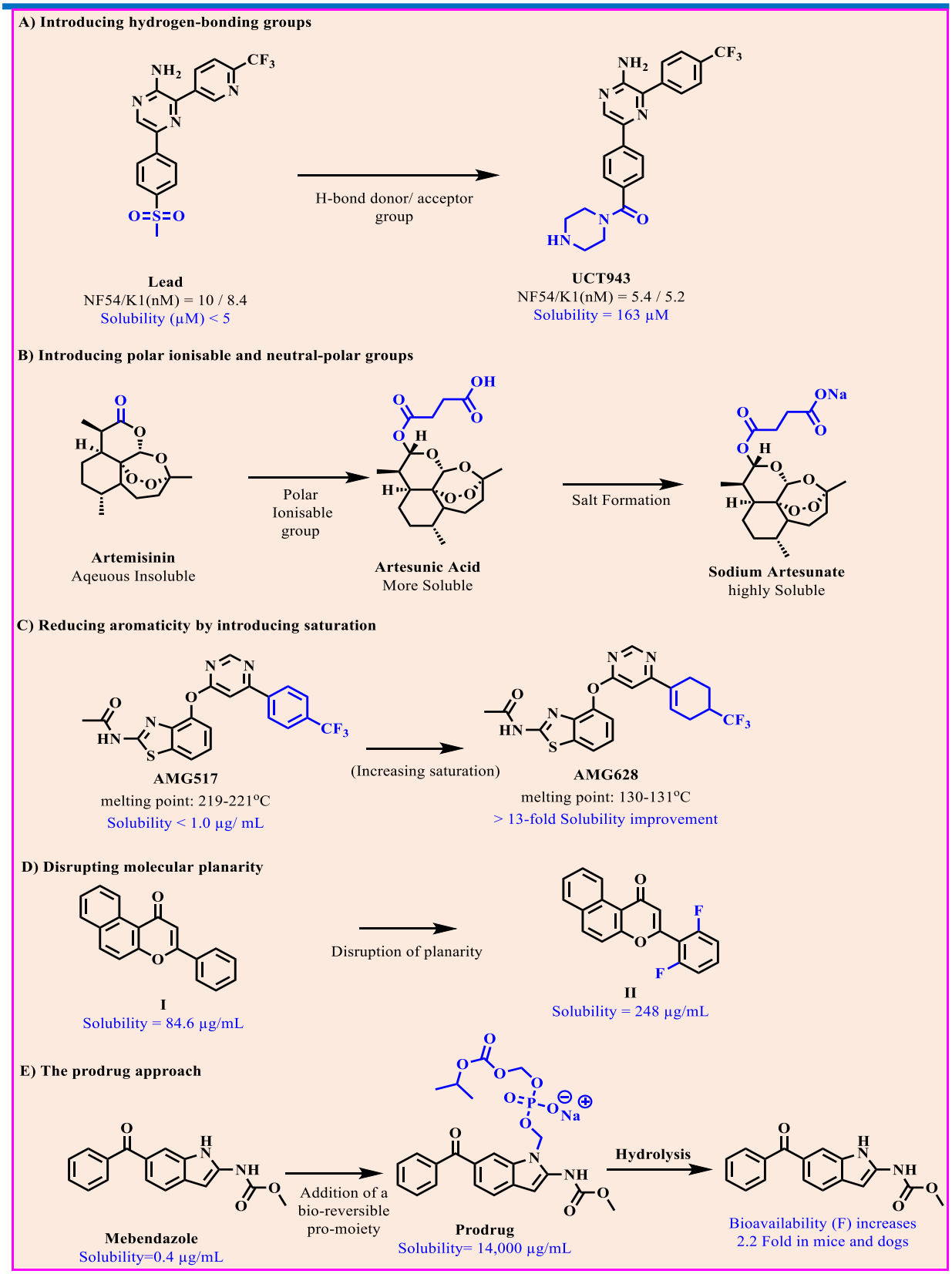

Figure 1.14: Selected approaches used to improve aqueous solubility

1.6 Drug metabolism and pharmacokinetics

In drug discovery, lead optimisation, evaluation of drug pharmacology and safety, clinical testing and development, and the final positioning of the drug product into the market are all significantly dependent upon the pharmacokinetics and drug metabolism profile. Medicinal chemists are usually tasked to identify the target enzyme or receptor and use experimental structure-activity relationships to increase the *in vitro* activity. However, *in vitro* activity alone does not guarantee good *in vivo* activity unless the drug is associated with good absorption, permeation, bioavailability and a desirable action duration or half-life.[137]

The drug's pharmacokinetic and metabolism profiles are the key determinants of bioavailability and the resulting *in vivo* therapeutic effect. A parent drug may, upon administration, be metabolised to either an active metabolite (metabolite that is able to exert the desirable therapeutic effect) or a reactive metabolite (a metabolite that is able to exert a toxic effect on biomolecules of the body such as glutathione thus, leading to metabolism-induced cytotoxicity). Such drug metabolism profiles should also be explored for regulatory purposes.[138] The kinetics of active metabolite formation, the basic mechanisms of the events involved in absorption, distribution, metabolism and excretion (ADME); the interaction of chemicals with the drug-metabolising enzymes, particularly cytochrome P450 (CYP) should as well be understood to facilitate prediction of the therapeutic outcome and provide ability to explain a drug's toxicity.[137]

1.7 Pyridobenzimidazoles: introduction and pharmacological properties

Pyridobenzimidazoles (PBIs) are fused ring heterocyclic aromatic compounds which have recently attracted attention in antimalarial, antischistosomal and antimycobacterial drug discovery.[63,111,139,140] The PBI pharmacophore comprises a tricyclic fused ring system that constitutes a benzene, the central imidazole and a pyridyl ring (figure 1.15).

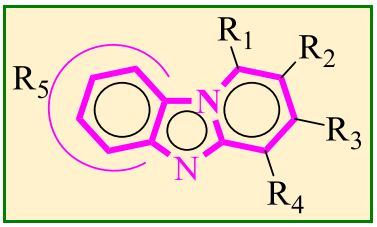

Figure 1.15: Pharmacophore of PBI

The PBI pharmacophore is synthetically diverse, chemically stable, and possesses vast biological and medicinal properties. These properties include inhibition of the synthesis of *b-1,6-glucan*, a cell wall component in fungus, anti-cancer, antiviral, analgesic, antibacterial, antitumor and antitubercular properties.[139,141–143] Selected compounds amongst numerous other chemotherapeutic agents are as shown in figure 1.16:

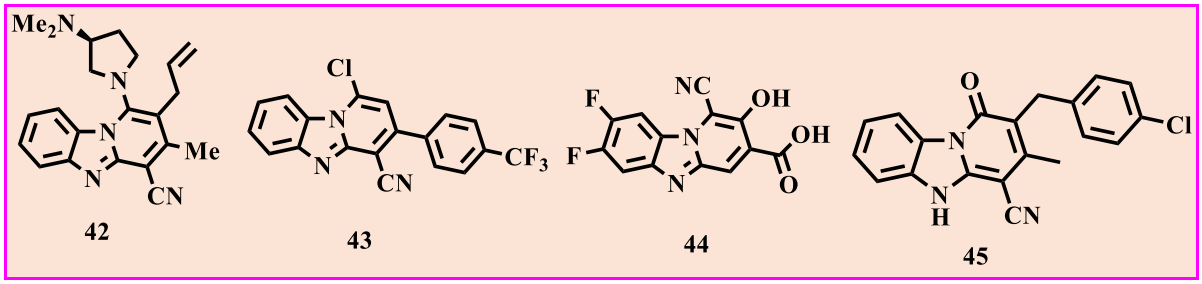

Figure 1.16: Bioactive PBIs- antibacterial (**42**), anticancer (**43**) antiviral (**44**) and antituberculosis (**45**).

The PBI scaffold is found in many pharmacologically relevant molecules including Rifaximin, an approved drug.[143] The PBI pharmacophore is, therefore, regarded as a privileged scaffold.[140] The scaffold has been used as a building block with many sites of modification to yield drug-like compounds. Consequently, medicinal chemistry explorations around the PBI nucleus have recently identified PBI analogues as novel antimalarial and antischistosomal agents.[63,111,140]

1.7.1 Antimalarial and antischistosomal properties of PBIs

The PBI core was recently shown to be a novel antimalarial chemotype.[63,140] The discovery of antimalarial properties of the PBI core stemmed from a medium-throughput screening (MTS) of 1440 commercially available compounds against the multidrug-resistant strain of *P.*

falciparum (K1).[63] Consequently, the hit compound **TDR15087** (**46**) (figure 1.17), was identified with moderate *in vitro* activity (IC_{50} = 170 - 370 nM) against *P. falciparum* GHA and W2 strains. Furthermore, 535 additional compounds were screened against the multidrug-resistant *P. falciparum* K1 strain but this time, with a view to exploring the effect of structure diversity around the PBI core. This led to the identification of the *N*-benzylpiperazinyl derivatives **TDR35885** (**47**) and **TDR44047** (**48**) (figure 1.17), which, in addition to greater *in vitro* antiplasmodium activity, were found to have better selectivity over the mammalian L-6 cell line.[63] Particularly, the activities against *P. falciparum* of these hit compounds which were uncovered in the second phase of PBI medium throughput screening showed an IC_{50} = 52 nM for the chloroquine sensitive (NF54) strain and IC_{50} = 50 - 78 nM against the resistance (K1) strain for **TDR35885** (**47**), whereas, IC_{50} = 53 nM for NF54 strain and 23 - 95 nM for the K1 strain was found for **TDR44047** (**48**).

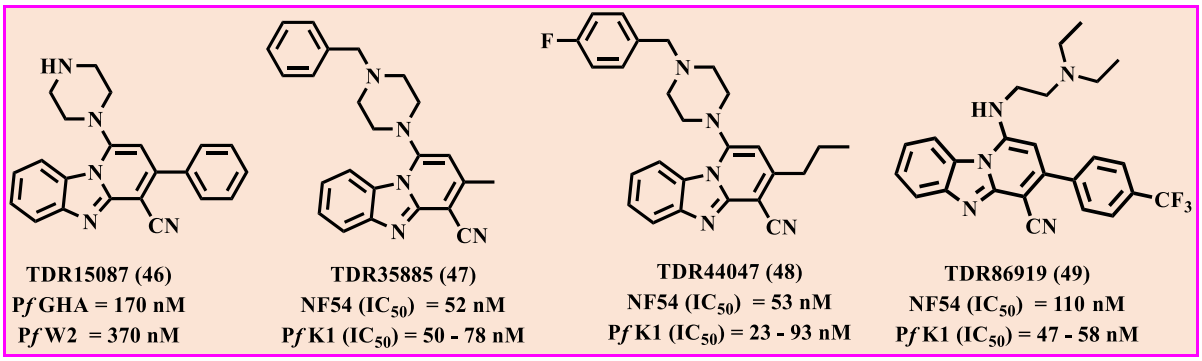

Figure 1.17: The PBI hit compounds identified from MTS.

However, all the 3 hit compounds (**46 – 48**) proved to be inactive in the standard *in vivo P. berghei* mouse model at doses of up to 4 x 100 mg/kg (ip), most likely because of a combination of poor solubility and metabolic stability.[63,140] Since there was no prior art with respect to the antimalarial activity of PBIs, compounds **46 – 48** inspired further medicinal chemistry explorations toward the design and synthesis of structural analogues, which were aimed at realising compounds with improved pharmacokinetic properties as well as enhanced pharmacological profiles. Consequently, the synthesis, structure-activity and structure-property relationship (SAR/SPR) studies of the 3-aryl derivatives with alkylamino side chains (at R1, figure 1.15) were undertaken. As a result, compound **49** (figure 1.17) with improved *in vitro* activity (IC_{50} = 47 nM) and about 3.5-fold more active than chloroquine (IC_{50} = 170 - 200 nM) on the drug-resistant K1 strain of *P. falciparum* was identified. Compound **49** was also found to be metabolised *in vitro* into an active metabolite, compound **50** (figure 1.18). Despite its reduced selectivity over L-6 mammalian cell line, compound **50** exhibited moderate activity,

about 10-fold higher metabolic stability and a relatively improved half-life compared to the parent compound **49**.[63] Thus, further medicinal chemistry exploration around compound **50** identified compound **51** (figure 1.18) with a combination of good *in vitro* antiplasmodium activity against the chloroquine-sensitive (CQ-S) and the resistant strains of *P. falciparum*. Moreover, compound **51** demonstrated an improved *in vivo* antimalarial efficacy when tested using the standard *P. berghei*-infected mouse model (figure 1.18).[63,140] Regrettably, like the others, this compound was associated with poor solubility.[111,140]

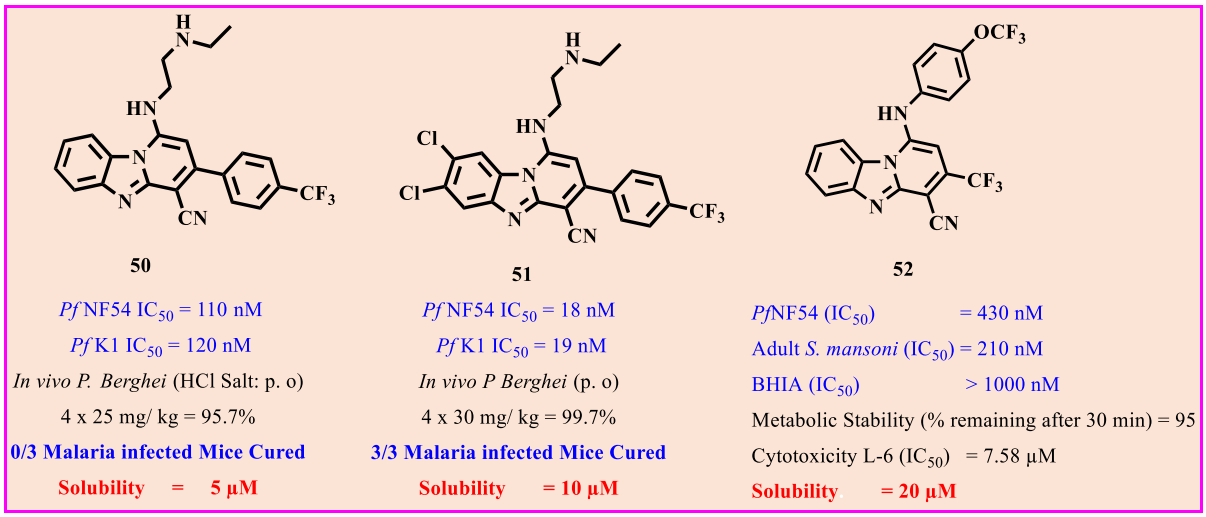

Figure 1.18: Antimalarial PBIs- Ndakala 2011 (**50**) and Singh 2017 (**51**) and GMP19-unpublished (**52**).

Amongst other front-runner compounds researched on and found to have a solubility liability albeit good antimalarial and interestingly, antischistosomal activity is **GMP-19** (**52**) (figure 1.18) which was derived in the year 2015 (unpublished).

Toward addressing sub-optimal solubility, while retaining or improving antiparasitic activity, this research endeavoured to synthesise and undertake SAR/ SPR exploration using the frontrunner compound, **GMP-19** as a template, having demonstrated good *in vitro* activity on schistosomes and *Plasmodium* parasites.

The strategies used in optimising solubility, involved the introduction of water-solubilising amines, amides and saturation, while the SAR/SPR expansion campaign involved the incorporation of chirality, germinal and α-methylbenzylamine substituents on the PBI core of **GMP-19**. Details of these strategies are outlined in subsequent chapters.

1.8 Aims and objectives

1.8.1 Objective

The main objective of this research was to enhance the solubility of antimalarial and antischistosomal pyrido[1,2-*a*]benzimidazole-based frontrunner compound **GMP-19**.

1.8.2 Hypothesis

Pyrido[1,2-*a*]benzimidazole-based compounds are potential novel antimalarial and antischistosomal drug leads with favorable potency, pharmacokinetics and physicochemical properties.

1.8.3 Specific Aims

i. To synthesise and characterise the antimalarial and antischistosomal Pyrido[1,2-*a*]benzimidazoles designed to improve solubility.

ii. To profile the synthesised compounds with respect to antiplasmodium and antischistosomal activities and solubility.

iii. To derive the antiplasmodium and antischistosomal as well as solubility profiles.

iv. To investigate the factors (e.g., melting point, cLogP, and retention time on Reverse-Phase HPLC) affecting solubility and deduce relationships.

v. To submit the selected frontrunner compounds with potent antiplasmodium and/or antischistosomal activities with good solubility for *in vitro* microsomal metabolic stability, and cytotoxicity profiling.

References

(1) Otten, M.; Aregawi, M.; Were, W.; Karema, C.; Medin, A.; Jima, D.; Kebede, W.; Gausi, K.; Komatsu, R.; Korenromp, E.; Low-Beer, D.; Grabowsky, M. Initial Evidence of Reduction of Malaria Cases and Deaths in Rwanda and Ethiopia Due to Rapid Scale-up of Malaria Prevention and Treatment. *Malar. J.* **2009**, *8* (1), 14.

(2) Cox, F. History of the Discovery of the Malaria Parasites and Their Vectors. **2010**, *3* (1), 5.

(3) International travel and health: http://www.who.int/ith/diseases/malaria/en/ (accessed Jun 29, **2018**).

(4) Delves, M.; Plouffe, D.; Scheurer, C.; Meister, S.; Wittlin, S.; Winzeler, E. A.; Sinden, R. E.; Leroy, D. The Activities of Current Antimalarial Drugs on the Life Cycle Stages of Plasmodium: A Comparative Study with Human and Rodent Parasites. *PLoS Med.* **2012**, (2), e1001169.

(5) Mordmüller, B.; Surat, G.; Lagler, H.; Chakravarty, S.; Ishizuka, A. S.; Lalremruata, A.; Gmeiner, M.; Campo, J. J.; Esen, M.; Ruben, A. J.; Held, J.; Calle, C. L.; Mengue, J. B.; Gebru, T.; Ibáñez, J.; Sulyok, M.; James, E. R.; Billingsley, P. F.; Natasha, K.; Manoj, A.; Murshedkar, T.; Gunasekera, A.; Eappen, A. G.; Li, T.; Stafford, R. E.; Li, M.; Felgner, P. L.; Seder, R. A.; Richie, T. L.; Sim, B. K. L.; Hoffman, S. L.; Kremsner, P. G. Sterile Protection against Human Malaria by Chemoattenuated PfSPZ Vaccine. *Nature* **2017**, (7642), 445–449.

(6) Dembélé, L.; Franetich, J.-F.; Lorthiois, A.; Gego, A.; Zeeman, A.-M.; Kocken, C. H. M.; Le Grand, R.; Dereuddre-Bosquet, N.; van Gemert, G.-J.; Sauerwein, R.; Vaillant, J.-C.; Hannoun, L.; Fuchter, M. J.; Diagana, T. T.; Malmquist, N. A.; Scherf, A.; Snounou, G.; Mazier, D. Persistence and Activation of Malaria Hypnozoites in Long-Term Primary Hepatocyte Cultures. *Nat. Med.* **2014**, *20* (3), 307–312.

(7) Liu, W.; Li, Y.; Shaw, K. S.; Learn, G. H.; Plenderleith, L. J.; Malenke, J. A.; Sundararaman, S. A.; Ramirez, M. A.; Crystal, P. A.; Smith, A. G.; Bibollet-Ruche, F.; Ayouba, A.; Locatelli, S.; Esteban, A.; Mouacha, F.; Guichet, E.; Butel, C.; Ahuka-Mundeke, S.; Inogwabini, B.-I.; Ndjango, J.-B. N.; Speede, S.; Sanz, C. M.; Morgan, D. B.; Gonder, M. K.; Kranzusch, P. J.; Walsh, P. D.; Georgiev, A. V.; Muller, M. N.; Piel, A. K.; Stewart, F. A.; Wilson, M. L.; Pusey, A. E.; Cui, L.; Wang, Z.; Färnert, A.; Sutherland, C. J.; Nolder, D.; Hart, J. A.; Hart, T. B.; Bertolani, P.; Gillis, A.; LeBreton, M.; Tafon, B.; Kiyang, J.; Djoko, C. F.; Schneider, B. S.; Wolfe, N. D.; Mpoudi-Ngole, E.; Delaporte, E.; Carter, R.; Culleton, R. L.; Shaw, G. M.; Rayner, J. C.; Peeters, M.;

Hahn, B. H.; Sharp, P. M. African Origin of the Malaria Parasite Plasmodium Vivax. *Nat. Commun.* **2014**, *5* (1), 3346.

(8) Collins, W. E.; Jeffery, G. M. Plasmodium Malariae: Parasite and Disease. *Clin. Microbiol. Rev.* **2007**, *20* (4), 579–592.

(9) Lee, K.-S.; Divis, P. C. S.; Zakaria, S. K.; Matusop, A.; Julin, R. A.; Conway, D. J.; Cox-Singh, J.; Singh, B. Plasmodium Knowlesi: Reservoir Hosts and Tracking the Emergence in Humans and Macaques. *PLoS Pathog.* **2011**, (4), e1002015.

(10) Kleinschmidt, I.; Mnzava, A. P.; Kafy, H. T.; Mbogo, C.; Bashir, A. I.; Bigoga, J.; Adechoubou, A.; Raghavendra, K.; Knox, T. B.; Malik, E. M.; Nkuni, Z. J.; Bayoh, N.; Ochomo, E.; Fondjo, E.; Kouambeng, C.; Awono-Ambene, H. P.; Etang, J.; Akogbeto, M.; Bhatt, R.; Swain, D. K.; Kinyari, T.; Njagi, K.; Muthami, L.; Subramaniam, K.; Bradley, J.; West, P.; Massougbodji, A.; Okê-Sopoh, M.; Hounto, A.; Elmardi, K.; Valecha, N.; Kamau, L.; Mathenge, E.; Donnelly, M. J. Design of a Study to Determine the Impact of Insecticide Resistance on Malaria Vector Control: A Multi-Country Investigation. *Malar. J.* **2015**, *14* (1), 282.

(11) Mueller, I.; Shakri, A. R.; Chitnis, C. E. Development of Vaccines for Plasmodium Vivax Malaria. *Vaccine* **2015**, *33* (52), 7489–7495.

(12) Lyke, K. E.; Ishizuka, A. S.; Berry, A. A.; Chakravarty, S.; DeZure, A.; Enama, M. E.; James, E. R.; Billingsley, P. F.; Gunasekera, A.; Manoj, A.; Li, M.; Ruben, A. J.; Li, T.; Eappen, A. G.; Stafford, R. E.; KC, N.; Murshedkar, T.; Mendoza, F. H.; Gordon, I. J.; Zephir, K. L.; Holman, L. A.; Plummer, S. H.; Hendel, C. S.; Novik, L.; Costner, P. J. M.; Saunders, J. G.; Berkowitz, N. M.; Flynn, B. J.; Nason, M. C.; Garver, L. S.; Laurens, M. B.; Plowe, C. V.; Richie, T. L.; Graham, B. S.; Roederer, M.; Sim, B. K. L.; Ledgerwood, J. E.; Hoffman, S. L.; Seder, R. A. Attenuated PfSPZ Vaccine Induces Strain-Transcending T Cells and Durable Protection against Heterologous Controlled Human Malaria Infection. *Proc. Natl. Acad. Sci.* **2017**, *114* (10), 2711–2716.

(13) Talisuna, A.; Grewal, P.; Rwakimari, J. B.; Mukasa, S.; Jagoe, G.; Banerji, J. Cost Is Killing Patients: Subsidising Effective Antimalarials. *Lancet* **2009**, *374* (9697), 1224–1226.

(14) Paloque, L.; Ramadani, A. P.; Mercereau-Puijalon, O.; Augereau, J.-M.; Benoit-Vical, F. Plasmodium Falciparum: Multifaceted Resistance to Artemisinins. *Malar. J.* **2016**, *15* (1), 149.

(15) Takala-Harrison, S.; Jacob, C. G.; Arze, C.; Cummings, M. P.; Silva, J. C.; Dondorp, A. M.; Fukuda, M. M.; Hien, T. T.; Mayxay, M.; Noedl, H.; Nosten, F.; Kyaw, M. P.;

Nhien, N. T. T.; Imwong, M.; Bethell, D.; Se, Y.; Lon, C.; Tyner, S. D.; Saunders, D. L.; Ariey, F.; Mercereau-Puijalon, O.; Menard, D.; Newton, P. N.; Khanthavong, M.; Hongvanthong, B.; Starzengruber, P.; Fuehrer, H.-P.; Swoboda, P.; Khan, W. A.; Phyo, A. P.; Nyunt, M. M.; Nyunt, M. H.; Brown, T. S.; Adams, M.; Pepin, C. S.; Bailey, J.; Tan, J. C.; Ferdig, M. T.; Clark, T. G.; Miotto, O.; MacInnis, B.; Kwiatkowski, D. P.; White, N. J.; Ringwald, P.; Plowe, C. V. Independent Emergence of Artemisinin Resistance Mutations Among Plasmodium Falciparum in Southeast Asia. *J. Infect. Dis.* **2015**, *211* (5), 670–679.

(16) Ariey, F.; Witkowski, B.; Amaratunga, C.; Beghain, J.; Langlois, A.-C.; Khim, N.; Kim, S.; Duru, V.; Bouchier, C.; Ma, L.; Lim, P.; Leang, R.; Duong, S.; Sreng, S.; Suon, S.; Chuor, C. M.; Bout, D. M.; Ménard, S.; Rogers, W. O.; Genton, B.; Fandeur, T.; Miotto, O.; Ringwald, P.; Le Bras, J.; Berry, A.; Barale, J.-C.; Fairhurst, R. M.; Benoit-Vical, F.; Mercereau-Puijalon, O.; Ménard, D. A Molecular Marker of Artemisinin-Resistant Plasmodium Falciparum Malaria. *Nature* **2014**, *505* (7481), 50–55.

(17) Bhatt, S.; Weiss, D. J.; Cameron, E.; Bisanzio, D.; Mappin, B.; Dalrymple, U.; Battle, K. E.; Moyes, C. L.; Henry, A.; Eckhoff, P. A.; Wenger, E. A.; Briët, O.; Penny, M. A.; Smith, T. A.; Bennett, A.; Yukich, J.; Eisele, T. P.; Griffin, J. T.; Fergus, C. A.; Lynch, M.; Lindgren, F.; Cohen, J. M.; Murray, C. L. J.; Smith, D. L.; Hay, S. I.; Cibulskis, R. E.; Gething, P. W. The Effect of Malaria Control on Plasmodium Falciparum in Africa between 2000 and 2015. *Nature* **2015**, *526* (7572), 207–211.

(18) World malaria report 2017 http://apps.who.int/iris/bitstream/handle/10665/259492/9789241565523eng.pdf;jsessionid=B834A47178EA220A9B1FCEA9D2FD9AA6?sequence=1 (accessed Aug 7, **2017**).

(19) Gething, P. W.; Patil, A. P.; Smith, D. L.; Guerra, C. A.; Elyazar, I. R.; Johnston, G. L.; Tatem, A. J.; Hay, S. I. A New World Malaria Map: Pla(1) Gething, P. W.; Patil, A. P.; Smith, D. L.; Guerra, C. A.; Elyazar, I. R.; Johnston, G. L.; Tatem, A. J.; Hay, S. I. A New World Malaria Map: Plasmodium Falciparum Endemicity in 2010. Malar. J. 2011, 10 (1), 378.Smodium Fal. *Malar. J.* **2011**, *10* (1), 378.

(20) Tatem, A. J.; Jia, P.; Ordanovich, D.; Falkner, M.; Huang, Z.; Howes, R.; Hay, S. I.; Gething, P. W.; Smith, D. L. The Geography of Imported Malaria to Non-Endemic Countries: A Meta-Analysis of Nationally Reported Statistics. *Lancet Infect. Dis.* **2017**, *17* (1), 98–107.

(21) Ohrt, C.; Sturrock, H. J.; Roberts, Kathryn W, J.; Gosling, R. D. Tackling Imported Malaria: An Elimination Endgame. *Am. J. Trop. Med. Hyg.* **2015**, *93* (1), 139–144.

(22) Askling, H.; Bruneel, F.; Burchard, G.; Castelli, F.; Chiodini, P.; G, M. P.; Lopez-Vélez, R.; Paul, M.; Petersen, E.; Popescu, C.; Ramharter, M.; Schlagenhauf, P. Management of Imported Malaria in Europe. *Malar. J.* **2012**, *11* (1), 328.

(23) Cotter, C.; Sturrock, H. J.; Hsiang, M. S.; Liu, J.; Phillips, A. A.; Hwang, J.; Gueye, C. S.; Fullman, N.; Gosling, R. D.; Feachem, R. G. The Changing Epidemiology of Malaria Elimination: New Strategies for New Challenges. *Lancet* **2013**, *382* (9895), 900–911.

(24) Where is Malaria Most Common? https://medellaup.com/wp-content/uploads/2017/11/where-is-malaria-most-common-1050x600.jpg (accessed Aug 7, **2018**).

(25) Magistrado, P. A.; Corey, V. C.; Lukens, A. K.; LaMonte, G.; Sasaki, E.; Meister, S.; Wree, M.; Winzeler, E.; Wirth, D. F. Plasmodium Falciparum Cyclic Amine Resistance Locus (PfCARL), a Resistance Mechanism for Two Distinct Compound Classes. *ACS Infect. Dis.* **2016**, (11), 816–826.

(26) 2016 World Malaria apps.who.int/iris/bitstream/10665/252038/1/9789241511711-eng.pdf?ua=1 (accessed Mar 16, **2017**).

(27) Dellicour, S.; Tatem, A. J.; Guerra, C. A.; Snow, R. W.; ter Kuile, F. O. Quantifying the Number of Pregnancies at Risk of Malaria in 2007: A Demographic Study. *PLoS Med.* **2010**, (1), e1000221.

(28) Hartman, T. K.; Rogerson, S. J.; Fischer, P. R. The Impact of Maternal Malaria on Newborns. *Ann. Trop. Paediatr.* **2010**, (4), 271–282.

(29) Baird, J. K. Resistance to Therapies for Infection by Plasmodium Vivax. *Clin. Microbiol. Rev.* **2009**, (3), 508–534.

(30) Njoroge, M.; Njuguna, N. M.; Mutai, P.; Ongarora, D. S. B.; Smith, P. W.; Chibale, K. Recent Approaches to Chemical Discovery and Development Against Malaria and the Neglected Tropical Diseases Human African Trypanosomiasis and Schistosomiasis. *Chem. Rev.* **2014**, (14), 11138–11163.

(31) Phyo, A. P.; Nkhoma, S.; Stepniewska, K.; Ashley, E. A.; Nair, S.; McGready, R.; Moo, C. L.; Al-Saai, S.; Dondorp, A. M.; Lwin, K. M.; Singhasivanon, P.; Day, N. P. J.; White, N. J.; Anderson, T. J. C.; Nosten, F. Emergence of Artemisinin-Resistant Malaria on the Western Border of Thailand: A Longitudinal Study. *Lancet.* **2012**, (7), 1960–1966.

(32) Bannister, L.; Mitchell, G. The Ins, Outs and Roundabouts of Malaria. *Trends Parasitol.* **2003**, *19* (5), 209–213.

(33) Silva, A. F.; Bastos, E. L.; Torres, M. D. T.; Costa-da-Silva, A. L.; Ioshino, R. S.; Capurro, M. L.; Alves, F. L.; Miranda, A.; de Freitas Fischer Vieira, R.; Oliveira, V. X. Antiplasmodium Activity Study of Angiotensin II via Ala Scan Analogs. *J. Pept. Sci.*

2014, (8), 640–648.

(34) Alano, P. Plasmodium Falciparum Gametocytes: Still Many Secrets of a Hidden Life. *Mol. Microbiol.* **2007**, *66* (2), 291–302.

(35) Wirth, D. F. The Parasite Genome: Biological Revelations. *Nature* **2002**, (6906), 495–496.

(36) Plasmodium parasite life cycle http://www.malwest.gr/Portals/0/EID_lec17_slide8-large%5B1%5D.jpg (accessed Aug 7, **2018**).

(37) Ashley, E. A. et al. Spread of Artemisinin Resistance in Plasmodium Falciparum Malaria. *N. Engl. J. Med.* **2014**, *371* (5), 411–423.

(38) O'Neill, P. M.; Barton, V. E.; Ward, S. A. The Molecular Mechanism of Action of Artemisinin—The Debate Continues. *Molecules* **2010**, *15* (3), 1705–1721.

(39) Malaria prophylaxis: https://en.wikipedia.org/wiki/Malaria_prophylaxis (accessed Mar 30, **2017**).

(40) Jacquerioz, F. A.; Croft, A. M. Drugs for Preventing Malaria in Travellers. In *Cochrane Database of Systematic Reviews*; Jacquerioz, F. A., Ed.; John Wiley & Sons, Ltd: Chichester, UK, **2009**.

(41) Dondorp, A. M.; Yeung, S.; White, L.; Nguon, C.; Day, N. P. J.; Socheat, D.; von Seidlein, L. Artemisinin Resistance: Current Status and Scenarios for Containment. *Nat. Rev. Microbiol.* **2010**, (8), 272–280.

(42) Dihydroartemisinin https://pubchem.ncbi.nlm.nih.gov/compound/dihydroartemisinin-#section=Top (accessed Mar 17, **2017**).

(43) Jiang, J. B.; Guo, X. B.; Li, G. Q. Antimalarial Studies on Qinghaosu. *Chin. Med. J. (Engl).* **1979**, (12), 811–816.

(44) Keiser, Jennifer; Utzinger, J. Antimalarials in the Treatment of Schistosomiasis. *Curr. Pharm. Des.* **2012**, (18), 3531–3538.

(45) 350 million treatments of Coartem® Dispersible delivered to over 50 countries http://www.mmv.org/achievements-challenges/achievements/coartem-d (accessed Mar 26, **2017**).

(46) Anthony, M. P.; Burrows, J. N.; Duparc, S.; JMoehrle, J.; Wells, T. N. The Global Pipeline of New Medicines for the Control and Elimination of Malaria. *Malar. J.* **2012**, *11* (1), 316.

(47) Emerging Infectious Diseases-Malaria https://wwwnc.cdc.gov/eid/spotlight/malaria (accessed Jun 4, **2018**).

(48) Sirima, S. B.; Cotte, A. H.; Konaté, A.; Moran, A. C.; Asamoa, K.; Bougouma, E. C.;

Diarra, A.; Ouédraogo, A.; Parise, M. E.; Newman, R. D. Malaria Prevention during Pregnancy: Assessing the Disease Burden One Year after Implementing a Program of Intermittent Preventive Treatment in Koup??La District, Burkina Faso. *Am. J. Trop. Med. Hyg.* **2006**, *75* (2), 205–211.

(49) Kremsner, P. G.; Krishna, S. Antimalarial Combinations. *Lancet* **2004**, *364* (9430), 285–294.

(50) Minta, A. A.; Tan, K. R.; Mace, K. E.; Arguin, P. M. Acute Malaria Infection after Atovaquone–proguanil Prophylaxis. *J. Travel Med.* **2017**, *24* (2).

(51) Galappaththy, G. N.; Tharyan, P.; Kirubakaran, R. Primaquine for Preventing Relapse in People with Plasmodium Vivax Malaria Treated with Chloroquine. *Cochrane Database Syst. Rev.* **2013**.

(52) Ashley, E. A.; Recht, J.; White, N. J. Primaquine: The Risks and the Benefits. *Malar. J.* **2014**, *13* (1), 418.

(53) Motshoge, T.; Ababio, G.; Aleksenko, L.; Souda, S.; Muthoga, C. W.; Mutukwa, N.; Tawe, L.; Ramatlho, P.; Gabaitiri, L.; Chihanga, S.; Mosweunyane, T.; Hamda, S.; Moakofhi, K.; Ntebela, D.; Peloewetse, E.; Mazhani, L.; Pernica, J. M.; Read, J.; Quaye, I. K.; Paganotti, G. M. Prevalence of G6PD Deficiency and Associated Haematological Parameters in Children from Botswana. *Infect. Genet. Evol.* **2018**, *63*, 73–78.

(54) Chu, C. S.; Bancone, G.; Moore, K. A.; Win, H. H.; Thitipanawan, N.; Po, C.; Chowwiwat, N.; Raksapraidee, R.; Wilairisak, P.; Phyo, A. P.; Keereecharoen, L.; Proux, S.; Charunwatthana, P.; Nosten, F.; White, N. J. Haemolysis in G6PD Heterozygous Females Treated with Primaquine for Plasmodium Vivax Malaria: A Nested Cohort in a Trial of Radical Curative Regimens. *PLOS Med.* **2017**, *14* (2), e1002224.

(55) Wellems, T. E.; Plowe, C. V. Chloroquine-Resistant Malaria. *J. Infect. Dis.* **2001**, *184* (6), 770–776.

(56) Sidhu, A. B. S.; Verdier-Pinard, D.; Fidock, D. A. Chloroquine Resistance in Plasmodium Falciparum Malaria Parasites Conferred by Pfcrt Mutations. *Science* (80) **2002**, *298* (5591), 210–213.

(57) Rea, E.; Holder, A. A.; Tewari, R. Plasmodium Peekaboo: PK4 Mediates Parasite Latency. *Cell Host Microbe* **2017**, *22* (6), 724–725.

(58) T. W. A. R. N. Clinical Determinants of Early Parasitological Response to ACTs in African Patients with Uncomplicated Falciparum Malaria: A Literature Review and Meta-Analysis of Individual Patient Data. *BMC Med.* **2015**, *13* (1), 212.

(59) Ashley, E. A. et al. Spread of Artemisinin Resistance in Plasmodium Falciparum Malaria. *N. Engl. J. Med.* **2014**, (5), 411–423.

(60) Wiegelmann, W.; Wildmeister, W.; Horster, F. A.; Solbach, H. G. The Effect of Dose on the Antimalarial Efficacy of Artemether-lumefantrine: A Systematic Review and Pooled Analysis of Individual Patient Data. *Lancet Infect. Dis.* **2015**, (6), 692–702.

(61) Van Thang, N.; Binh, T. Q.; Van Nam, N.; Kager, P. A.; de Vries, P. J.; Long, H. P.; Giao, P. T. Artemisinin for Treatment of Uncomplicated Falciparum Malaria: Is There a Place for Monotherapy? *Am. J. Trop. Med. Hyg.* **2001**, *65* (6), 690–695.

(62) Gbotosho, G. O.; Akinola, O. A Localised Threat to an Excellent Antimalarial Drug. *Lancet Infect. Dis.* **2015**, (6), 623–624.

(63) Ndakala, A. J.; Gessner, R. K.; Gitari, P. W.; October, N.; White, K. L.; Hudson, A.; Fakorede, F.; Shackleford, D. M.; Kaiser, M.; Yeates, C.; Charman, S. A.; Chibale, K. Antimalarial Pyrido[1,2- a]Benzimidazoles. *J. Med. Chem.* **2011**, (54), 4581–4589.

(64) Mbengue, A.; Bhattacharjee, S.; Pandharkar, T.; Liu, H.; Estiu, G.; Stahelin, R. V.; Rizk, S. S.; Njimoh, D. L.; Ryan, Y.; Chotivanich, K.; Nguon, C.; Ghorbal, M.; Lopez-Rubio, J.-J.; Pfrender, M.; Emrich, S.; Mohandas, N.; Dondorp, A.; Wiest, O.; Haldar, K. A Molecular Mechanism of Artemisinin Resistance in Plasmodium Falciparum Malaria. *Nature* **2015**, *520* (7549), 683–687.

(65) W. H. O. World Malaria Reports 2010 - 2017 http://www.who.int/malaria/publications/world_malaria_report/en/ (accessed Nov 13, **2018**).

(66) Ridley, R. G. Medical Need, Scientific Opportunity and the Drive for Antimalarial Drugs. *Nature* **2002**, (6872), 686–693.

(67) 14 compounds in preclinical and clinical development https://www.mmv.org/our-impact/achievements/14-compounds-preclinical-and-clinical-development (accessed Aug 7, **2018**).

(68) White, M.; Verity, R.; Griffin, J.; Asante, K.; Owusu-Agyei, S.; Greenwood, B.; Drakeley, C.; Gesase, S.; Lusingu, J.; Ansong, D.; Adjei, S.; Agbenyega, T.; Ogutu, B.; Otieno, L.; Otieno, W.; Agnandji, S. T.; Lell, B.; Kremsner, P.; Hoffman, I.; Martinson, F.; Kamthunzu, P.; Tinto, H.; Valea, I.; Sorgho, H.; Oneko, M.; Otieno, K.; Hamel, M. J.; Salim, N.; Mtoro, A.; Abdulla, S.; Aide, P.; Sacarlal, J.; Aponte, J.; Njuguna, P.; Marsh, K.; Bejon, P.; Riley, E.; Ghani, A. Immunogenicity of the RTS,S/AS01 Malaria Vaccine and Implications for Duration of Vaccine Efficacy: Secondary Analysis of Data from a Phase 3 Randomised Controlled Trial. *Lancet Infect. Dis.* **2015**, (12), 1450–1458.

(69) Macintyre, F.; Baker, M.; Möhrle, J. J. Antimalarial Activity of Artefenomel (OZ439),

a Novel Synthetic Antimalarial Endoperoxide, in Patients with Plasmodium Falciparum and Plasmodium Vivax Malaria : An Open-Label Phase 2 Trial. *Lancet Infect. Dis.* **2016**, *16*, 61–69.

(70) Leong, F. J.; Li, R.; Jain, J. P.; Lefèvre, G.; Magnusson, B.; Diagana, T. T.; Pertel, P. A First-in-Human Randomized, Double-Blind, Placebo-Controlled, Single- and Multiple-Ascending Oral Dose Study of Novel Antimalarial Spiroindolone KAE609 (Cipargamin) To Assess Its Safety, Tolerability, and Pharmacokinetics in Healthy Adult Volunteers. *Antimicrob. Agents Chemother.* **2014**, *58* (10), 6209–6214.

(71) Kuhen, K. L.; Chatterjee, A. K.; Rottmann, M.; Gagaring, K.; Borboa, R.; Buenviaje, J.; Chen, Z.; Francek, C.; Wu, T.; Nagle, A.; Barnes, S. W.; Plouffe, D.; Lee, M. C. S.; Fidock, D. A.; Graumans, W.; van de Vegte-Bolmer, M.; van Gemert, G. J.; Wirjanata, G.; Sebayang, B.; Marfurt, J.; Russell, B.; Suwanarusk, R.; Price, R. N.; Nosten, F.; Tungtaeng, A.; Gettayacamin, M.; Sattabongkot, J.; Taylor, J.; Walker, J. R.; Tully, D.; Patra, K. P.; Flannery, E. L.; Vinetz, J. M.; Renia, L.; Sauerwein, R. W.; Winzeler, E. A.; Glynne, R. J.; Diagana, T. T. KAF156 Is an Antimalarial Clinical Candidate with Potential for Use in Prophylaxis, Treatment, and Prevention of Disease Transmission. *Antimicrob. Agents Chemother.* **2014**, *58* (9), 5060–5067.

(72) McCarthy, J. S.; Lotharius, J.; Rückle, T.; Chalon, S.; Phillips, M. A.; Elliott, S.; Sekuloski, S.; Griffin, P.; Ng, C. L.; Fidock, D. A.; Marquart, L.; Williams, N. S.; Gobeau, N.; Bebrevska, L.; Rosario, M.; Marsh, K.; Möhrle, J. J. Safety, Tolerability, Pharmacokinetics, and Activity of the Novel Long-Acting Antimalarial DSM265: A Two-Part First-in-Human Phase 1a/1b Randomised Study. *Lancet Infect. Dis.* **2017**, *17* (6), 626–635.

(73) Mzayek, F.; Deng, H.; Mather, F. J.; Wasilevich, E. C.; Liu, H.; Hadi, C. M.; Chansolme, D. H.; Murphy, H. A.; Melek, B. H.; Tenaglia, A. N.; Mushatt, D. M.; Dreisbach, A. W.; Lertora, J. J. L.; Krogstad, D. J. Randomized Dose-Ranging Controlled Trial of AQ-13, a Candidate Antimalarial, and Chloroquine in Healthy Volunteers. *PLoS Clin. Trials* **2007**, *2* (1), e6.

(74) Younis, Y.; Douelle, F.; Feng, T.-S.; Cabrera, D. G.; Manach, C. Le; Nchinda, A. T.; Duffy, S.; White, K. L.; Shackleford, D. M.; Morizzi, J.; Mannila, J.; Katneni, K.; Bhamidipati, R.; Zabiulla, K. M.; Joseph, J. T.; Bashyam, S.; Waterson, D.; Witty, M. J.; Hardick, D.; Wittlin, S.; Avery, V.; Charman, S. A.; Chibale, K. 3,5-Diaryl-2-Aminopyridines as a Novel Class of Orally Active Antimalarials Demonstrating Single Dose Cure in Mice and Clinical Candidate Potential. *J. Med. Chem.* **2012**, *55* (7), 3479–

3487.

(75) White NJ, Pukrittayakamee S, Phyo AP, Rueangweerayut R, Nosten F, Jittamala P, Jeeyapant A, Jain JP, Lefèvre G, L. R.; Magnusson B, Diagana TT, L. F. Spiroindolone KAE609 for Falciparum and Vivax Malaria. *N. Engl. J. Med.* **2014**, (5), 403–410.

(76) Okombo, J.; Chibale, K. Recent Updates in the Discovery and Development of Novel Antimalarial Drug Candidates. *Medchemcomm* **2018**, *9* (3), 437–453.

(77) Spillman, N. J.; Allen, R. J. W.; McNamara, C. W.; Yeung, B. K. S.; Winzeler, E. A.; Diagana, T. T.; Kirk, K. Na+ Regulation in the Malaria Parasite Plasmodium Falciparum Involves the Cation ATPase PfATP4 and Is a Target of the Spiroindolone Antimalarials. *Cell Host Microbe* **2013**, *13* (2), 227–237.

(78) Le Manach, C.; Nchinda, A. T.; Paquet, T.; Gonzàlez Cabrera, D.; Younis, Y.; Han, Z.; Bashyam, S.; Zabiulla, M.; Taylor, D.; Lawrence, N.; White, K. L.; Charman, S. A.; Waterson, D.; Witty, M. J.; Wittlin, S.; Botha, M. E.; Nondaba, S. H.; Reader, J.; Birkholtz, L.-M.; Jiménez-Díaz, M. B.; Martínez, M. S.; Ferrer, S.; Angulo-Barturen, I.; Meister, S.; Antonova-Koch, Y.; Winzeler, E. A.; Street, L. J.; Chibale, K. Identification of a Potential Antimalarial Drug Candidate from a Series of 2-Aminopyrazines by Optimization of Aqueous Solubility and Potency across the Parasite Life Cycle. *J. Med. Chem.* **2016**, *59* (21), 9890–9905.

(79) Jiménez-Díaz, M. B.; Ebert, D.; Salinas, Y.; Pradhan, A.; Lehane, A. M.; Myrand-Lapierre, M.-E.; O'Loughlin, K. G.; Shackleford, D. M.; Justino de Almeida, M.; Carrillo, A. K.; Clark, J. A.; Dennis, A. S. M.; Diep, J.; Deng, X.; Duffy, S.; Endsley, A. N.; Fedewa, G.; Guiguemde, W. A.; Gómez, M. G.; Holbrook, G.; Horst, J.; Kim, C. C.; Liu, J.; Lee, M. C. S.; Matheny, A.; Martínez, M. S.; Miller, G.; Rodríguez-Alejandre, A.; Sanz, L.; Sigal, M.; Spillman, N. J.; Stein, P. D.; Wang, Z.; Zhu, F.; Waterson, D.; Knapp, S.; Shelat, A.; Avery, V. M.; Fidock, D. A.; Gamo, F.-J.; Charman, S. A.; Mirsalis, J. C.; Ma, H.; Ferrer, S.; Kirk, K.; Angulo-Barturen, I.; Kyle, D. E.; DeRisi, J. L.; Floyd, D. M.; Guy, R. K. (+)-SJ733, a Clinical Candidate for Malaria That Acts through ATP4 to Induce Rapid Host-Mediated Clearance of Plasmodium. *Proc. Natl. Acad. Sci.* **2014**, *111* (50), E5455–E5462.

(80) Abbat, S.; Jain, V.; Bharatam, P. V. Origins of the Specificity of Inhibitor P218 toward Wild-Type and Mutant Pf DHFR: A Molecular Dynamics Analysis. *J. Biomol. Struct. Dyn.* **2015**, *33* (9), 1913–1928.

(81) Shafiq, N.; Rajagopalan, S.; Kushwaha, H. N.; Mittal, N.; Chandurkar, N.; Bhalla, A.; Kaur, S.; Pandhi, P.; Puri, G. D.; Achuthan, S.; Pareek, A.; Singh, S. K.; Srivastava, J.

S.; Gaur, S. P. S.; Malhotra, S. Single Ascending Dose Safety and Pharmacokinetics of CDRI-97/78: First-in-Human Study of a Novel Antimalarial Drug. *Malar. Res. Treat.* **2014**, *2014*, 1–10.

(82) MMV-supported projects https://www.mmv.org/research-development/mmv-supported-projects (accessed Aug 7, **2018**).

(83) Hotez, P.; Molyneux, D.; Fenwick, A.; Kumaresan, J.; Sachs, S.; Sachs, J.; Savioli, L. Control of Neglected Tropical Diseases. *N. Engl. J. Med.* **2007**, (10), 1018–1027.

(84) Colley, D. G.; Bustinduy, A. L.; Secor, W. E.; King, C. H. Human Schistosomiasis. *Lancet* **2014**, *383* (9936), 2253–2264.

(85) Blair, D.; Davis, G.; Wu, B. Evolutionary Relationships between Trematodes and Snails Emphasizing Schistosomes and Paragonimids. *Parasitology* **2001**, *123* (07).

(86) Lockyer, A. E.; Jones, C. S.; Noble, L. R.; Rollinson, D. Trematodes and Snails: An Intimate Association. *Can. J. Zool.* **2004**, *82* (2), 251–269.

(87) Allan, F.; Dunn, A. M.; Emery, A. M.; Stothard, J. R.; Johnston, D. A.; Kane, R. A.; Khamis, A. N.; Mohammed, K. A.; Rollinson, D. Use of Sentinel Snails for the Detection of Schistosoma Haematobium Transmission on Zanzibar and Observations on Transmission Patterns. *Acta Trop.* **2013**, *128* (2), 234–240.

(88) Sanogo, B.; Yuan, D.; Zeng, X.; Zhang, Y.; Wu, Z. Diversity and Compatibility of Human Schistosomes and Their Intermediate Snail Hosts. *Trends Parasitol.* **2018**, *34* (6), 493–510.

(89) Naghavi, M. et al. Global, Regional, and National Age-Sex Specific Mortality for 264 Causes of Death, 1980–2016: A Systematic Analysis for the Global Burden of Disease Study 2016. *Lancet* **2017**, *390* (10100), 1151–1210.

(90) Schistosomiasis: WHO reports substantial treatment progress for school-age children http://www.who.int/neglected_diseases/news/WHO_schistosomiasis_reports_substantial_treatment_progress_sac/en/ (accessed Jun 29, **2018**).

(91) Current global distribution of schistosomiasis, stratified according to country-specific prevalence estimates. https://www.researchgate.net/Current-global-distribution-of-schistosomiasis-stratified-according-to-country-specific_fig2_46218355 (accessed Aug 2, **2018**).

(92) Steinmann, P.; Keiser, J.; Bos, R.; Tanner, M.; Utzinger, J. Schistosomiasis and Water Resources Development: Systematic Review, Meta-Analysis, and Estimates of People at Risk. *Lancet Infect. Dis.* **2006**, (7), 411–425.

(93) Schistosomiasis http://www.who.int/mediacentre/factsheets/fs115/en/ (accessed Mar

24, **2017**).

(94) Giannelli, A.; Cantacessi, C.; Colella, V.; Dantas-Torres, F.; Otranto, D. Gastropod-Borne Helminths: A Look at the Snail–Parasite Interplay. *Trends Parasitol.* **2016**, *32* (3), 255–264.

(95) Pila, E. A.; Li, H.; Hambrook, J. R.; Wu, X.; Hanington, P. C. Schistosomiasis from a Snail's Perspective: Advances in Snail Immunity. *Trends Parasitol.* **2017**, *33* (11), 845–857.

(96) Gryseels, B.; Polman, K. Human Schistosomiasis. *Lancet* **2006**, *368* (9541), 1106–1118.

(97) Schistosoma spp. life cycle https://web.stanford.edu/group/parasites/ParaSites2003/Schistosomiasis/cycle.htm (accessed Aug 7, **2018**).

(98) Schistosoma http://parasite.org.au/para-site/text/schistosoma-text.html (accessed Apr 5, 2017).

(99) Cioli, D. Chemotherapy of Schistosomiasis: An Update. *Parasitol. Today* **1998**, (10), 418–422.

(100) Cioli, D.; Pica-Mattoccia, L.; Archer, S. Antischistosomal Drugs: Past, Present … and Future? *Pharmacol. Ther.* **1995**, (1), 35–85.

(101) Fenwick, A.; Savioli, L.; Engels, D.; Robert Bergquist, N.; Todd, M. H. Drugs for the Control of Parasitic Diseases: Current Status and Development in Schistosomiasis. *Trends Parasitol.* **2003**, (11), 509–515.

(102) Xiao, S. H.; Keiser, J.; Chen, M. G.; Tanner, M.; Utzinger, J. Research and Development of Antischistosomal Drugs in the People's Republic of China. A 60-Year Review. *Adv. Parasitol.* **2010**, *73* (C), 231–295.

(103) Meyer, T.; Sekljic, H.; Fuchs, S.; Bothe, H.; Schollmeyer, D.; Miculka, C. Taste, A New Incentive to Switch to (R)-Praziquantel in Schistosomiasis Treatment. *PLoS Negl. Trop. Dis.* **2009**, (1), e357.

(104) Caffrey, C. R. Chemotherapy of Schistosomiasis: Present and Future. *Curr. Opin. Chem. Biol.* **2007**, (*11*), 433–439.

(105) Cioli, D.; Botros, S. S.; Wheatcroft-Francklow, K.; Mbaye, A.; Southgate, V.; Tchuenté, L. A. T.; Pica-Mattoccia, L.; Troiani, A. R.; Seif El-Din, S. H.; Sabra, A. N. A.; Albin, J.; Engels, D.; Doenhoff, M. J. Determination of ED50 Values for Praziquantel in Praziquantel-Resistant and -Susceptible Schistosoma Mansoni Isolates. *Int. J. Parasitol.* **2004**, (8), 979–987.

(106) Wang, X.; Dong, Y.; Wittlin, S.; Charman, S. A.; Chiu, F. C. K.; Chollet, J.; Katneni, K.; Mannila, J.; Morizzi, J.; Ryan, E.; Scheurer, C.; Steuten, J.; Santo Tomas, J.; Snyder,

C.; Vennerstrom, J. L. Comparative Antimalarial Activities and ADME Profiles of Ozonides (1,2,4-Trioxolanes) OZ277, OZ439, and Their 1,2-Dioxolane, 1,2,4-Trioxane, and 1,2,4,5-Tetraoxane Isosteres. *J. Med. Chem.* **2013**, *56* (6), 2547–2555.

(107) Siqueira, L. da P.; Fontes, D. A. F.; Aguilera, C. S. B.; Timóteo, T. R. R.; Ângelos, M. A.; Silva, L. C. P. B. B.; de Melo, C. G.; Rolim, L. A.; da Silva, R. M. F.; Neto, P. J. R. Schistosomiasis: Drugs Used and Treatment Strategies. *Acta Trop.* **2017**, *176*, 179–187.

(108) Njoroge, M.; Njuguna, N. M.; Mutai, P.; Ongarora, D. S. B.; Smith, P. W.; Chibale, K. Recent Approaches to Chemical Discovery and Development Against Malaria and the Neglected Tropical Diseases Human African Trypanosomiasis and Schistosomiasis. *Chem. Rev.* **2014**, (22), 11138–11163.

(109) Meuldermans, W.; Hendrickx, J.; Lauwers, W.; Hurkmans, R.; Swysen, E.; Heykants, J. Excretion and Biotransformation of Astemizole in Rats, Guinea-Pigs, Dogs, and Man. *Drug Dev. Res.* **1986**, (1–4), 37–51.

(110) Alexis Nzila, Z. M.; Chibale, &. K. Drug Repositioning in the Treatment of Malaria and TB. *Futur. Med. Chem* **2011**, *3* (11), 1413–1426.

(111) Okombo, J.; Singh, K.; Mayoka, G.; Ndubi, F.; Barnard, L.; Njogu, P. M.; Njoroge, M.; Gibhard, L.; Brunschwig, C.; Vargas, M.; Keiser, J.; Egan, T. J.; Chibale, K. Antischistosomal Activity of Pyrido[1,2- a]Benzimidazole Derivatives and Correlation with Inhibition of β-Hematin Formation. *ACS Infect. Dis.* **2017**, *3* (6), 411–420.

(112) Delcroix, M.; Sajid, M.; Caffrey, C. R.; Lim, K.-C.; Dvořák, J.; Hsieh, I.; Bahgat, M.; Dissous, C.; McKerrow, J. H. A Multienzyme Network Functions in Intestinal Protein Digestion by a Platyhelminth Parasite. *J. Biol. Chem.* **2006**, *281* (51), 39316–39329.

(113) Chen, M. M.; Shi, L.; Sullivan, D. J. Haemoproteus and Schistosoma Synthesize Heme Polymers Similar to Plasmodium Hemozoin and β-Hematin. *Mol. Biochem. Parasitol.* **2001**, *113* (1), 1–8.

(114) Oliveira, M. F. M. A.; Torres, C. R.; Oliveira, P. L.; Rumjanek, F. D.; Souza, W. De. Haemozoin in Schistosoma Mansoni. *Mol. Biochem. Parasitol.* **2000**, *111*, 217–221.

(115) Ingram, K.; Ellis, W.; Keiser, J. Antischistosomal Activities of Mefloquine-Related Arylmethanols. *Antimicrob. Agents Chemother.* **2012**, *56* (6), 3207–3215.

(116) Chen, D. J., et al. Experimental Studies on Antischistosomal Activity of Qinghaosu. *Chin. Med. J. (Engl).* **1980**, (60), 422–425.

(117) Le, W.; You, J. Yang, Y.; Mei, J.; Guo, H.; Yang, H. Zang, C. Studies on the Efficacy of Artemether in Experimental Schistosomiasis. *Acta Pharm. Sin* **1982**, (17), 187–193.

(118) Xiao, S.; Keiser, J.; Chollet, J.; Utzinger, J.; Dong, Y.; Endriss, Y.; Vennerstrom, J.;

Tanner, M. In Vitro and In Vivo Activities of Synthetic Trioxolanes against Major Human Schistosome Species. *Antimicrob. Agents Chemother.* **2007**, *51* (4), 1440–1445.

(119) Pradines, V.; Portela, J.; Boissier, J.; Coslédan, F.; Meunier, B.; Robert, A. Trioxaquine PA1259 Alkylates Heme in the Blood-Feeding Parasite Schistosoma Mansoni. *Antimicrob. Agents Chemother.* **2011**, *55* (5), 2403–2405.

(120) Cosledan, F.; Fraisse, L.; Pellet, A.; Guillou, F.; Mordmuller, B.; Kremsner, P. G.; Moreno, A.; Mazier, D.; Maffrand, J.-P.; Meunier, B. Selection of a Trioxaquine as an Antimalarial Drug Candidate. *Proc. Natl. Acad. Sci.* **2008**, *105* (45), 17579–17584.

(121) Savjani, K. T.; Gajjar, A. K.; Savjani, J. K. Drug Solubility: Importance and Enhancement Techniques. *ISRN Pharm.* **2012**, (10), 1–10.

(122) Hamada, Y. Recent Progress in Prodrug Design Strategies Based on Generally Applicable Modifications. *Bioorg. Med. Chem. Lett.* **2017**, *27* (8), 1627–1632.

(123) Wexler, D. S.; Gao, L.; Anderson, F.; Ow, A.; Nadasdi, L.; McAlorum, A.; Urfer, R.; Huang, S.-G. Linking Solubility and Permeability Assays for Maximum Throughput and Reproducibility. *J. Biomol. Screen.* **2005**, *10* (4), 383–390.

(124) Censi, R.; Di Martino, P. Polymorph Impact on the Bioavailability and Stability of Poorly Soluble Drugs. *Molecules* **2015**, *20* (10), 18759–18776.

(125) Williams, H. D.; Trevaskis, N. L.; Charman, S. A.; Shanker, R. M.; Charman, W. N.; Pouton, C. W.; Porter, C. J. H. Strategies to Address Low Drug Solubility in Discovery and Development. *Pharmacol. Rev. Pharmacol Rev* **2013**, *65* (January), 315–499.

(126) Khadka, P.; Ro, J.; Kim, H.; Kim, I.; Kim, J. T.; Kim, H.; Cho, J. M.; Yun, G.; Lee, J. Pharmaceutical Particle Technologies: An Approach to Improve Drug Solubility, Dissolution and Bioavailability. *Asian J. Pharm. Sci.* **2014**, *9* (6), 304–316.

(127) Ishikawa, M.; Hashimoto, Y. Improvement in Aqueous Solubility in Small Molecule Drug Discovery Programs by Disruption of Molecular Planarity and Symmetry. *J. Med. Chem.* **2011**, (6), 1539–1554.

(128) Rutkowska, E.; Pajak, K.; Jóźwiak, K. Lipophilicity--Methods of Determination and Its Role in Medicinal Chemistry. *Acta Pol. Pharm.* **2013**, (1), 3–18.

(129) Palucki, M.; Higgins, J.; Kwong, E.; Templeton, A. Strategies at the Interface of Drug Discovery and Development: Early Optimization of the Solid State Phase and Preclinical Toxicology Formulation for Potential Drug Candidates. *J. Med. Chem.* **2010**, (53), 5897–5905.

(130) Low, Y. W. (Ivan); Blasco, F.; Vachaspati, P. Optimised Method to Estimate Octanol Water Distribution Coefficient (LogD) in a High Throughput Format. *Eur. J. Pharm.*

Sci. **2016**, (12,) 110–116.

(131) Lovering, F.; Bikker, J.; Humblet, C. Escape from Flatland: Increasing Saturation as an Approach to Improving Clinical Success. *J. Med. Chem.* **2009**, (52), 6752–6756.

(132) Kasuga, J.; Ishikawa, M.; Yonehara, M.; Makishima, M.; Hashimoto, Y.; Miyachi, H. Improvement of Water-Solubility of Biarylcarboxylic Acid Peroxisome Proliferator-Activated Receptor (PPAR) δ-Selective Partial Agonists by Disruption of Molecular Planarity/Symmetry. *Bioorg. Med. Chem.* **2010**, (20), 7164–7173.

(133) Li, Y.; Zhu, Y.-M.; Jiang, H.-J.; Pan, J.-P.; Wu, G.-S.; Wu, J.-M.; Shi, Y.-L.; Yang, J.-D.; Wu, B.-A. Synthesis and Antimalarial Activity of Artemisinin Derivatives Containing an Amino Group. *J. Med. Chem.* **2000**, *43* (8), 1635–1640.

(134) Serajuddin, A. T. M. Salt Formation to Improve Drug Solubility. *Adv. Drug Deliv. Rev.* **2007**, *59* (7), 603–616.

(135) Jornada, D.; dos Santos Fernandes, G.; Chiba, D.; de Melo, T.; dos Santos, J.; Chung, M. The Prodrug Approach: A Successful Tool for Improving Drug Solubility. *Molecules* **2015**, *21* (1), 42.

(136) Zimmermann, S. C.; Tichý, T.; Vávra, J.; Dash, R. P.; Slusher, C. E.; Gadiano, A. J.; Wu, Y.; Jančařík, A.; Tenora, L.; Monincová, L.; Prchalová, E.; Riggins, G. J.; Majer, P.; Slusher, B. S.; Rais, R. N-Substituted Prodrugs of Mebendazole Provide Improved Aqueous Solubility and Oral Bioavailability in Mice and Dogs. *J. Med. Chem.* **2018**, *61* (9), 3918–3929.

(137) Lin, J. H.; Lu, A. Y. H. Role of Pharmacokinetics and Metabolism in Drug Discovery and Development. *Pharmacol. Rev.* **1997**, (4), 403–449.

(138) *Pharmacokinetics and Metabolism in Drug Design*; Smith, D. A., Allerton, C., Kalgutkar, A. S., van de Waterbeemd, H., Walker, D. K., Eds.; Wiley-VCH Verlag GmbH & Co. KGaA: Weinheim, Germany, 2012.

(139) Pieroni, M.; Tipparaju, S. K.; Lun, S.; Song, Y.; Sturm, A. W.; Bishai, W. R.; Kozikowski, A. P. Pyrido[1,2- a]Benzimidazole-Based Agents Active Against Tuberculosis (TB), Multidrug-Resistant (MDR) TB and Extensively Drug-Resistant (XDR) TB. *ChemMedChem* **2011**, *6* (2), 334–342.

(140) Singh, K.; Okombo, J.; Brunschwig, C.; Ndubi, F.; Barnard, L.; Wilkinson, C.; Njogu, P. M.; Njoroge, M.; Laing, L.; Machado, M.; Prudêncio, M.; Reader, J.; Botha, M.; Nondaba, S.; Birkholtz, L.-M.; Lauterbach, S.; Churchyard, A.; Coetzer, T. L.; Burrows, J. N.; Yeates, C.; Denti, P.; Wiesner, L.; Egan, T. J.; Wittlin, S.; Chibale, K. Antimalarial Pyrido[1,2- a]Benzimidazoles: Lead Optimization, Parasite Life Cycle Stage Profile,

Mechanistic Evaluation, Killing Kinetics, and in Vivo Oral Efficacy in a Mouse Model. *J. Med. Chem.* **2017**, (4), 1432–1448.

(141) Takeshita, H.; Watanabe, J.; Kimura, Y.; Kawakami, K.; Takahashi, H.; Takemura, M.; Kitamura, A.; Someya, K.; Nakajima, R. Novel Pyridobenzimidazole Derivatives Exhibiting Antifungal Activity by the Inhibition of β-1,6-Glucan Synthesis. *Bioorg. Med. Chem. Lett.* **2010**, (13), 3893–3896.

(142) Kotovskaya, S. K.; Baskakova, Z. M.; Charushin, V. N.; Chupakhin, O. N.; Belanov, E. F.; Bormotov, N. I.; Balakhnin, S. M.; Serova, O. A. Synthesis and Antiviral Activity of Fluorinated Pyrido[1,2-a]Benzimidazoles. *Pharm. Chem. J.* **2005**, (11), 574–578.

(143) Jiang, Z. D.; DuPont, H. L. Rifaximin: In Vitro and in Vivo Antibacterial Activity – A Review. *Chemotherapy* **2005**, *51* (1), 67–72.

2. SYNTHESIS AND CHARACTERIZATION OF TARGET COMPOUNDS

2.1 Introduction

Here, the design, synthesis, and spectroscopic and physical characterization of the synthesized PBI analogues are discussed. The expansion and exploration of structure-activity relationship (SAR) and structure-property relationship (SPR) studies on this series of compounds involved carrying out chemical modifications around the PBI core scaffold. Substituent groups with molecular features likely to improve solubility as well as drug metabolism and pharmacokinetic (DMPK) properties of the target analogues were incorporated.

In the preliminary stage, the design of SAR/SPR studies involved incorporating α-methylbenzylamine moieties into the PBI motif. The incorporation of these features was postulated to disrupt molecular planarity, introduce saturation, and enhance hydrogen bonding properties. Recently, Cui *et al.* reported an anticancer medicinal chemistry optimization campaign in which an α-methylbenzyl substituent (2,6-dichloro-3-fluoro-α-methyl-benzyl) was incorporated into a lead anticancer drug scaffold to deliver the anticancer drug crizotinib.[1] Furthermore, Tanaji incorporated a *gem*-dimethyl group to obtain clinically relevant drugs.[2] This report highlighted the importance of protruding lipophilic methyl groups in improving target binding efficiency, and thus increasing bioactivity. Additionally, phenyl ring substituents were selected in such a way as to incorporate representative Craig plot groups from each of the four quadrants depicted in figure 2.1. In this regard, a plot of Hammett constants (σ) which represents the electronic effect of various atoms or groups of atoms relative to hydrogen against hydrophobicity (π) values[3,4] played a significant role in guiding the selection of various substituents. The selected Craig plot groups and their corresponding quadrants include F, Cl, and OCF_3 (1^{st}), CH_3SO_2 (2^{nd}), OCH_3 and OH (3^{rd}), and Me (4^{th}). These groups were fixed at the *para*-position of the substituent benzylamine ring, and a few were added to the *ortho*-position for control purposes.

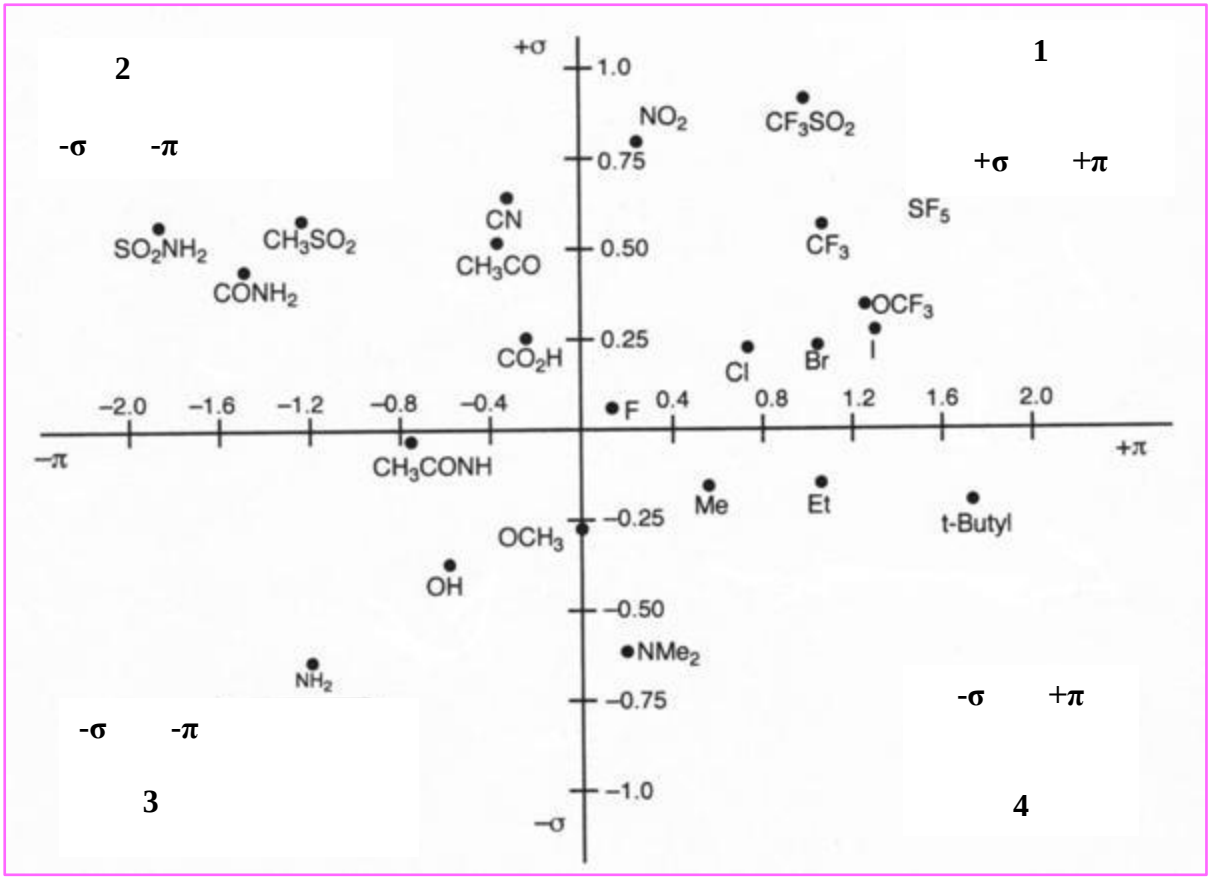

Figure 2.1: Craig plot substituents incorporated in structure-activity and -property relationship studies around novel antimalarial and antischistosomal pyrido[1,2-*a*]benzimidazole analogues[3]

With the next phase of SAR/SPR studies, factors that would affect the solubility of PBI compounds will be evaluated. Established organic synthetic methods were used to synthesize the target compounds.

The asexual blood stage antiplasmodium activities of all analogues synthesized were evaluated against both the chloroquine-sensitive *P. falciparum* NF54 and the multi-drug-resistant K1 strains. The in vitro gametocytocidal activity of the compounds was also determined using the *P. falciparum* NF54 strain. Furthermore, compounds were subjected to *in vitro* antischistosomal activity evaluation against both NTS and adult *Schistosoma mansoni* liver flukes. Finally, the apparent solubility of the analogues was evaluated using turbidimetric and HPLC-based kinetic solubility assays.

2.2 Design

2.2.1 α-Methylbenzylamine-substituted PBI analogues in SAR 1.1 to 1.4

In the design of SAR 1 target analogues, it was postulated that making structural modifications at position C-1 of the pyridinyl ring, and at positions, C-8 and -9 of the phenyl ring of the PBI motif would be essential in exploring and expanding the SAR/SPR studies on this series of compounds. Consequently, although compounds synthesized in SAR 1.1 to 1.4 and SAR 2.1 to 2.5 studies were diversified, the PBI motif was maintained (figure 2.2).

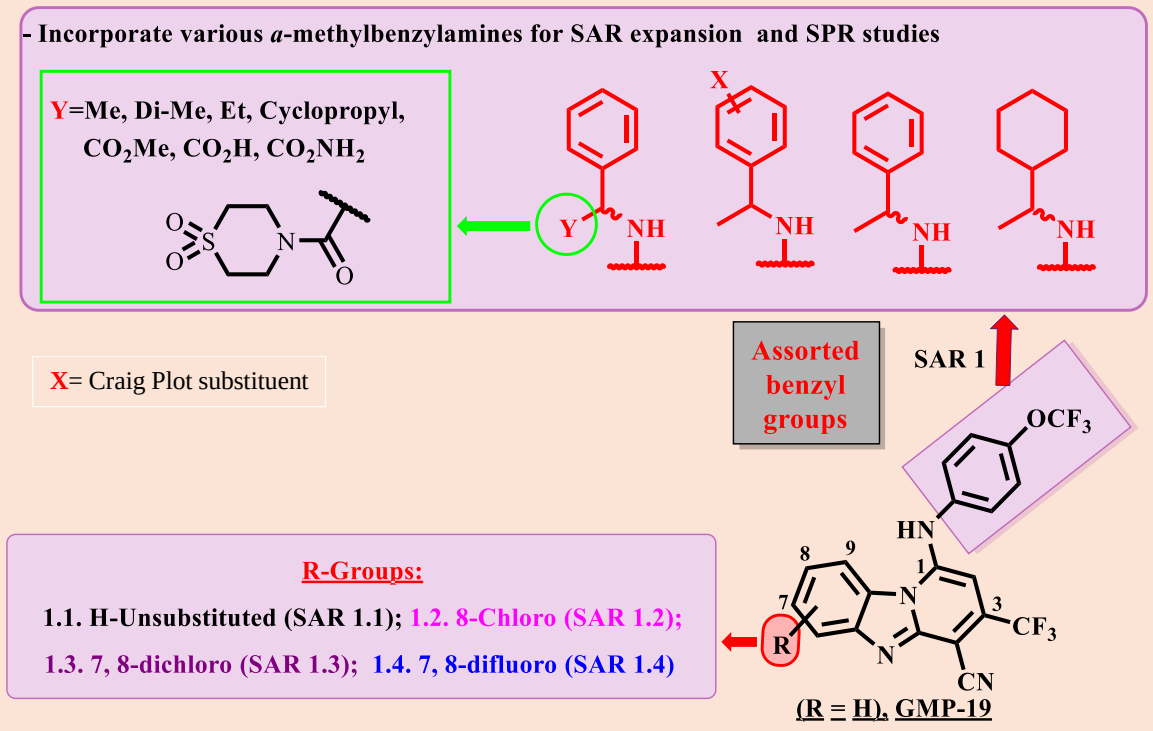

Figure 2.2: Design of PBI analogues in structure-activity relationship (SAR) studies 1.1 to 1.4

In order to introduce structural diversity and explore different chemical spaces, the 4-(trifluoromethoxy)aniline moiety of **GMP-19** was replaced with assorted α-methylbenzylamine substituents at C-1 of the PBI core (SAR 1.1). Consequently, analogues showing high biological activity were further modified by incorporating electron-withdrawing mono-atomic substituent groups such as chloro and fluoro atoms, respectively (SAR 1.2 and 1.4). These substitutions were made at positions C-7 and/or C-8 of the core scaffold, while the α-methylbenzylamine substituents that retained high biological activity were maintained at C-1. These modifications were, in addition to SAR expansion, envisaged to improve metabolic stability and/or solubility.

2.2.2 α-Methylbenzylamine-substituted PBI analogues in SAR 2.1 to 2.5

The design of SAR 2 analogues incorporating molecular features known to improve compound solubility. In this regard, polar hydrogen-bonding and water-solubilizing groups were incorporated into the phenyl (SAR 2.1 and 2.2) and pyridinyl rings at C-1 (SAR 2.3, figure 2.3). Thus, amides (SAR 2.1) and amino moieties, such as morpholinyl and piperazinyl groups (SAR 2.2), were introduced into the left-hand side (LHS) of the core scaffold.

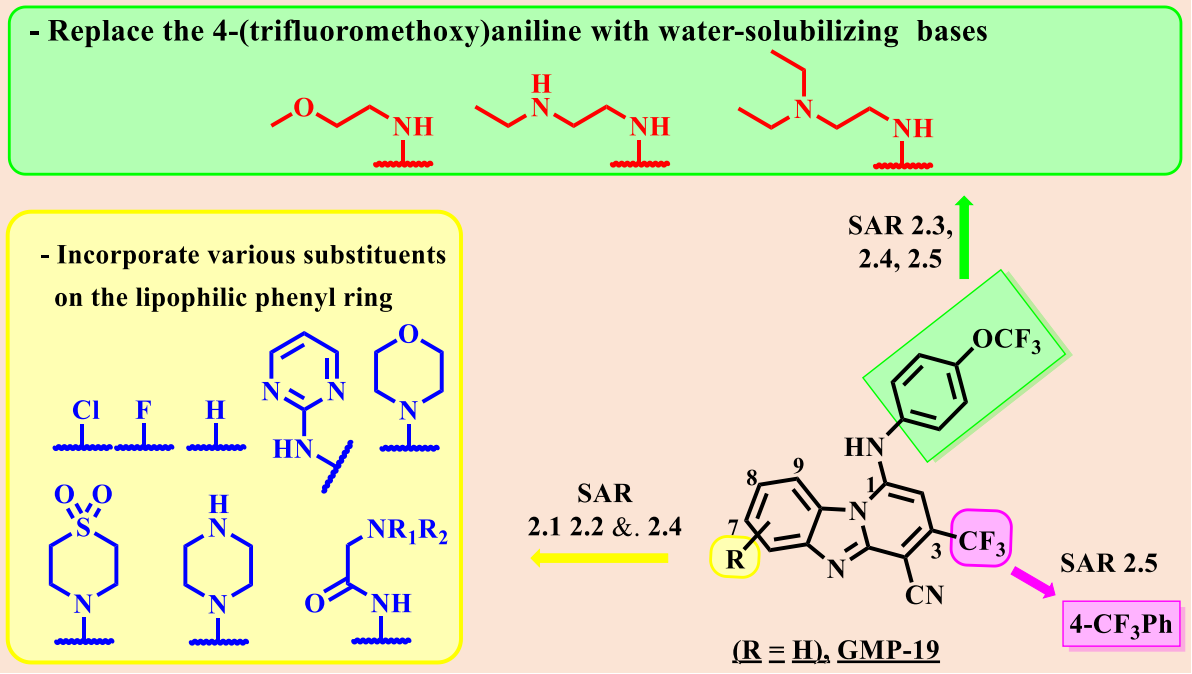

Figure 2.3: Design of PBI analogues in structure-activity relationship (SAR) studies 2.1 to 2.5

Initially, the 4-(trifluoromethoxy)aniline (4-OCF_3Ph) moiety of **GMP-19** was maintained while making structural changes to the phenyl ring. Once the *R* portion of the core scaffold was optimized to a degree with respect to solubility and biological activity, the optimal group was fixed at this position. In this regard, the morpholino group was identified as showing the best balance of aqueous solubility and biological activity. Consequently, the 4-OCF_3Ph moiety was replaced with basic side chains (SAR 2.3). Upon optimization of the right-hand side (RHS) with respect to solubility and biological activity, the next phase of SAR focused on replacing the trifluoromethyl (CF_3) moiety of the **GMP-19** template with a 4-trifluoromethylphenyl (4-CF_3Ph) group at C-3 on the RHS. Although replacing CF_3 with a 4-CF_3Ph group resulted in increased lipophilicity, the overall design strategy was to combine the highly improved solubility of SAR 2.4 analogues with an improved antiplasmodium activity that is associated with the 4-PhCF_3 moiety.[5]

2.3 Synthesis of SAR 1 and 2 compounds

Although numerous synthetic studies have reported diverse protocols for the synthesis of the same heterocyclic PBI core, the synthesis technique used in this study was based on the work of Rida *et al.*[6] and Ndakala *et al.*[5] Furthermore, the work of Paul *et al*.[7] formed the basis and reference for the synthesis of target analogues that required carbon-to-amine coupling (C-N bond formation). In this regard, the Buchwald-Hartwig palladium (0)-catalyzed amination protocol was used. A 1-ethyl-3-(3-dimethylaminopropyl)carbodiimide (EDCI)-mediated coupling protocol[8–10] was used to synthesize the target amides.

Target compounds for the initial phase of the SAR study were synthesized using the synthetic protocol outlined below in figure 2.4. Condensation of a commercially available and appropriately substituted benzene-1,2-diamine with an ethyl 2-cyanoacetate under reflux conditions produced a bicyclic-benzimidazole acetonitrile intermediate, which underwent further condensation to yield a suitably substituted oxo-/hydroxyl-functionalized tricyclic PBI intermediate that was subsequently converted into a chlorinated intermediate. Microwave-assisted regio-selective amination was performed to produce target molecules for the SAR 1.1 to 1.4 study. Among the intermediate analogues at this stage, those with suitable functionalities were subjected to further reactions, such as base-catalyzed hydrolysis of the ester group to deliver intermediate acids for subsequent amide coupling. Moreover, the analogues that possessed suitable halogens on the phenyl ring of the core scaffold underwent Buchwald-Hartwig palladium-catalyzed amination reactions to produce SAR 2.1 to 2.5 compounds. SAR 1.1 to 1.4 and SAR 2.1 to 2.5 target compounds were obtained via the 4 and 6-step synthetic procedures outlined in figure 2.4 and 2.7, respectively. The isolated yields are tallied in figures 2.5, 2.6, and 2.8.

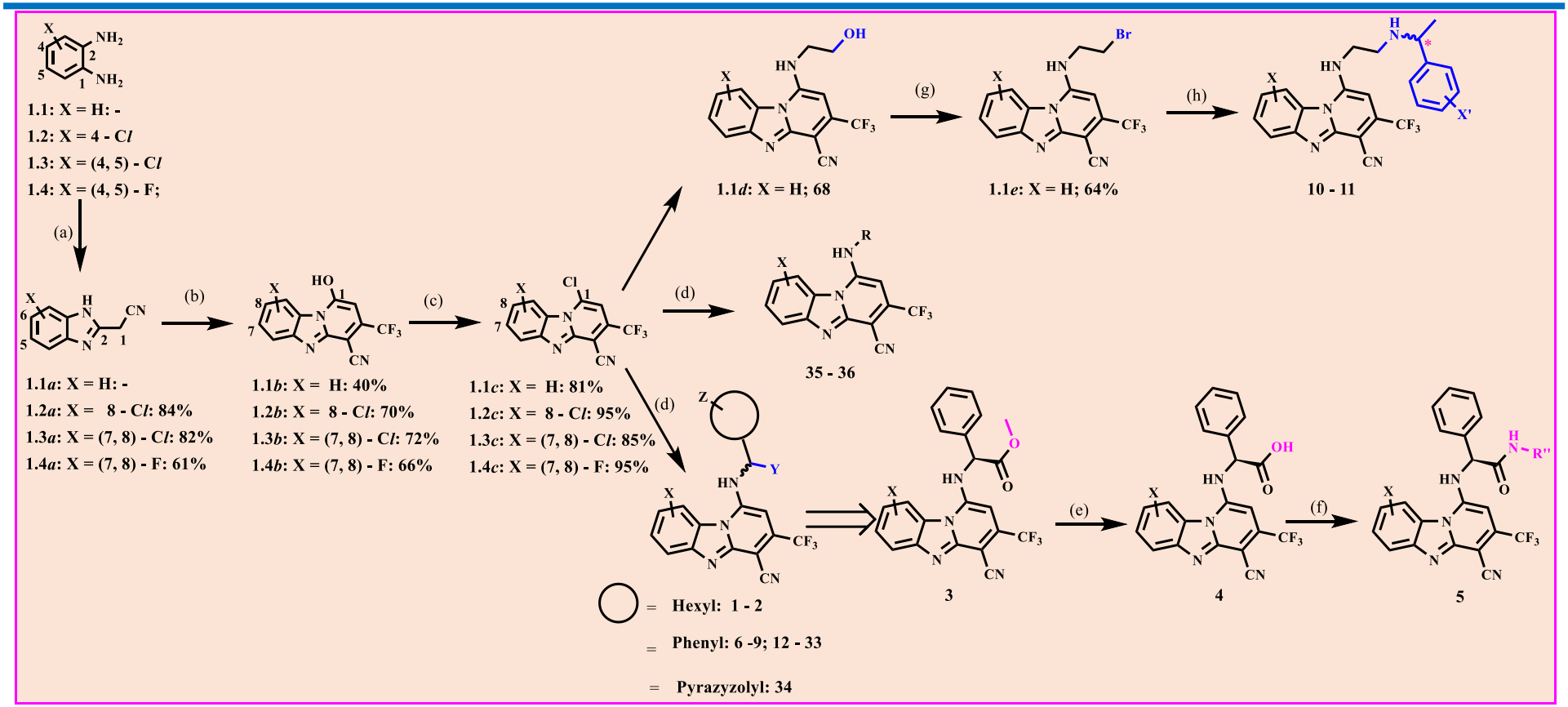

Figure 2.4: Synthesis of compounds in structure-activity relationship (SAR) studies 1.1 to 1.4

Reagents and conditions: (a) Ethyl cyanoacetate, dimethylformamide (DMF), 160 °C, 3 h; (b) ethyl 4,4,4-trifluoro-3-oxobutanoate, NH_4OAc, 145 °C, 2 h; (c) $POCl_3$, 130 °C, 3 h; (d) amine, triethylamine (TEA), tetrahydrofuran (THF), 80 °C, microwave (150 W), 20 min; (e) i. 2.0 M KOH, MeOH, 25 °C, 10 min.; ii. 2.0 M HCl; (f) 1-ethyl-3-(3-dimethylaminopropyl)carbodiimide, 4-dimethylaminopyridine, methylene dichloride (DCM), 0-25 °C, 2 h; (g) CBr_4, PPh_3, DMF, 25 °C, 10 min.; (h) K_2CO_3, DMF, 75 °C, 2 h.

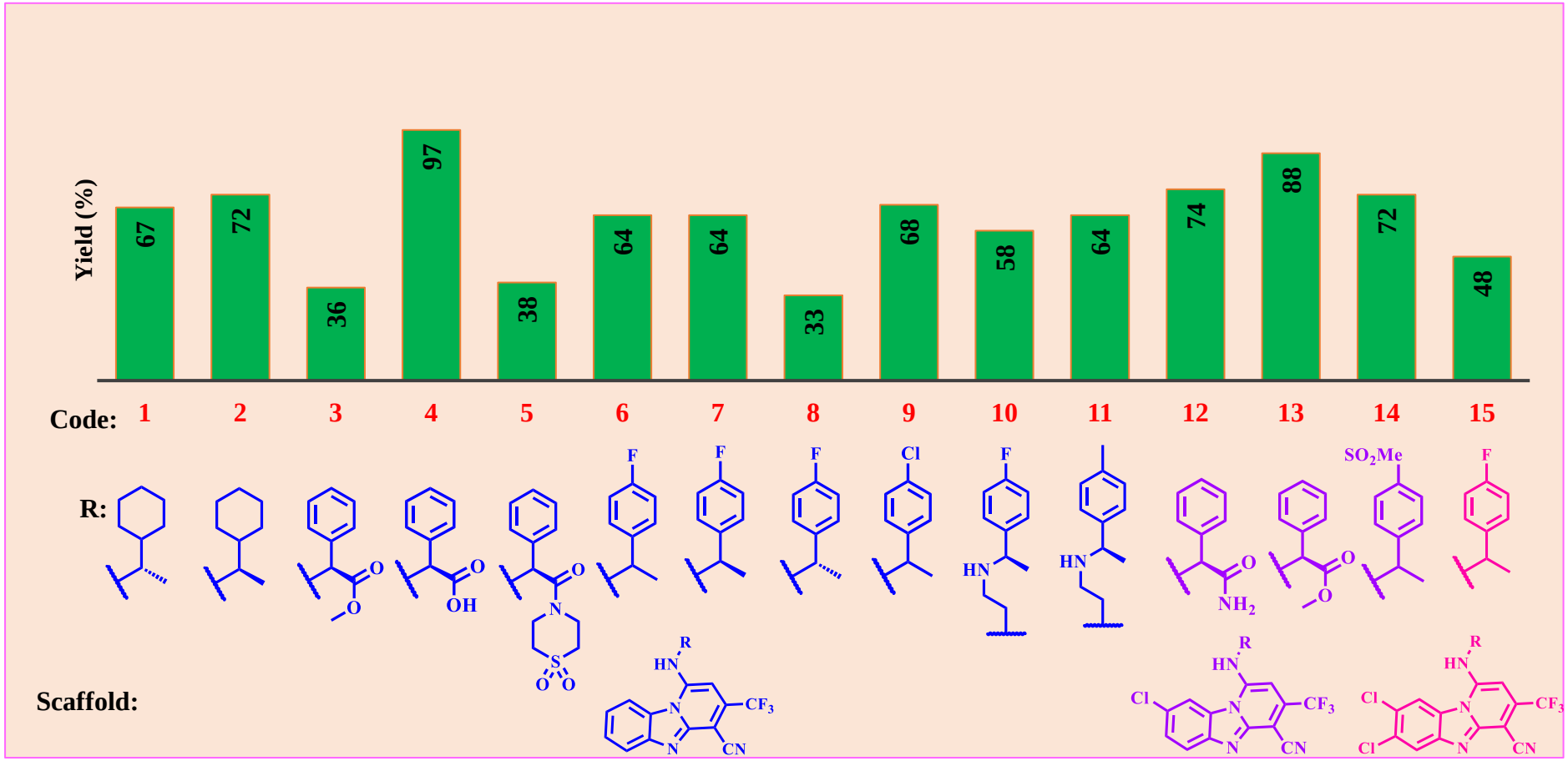

Figure 2.5: Yield for compounds synthesized in structure-relationship (SAR) studies 1.1 (compounds **1-11**), 1.2 (**12-14**), and 1.3 (**15**)

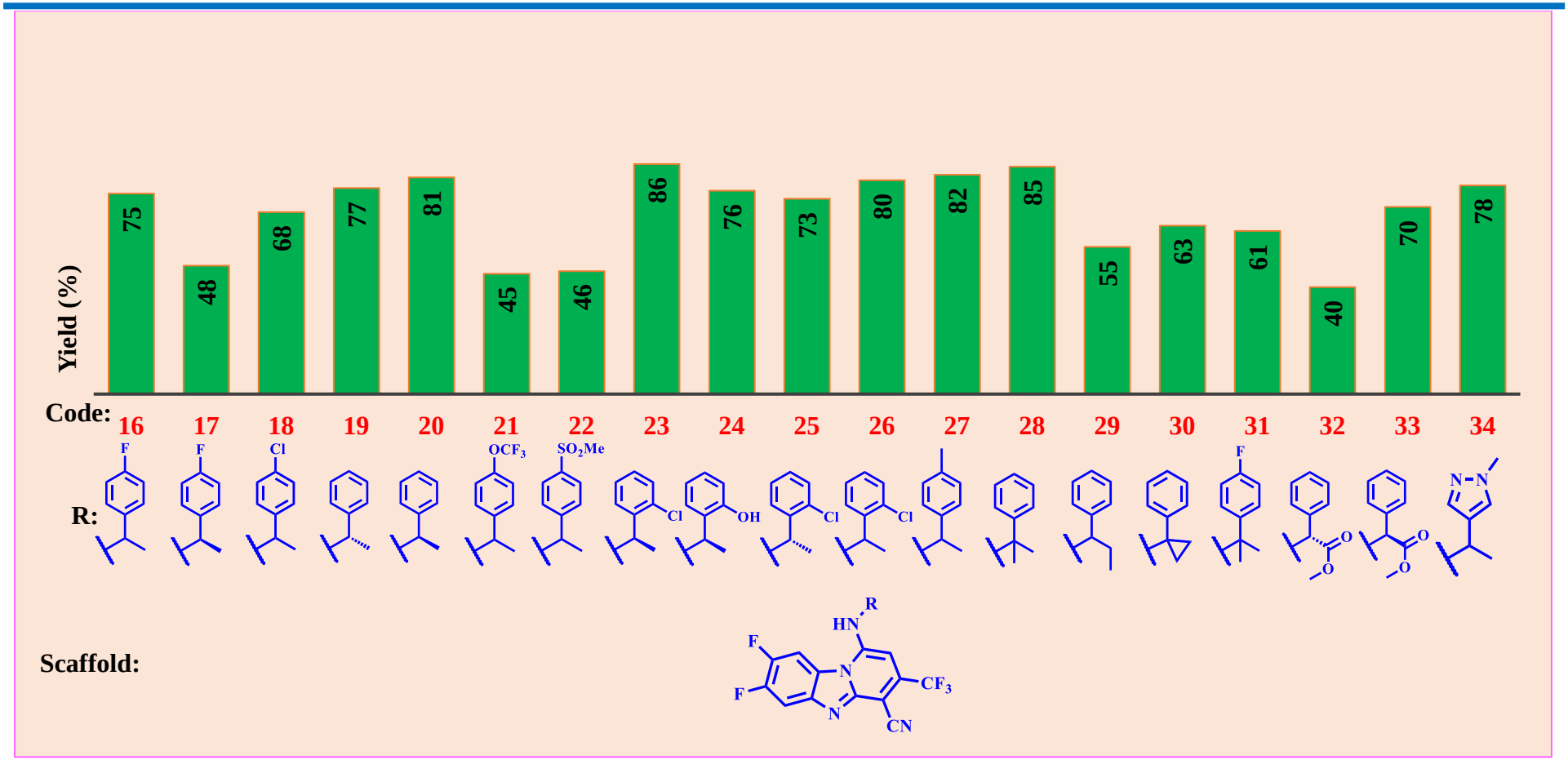

Figure 2.6: Yield for compounds synthesized in structure-relationship (SAR) study 1.4 (compounds **16-34**)

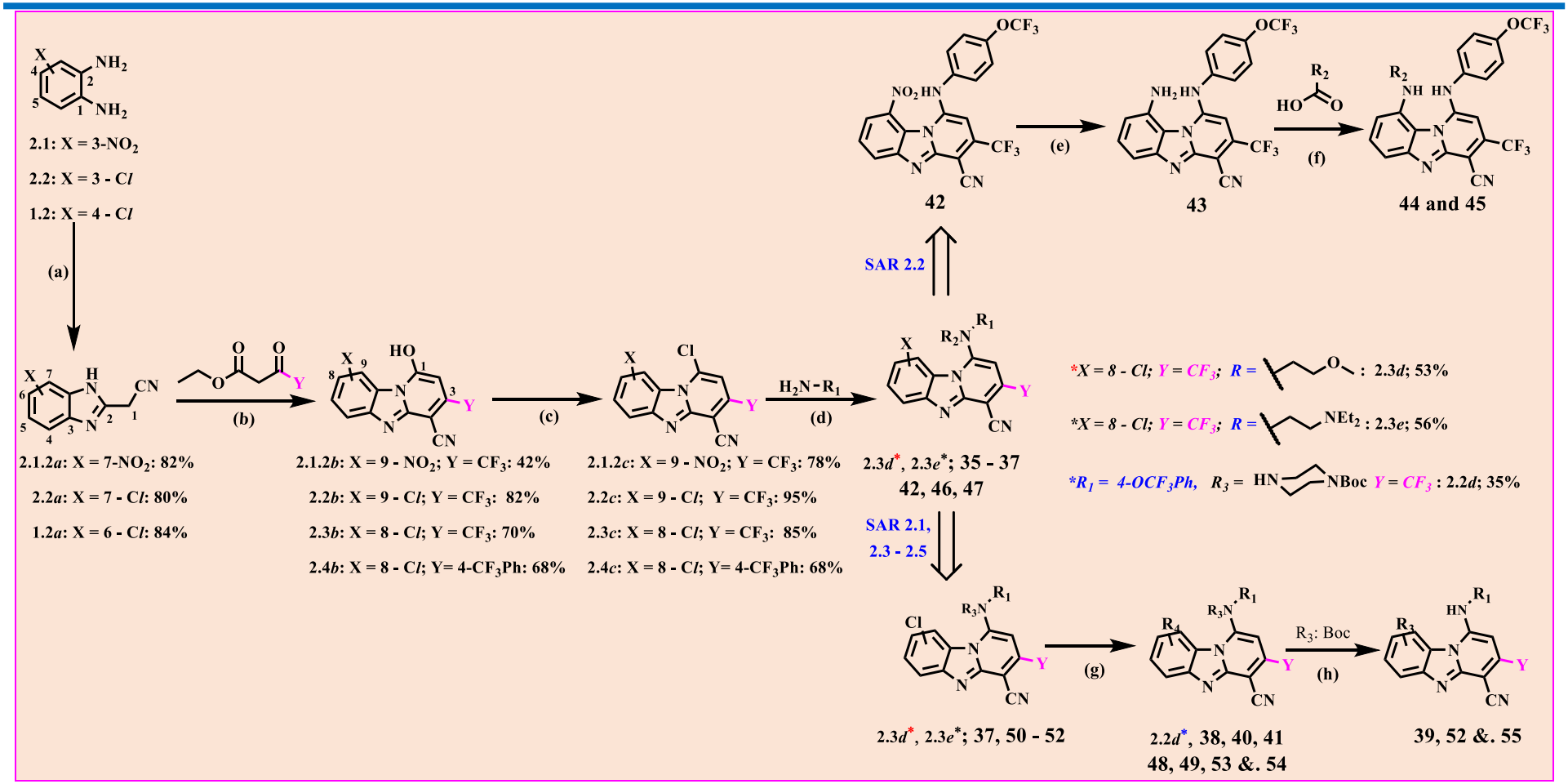

Figure 2.7: Synthesis of compounds in structure-activity relationship (SAR) studies 2.1 to 2.5

Reagents and conditions: (a) Ethyl cyanoacetate, DMF, 160 °C, 3 h; (b) NH_4OAc, 145 °C, 2 h; (c) $POCl_3$, 130 °C, 3 h; (d) TEA, THF, 80 °C, microwave (150 W), 20 min; (e) NH_4Cl, Fe, MeOH:H_2O (1:1), 65 °C, 45 min; (f) DCM, EDCI, DMAP, 0 °-25 °C, 6-12 h; (g) amine, $Pd_2(dba)_3$, RuPhos, Cs_2CO_3, 1,4-dioxane/ DMF (1:1), 80 to 110 °C; (h) 2.0 M HCl, 25 °C, 1 h

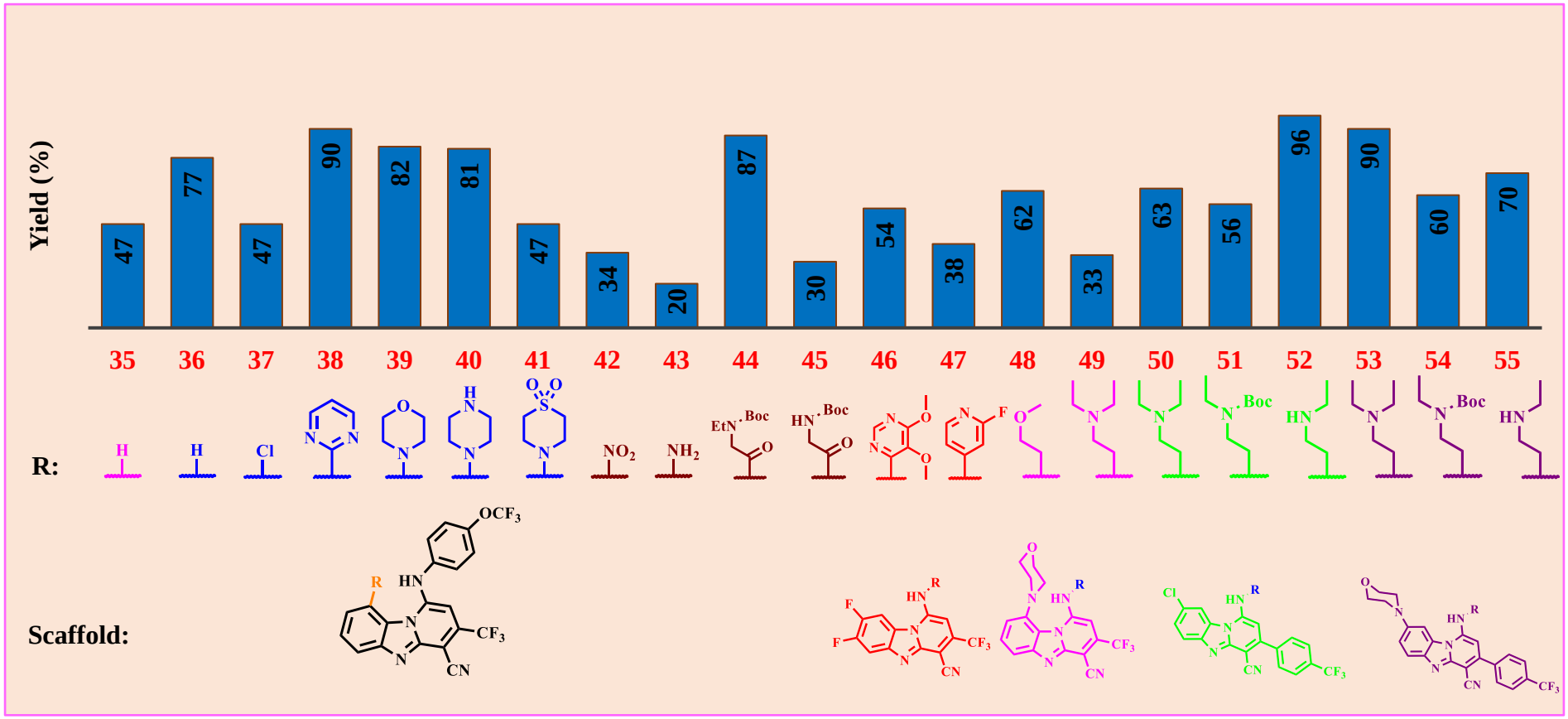

Figure 2.8: Yield for compounds synthesized in structure-relationship (SAR) studies 2.1 (compounds **35-41**), 2.2 (**42-45**), 2.3 (**46-47**), 2.4 (**48-49**), and 2.4 (**50-55**)

2.4 Mechanistic details and spectroscopic analyses of SAR 1 intermediate and target compounds

Details of selected key reaction steps leading to the formation of critical intermediates and selected final analogues and the proton nuclear magnetic resonance (^{1}H NMR) spectroscopy analyses of representative compounds are described here. The unsubstituted benzimidazole acetonitrile intermediate **1.1*a*** (figure 2.4) was commercially available and used as purchased, and the symmetrically and asymmetrically substituted benzimidazole acetonitrile intermediates **1.2*a*, 1.4*a*, 2.1.1*a*, 2.1.2*a*** and **2.2*a*** (figures 2.4 and 2.7) were obtained from commercially available and appropriately halogenated and nitro-substituted benzene-1,2-diamine precursors. These precursors include the 4-chloro (**1.2**), 4,5-dichloro (**1.3**), 4,5-difluoro (**1.4**), 3-chloro (**2.2**), and 3-nitro (**2.1**) benzene-1,2-diamine moieties (figures 2.4 and 2.7). The formation of various benzimidazole acetonitrile intermediates used in this study is exemplified by the formation of the symmetrically substituted 2-(5,6-difluoro-1*H*-benzo[*d*]imidazol-2-yl)acetonitrile (compound **1.4*a***, figure 2.9). The consecutive steps involved in the condensation reaction required for the formation of **1.4*a*** include the nucleophilic addition of the amino group in compound **1.4** to the carbonyl carbon of ethyl cyanoacetate (figure 2.9).

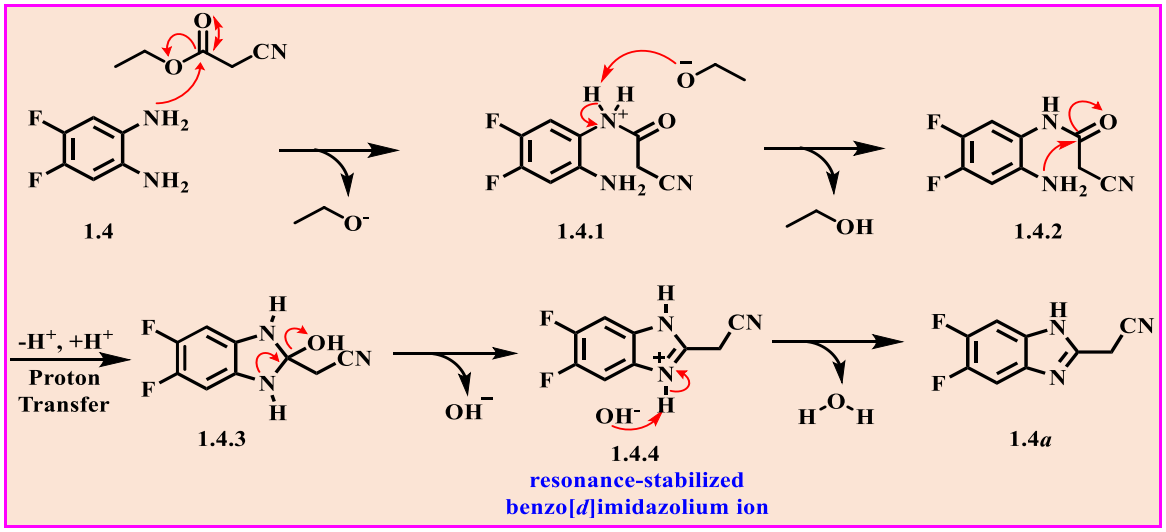

Figure 2.9: Mechanism of formation of 2-(1*H*-benzo[*d*]imidazol-2-yl)acetonitrile (**1.4*a***)

Next, ethoxide ion-mediated deprotonation of the intermediate **1.4.1** occurs. An intramolecular nucleophilic addition takes place, leading to a ring closure and a subsequent proton transfer to form **1.4.3**. A dehydration reaction leads to the formation of 2-(cyanomethyl)-1*H*-benzo[*d*]imidazol-3-ium ion, intermediate **1.4.4**. Charge stabilization of **1.4.4** then occurs by means of a hydroxide mediated proton abstraction that leads to the formation of the desired

product, **1.4*a***. The mono-, di-chlorinated, and 7-nitro benzimidazole acetonitrile intermediates (**1.2*a***, **1.3*a*, 2.1*a*,** and **2.2*a***) were synthesized following the steps outlined in figure 2.9.

The structure of **1.4*a*** was confirmed via 1D ^{1}H NMR spectroscopy, and the following signals were identified: highly deshielded **NH** proton (**H^{4}**) peak at δ = 12.8 ppm, two electronically equivalent aromatic proton signals at δ = 7.6 ppm (**H^{2}** and **H^{3}**), and a sharp singlet peak at δ = 4.4 ppm, corresponding to the two relatively shielded methylene protons (**H^{1}**). Although the F-H-coupling was not evident at this stage, the ^{19}F-NMR showed the presence of the two fluorine atoms and the ^{1}H NMR spectrum obtained (figure 2.10) was consistent with the structure of compound **1.4*a*.**

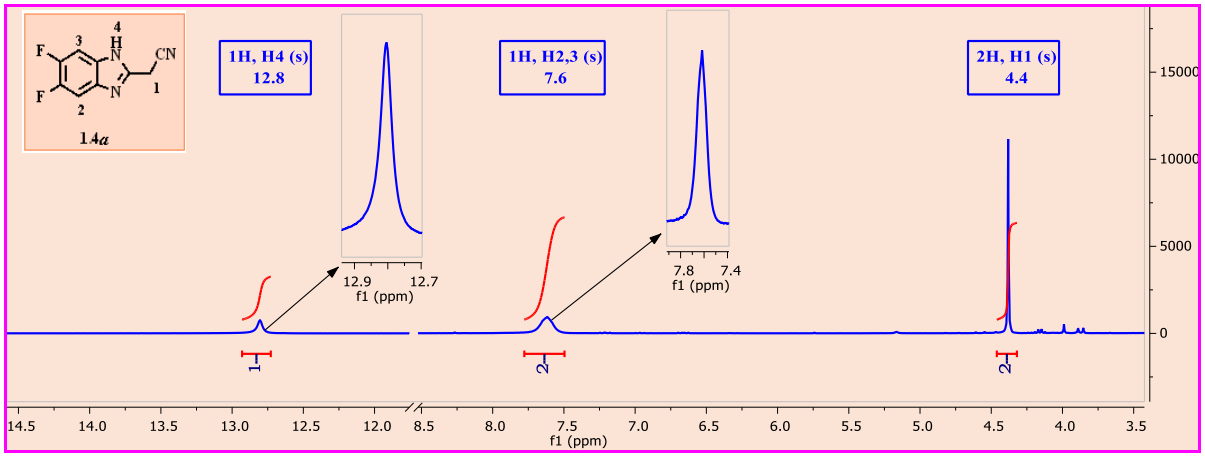

Figure 2.10: 1D ^{1}H nuclear magnetic resonance spectroscopy spectrum of **1.4*a*** showing the **NH** (**H^{4}**) and the methylene (**H^{1}**) proton singlet peaks at δ = 12.8 ppm and δ = 4.4 ppm, respectively in DMSO-d_6 at 300 MHz

The intermediate **1.4*a*** was progressed further to a condensation reaction. The ammonium acetate ion then deprotonates one of the partially acidic methylene protons of **1.4*a*** and forms a resonance-stabilized methanide ion. The nucleophilic addition of the methanide ion onto a more electrophilic carbonyl (*keto*) carbon of the *beta*-ketoester occurs next. Consequently, the hydroxyl group is converted into a suitable leaving group by protonation. The dehydration that occurs via an E2 elimination mechanism leads to the formation of the C-C π-bond (figure 2.11). Furthermore, the protonation of the carbonyl oxygen of the ester group increases the electrophilicity of the carbonyl carbon and thus facilitates an intramolecular nucleophilic addition, which is followed by elimination and aromatization steps to form the oxo/hydroxyl intermediate **1.4*b***. The spectroscopic results in figure 2.12 indicate an increase in the number of the aromatic signals and confirm the formation of the compound.

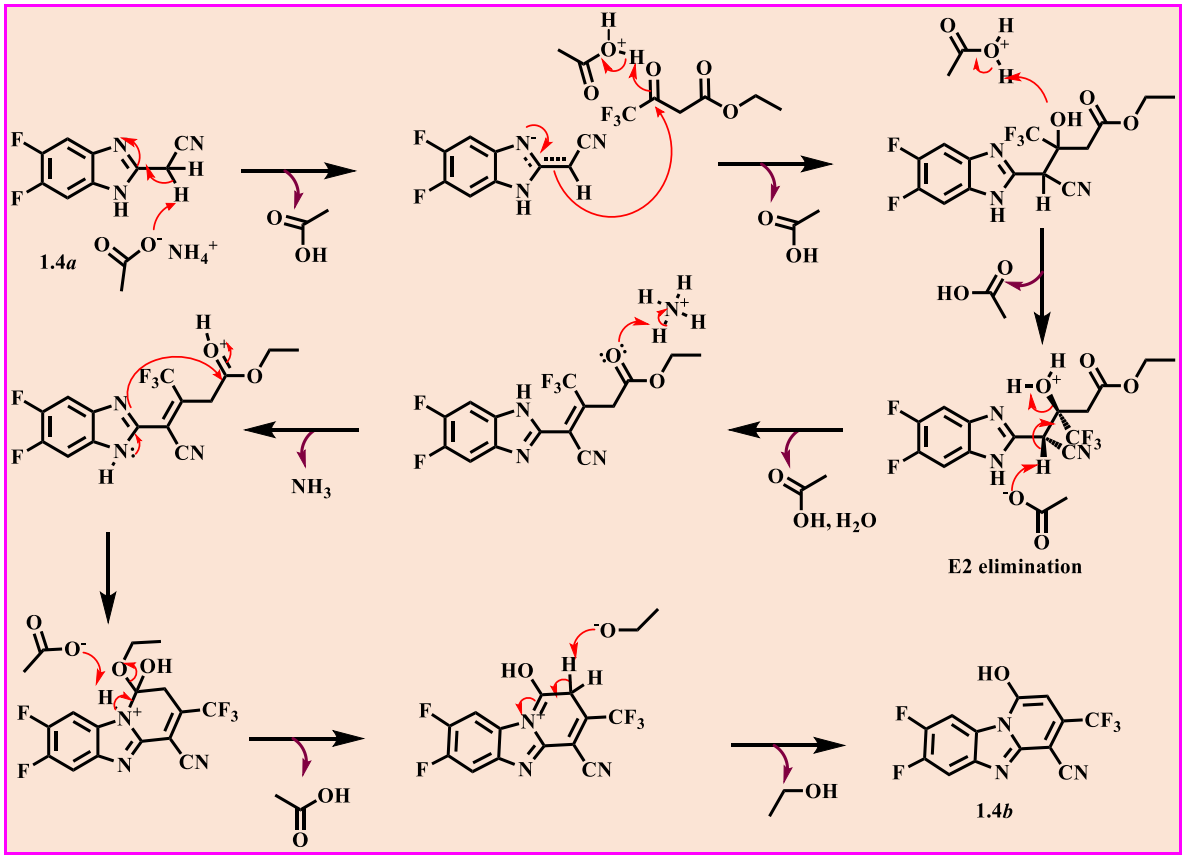

Figure 2.11: Mechanism of formation of intermediate **1.4*b***

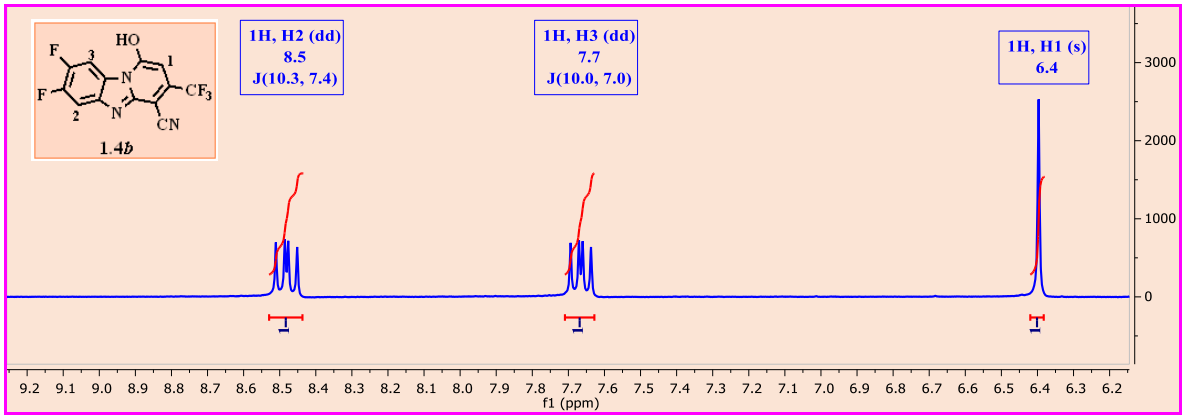

Figure 2.12: 1D ^{1}H nuclear magnetic resonance spectrum of **1.4*b*** showing aromatic signals in DMSO-d_6 at 300 MHz

A singlet peak that integrates for one proton (**1H**) is evident at δ = 6.4 ppm, and this corresponds to the newly introduced proton **H^{1}**. Additionally, a separation of signals and a change in the splitting pattern of **H^{2}** and **H^{3}** in **1.4*b*** were observed. The presence of the **OH** on the RHS affected the electronic environment between the two protons, thus leading to the observed peak separation, which was not previously observed on the 1D ^{1}H NMR spectrum of **1.4*a***. Moreover, the observed doublet of doublets (dd) splitting pattern is attributed to the presence of fluorine

atoms, which influence the electronic environment of the protons via fluorine-to-proton spin-spin coupling. The β-fluorine splits a proton into a doublet whereupon the magnetic influence of the γ-fluorine nucleus through long-range coupling leads to further splitting. Therefore, the two fluorine atoms present between the two protons on the LHS of compound **1.4*b*** caused $\mathbf{H^2}$ and $\mathbf{H^3}$ to split into the observed pattern.

Chlorination of **1.4*b*** led to the formation of the common amination intermediate **1.4*c*,** which displayed downfield migration of the singlet peak from δ = 6.4 in **1.4*b*** to δ = 7.7 ppm in **1.4*c*** (figure 2.13). The shift is attributed to the stronger deshielding effect of the chloro atom on $\mathbf{H^1}$ compared to that of the hydroxyl group.

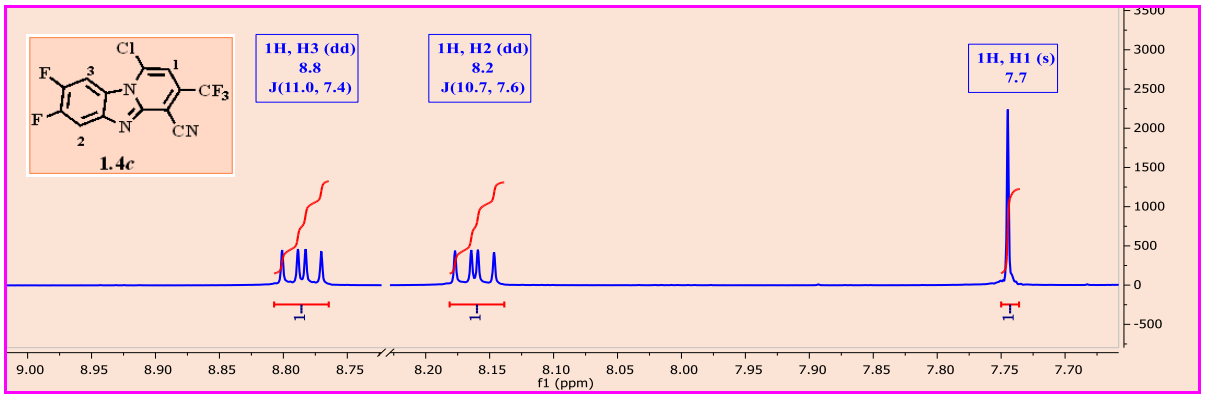

Figure 2.13: 1D ^{1}H nuclear magnetic resonance spectrum of **1.4*c*** showing aromatic signals in DMSO-d_6 at 600 MHz

The amination of **1.4*c*** involved nucleophilic aromatic substitution involving an amino group of the α-methylbenzylamine (or any appropriate amine) (figure 2.14).

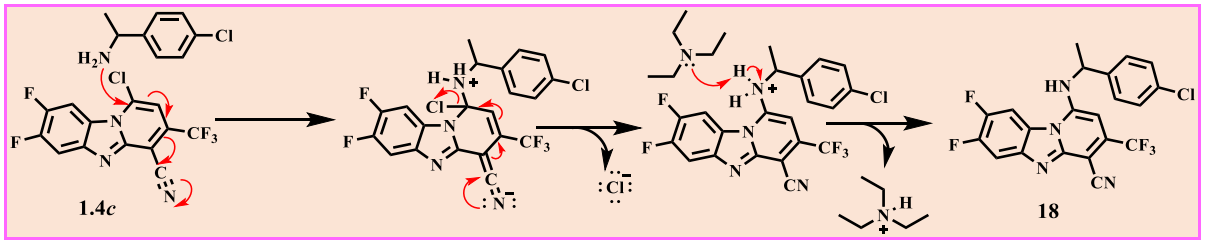

Figure 2.14: Mechanism of the aromatic nucleophilic addition (SNAr) of amines

The successful formation of compound **18** was confirmed via 1D ^{1}H NMR spectroscopy (figure 2.15). The spectrum signals are consistent with the structure of the compound.

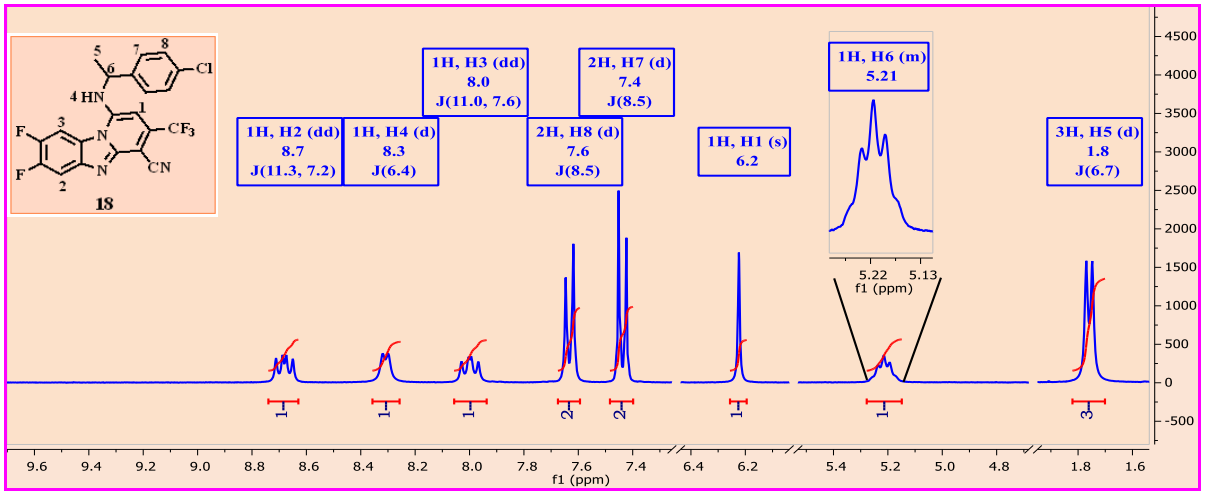

Figure 2.15: 1D ^{1}H nuclear magnetic resonance spectrum of compound **18** showing the newly introduced protons corresponding to the amino, methyl, methylene, and additional aromatic groups in DMSO-d_6 at 300 MHz

Two symmetrical signals typical of a *para*-substituted phenyl ring were identified in the aromatic region.[11] The clear separation of the symmetrical doublet peaks arising from **1H^{8}** (δ = 7.6 ppm, *J* = 8.5 Hz) and **1H^{7}** (δ = 7.4 ppm, *J* = 8.5 Hz) is attributed to the presence of a deshielding chloro atom at the *para*-position of the benzyl ring. In addition, the methine proton (**1H^{6}**: δ = 5.2 ppm) at the α-position, which appeared as a slightly deshielded multiplet was a key diagnostic feature to confirm the formation of the target compound. Furthermore, a doublet peak identified upfield in the aliphatic region integrating for three protons (**3H^{5}**, δ = 1.8 ppm, *J* = 6.7 Hz), indicating the presence of a methyl group. Moreover, the existence of a doublet peak identified downfield at **1H^{4}** (δ = 8.3 pm; *J* = 6.4 Hz) indicates the presence of an amino functional group on the molecule, which is attributed to the vicinal spin-spin coupling with **H^{6}** (figure 2.15).

Several other analogues in this section were derived and characterized and showed similar spectral features to those of compound **18**. The 1D ^{1}H NMR spectrum of analogue **15** and the structure of this compound is also shown in figure 2.16. Unlike the complex multiplicities observed with compound **18**, compound **15** showed well-resolved singlet peaks corresponding to **1H^{3}** (δ = 7.9 ppm) and **1H^{2}** (δ = 8.4 ppm). Further diagnostics performed to confirm the structure of compound **15** included identification of the presence of the symmetrical doublet peaks due to *para*-fluoro substitution on the benzylamine moiety. In this regard, the newly introduced protons **2H^{8}** (δ = 7.2 ppm, *J* = 8.9 Hz) exhibited a well-resolved triplet (t) due to equal vicinal spin-spin coupling with **H^{7}** and the fluoro (**F**) atom. On the other hand, **2H^{7}** (δ =

7.6 ppm, J = 8.5, 5.4 Hz) split into dd arising from a vicinal coupling with **H**^{8} and a long-range coupling to **F**.

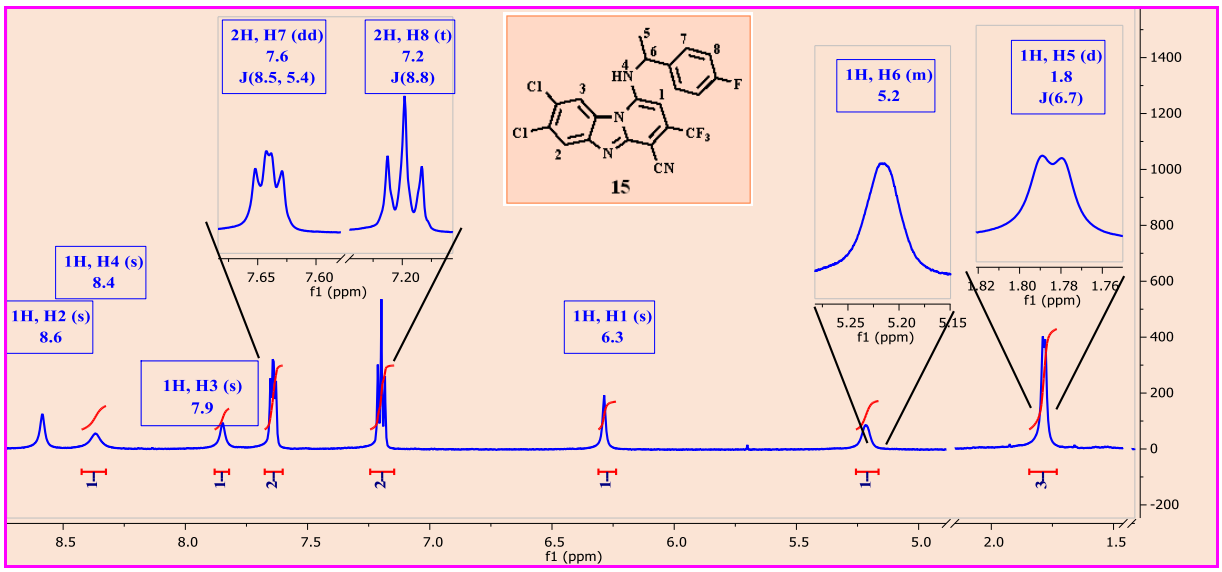

Figure 2.16: 1D ^{1}H nuclear magnetic resonance spectrum of compound **15** showing the presence of a symmetrically-substituted benzyl moiety in DMSO-d_6 at 600 MHz

The appearance of a multiplet peak corresponding to **1H**^{6} (δ = 5.2 ppm) upfield confirmed the presence of an α-methine proton. Another vicinal coupling of **H**^{6} to the neighbouring amino-**NH** proton **H**^{4} led to further splitting which brought about the observed multiplet splitting pattern. On the other hand, a broad singlet was observed at δ = 8.4 ppm due to **H**^{4}. Moreover, the presence of the methyl group was confirmed by the appearance of a clearly resolved doublet peak upfield at δ = 1.8 ppm, J = 6.7 Hz, which integrated into three protons (3**H**), corresponding to the methyl protons **H**^{5}.

Furthermore, analogues with an unsubstituted phenyl ring of the PBI nucleus, such as compound **9,** are among the target compounds synthesized in this SAR study. The 1D ^{1}H NMR spectrum confirming the formation of this representative compound is displayed in figure 2.17.

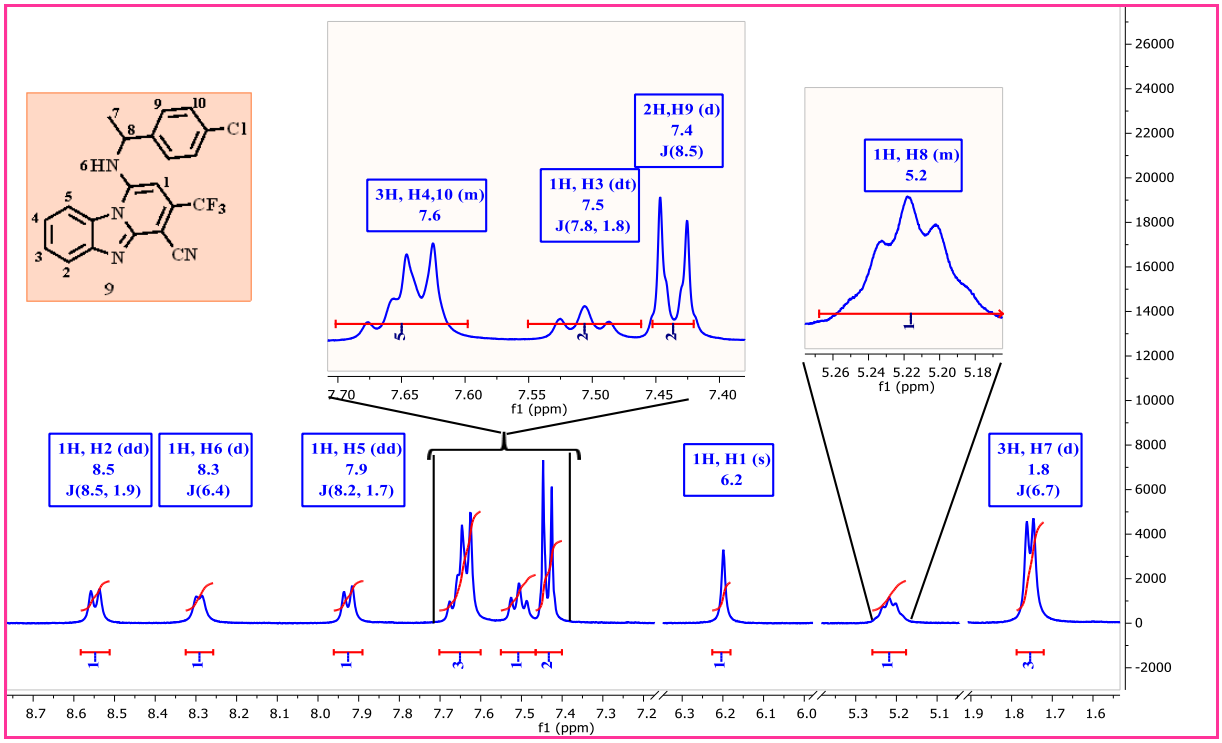

Figure 2.17: 1D ^{1}H nuclear magnetic resonance spectrum of compound **9** showing methyl (H^{7}) and methylene (H^{8}) protons at δ = 1.8 ppm and δ = 5.2 ppm in DMSO-d_6 at 400 MHz

The diagnostic features identified as characteristic of aminated final molecules such as compounds **18** and **15** are also evident in the ^{1}H NMR spectrum of compound **9**. Briefly, such features include the symmetrical splitting of the *para*-substituted benzyl protons (**H^{10}** and **H^{9}**, δ = 7.6 and δ = 7.4 ppm, respectively), the presence of the methine peak (**H^{8}**, δ = 5.2 ppm), the methyl peak (**H^{7}**, δ = 1.8 ppm), and a broad doublet peak corresponding to the **NH** (**H^{6}**) at δ = 8.3 ppm downfield. Additionally, as theoretically expected, the core scaffold showed doublet of doublets peaks downfield corresponding to **1H^{2}** (δ = 8.6, ppm, *J* = 8.5, 1.9 Hz) and **1H^{5}** (δ = 7.9 ppm, *J* = 8.2, 1.7 Hz). The peak identified as **H^{4}** coalesced with **H^{10}** at approximately δ = 7.6 ppm, thus making it difficult to determine the multiplicity. A doublet of triplets (dt) and singlet peaks corresponding to the aromatic protons **1H^{3}** (δ = 7.5 ppm) and **1H^{1}** (δ = 6.2 ppm) were observed.

Furthermore, unsubstituted core scaffold-based analogues possessing a carboxylate group were derivatized by the introduction of water-solubilizing amide functionality. An amidated analogue (**5**), its precursors, and the corresponding 1D ^{1}H NMR spectra are shown in figure 2.18.

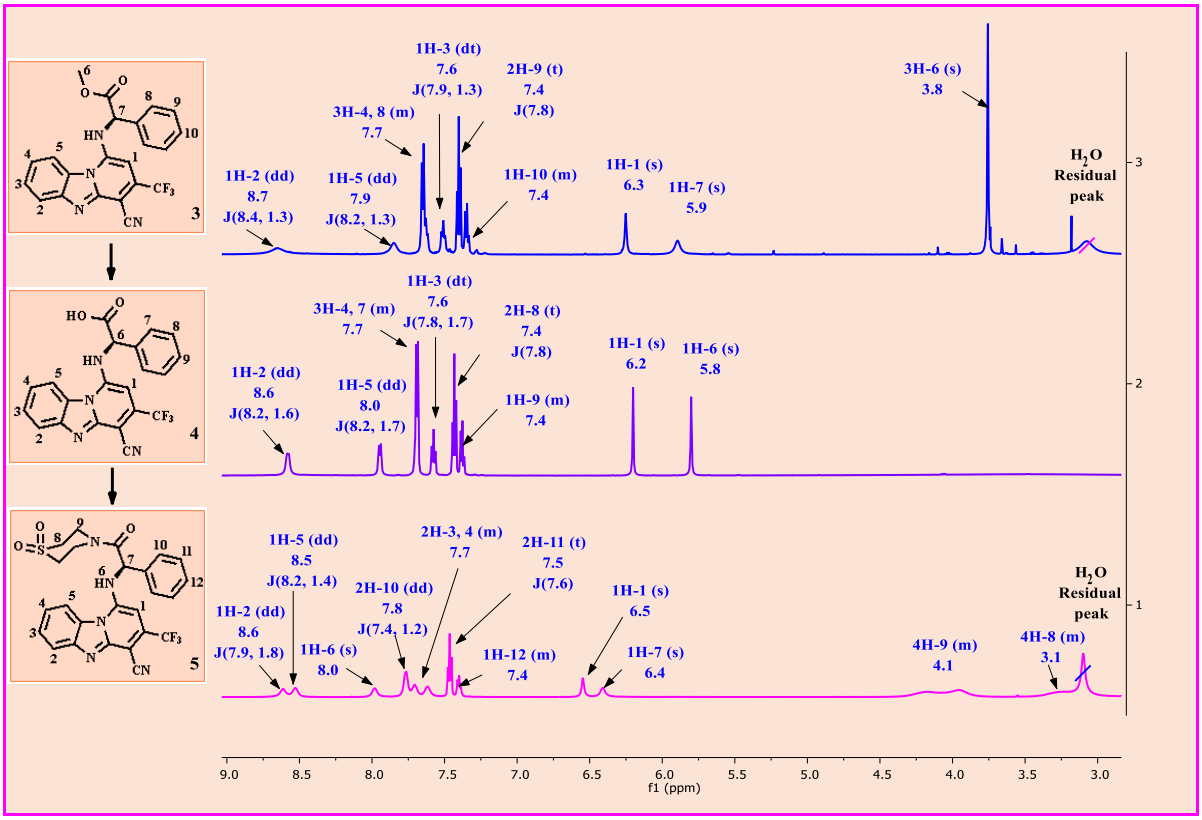

Figure 2.18: 1D ^{1}H nuclear magnetic resonance spectra of compounds **3** (ester), **4** (acid), and **5** (amidated target product) in DMSO-d_6 at 400 MHz

The existence of a singlet peak corresponding to the methyl ester protons **3H^{6}** (δ = 3.8 ppm) of **3** and its consequent disappearance from the spectrum of **4** indicates the presence and successful demethylation of the methyl group of compound **3**. Consequently, the appearance of the symmetrical 1,1-dioxidothiormopholinyl doublet peaks in **5** (**H^{9}** and **H^{8}**, δ = 4.1 and 3.1 ppm, respectively) on the lower spectrum indicates the presence of this amidated compound. Although the chemical shifts in **5** appeared slightly migrated downfield, the α-methine proton of compounds **3**, **4**, and **5** are represented by the synonymous signals at **H^{7}, H^{6}**, and **H^{7}** respectively (δ = 5.9, 5.8, and 6.4 ppm, respectively). Although the **NH** proton was not visible in precursors **3** and **4**, its presence in **5** (**1H^{6}**) at δ = 8.0 ppm confirms the presence of the amino group. Additionally, other characteristic features were observed, such as a singlet peak corresponding to **H^{1}** at approximately δ = 6.2 to 6.5 ppm, unsubstituted benzyl aromatic proton signals at approximately δ = 7.5 to 7.8 ppm and shielded and unshielded phenyl protons appearing at approximately δ = 7.4 to 7.8 ppm and δ = 7.9 to 8.6 ppm, respectively.

2.5 Mechanistic details and spectroscopic analyses of SAR 2 intermediate and target compounds

Here, the formation of key intermediate analogues and selected representative synthesized target compounds modified with various water-solubilizing groups at different positions of the phenyl and pyridyl rings of the PBI core scaffold are discussed. Because most of the starting precursors were asymmetric, the core scaffolds formed in isomeric forms. Nitro-substituted analogues showed the cleanest separation of the isomers, and their corresponding intermediate and target analogues are therefore used to facilitate spectroscopic evaluations and discussions here.

2.5.1 Synthesis of amide compounds

Although the symmetrical disubstituted benzimidazole acetonitrile intermediates derived in figure 2.7 only produced a monomeric compound, the corresponding monosubstituted asymmetric benzimidazole acetonitrile intermediate formed isomers. The presence of the isomeric compounds was confirmed via liquid chromatography-mass spectrometry (LC-MS), which revealed two distinct signals with the same *m/z* value (200.9) at 3.06 and 3.18 minutes, respectively. The formation of isomers is thought to arise from deprotonation of the benzimidazolium ion via two possible routes (figure 2.19).

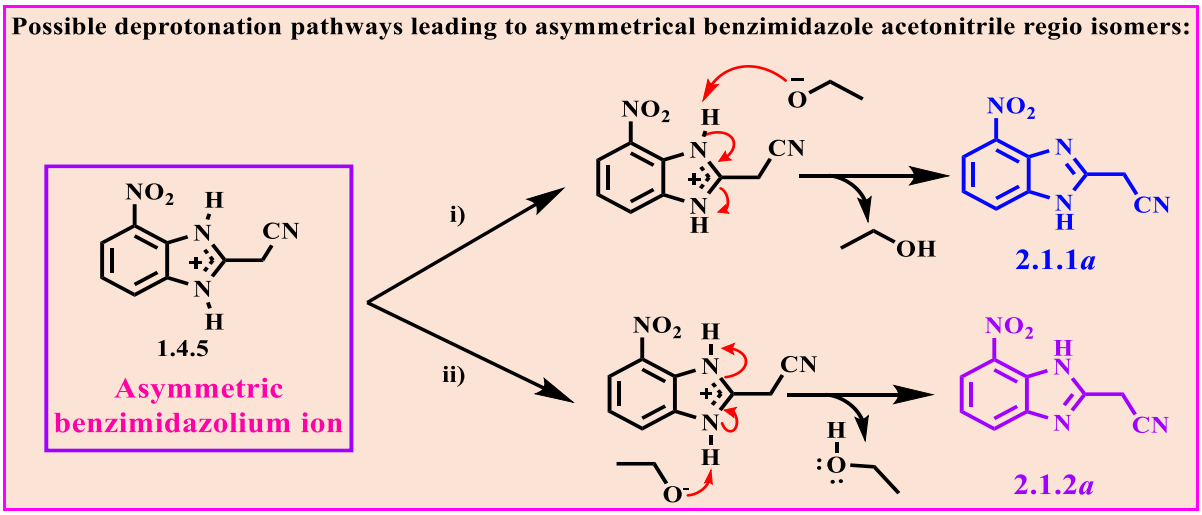

Figure 2.19: Mechanistic details of the formation of isomeric compounds **2.1.1*a*** and **2.1.2*a***

Interestingly, the two isomers were separated by trituration in diethyl ether and obtained as solid residue (yellow) and etheryl solution (orange solid after drying). The spectroscopic analysis of these isolates confirmed the formation and existence of the two isomeric products. The two structures were distinguished by the spin-spin coupling constants and the splitting patterns on their respective 1D ^{1}H NMR spectra shown below in figure 2.20.

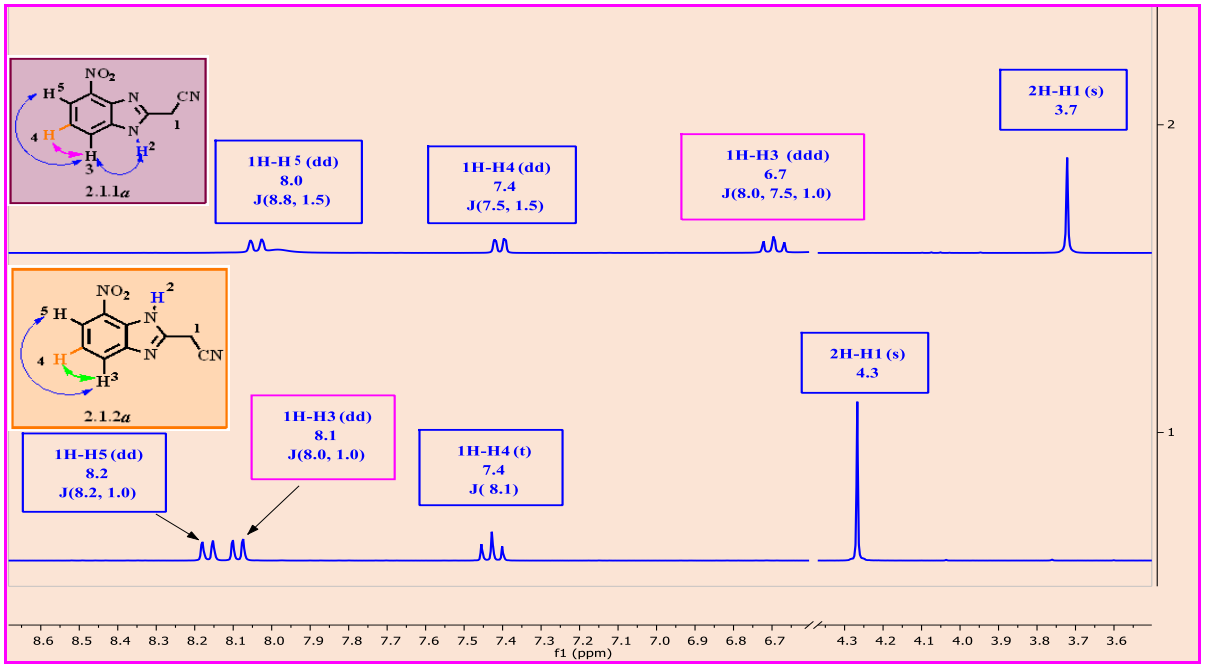

Figure 2.20: 1D ^{1}H nuclear magnetic resonance spectra of regio-isomeric compounds **2.1.1*a*** and **2.1.2*a*** showing the difference in splitting patterns of **2.1.1*a*-H^4** and **2.1.2*a*-H^4** in CD_3CN-d_3 at 400 MHz

Possible spin-spin coupling interactions that are likely to bring about the observed spectroscopic results from the two isomers are shown in figure 2.20. The **H^3** of compound **2.1.1*a*** exhibited a doublet of the doublets of doublets with coupling constants J = 8.0, 7.5, 1.0 Hz (figure 2.20).

The observed splitting pattern is due to a vicinal coupling with **H^4** (magenta), which is further split by two long-range couplings with **H^5** (blue) and the **NH** proton **H^2** (green), respectively (figure 2.21). On the contrary, **H^3** of compound **2.1.2*a*** exhibited a clearly resolved doublet of doublet (dd) peak (J = 8.0, 1.0 Hz) due to vicinal coupling with **H^4** (t, J = 8.1 Hz, magenta) and only one long-range coupling with **H^5** (dd, J = 8.2, 1.0 Hz, blue). This implies that **H^2** on **2.1.1*a*** occupies a different position, as has been proposed with compound **2.1.2*a***. The new position (five bonds away) prevents any long-range coupling that would bring about further splitting as observed with **2.1.1*a***. Additionally, the spectrum of compound **2.1.1*a*** showed widely separated double doublets corresponding to **1H^4** and **1H^5** (δ = 7.4 and 8.0 ppm, J = 7.5, 1.5 and 8.8, 1.5 Hz, respectively), while compound **2.1.2*a*** exhibited closely spaced double doublets (**1H^3** and **1H^5**, δ = 8.1 and 8.2 ppm, J = 8.0, 1.0 and 8.2, 1.0

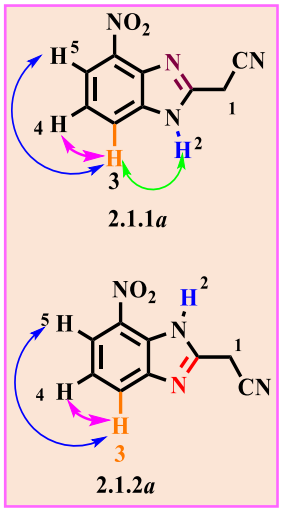

Figure 2.21: H^4-spin-spin interactions on **2.1.1*a*** and **2.1.2*a***

Hz, respectively). The deshielding effect of the Sp^2-hybridized nitrogen (red) appears to be responsible for the downfield migration of the signals.

Next, compounds **2.1.1*a*** and **2.1.2*a*** (figure 2.21) underwent the reaction shown in step (ii), figure 2.7. The proposed mechanistic steps and details leading to the formation of monomeric intermediate compounds **2.1.1*b*** and **2.1.2*b*** are similar to those outlined in figure 2.9. Both compounds were diagnostically characterized by the loss of a proton and the downfield migration of the respective singlet peaks from δ = 3.7 and δ = 4.3 ppm, corresponding to the aromatic proton $\mathbf{H^1}$ of compounds **2.1.1*a*** and **2.1.2*a*** respectively, to δ = 6.1 and δ = 6.4 ppm, corresponding to $\mathbf{H^1}$ of compounds **2.1.1*b*** and **2.1.2*b*,** respectively (figure 2.22).

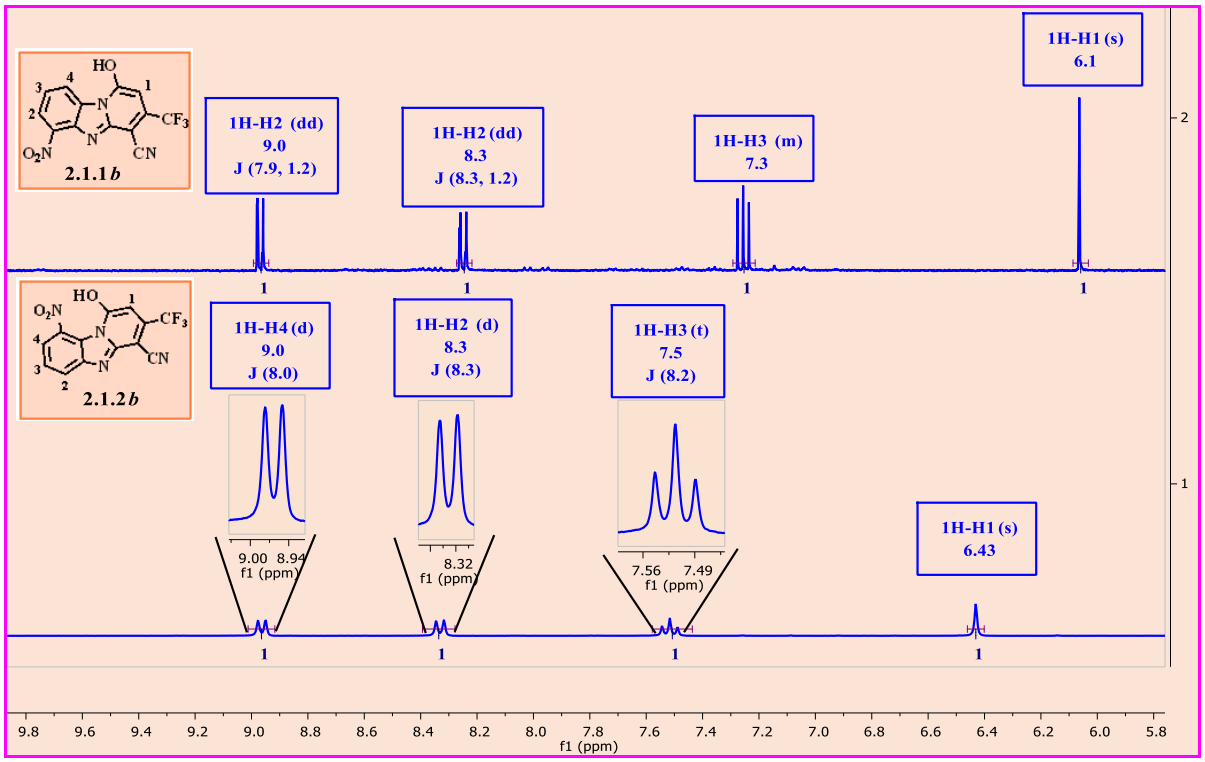

Figure 2.22: 1D ^{1}H nuclear magnetic spectra of the isomeric hydroxyl intermediates **2.1.1*b*** and **2.1.2*b*** in CD_3CN-d_3 at 400 MHz

Respective aromatic nucleophilic substitution reactions (SNAr, section 2.4) on hydroxyl-functionalized intermediate compounds **2.1.1*b*** and **2.1.2*b*** delivered the corresponding chlorinated compounds **2.1.1*c*** and **2.1.2*c*** (Fig. 2.22.1). The ^{1}H NMR spectrum (data not shown) was consistent with the structure of the chlorinated compounds. Consequently, the amination of **2.1.2*c*** produced the nitro-substituted intermediate compound **42**. The formation of compound **42** was confirmed via 1D ^{1}H NMR spectroscopy. The newly introduced *para*-substituted phenyl group resulted in the

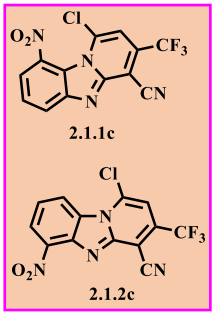

Fig. 2.22.1: The Chloro analogues **2.1.1c** &. **2.1.2c**

symmetrical and clear doublet peaks at approximately δ = 7.4 to 7.5 ppm corresponding to **H**^{5} and **H**^{6}, respectively (figure 2.23).

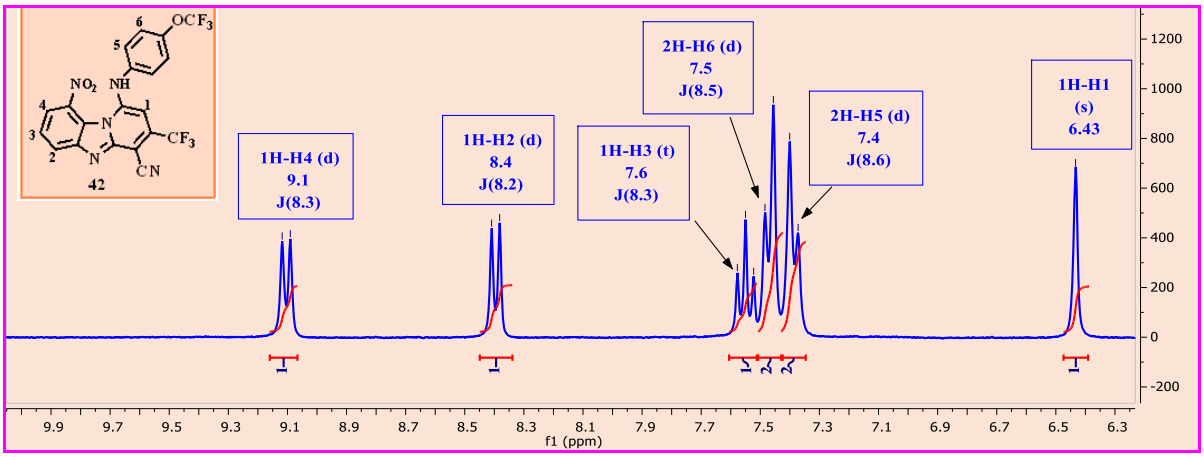

Figure 2.23: 1D ^{1}H nuclear magnetic resonance spectrum of compound **42**. The symmetric doublet peaks at approximately δ = 7.4 to 7.5 ppm confirm the amination and the presence of a *para*-substituted benzyl moiety in DMSO-d_6 at 300 MHz

The nitro group was selectively reduced to form compound **43,** whose structure was confirmed via 1D ^{1}H NMR spectroscopy. A singlet peak at δ = 3.3 ppm, which integrated for two upfield protons, was identified and corresponds to the new aniline protons (**H**^{5}, figure 2.24).

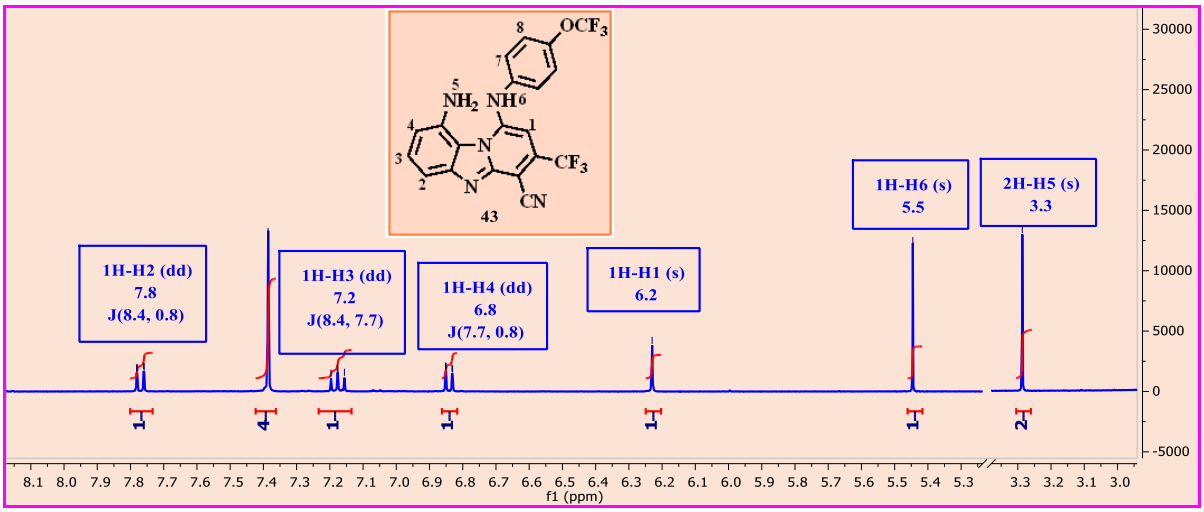

Figure 2.24: 1D ^{1}H nuclear magnetic resonance spectrum for compound **43**, showing a sharp singlet peak at δ = 3.3 ppm corresponding to the new aniline protons (**H**^{5}) in CD_3CN-d_3 at 400 MHz

The subsequent amidation of compound **43** with appropriate carboxylic acids led to the formation of the desired amide compounds **44** and **45,** as shown in figures 2.25 and 2.26.

Formation of the amide bond involves deprotonation of the substituent carboxylic acid by the nitrogen lone electron pair of EDCI, thereby making the imide carbon even more electrophilic

(figure 2.25). A nucleophilic attack on protonated EDCI by the carboxylate ion produced the *O*-acylisourea mixed ester, which was trapped by DMAP.[12] The addition of a suitable amino substrate to the activated complex (**Y**) led to the formation of the desired amide bond.

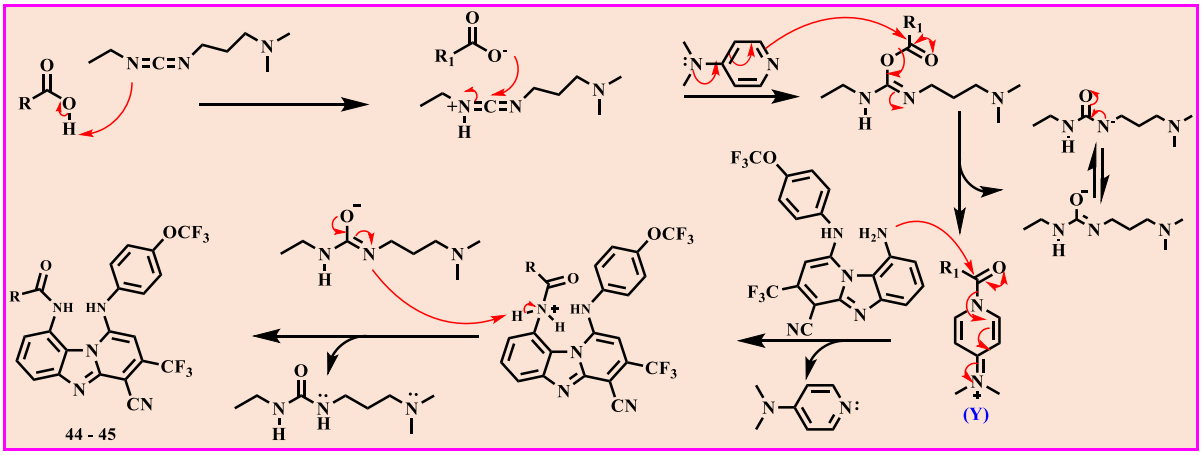

Figure 2.25: Amide bond formation mechanism[13,14]

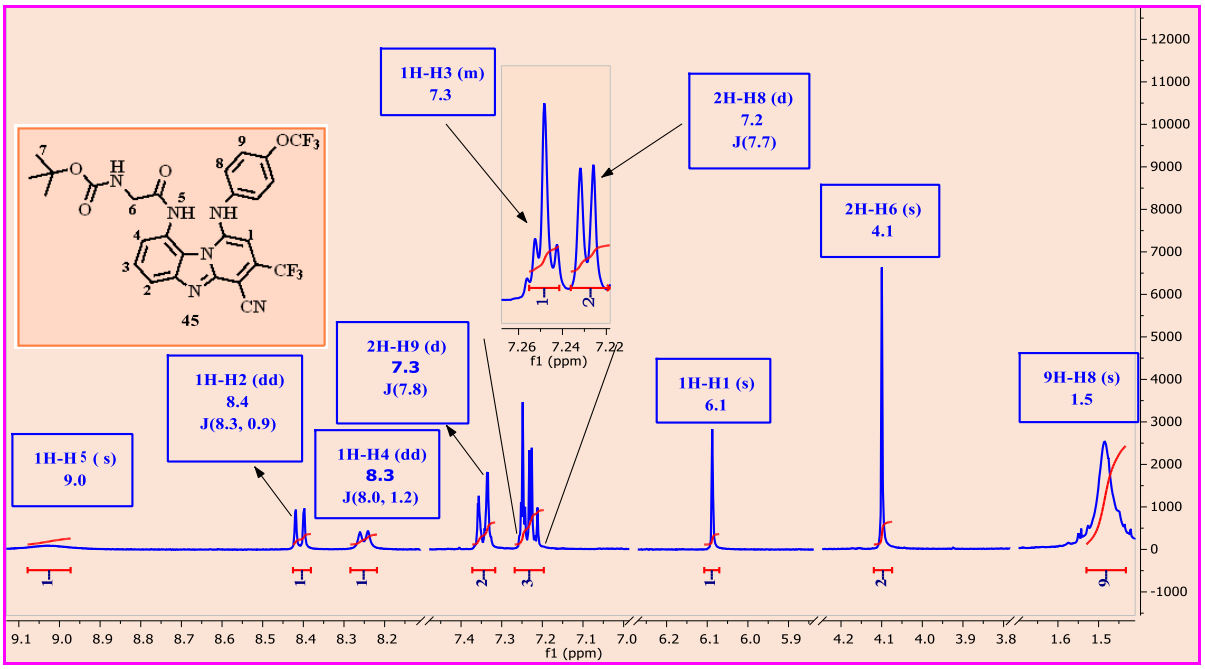

Figure 2.26: 1D ^{1}H nuclear magnetic resonance spectrum of amidated compound **45** showing the upfield singlet peaks corresponding to carbamate (**H**^{7}, δ = 3.3 ppm) and methylene protons (**H**^{6}, δ = 3.3 ppm) in CD_3CN-d_3 at 400 MHz

The appearance of upfield aliphatic proton signals corresponding to carbamate and methylene protons (**H**^{7}, δ = 1.5 ppm and **H**^{6}, δ = 4.1 ppm, respectively, figure 2.26), in addition to the other spectral features described earlier with regard to compound **43** (figure 2.24), confirmed the formation and the structure of amidated product compound **45**.

2.5.2 Synthesis of amine-substituted analogues

In addition to polar carbonyl-functionalized analogues, aryl-aminated analogues were also explored with regard to solubility improvement. The steps involved in the synthesis of aryl halide intermediates are outlined in figure 2.7 (steps *i-iv*), and the proposed formation mechanisms are similar to those outlined in figures 2.9, 2.11, and 2.14. A typical aryl chloride (**37**) (*ortho*-chloro*)* with its 1D ^{1}H NMR spectrum is shown in figure 2.27.

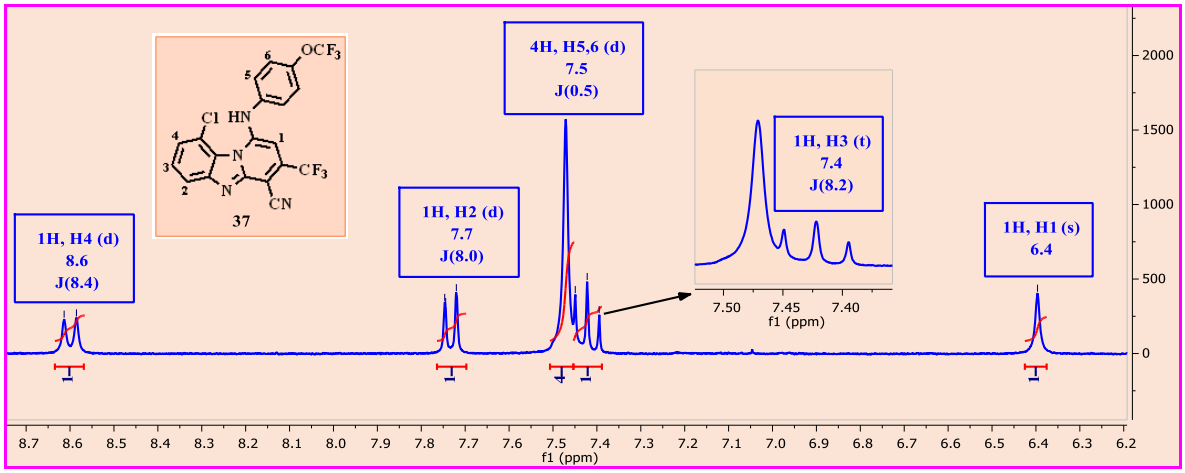

Figure 2.27: 1D ^{1}H nuclear magnetic resonance spectrum of compound **37**, showing the four methoxy aniline protons coalescing as a single peak in DMSO-d_6 at 300 MHz

A Buchwald-Hartwig amination reaction was conducted to transform aryl halides into target aryl amine analogues. as shown below in figure 2.28.

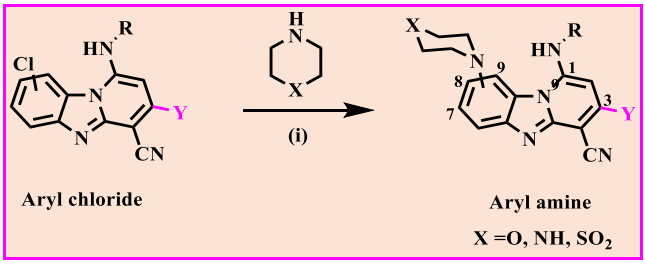

Figure 2.28: The Buchwald-Hartwig amination: reagents and conditions: i) amine, $Pd_2(dba)_3$, RuPhos, Cs_2CO_3, 1,4-dioxane/DMF, 80 to 110 °C[13]

The Buchwald-Hartwig cross-coupling reaction proceeds via a catalytic cycle as shown in figure 2.29. Four major steps, including oxidative addition, ligand coordination, transmetalation, and reductive elimination, are involved in completing this amination reaction. The oxidative addition of the aryl halide to the palladium (0) complex ($Pd_2(dba_3)$) catalyst occurs, after which the amine coordinates to the palladium metal centre. Deprotonation of the amine by a base, in this case, Cs_2CO_3, generates the highly nucleophilic amide ion, which then substitutes the chlorine atom. The final aminated product is formed via a reductive elimination

step while the ligand-bound palladium (Pd(0)) catalyst is regenerated to continue the cycle (figure 2.29).[5]

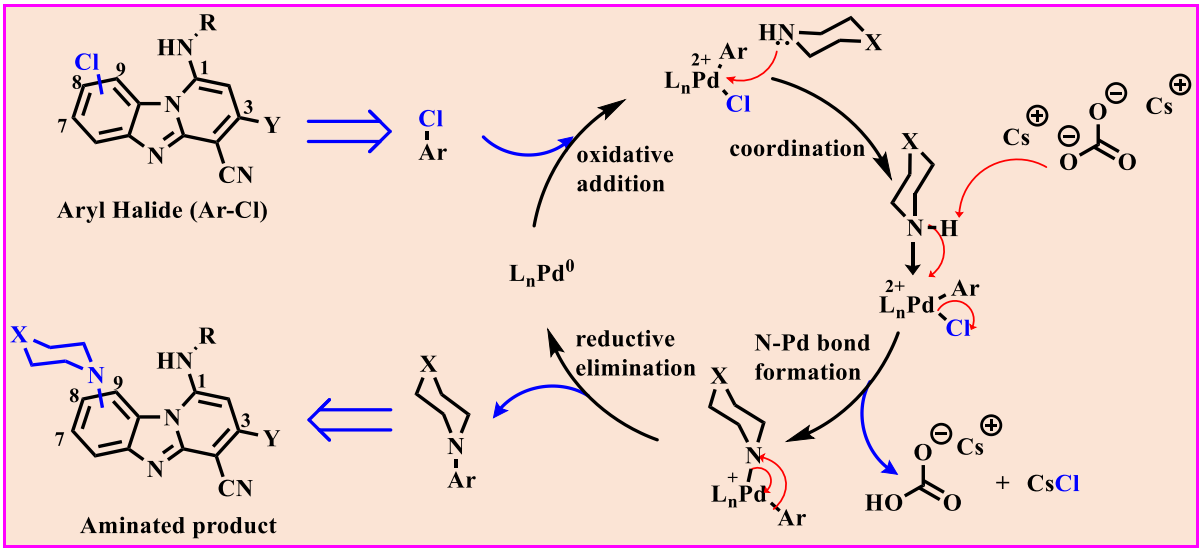

Figure 2.29: Catalytic cycle for the Buchwald-Hartwig amination[7,15,16]

Analogues synthesized via the Buchwald-Hartwig cross coupling protocol shown in figure 2.29 include piperazinyl- and the morpholinyl-substituted analogues, among others. A representative Buchwald-Hartwig aminated analogue (**41**) and its 1D ^{1}H NMR spectrum is shown in figure 2.30. Successful amination was confirmed by the appearance of the symmetrical 1,1-dioxidothiomorpholinyl signals in the aliphatic region upfield. The well-resolved triplet peaks identified at δ = 4.2 ppm and δ = 3.2 ppm correspond to **H^{5}** and **H^{6}**, respectively, integrating for four methylene protons (**4H**) each. Furthermore, thiomorpholinyl signals were identified with very close spin-spin coupling constants (**H^{5}** and **H^{6}**, *J* = 5.2 and 5.2 Hz, respectively) suggesting that the protons **H^{5}** and **H^{6}** are next to each other. Moreover, the four protons of the *para*-substituted phenyl group resonated into unclearly resolved symmetrical signals integrating for four (04) protons (**4H$^{7,\ 8}$** δ = 7.4 ppm) in the aromatic region. Although the symmetry of the phenyl signal was not clearly separated into the expected doublet peaks, it was not as coalesced as was observed for compound **37** (figure 2.27).

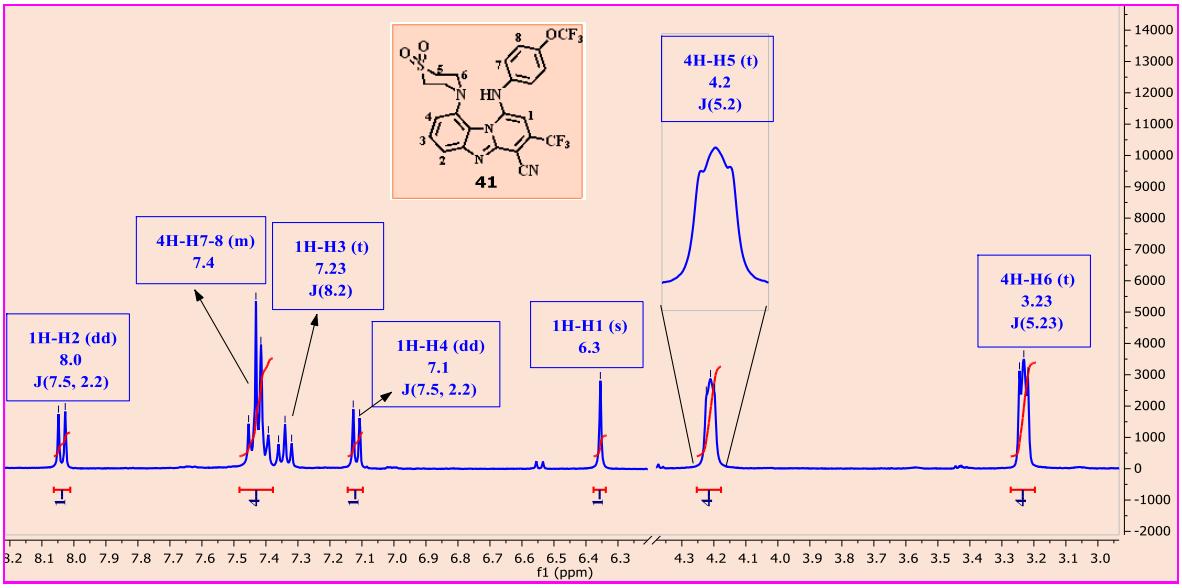

Figure 2.30: 1D ^{1}H nuclear magnetic resonance spectrum of compound **41** showing typical thiomorpholine dioxide protons signals upfield in CD_3CN-d_3 at 400 MHz

Generally, the *ortho*-substituted aryl amine target analogues were obtained in low yields presumably due to the competitive and dominant formation of the dehalogenated-hydrogenated by-product shown in figure 2.30.1. The bulkiness of the cyclic amine moiety may have affected ligand coordination during the amination process at 9th position (*ortho*) of the core-scaffold leading to 90% formation of the side-product at the expense of the desired product whenever amination was attempted at this position. On the other hand, the *meta* position (C-7) was less sterically hindered and thus readily facilitated amine couplings. Highly improved yields (>70%) were accordingly observed. An example of a *meta*-aminated target analogue (**49**) and its 1D ^{1}H NMR spectrum are shown in figure 2.31 below. Diagnostic spectral features include a high number of aliphatic signals upfield. Here, a triplet peak that integrated for six protons (**6H**) at δ = 1.1 ppm corresponding to two methyl group protons (**H^{11}**) was observed. Additionally, a well-resolved quartet that integrated for four protons (**4H**, **H^{10}**) corresponding to the two electronically equivalent methylene groups was identified slightly downfield at δ = 2.8 ppm. Moreover, the presence of the symmetrical triplet peaks corresponding to the methylene protons **2H^{9}** and **2H^{8}** (δ = 3.0 and 3.6 ppm, J = 5.9 and 6.1 Hz, respectively) further indicated the presence of the ethylene linker of the basic side chain (figure 2.31).

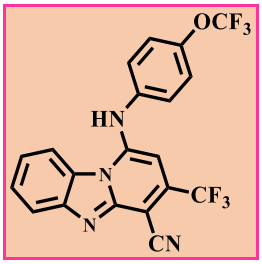

Fig. 2.30.1: Structure of the arene: halogenated-hydrogenated by-product

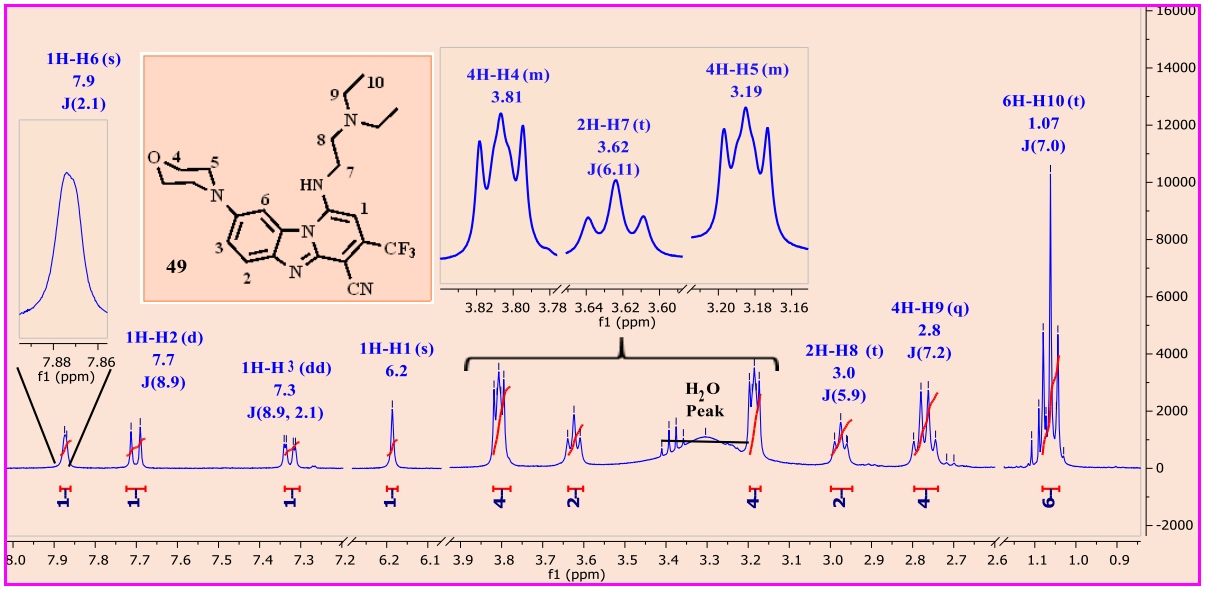

Figure 2.31: 1D ^{1}H nuclear magnetic resonance spectrum of the morpholine-acyclic-base substituted final analogue **49** in DMSO-d_6 at 400 MHz

Moreover, the presence of the morpholino group was identified by the appearance of two symmetrical morpholinyl multiplet peaks that integrated for four protons (**4H**) each at δ = 3.8 ppm and δ = 3.2 ppm, corresponding to the methylene protons $\mathbf{H^4}$ and $\mathbf{H^5}$. Additionally, the *meta*-aminated core scaffold was distinguished from the *para*-substituted by the existence of a doublet peak (J = 2.1 Hz) that integrated for one proton (**1H**, $\mathbf{H^6}$) resonating downfield at δ = 7.9 ppm. Its poorly resolved doublet peak is rationalized by the small spin-spin coupling constant resulting from long-range coupling with $\mathbf{H^3}$ Additionally, a dd peak that integrated into one proton $\mathbf{H^3}$ (J = 8.9, 2.1 Hz) was identified at δ = 7.3 ppm. This splitting pattern is explained by the strong vicinal spin-spin coupling of $\mathbf{H^3}$ with $\mathbf{H^2}$ and long-range coupling with $\mathbf{H^6}$, respectively. Finally, as expected, $\mathbf{H^2}$ split into a clear doublet that was identified at δ = 7.7 ppm (J = 8.9) due to strong vicinal spin-spin coupling with $\mathbf{H^3}$.

A total of 55 analogues were synthesized for SAR/SPR studies. 1D ^{1}H NMR spectroscopy was used to characterize the synthesized analogues. The characterization details are outlined in Chapter 6. The 1D ^{1}H NMR results were consistent with the various structures of the analogues and no advanced techniques were employed to complete the characterization of any compound. The analogues were submitted for solubility and *in vitro* pharmacological evaluations. In the next chapter, the pharmacological activity and solubility of the compounds synthesized are discussed.

References

(1) Cui, J. J.; McTigue, M.; Kania, R.; Edwards, M. Case History: Xalkori™ (Crizotinib), a Potent and Selective Dual Inhibitor of Mesenchymal Epithelial Transition (MET) and Anaplastic Lymphoma Kinase (ALK) for Cancer Treatment; 2013; pp 421–434.

(2) Talele, T. T. Natural-Products-Inspired Use of the Gem -Dimethyl Group in Medicinal Chemistry. *J. Med. Chem.* **2018**, *61* (6), 2166–2210.

(3) Craig, P. N. Interdependence between Physical Parameters and Selection of Substituent Groups for Correlation Studies. *J. Med. Chem.* **1971**, *14* (8), 680–684.

(4) Thomas G. *Fundamentals of Medicinal Chemistry*; John Wiley &. Sons Ltd: London, **2003**.

(5) Ndakala, A. J.; Gessner, R. K.; Gitari, P. W.; October, N.; White, K. L.; Hudson, A.; Fakorede, F.; Shackleford, D. M.; Kaiser, M.; Yeates, C.; Charman, S. A.; Chibale, K. Antimalarial Pyrido[1,2- a]Benzimidazoles. *J. Med. Chem.* **2011**, No. 54, 4581–4589.

(6) Rida, S. M.; Soliman, F. S. G.; Badawey, E.-S. A. M.; El-Ghazzawi, E.; Kader, O.; Kappe, T. Benzimidazole Condensed Ring Systems. 1 . Syntheses and Biological Investigations of Some Substituted Pyrido[1,2- a]Benzimidazoles. *J. Heterocycl. Chem.* **1988**, *25* (4), 1087–1093.

(7) Paul, F.; Patt, J.; Hartwig, J. F. Palladium-Catalyzed Formation of Carbon-Nitrogen Bonds. Reaction Intermediates and Catalyst Improvements in the Hetero Cross-Coupling of Aryl Halides and Tin Amides. *J. Am. Chem. Soc.* **1994**, *116* (13), 5969–5970.

(8) Carpino, L. A.; El-Faham, A. The Diisopropylcarbodiimide/ 1-Hydroxy-7-Azabenzotriazole System: Segment Coupling and Stepwise Peptide Assembly. *Tetrahedron* **1999**, *55* (22), 6813–6830.

(9) Figlus, M.; Tarruella, A. C.; Messer, A.; Sollis, S. L.; Hartley, R. C. Low Molecular Weight MPEG-Assisted Organic Synthesis. *Chem. Commun.* **2010**, *46* (24), 4405.

(10) Al-Warhi, T. I.; Al-Hazimi, H. M. A.; El-Faham, A. Recent Development in Peptide Coupling Reagents. *J. Saudi Chem. Soc.* **2012**, *16* (2), 97–116.

(11) Jacobsen, J. P.; Schaumburg, K. 1H and 2H NMR Spectra of Chlorobenzene and Bromobenzene in Liquid Crystalline Phase. *J. Magn. Reson.* **1977**, *28* (1), 1–7.

(12) Rebek, J.; Feitler, D. Mechanism of the Carbodiimide Reaction. II. Peptide Synthesis on the Solid Phase. *J. Am. Chem. Soc.* **1974**, *96* (5), 1606–1607.

(13) Rebek, J.; Feitler, D. Improved Method for the Study of Reaction Intermediates. Mechanism of Peptide Synthesis Mediated by Carbodiimides. *J. Am. Chem. Soc.* **1973**,

No. 95, 4052–4053.

(14) Montalbetti, C. A. G. N.; Falque, V. Amide Bond Formation and Peptide Coupling. *Tetrahedron* **2005**, *61* (46), 10827–10852.

(15) Hartwig, J. F.; Richards, S.; Baran, D. Influences on the Relative Rates for C - N Bond-Forming Reductive Elimination and -Hydrogen Elimination of Amides . A Case Study on the Origins of Competing Reduction in the Palladium-Catalyzed Amination of Aryl Halides. **1996**, No. 11, 3626–3633.

(16) Guram, A. S.; Buchwald, S. L. Palladium-Catalyzed Aromatic Aminations with in Situ Generated Aminostannanes. *J. Am. Chem. Soc.* **1994**, *116*, 7901–7902.

3. PHARMACOLOGICAL AND SOLUBILITY EVALUATION

3.1 Introduction

In this chapter, the *in vitro* antiplasmodium activity against asexual blood-stage parasites, gametocytocidal and antischistosomal activities, as well as the solubility of the synthesized PBI target compounds are discussed. The antiparasitic activities of the analogues were evaluated in the chloroquine-sensitive NF54 (SAR 1.1 to 1.4 and SAR 2.1 to 2.4 compounds) and the chloroquine-resistant K1 (SAR 2.1 to 2.4) strains of the human malaria parasite *P. falciparum.* Furthermore, the *in vitro* antischistosomal activities of SAR 1.1 to 1.4 analogues were assessed against both newly transformed schistosomula (NTS) and adult worms or adult liver flukes of *Schistosoma mansoni*. SAR 2.1 to 2.4 analogues were only screened against the adult liver flukes of *S. mansoni*. Besides the antiparasitic activities, compound solubility is also discussed here.

3.2 SAR 1: Assessment of the solubility and *in vitro* antiplasmodium, gametocytocidal, and antischistosomal activities of SAR 1.1 to 1.4 analogues

Here, the 4-(trifluoromethoxy)aniline moiety at C-1 on the pyridyl ring of **GMP-19** was replaced with various α-methylbenzylamine moieties (figure 3.1).

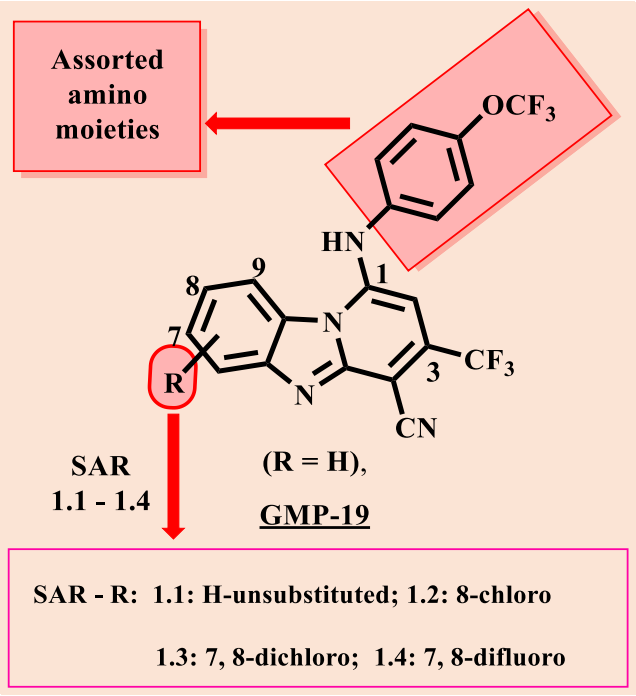

Figure 3.1: Design of SAR 1.1 to 1.4 analogues

Various moieties were incorporated to introduce moderate saturation and to potentially disrupt molecular planarity. Indeed, the introduction of saturation has been shown to lead to improved

solubility.[1,2] Furthermore, although electron-withdrawing atoms such as fluoro and chloro groups were incorporated on the phenyl ring at C-7 and C-8, the 3-CF_3 group on the pyridyl ring of the PBI core was kept constant. Previous studies have shown that the left-hand side (LHS) phenyl ring of the PBI core is a metabolic hotspot (Mayoka, unpublished data). In efforts to potentially block metabolism on this site, fluoro and chloro groups were appended onto the LHS phenyl ring. This is in view of the fact that drug molecules containing electron-withdrawing groups undergo reduced cytochrome P450 (CYP)-mediated oxidation.[3,4] A diverse set of target compounds with varying antiparasitic activities and solubility were identified. The *in vitro* antiplasmodium and antischistosomal activities and solubility values are summarized in figure 3.2.

3.2.1 Assessment of the solubility and *in vitro* antiplasmodium activities of SAR 1 analogues

A PBI core scaffold with no substitution on the phenyl ring was used in the first phase of this SAR study (figure 3.2). Fully saturated amino moieties such as (*R*) and *S*-1-cyclohexylethan-1-amine (analogues **1** and **2**) were randomly sampled and incorporated at C-1 of the PBI core. However, these substitutions were detrimental to antiplasmodium activity (**1**, IC_{50} = 3.070 μM; and **2**, IC_{50} = 2.757 μM) relative to IC_{50} = 0.430 μM of the frontrunner **GMP-19**. Additionally, both analogues demonstrated poor solubility (< 10 μM), which may be attributed to the highly lipophilic nature of the incorporated substituents. In the same SAR, α-carboxylate benzylamine-substituted analogues and their corresponding amide derivatives exhibited improved solubility at the expense of antiplasmodium activity. In this regard, the methyl ester **3** (solubility = 30 μM), its carboxylic acid form **4** (solubility = 150 μM), and the 1,1-dioxidothiomorpholinyl amidated derivative **5** (solubility = 50 μM) exhibited 6-, 30-, and 10-fold increases in solubility, respectively, compared to **GMP-19** (solubility = 5 μM). All three analogues (IC_{50} = 6.000 μM) exhibited a 14-fold reduction in antiplasmodium potency relative to **GMP-19** (IC_{50} = 0.430 μM, figure 3.2). Furthermore, the effect of introducing an electron-withdrawing group on the phenyl ring of the substituent benzylamine was investigated. Although not as active as **GMP-19**, the *para*-fluorinated racemic compound **6** (IC_{50} = 1.274 μM) demonstrated a 5-fold increase in potency compared to compounds **1** to **5,** but a 3-fold reduction in potency compared to **GMP-19**. Compound **7**, the resolved pure *R*-enantiomer, showed even higher activity (IC_{50} = 0.875 μM), with a 2-fold increase in antiplasmodium potency compared to the racemic form, compound **6,** and the *S*-enantiomer, compound **8** (IC_{50} = 2.039 μM).

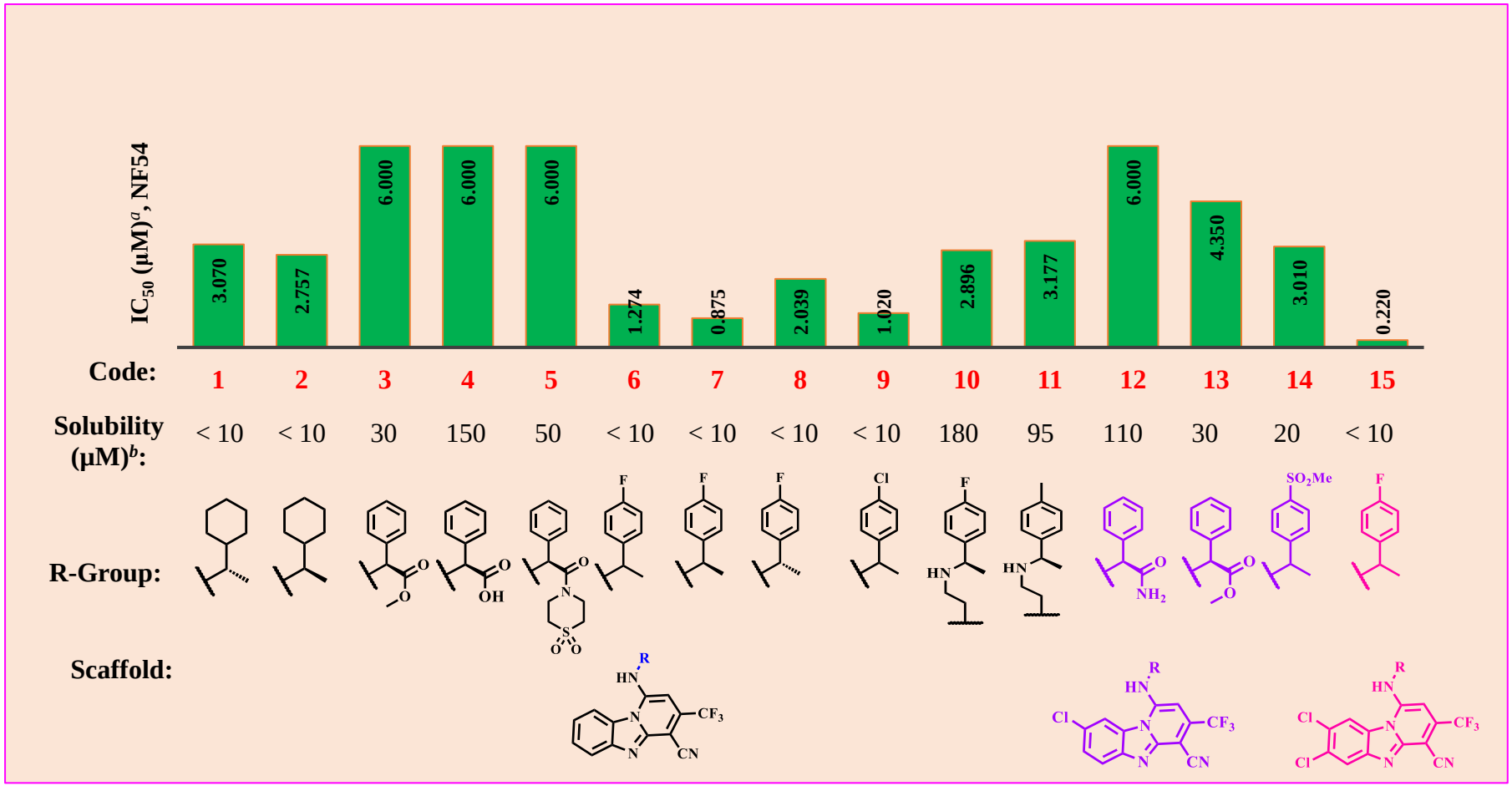

Figure 3.2: Solubility and *in vitro* antiplasmodium activity of SAR 1.1 to 1.3 compounds

SAR 1.1, black; SAR 1.2, purple, and SAR 1.3, pink

[a]Mean values were calculated from at least two independent experiments on the *P. falciparum* strain NF54 (individual values within ± 2-fold). Artesunate (IC_{50} = 0.007 µM) and chloroquine (IC_{50} = 0.012 µM) were used as reference drugs.

[b]Determined using a turbidimetric method[5]

Thus, the reduced activity of the racemic form **6** may be attributed to the antagonistic effect of the *S*-enantiomer. In addition, compound **9** (IC_{50} = 1.020 μM), a racemate similar to the fluoro-substituted analogue **6** but possessing a chloro group, was equipotent to compound **6**. This indicates that the nature of the halogen at the *para* position of the substituent phenyl ring is irrelevant to antiplasmodium potency. Furthermore, incorporating a 2-carbon methylene spacer between the two nitrogen atoms (the PBI core scaffold-linked N and the α-methylene carbon-linked N of the substituent benzylamine moiety) resulted in improved solubility at the expense of biological activity, as demonstrated by compounds **10** and **11** (**10**: solubility = 180 μM, IC_{50} = 2.896 μM; **11**: solubility = 150 μM, IC_{50} = 3.177 μM), which exhibited 2- and 7-fold lower antiplasmodium activity relative both compounds **10**, **11** and **GMP-19**, respectively.

The next phase of SAR exploration involved introducing substitutions on the phenyl ring of the PBI core scaffold. Initially, a mono-substitution involving a chloro atom was introduced on the phenyl ring of the core scaffold at C-8. The effect of 8-chloro substitution on antiplasmodium activity was evaluated at the same time, thus providing prospects for SAR expansion. The poor antiplasmodium activity of compound **13** (IC_{50} = 4.35 μM) was comparable to that of the unsubstituted compound **3** (IC_{50} = 6.00 μM). Generally, 8-chloro mono-substitution had a negative impact on antiplasmodium activity. Compounds **12**, **13,** and **14** showed 14-, 10-, and 7-fold decreases in potency relative to that of **GMP-19**. Although poor antiplasmodium activity was demonstrated, the amide-substituted analogue **12** exhibited the highest improvement in solubility (solubility = 80 μM) compared to the other two analogues **13** and **14** (solubility = 30 and 20 μM, respectively). The difference in solubility between the amide-substituted compound **12** and the methyl ester-substituted compound **13** may be attributed to the enhanced hydrogen-bond donor and acceptor properties of compound **12**.

In the next SAR study, double substitution on the phenyl ring of the core scaffold was investigated. This modification resulted in drastically improved antiplasmodium activity, as demonstrated by the 7,8-dichlorinated analogue **15** (IC_{50} = 0.220 μM, figure 3.2). Although this analogue exhibited the strongest antiplasmodium activity compared to both **GMP-19** and the rest of the compounds in SAR 1, further generation of dichlorinated analogues in this series was not undertaken due to the increased lipophilicity in such analogues. Thus, substitutions that could provide reduced lipophilicity while retaining antiplasmodium activity were explored. Consequently, the chloro groups in compound **15** were replaced with fluoro atoms, producing a slightly less lipophilic 7,8-difluorinated racemic analogue (compound **16**, figure

3.3). Interestingly, compound **16** demonstrated improved antiplasmodium activity (IC_{50} = 0.140 μM) and was three times more potent compared to **GMP-19**. This increase in pharmacological activity triggered interest in the respective pure enantiomers. The pure *R*-enantiomer (compound **17)** demonstrated even greater antiplasmodium potency (IC_{50} = 0.022 μM), with 7- and 20-fold improvements in antiplasmodium activity compared to the racemic analogue compound **16** and the front-runner compound **GMP-19**, respectively. This indicates that the *S*-enantiomer may be antagonizing the antiplasmodium activity of its *R*-counterpart. However, the *S*-enantiomer should be obtained and tested to confirm these hypotheses. Similarly, while the fluoro groups were maintained at the C-7 and C-8 positions of the PBI core scaffold, the fluoro atom at the *para*-position of the α-methylbenzylamine moiety was replaced with a chloro atom to produce a racemic analogue (compound **18**). The resulting racemic mixture was three times more potent (IC_{50} = 0.051 μM) than the corresponding *para*-fluorophenyl-based racemic compound **16**. Unfortunately, the enantiomerically pure derivatives of compound **18** could not be obtained as none of the pure forms of the amine starting materials were available at the time of completing the programme. Furthermore, as the 7,8-difluoro substitution on the phenyl ring of the PBI core was maintained, the introduction of additional Craig plot substituents possessing positive and negative inductive effects on the phenyl ring of the α-methylbenzylamine moiety was investigated. The unsubstituted pure enantiomeric compounds **19** (*S*) and **20** (*R*) served as controls for the enantiomerically pure analogues, which demonstrated similar sub-micromolar antiplasmodium activities (IC_{50} = 0.340 and 0.250 μM, respectively, figure 3.3).

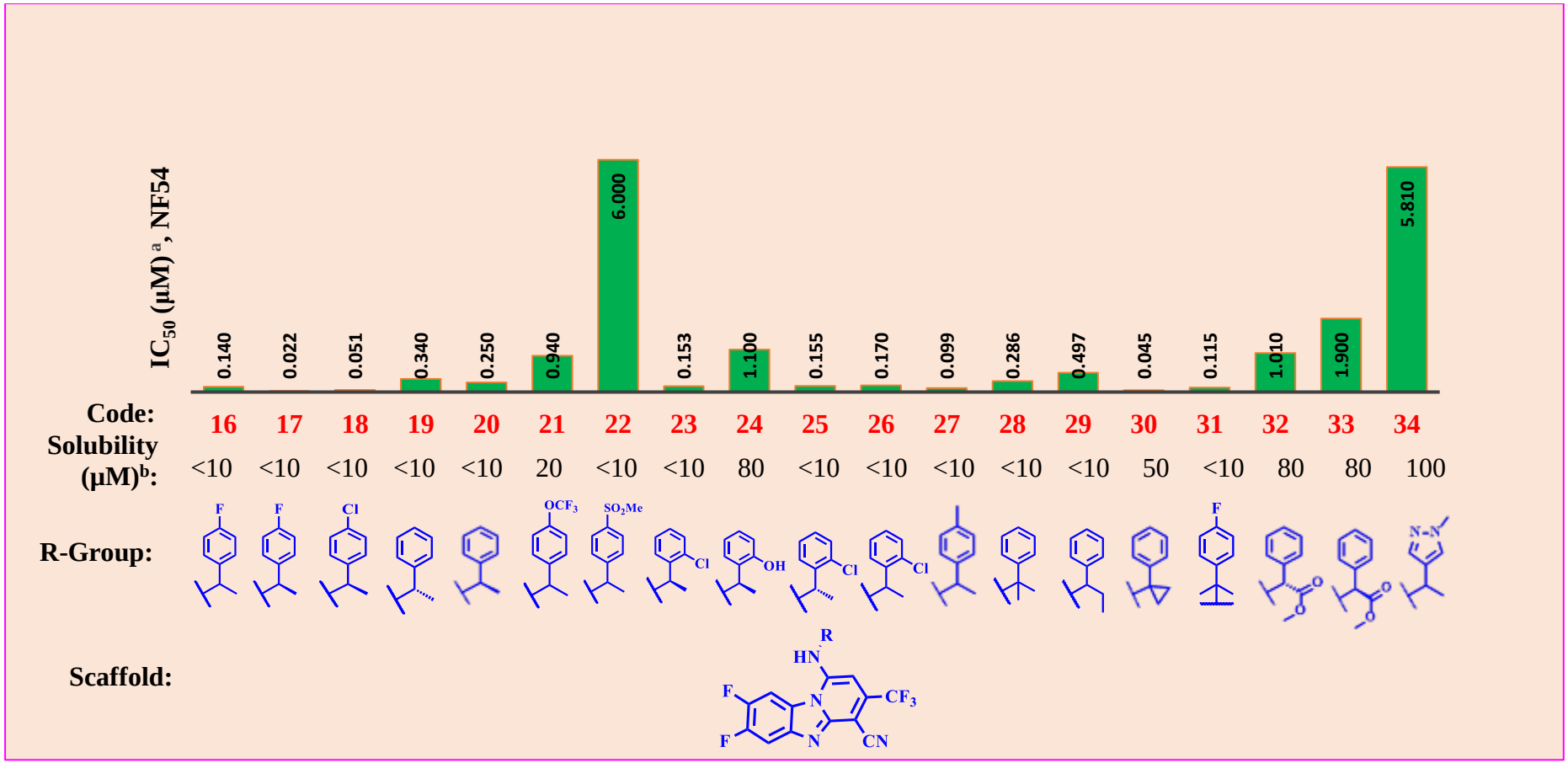

Figure 3.3: Solubility and *in vitro* antiplasmodium activity of SAR 1.4 compounds

[a]Mean values were calculated from at least two independent experiments on the *P. falciparum* strain NF54 (individual values within ± 2-fold). Artesunate (IC_{50} = 0.007 µM) and chloroquine (IC_{50} = 0.012 µM) were used as reference drugs.

[b]Determined using a turbidimetric method[5]

Amongst the representative substituent groups, the OCF_3-substituted analogue **21** (IC_{50} = 0.940 μM) exhibited higher antiplasmodium activity than the sulfone-substituted compound **22** (IC_{50} = 6.000 μM). In addition, although the *ortho*-chloro *R*-α-methylbenzylamine-substituted compound **23** (IC_{50} = 0.153 μM) demonstrated equipotent antiplasmodium activity compared to the unsubstituted analogue **20** (IC_{50} = 0.250 μM), its *S*-counterpart (**25,** IC_{50} = 0.155 μM) demonstrated a 2-fold increase in potency relative to compound **19** (IC_{50} = 0.340 μM). Similarly, the enantiomerically pure isomers **23** and **25** demonstrated equipotent antiplasmodium activities (IC_{50} = 0.153 and 0.155 μM, respectively), thus suggesting that potency is not stereoselective. Similarly, the *ortho*-chloro racemate forms **26**, **25** (*S*), and **23** (*R*; IC_{50} = 0.153, 0.155, and 0.170 μM, respectively) all demonstrated equipotent activity relative to each other. Furthermore, the substitution of the H with an OH group on the *ortho* position resulted in significant loss of antiplasmodium activity as demonstrated by compound **24** (IC_{50} = 1.100 μM), which exhibited a 4-fold decrease in antiplasmodium activity relative to the unsubstituted compound **20**. Additionally, when the electron-withdrawing and electron-donating groups were compared, the *ortho*-chloro analogue **23** exhibited greater activity (IC_{50} = 0.153 μM) than the *ortho*-phenolic analogue **24** (IC_{50} = 1.100 μM). This demonstrates a 7-fold increase in potency in favour of the lipophilic electron-withdrawing chloro group. Additionally, as demonstrated by the racemic mixtures **18** (*para*, IC_{50} = 0.051 μM) and **26** (*ortho*, IC_{50} = 0.170 μM), *para*-chloro substitution resulted in a 3-fold increase in activity compared to *ortho* substitution. Moreover, the racemic *para*-tolylamine-substituted analogue **27** (IC_{50} = 0.099 μM) exhibited comparable activity to the *para*-fluoro compound **16** (IC_{50} = 0.140 μM) and demonstrated a 2-fold decrease in potency compared to the *para*-chloro-substituted analogue **18** (IC_{50} = 0.051 μM). Furthermore, compound **27** demonstrated 9- and >60-fold increases in antiplasmodium potency relative to the electron-rich OCF_3-substituted analogue **21** (IC_{50} = 0.940 μM) and the sulfone moiety-substituted analogue **22** (IC_{50} = 6.000 μM), respectively. The effect of lipophilic benzylamine substituent moieties and the corresponding activity can be summarized as follows: chloro (**18**: IC_{50} = 0.051 μM) > methyl (**27**: IC_{50} = 0.099 μM) > fluoro (**16**: IC_{50} = 0.140 μM) > OCF_3 (**21**: IC_{50} = 0.940 μM).

Further antiplasmodium SAR studies on the 7,8-difluorinated PBI core scaffold involved variations on the α-methylene carbon of the α-methylbenzylamine moieties. The α-cyclopropyl-substituted benzylamine moiety conferred the greatest potency to compound **30** (IC_{50} = 0.045 μM), while the α-germinal dimethylbenzylamine-substituted analogue **28** (IC_{50} = 0.286 μM) and the α-ethylbenzylamine-substituted analogue **29** (IC_{50} = 0.497 μM) showed

lower activities. The closed ring cyclopropyl group at the α-carbon in compound **30** appears to be crucial to antiplasmodium potency, with 6- and 11-fold increases in activity observed in relation to its linear counterparts **28** and **29,** respectively. α-Carboxylate benzylamine substituents on the same 7,8-difluorinated core scaffold were revisited. Although a significant improvement in the antiplasmodium activities of the α-carboxylate benzylamine analogues was achieved compared to the unsubstituted versions shown in figure 3.2, the carboxylate analogues generally exhibited lower activity (*S*-enantiomer **32**: IC_{50} = 1.010 μM, and *R*-enantiomer **33**: IC_{50} = 1.900 μM, figure 3.3). A snapshot contracted heterocyclic aromatic amine SAR revealed significant loss in antiplasmodium activity from the five-membered ring pyrazolylamine-substituted analogue **34** (IC_{50} = 5.810 μM).

A few analogues of the 7,8-difluorinated PBI core scaffold exhibited encouraging solubility profiles. Although only one analogue (**30**) of this part of the SAR also demonstrated sub-micromolar antiplasmodium activity (IC_{50} = 0.045 μM), the other analogues demonstrated high solubility at the expense of *in vitro* antiplasmodium potency. The *para*-phenolic compound **24** (solubility = 80 μM), α-carboxylate compounds **32** and **33** (solubility = 80 μM), and the pyrazolylamine-substituted analogue **34** (solubility = 80 μM) were amongst the analogues showing encouraging solubility but low antiplasmodium potency. The OCF_3-substituted analogue **21** (solubility = 20 μM) showed low solubility in combination with sub-micromolar antiplasmodium potency. Unfortunately, the rest of the compounds in this series demonstrated poor solubility (< 10 μM).

3.2.2 *In vitro* gametocytocidal activity evaluation of SAR 1 analogues

In this section, the gametocytocidal activities of the previously described α-methylbenzylamine-substituted PBI analogues are discussed. Preliminary evaluation of these analogues revealed potency at both the early and late stages of gametocytogenesis. Their inhibitory effects were determined after treatment with 1.0 and 5.0 μM (figure 3.4). Interestingly, some analogues showed gametocytocidal activity at both the early and late stages.

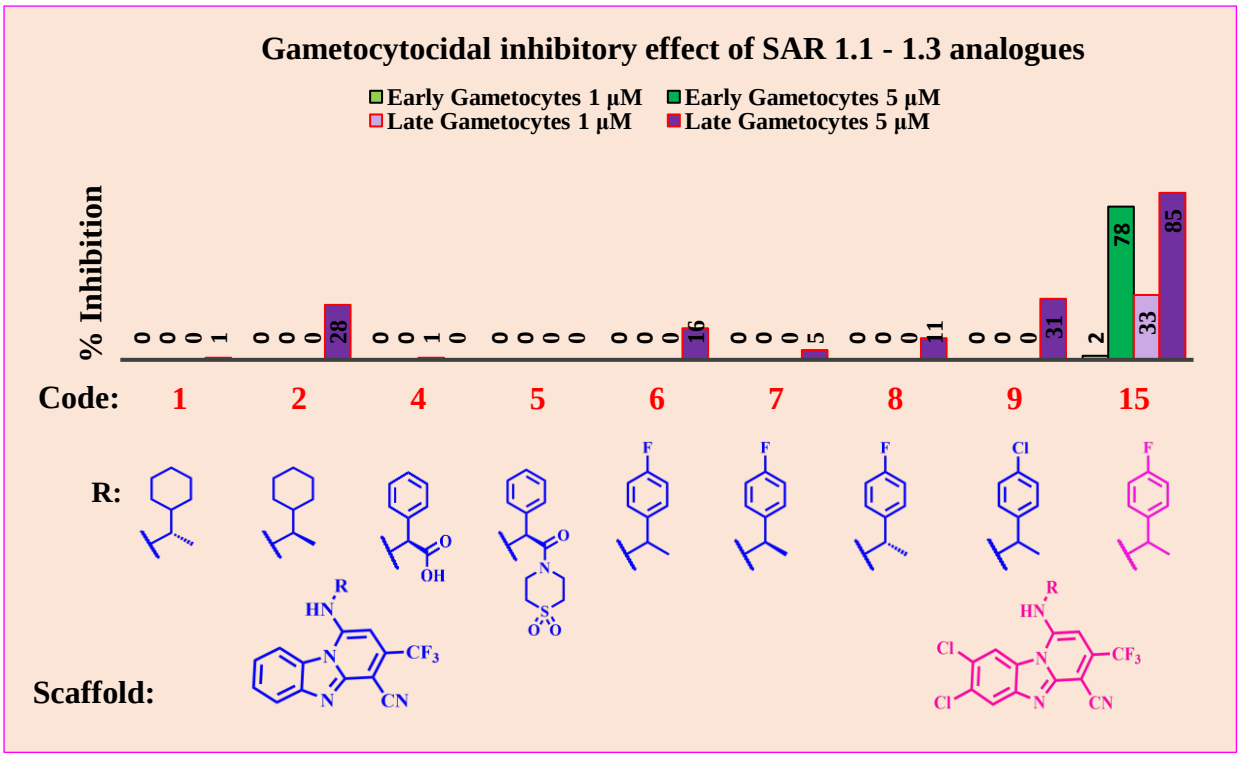

	Reference drugs (1.0 µM)	Early gametocytes	Late gametocytes
1	**Methylene blue**	93% (luc)	90% (luc), 50% (ATP)
2	**Dihydroartemisinin**	75% (luc)	70% (luc), 15% (ATP)
3	**MMV048**	77% (n=3)	92% (n=3)

Figure 3.4: *In vitro* gametocytogenesis inhibitory effect of SAR 1.1 to 1.3 compounds on early- and late-stage *Plasmodium falciparum* NF54 gametocytes

luc**,** parasite viability measured via luciferase reporter assay; ATP**,** parasite viability measured via ATP bioluminescence assay[6]

Although the monochlorinated core scaffold (SAR 1.2) exhibited inactivity at the sexual stages of parasite development, analogues derived from the unsubstituted phenyl ring of the core scaffold displayed <32% gametocytogenesis inhibition at both 1.0 and 5.0 µM test concentrations. Analogue **15**, which contained a 7,8-dichlorinated core scaffold, demonstrated significant improvement in gametocytocidal activity at 5 µM. However, this compound exhibited approximately 37- and 3-fold decreases in potency against the early and late stages of parasite development, respectively, at 1.0 µM relative to the control drug and Phase II clinical candidate MMV048. Moreover, the analogues derived from a 7,8-difluorinated core scaffold generally exhibited significantly improved gametocytocidal activity (figure 3.5). Compound **16** showed 15 and 72% inhibition of early- and late-stage parasites at 1.0 µM, respectively, or 7- and 2-fold increases in potency relative to analogue **15**. Additionally, compound **16** exhibited late-stage activity at 1.0 µM equal to that of **MMV048** (72 and 92% inhibition at 1.0 µM for compound **16** and **MMV048**, respectively), and 5-fold lower early-

stage gametocyte inhibition (15 and 77% early-stage inhibition at 1.0 µM, respectively). Furthermore, compound **16** (racemate) demonstrated equipotent gametocytocidal activity to that of the pure *R*-enantiomer **17** (15 and 19% early-stage inhibition at 1.0 µM, 88 and 90% early-stage inhibition at 5.0 µM, 72 and 77% late-stage inhibition at 1.0 µM, and 88 and 90% late-stage inhibition at 5.0 µM for compounds **16** and **17**, respectively). Moreover, although compound **16** exhibited late-stage activity comparable to that of compound **18**, a 2-fold increase in early-stage gametocytocidal potency was observed relative to compound **16** (19 and 42% inhibition at 1.0 µM for compounds **16** and **18**, respectively). In addition, the presence of a fluoro atom on the *para*-position of the benzylamine ring was essential to gametocytocidal activity, as was demonstrated by the lack of activity of the unsubstituted *R*-enantiomer (compound **20**). Furthermore, replacement of a fluoro or chloro group with OCF_3, SO_2Me, or Me was detrimental to gametocytocidal activity, as was demonstrated by compounds **21**, **22,** and **27,** which generally exhibited poor activity at both the early and late stages of gametocytogenesis. In this regard, gametocytocidal activity appears to be favoured by electron-withdrawing lipophilic substituents on the benzylamine substituents as demonstrated by the >4-fold reduction in activity of the electron-rich analogue **24** (21% early-stage gametocytes inhibition at 5.0 µM) relative to that of the lipophilic analogue **25** (90% early-stage gametocyte inhibition at 5.0 µM). Although the open α-germ-dimethylbenzylamine-substituted analogue **28** and its isomeric analogue **29** exhibited negligible gametocytocidal activity, the α-cyclopropyl benzylamine-substituted analogue **30** demonstrated the highest early-stage gametocytocidal activity (72 and 97% inhibition at 1.0 and 5.0 µM, respectively). Although compound **30** only displayed stage-specific activity toward early gametocytes, this compound demonstrated activity equal to that of **MMV048** (77% inhibition at 1.0 µM) against this stage. The *R*- and *S*-α-carboxylate benzylamine-substituted analogues showed comparably low gametocytocidal activity. This weak activity is demonstrated by compounds **32** and **33** (56 and 64% inhibition at 5.0 µM, respectively) against late-stage gametocytes, while the 5-membered heterocyclic amine-substituted analogue **34** exhibited a complete lack of gametocytocidal activity.

Although some compounds such as **16**, **17**, **18,** and **25** demonstrated dual-stage activity, compound **30** exhibited stage-specific action against early gametocytes. Lipophilic substitutions conferred greater gametocytocidal activity relative to electron-rich hydrophilic substitutions.

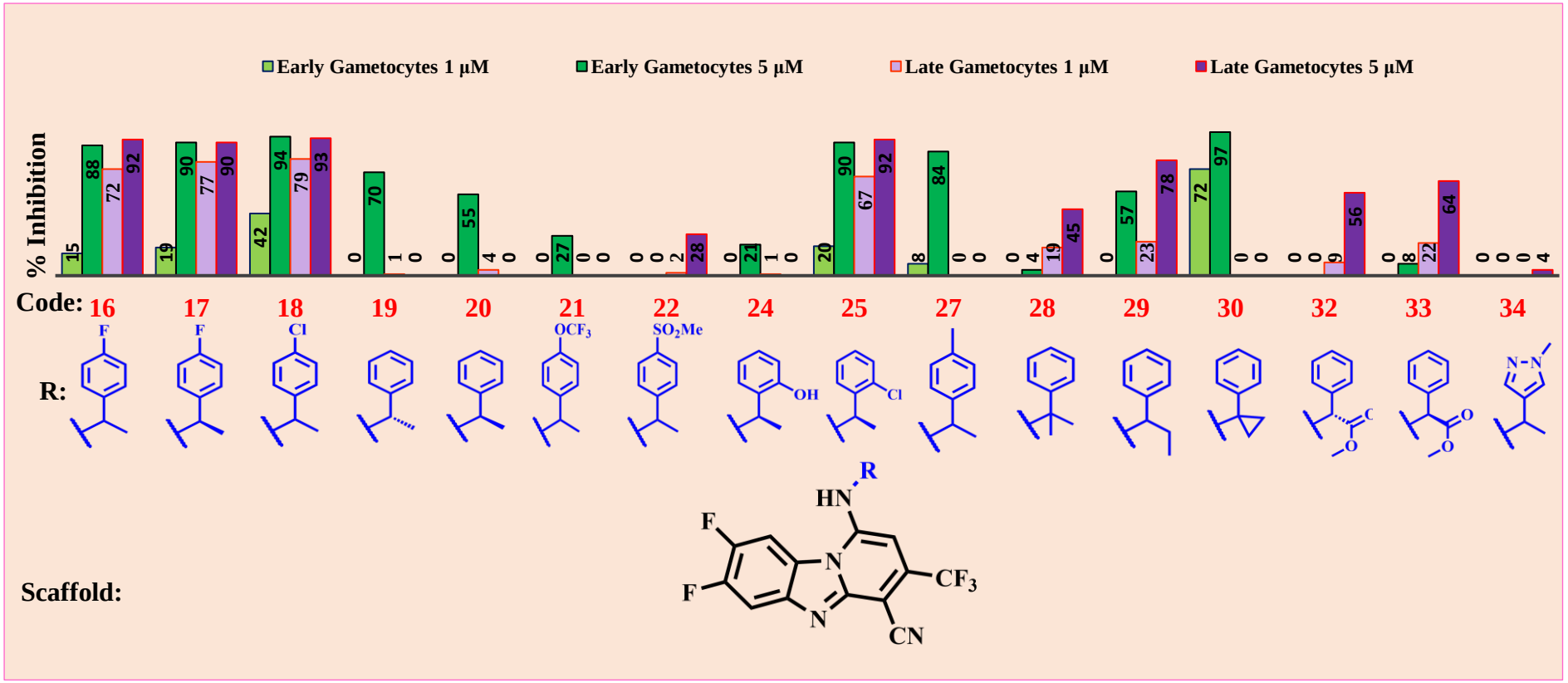

	Reference drugs	Early gametocytes	Late gametocytes
1	**Methylene blue**	93% (luc)	90% (luc), 50% (ATP)
2	**Dihydroartemisinin**	75% (luc)	70% (luc), 15% (ATP)
3	**MMV048**	77% (n=3)	92% (n=3)

Figure 3.5: *In vitro* gametocytogenesis inhibitory effect of SAR 1.4 compounds on early- and late-stage *Plasmodium falciparum* NF54 gametocytes

luc, parasite viability measured by luciferase reporter assay; **ATP**, parasite viability measured by ATP bioluminescence assay[6]

3.2.3 *In vitro* antischistosomal evaluation of SAR 1 analogues

This antischistosomal activity of the previously described α-methylbenzylamine-substituted PBI analogues is described here. Although the IC_{50} values of the analogues described here (compounds **1** to **34)** were not determined, a preliminary single-point screen of some of these compounds revealed strong antischistosomal properties. The compounds' inhibitory effects were determined at 10.00 µM, 1.00 µM, and 0.37 µM test concentrations. Interestingly, although a few analogues showed high activity against both NTS (juvenile worms) and adult schistosomes, most of the compounds tested showed greater inhibition against juvenile worms. Activity against NTS does not only attract attention for further exploration of this series of compounds but is also an indicator of the potential of this class of compounds to supplement the medical gap in treating schistosomiasis, as the current clinical drug (praziquantel) is only active against adult worms. Details of these compounds and their antischistosomal activities at various concentrations are presented in figures 3.6, 3.7, and 3.8.

3.2.4 *In vitro* activity against adult schistosomes

Except for the four analogues shown in figure 3.6, SAR 1.1 to 1.4 compounds generally demonstrated poor activity against adult schistosomes at both 10.00 µM and 1.00 µM. Of all the analogues synthesized from the unsubstituted ring of the PBI core (SAR 1.1), only three compounds (**6**, **7,** and **8**, figure 3.6) exhibited inhibitory effects (29 to 60% inhibition at 10.00 µM). Although inactivity was also observed with analogues bearing a 7,8-difluorinated PBI core scaffold (SAR 1.4), one analogue (compound **18**) demonstrated strong antischistosomal activity with 100% inhibition at both 10.00 and 1.00 µM, as shown in figure 3.6. Other compounds showed no activity and are therefore not included in this figure.

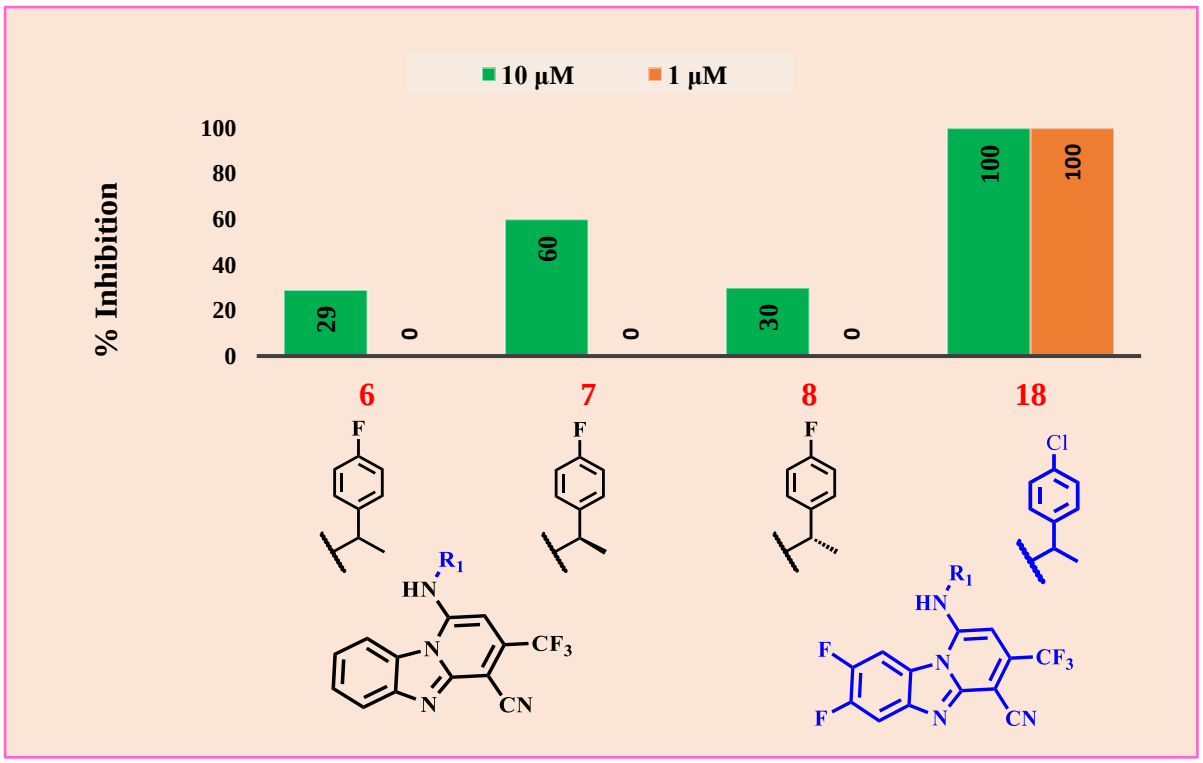

Figure 3.6: *In vitro* antischistosomal activity of SAR 1.1 to 1.4 compounds against adult *Schistosoma mansoni* worms

Control: praziquantel, 100 % inhibition at 0.37 µM

3.2.5 *In vitro* activity against newly transformed schistosomula (NTS)

Similar to that observed against adult worms, analogues derived from the PBI core scaffold bearing an unsubstituted phenyl ring showed little to no activity against NTS. In addition, the α-carboxylate benzylamine-substituted analogues and their corresponding amide derivatives exhibited poor antischistosomal activity against NTS even at the highest test concentration, as demonstrated by compounds **4** and **5** (35 and 55 % inhibition at 10.00 µM, respectively, figure 3.7). The most active analogue in this category, compound **6,** showed 100, 38, and 19% inhibition at 10.00, 1.00, and 0.37 µM respectively. Although still low, the chloro-substituted core scaffold showed improved antischistosomal activity against NTS as demonstrated by the α-carboxylate benzylamine-substituted analogues. A significant improvement in antischistosomal activity was observed by the introduction of a chloro atom on the phenyl ring of the PBI core. In this regard, the antischistosomal inhibitory effects of compound **4** increased from 35% and 0% to 100% and 24% for compound **13**, at 10.0 and 1.0 µM, respectively, after introducing a chloro atom at C-8 (SAR 1.2).

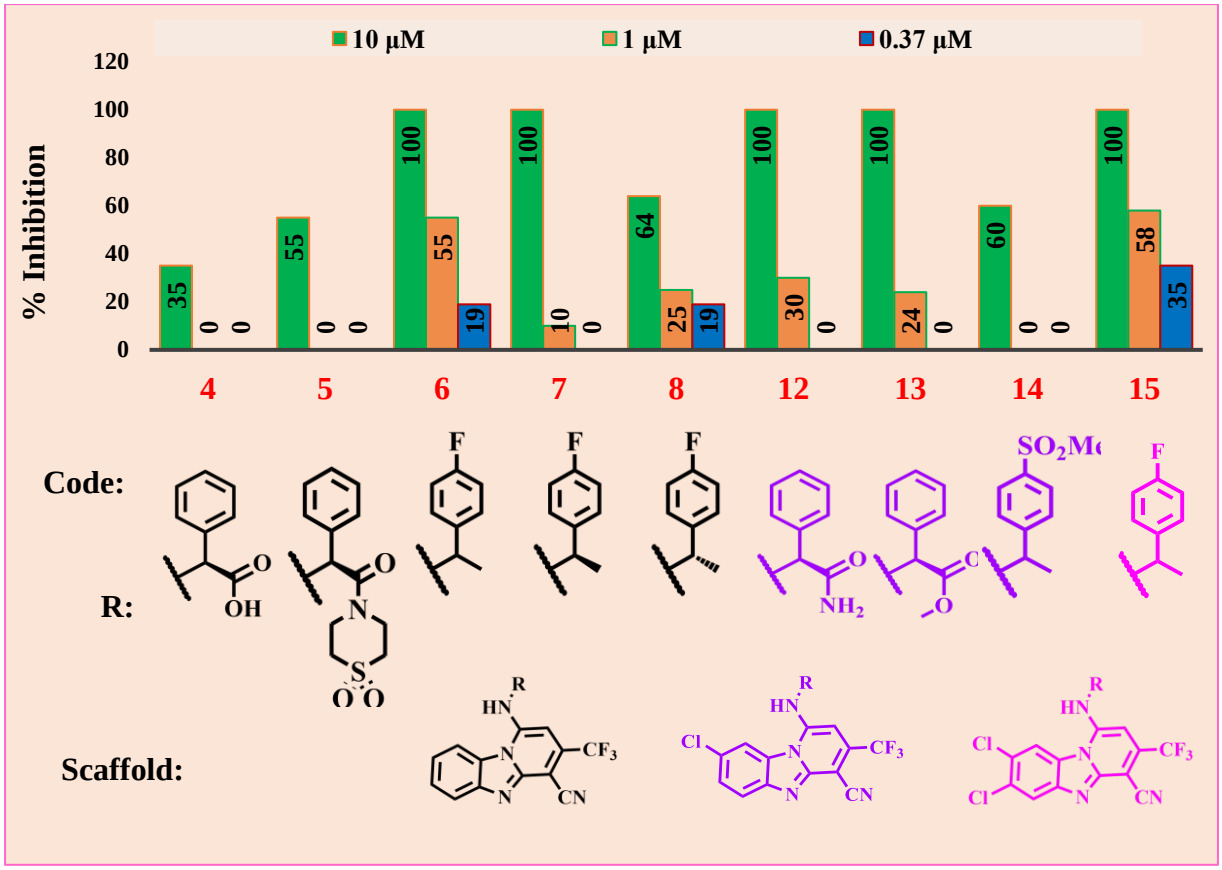

Figure 3.7: In vitro antischistosomal activity of SAR 1.1 to 1.3 compounds against newly transformed schistosomula **(NTS)**

SAR 1.1, black (unsubstituted core); SAR 1.2, magenta (8-chloro); SAR 1.3, pink (7, 8-dichloro)
Control: praziquantel, 100% inhibition at 0.37 µM

This improvement in antischistosomal activity corresponds to a 3-fold increase in favour of the monochlorinated phenyl of the PBI core scaffold. The primary amide (compound **12)** also exhibited improved activity (100% inhibition at 10.00 µM, and 30% inhibition at 1.0 µM) compared to the α-carboxylate benzylamine-substituted analogues derived from the unsubstituted phenyl ring of the PBI core. The *para*-sulfonyl benzylamine-substituted analogue showed 60% inhibition at 10.0 µM while no activity was observed at both 1.0 and 0.37 µM test concentrations. The effect of phenyl ring disubstitution of the PBI core scaffold on activity was also examined. The benzylamine moiety of compound **6,** which resulted in the greatest activity in this portion of the SAR study, was incorporated into the 7,8-dichlorinated (SAR 1.3) PBI core scaffold to produce compound **15**. An improvement in activity was observed from 100, 38, and 19% to 100, 58, and 35% by compound **6** and **15** respectively, at 10.00, 1.00, and 0.37 µM test concentrations.

Introduction of the 7,8-difluoro substitution on the phenyl ring of the PBI core scaffold (figure 3.8) provided further opportunities to expand the SAR study by reducing the cytotoxicity that was observed with the dichlorinated core scaffold (Mayoka, unpublished data), in addition to reducing both molecular weight and lipophilicity. Interestingly, analogues that were derived from this portion of the SAR study demonstrated a drastic improvement in antischistosomal activity, as shown by the 7,8-difluoro-substituted phenyl analogue **16** (100% inhibition at both 10.0 and 1.0 μM, and 48% inhibition at 0.37 μM, figure 3.8**)** in comparison with the 7,8-dichloro-substituted analogue **15** (100, 58, and 35% inhibition at 10.00, 1.00, and 0.37 μM test concentrations, respectively**,** figure 3.7**)**. Enantiomerism did not affect antischistosomal activity, as was demonstrated by the racemic analogue **16** and the pure enantiomer **17** (*R*), both of which exhibited 100% inhibition at both 10.0 and 1.0 μM, and 48 and 35% inhibition at 0.37 μM, respectively. Equipotency was also observed in the enantiomerically pure analogues **19** (*R*) and **20** (*S*), both of which exhibited 100% inhibition at 10.0 and 1.0 μM, and 21 and 25% inhibition at 0.37 μM, respectively. Furthermore, the *R*- and *S*-α-carboxylate benzylamine-substituted analogues also displayed similar antischistosomal activities, as was demonstrated by compound **32** (*S*; 100, 73, and 17% inhibition at 10.00, 1.00, and 0.37 μM, respectively) and compound **33** (*R*; 100% inhibition at both 10.0 and 1.0 μM, and 19% inhibition at 0.37 μM). Moreover, the α-methyl ester substitution on the substituent amine did not affect activity, as shown by compound **19** (100% inhibition at both 10.0 and 1.0 μM, and 21% at 0.37 μM), compound **33** (100% inhibition at both 10.0 and 1.0 μM, and 19% at 0.37 μM), compound **20** (100% inhibition at 10.0 and 1.0 μM, and 25% at 0.37 μM), and compound **32** (100, 73, and 17% inhibition at 10.00, 1.00, and 0.37 μM, respectively). Interestingly, α-cyclopropyl benzylamine-substituted analogue **30** exhibited impressive potency against NTS at 0.37 μM (69% inhibition), while demonstrating 100% inhibition at both 10.00 and 1.00 μM. Furthermore, substitution of the fluoro with the chloro group at the *para*-position of the benzylamino moiety did not affect the antischistosomal potency as shown by compounds **16** and **18**, which both showed 100% inhibition at 10.0 and 1.0 μM, and 48 and 31% inhibition at 0.37 μM, respectively.

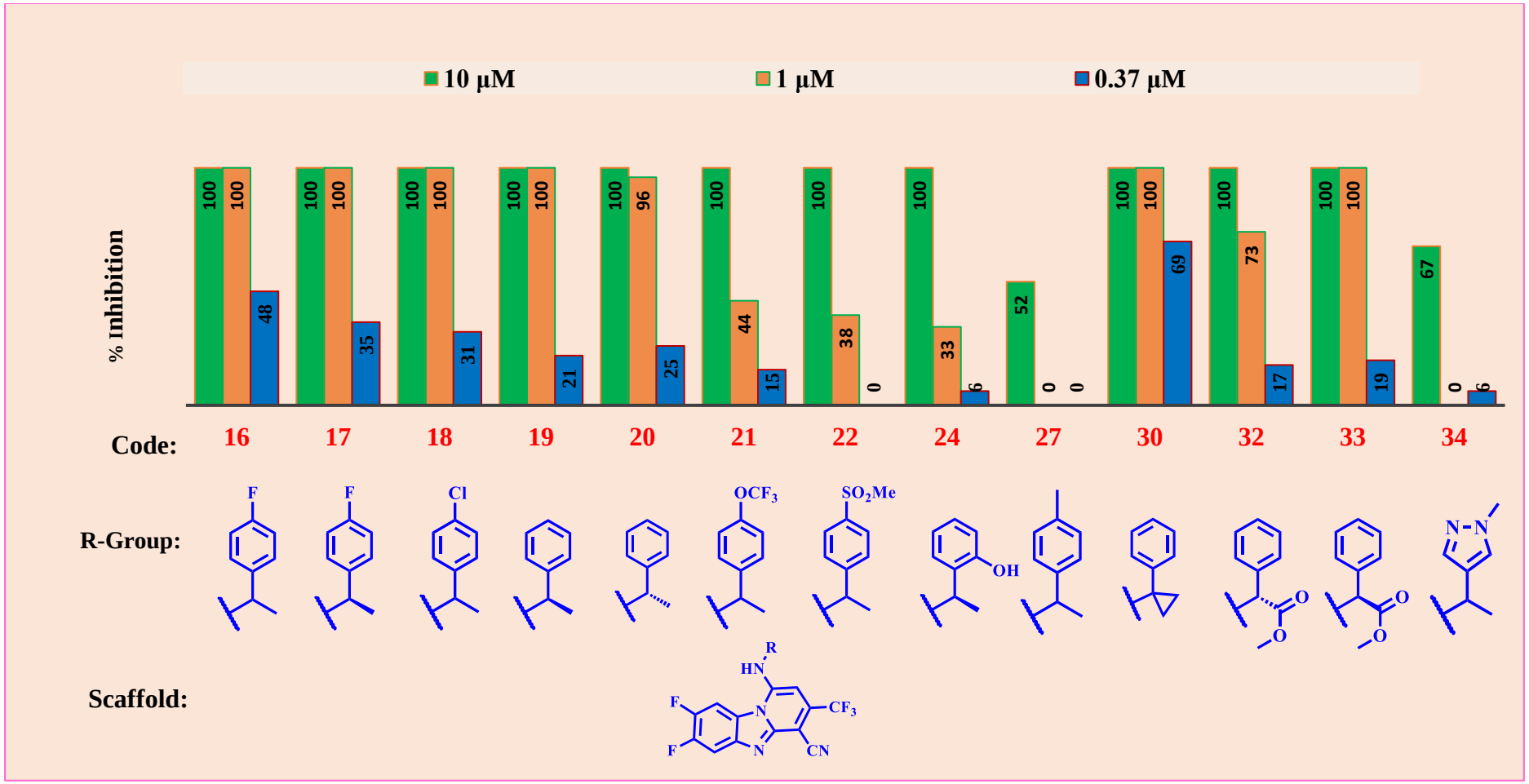

Figure 3.8: *In vitro* antischistosomal activity of SAR 1.4 (7,8-difluorinated core) compounds against newly transformed schistosomula (NTS)
Control: praziquantel, 100% inhibition at 0.37 µM

Similarly, the presence or absence of the fluoro atom on the benzyl ring did not affect antischistosomal activity, as shown by compounds **17** and **19,** which both exhibited 100% inhibition at 10.0 and 1.0 µM, and 35 and 21% inhibition at 0.37 µM, respectively. However, compound **16** (100% inhibition at both 10.0 and 1.0 µM, and 48% inhibition at 0.37 µM) and compound **27** (52% inhibition at 10.0 µM and no inhibition at both 1.0 and 0.37 µM) demonstrate the importance of including an electron-withdrawing group on the benzyl ring. The presence of the hydroxyl, trifluoromethyl, and sulfone groups led to a loss of antischistosomal activity. The inactivity of the analogues following the substitution of these groups is demonstrated by the trifluoromethyl-substituted analogue **21** (100, 44, and 15% inhibition at 10.00, 1.00, and 0.37 µM, respectively), the sulfone-based analogue **22** (100 and 38% inhibition at 10.00 and 1.00, respectively, and no activity shown at 0.37 µM), and the *meta*-hydroxyl-substituted analogue **24** (100, 33, and 6% inhibition at 10.00, 1.00, and 0.37 µM, respectively). The contraction of the ring of the substituent amino moiety resulted in the loss of antischistosomal activity as demonstrated by the pyrazolylamine-substituted analogue **34,** which showed 67% inhibition at 10.0 µM and <10% inhibition at 1.0 and 0.37 µM.

3.3 SAR 2: Assessment of the solubility and *in vitro* antiplasmodium and antischistosomal activities of LHS-modified PBI analogues

This phase of SAR and structure-property relationship (SPR) studies were aimed at improving physicochemical properties. Although enhancement of solubility was the major focus, modifications that could produce analogues with improved *in vitro* antiparasitic activity were highly sought. The PBI nucleus underwent modifications including the incorporation of hydrophilic amino moieties (figure 3.9). Antiplasmodium activity evaluation of the analogues was carried out in both NF54 and K1 *P. falciparum* strains, and the antischistosomal evaluation was performed against *S. mansoni*. Compounds with a range of low to high solubility and antiparasitic activities were obtained. The *in vitro* antiparasitic activities (IC_{50} values) and corresponding solubility values for various target compounds are shown in figures 3.10-3.12. For the sake of brevity, the discussion of all the antiplasmodium results will be based on potency against the chloroquine-sensitive (*Pf*NF54) malaria parasite strain.

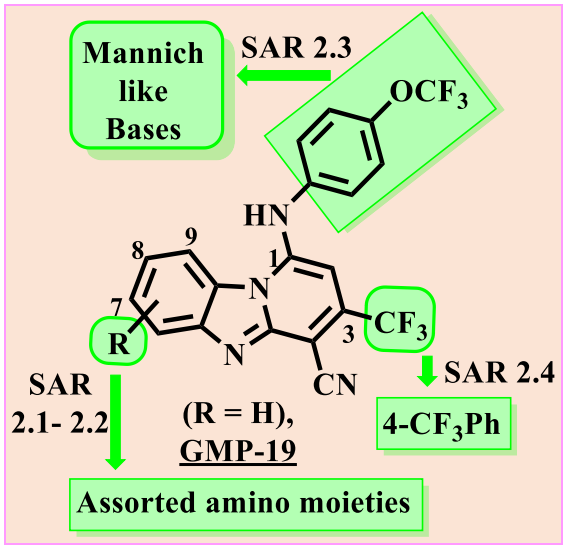

Figure 3.9: Points of modification in the SAR 2 study

3.3.1 Assessment of the solubility and *in vitro* antiplasmodium activities of SAR 2 analogues

The front-runner compound **GMP-19** (compound **35)** was used as a control in the antiplasmodium evaluation. Although similar IC_{50} values were obtained for the resynthesized material of **GMP-19** (compound **36**, IC_{50} = 0.25 µM) and previously synthesized material against the K1 strain, an unexpected 3-fold difference in activity was noted against the NF54 strain (IC_{50} = 0.43 and 0.17 µM for compound **35** and **36**, respectively). The derivatives demonstrated antiplasmodium potencies ranging from low to high, as shown in figure 3.10. Generally, moderately lipophilic groups around the PBI core influenced potency. The loss of potency observed upon replacing the morpholine with a piperazine group (compound **39,** IC_{50} = 0.18 µM, and **40**, IC_{50} = 9.60 µM) indicates that introduction of the polar NH group was detrimental to activity. Furthermore, the phenyl ring on the LHS of the PBI core was modified by incorporating polar non-ionizable amide functionalities. These analogues include a lipophilic *N*-ethylated amide compound **44**, which demonstrated poor antiplasmodium activity (IC_{50} > 10 µM). However, the moderately lipophilic *N*-des-ethyl amidated analogue **45** demonstrated a >37-fold improvement in antiplasmodium activity (IC_{50} = 0.27 µM) compared to compound **44** (figure 3.10).

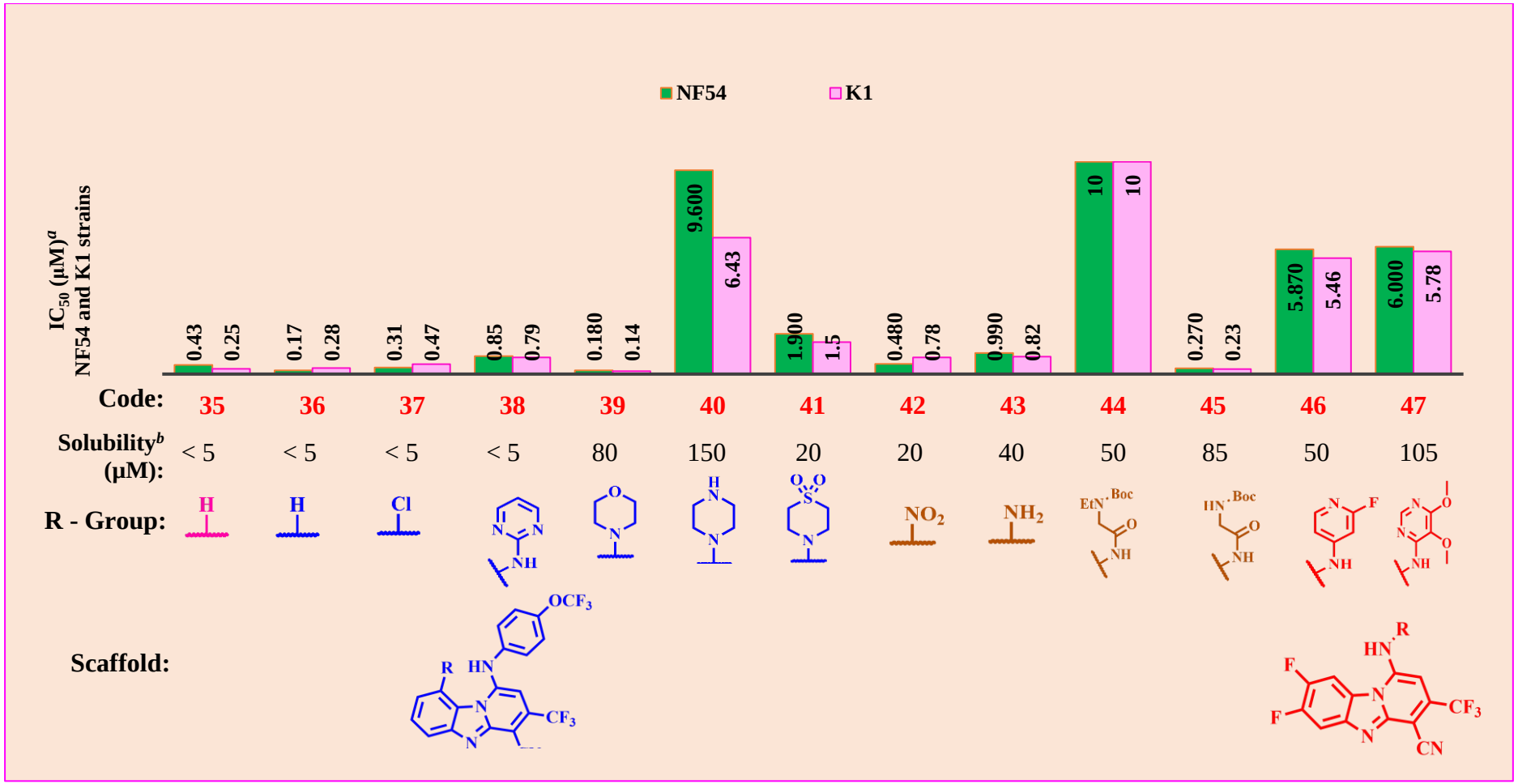

Figure 3.10: Solubility and *in vitro* antiplasmodium activity of SAR 2.1 to 2.3 compounds

SAR 2.1, blue; SAR 2.2, brown; SAR 2.3, red

[a]Mean values were calculated from at least two independent experiments on the *P. falciparum* strains NF54 and K1 (individual values within ± 2-fold). Artesunate (IC_{50} = 0.007 µM in NF54 and 0.930 ng/mL in K1) and chloroquine (IC_{50} = 0.012 µM in NF54 and 86 ng/mL in K1) were used as reference drugs.

[b]Kinetic solubility determined via UHPLC

The introduction of polar heterocyclic aromatic amino moieties was detrimental to antiplasmodium activity but caused a significant improvement in solubility, as demonstrated by compounds **46** (IC_{50} = 5.87 µM; solubility = 50 µM) and **47** (IC_{50} = 6.00 µM; solubility = 105 µM). However, the highly polar and basic piperazinyl-substituted analogue **40** (solubility = 150 µM) demonstrated a 2-fold improvement in solubility compared to the less polar morpholinyl-substituted analogue **39** (solubility = 80 µM). However, a 4-fold decrease in solubility was observed when the morpholine moiety of compound **40** was substituted with a 1,1-dioxidothiomorpholine group as in compound **41** (solubility = 20 µM). Sulfone- and the nitro-substituted compounds have been reported to have the unfavourable energy for hydrogen-bonding interactions with water molecules (this is discussed in more details in chapter 4).[7,8] Moreover, a 2-fold improvement in aqueous solubility was observed upon substituting the nitro group of compound **42** (solubility = 20 µM) with an amino group in analogue **43** (solubility = 40 µM). The improvement in solubility was further observed with polar non-ionizable amide-functionalized analogues such as the *N*-ethylated amide compound **44** (solubility = 50 µM) and the *N*-des-ethyl amidated compound **45** (solubility = 85 µM). Thus, amide derivative **45** showed a 2-fold improvement in solubility compared to compound **44**. Except for compound **38** (solubility <5 µM), aromatic moieties conferred greater solubility, as shown by compounds **46** and **47** (solubility <50 and 105 µM, respectively).

Based on the antiplasmodium and solubility evaluation, compound **39** was identified as an optimally active analogue and the morpholinyl substituent was therefore fixed on the phenyl ring in the next phase of the SAR study. As a result, the 4-(trifluoromethoxy)aniline substituent on the pyridyl ring of the core scaffold was substituted with saturated basic amino moieties to produce target analogues shown in figure 3.11 below. However, such substitutions initially produced analogues with reduced *in vitro* antiplasmodium activities, translating to a >30-fold loss in potency against the *Pf*NF54 strain compared to that of compound **39**. Such analogues include compounds **48** (IC_{50} = 6.000 µM) and **49** (IC_{50} = 4.940 µM, figure 3.12). In an attempt to probe the effect of re-introducing aromatic properties, the 4-(trifluoromethyl)phenyl moiety was incorporated in place of the trifluoromethyl group at C-3. A drastic improvement in antiplasmodium activity was observed as demonstrated by compound **53** (IC_{50} = 0.670 µM). Although low, the carbamate-substituted analogue **51** demonstrated antiplasmodium activity comparable to that of the *N*-ethylated amino analogue **50** (IC_{50} = 0.710 µM).

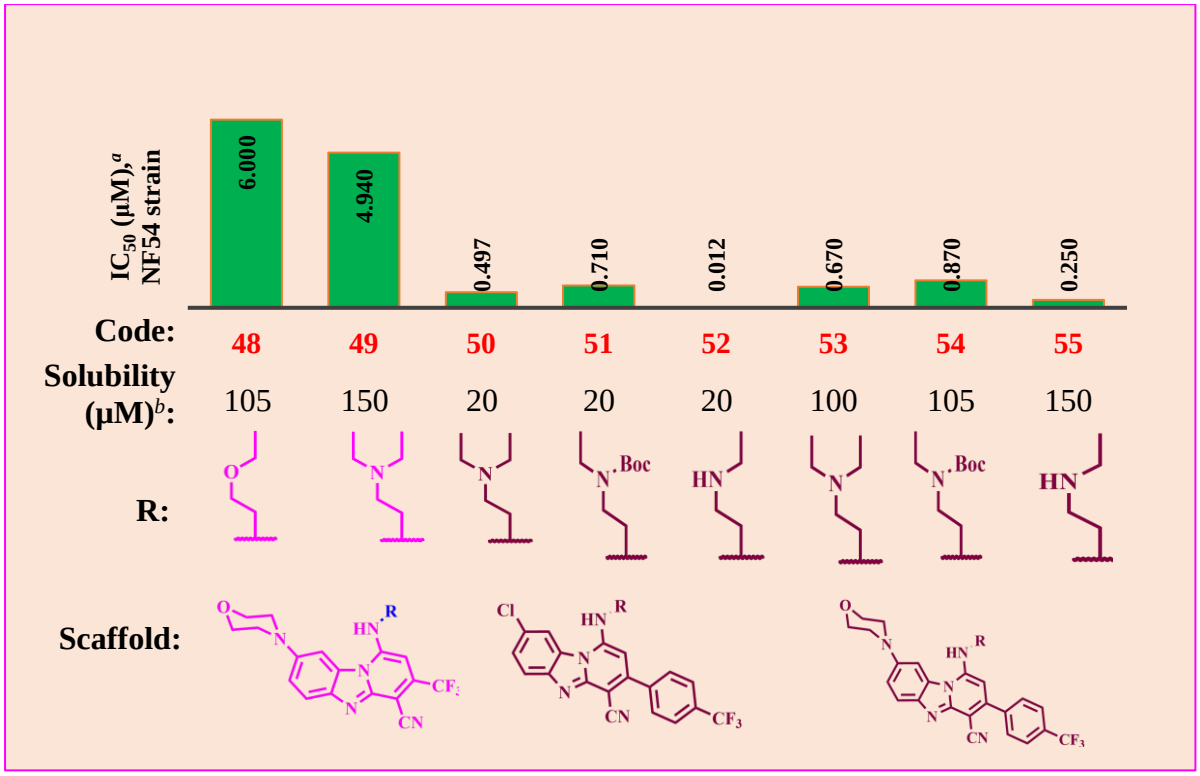

Figure 3.11: Solubility and in vitro antiplasmodium activity of SAR 2.4 and 2.5 compounds SAR 2.4, pink; SAR 2.5, brown

[a]Mean values were calculated from at least two independent experiments on the P. falciparum strains NF54 and K1 (individual values within ± 2-fold). Artesunate (IC_{50} = 0.007 µM in NF54 and 0.0024 µM in K1) and chloroquine (IC_{50} = 0.012 µM in NF54 and 0.270 µM in K1) were used as reference drugs.
[b]Kinetic solubility determined via UHPLC

Interestingly, a dramatic improvement in antiplasmodium activity was observed in the *N*-des-ethyl aminated compound **52** (IC_{50} < 0.012 µM), thus demonstrating a >40-fold improvement in antiplasmodium activity compared to that of the *N*-ethylated analogue **50**. Moreover, compound **52** demonstrated >59-fold improvement in antiplasmodium potency compared to the carbamate *N*-carbamate aminated analogue **51**. A slight loss of antiplasmodium activity was observed with the morpholine substituted analogue **53** (IC_{50} = 0.670 µM) relative to that of the chloro-substituted analogue **50**. Furthermore, similar activities were observed in the carbamate-based analogues **54** and **51** (IC_{50} = 0.870 and 0.710 µM, respectively). Interestingly, sub-micromolar antiplasmodium potency was retained with the fully substituted (*N*-des-ethyl/morpholine aminated) analogue **55** (IC_{50} = 0.250 µM). The final analogue (**55**), however, demonstrated a >12-fold decrease in activity compared to compound **52**. Similar sub-micromolar antiplasmodium activities were observed in the *N*-ethylated and *N*-carbamate aminated analogues **53** and **54** (IC_{50} = 0.670 and 0.870 µM, respectively). Furthermore, the *N*-des-ethyl/morpholine aminated analogue **55** demonstrated improved activity, translating to

approximately a 3-fold increase compared to both the *N*-ethylated and *N*-carbamate aminated analogues **53** and **54**. Moreover, these analogues demonstrated low to moderate solubility, although the analogues with a trifluoromethyl group at position C-3 did so at the expense of antiplasmodium potency. Compounds that demonstrated improvement in kinetic solubility at the expense of antiplasmodium activity include compounds **48** and **49** (solubility = 105 and 150 µM, respectively). The substitution of a CF_3 group with a 4-CF_3Ph moiety at the C-3 position resulted in low solubility for the chloro-substituted intermediate analogues **50** to **52** (solubility = 20 µM). The poor solubility of these analogues may be attributed to the anticipated π–stacking due to the planar conformations. Not surprisingly, solubility was restored upon substitution of a chloro group with a morpholine moiety on the core scaffold. Compounds **53** and **54** (solubility = 100 and 105 µM, respectively) demonstrated a 5-fold improvement in solubility compared to the corresponding chloro-substituted analogues **50** and **51**. Moreover, analogue **55** (solubility = 150 µM) showed a >7-fold improvement in solubility compared to its corresponding chlorinated analogue **53**. Density functional theory (DFT) calculations revealed that in the lowest energy state, the morpholine-substituted analogues assume an anti-coplanar conformation. These conformations disrupt molecular symmetry to reduce π–stacking and are thought to be responsible for the high solubility demonstrated by compounds **49** and **55**. Although some 3-dimension character was observed, compounds such as **28** exhibited poor solubility because of residual planarity (figure 3.12).

Code	Structure	DFT lowest energy conformation
49	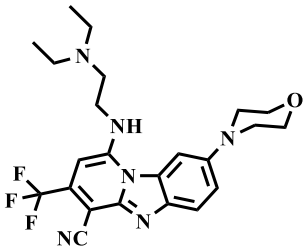	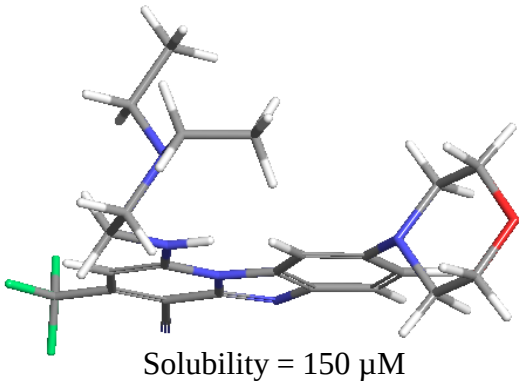 Solubility = 150 µM IC_{50} NF54 = 4.94 µM
55	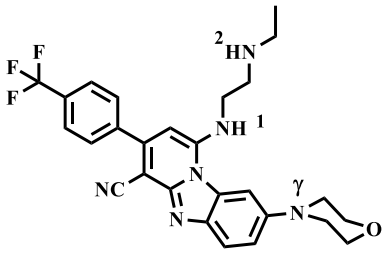	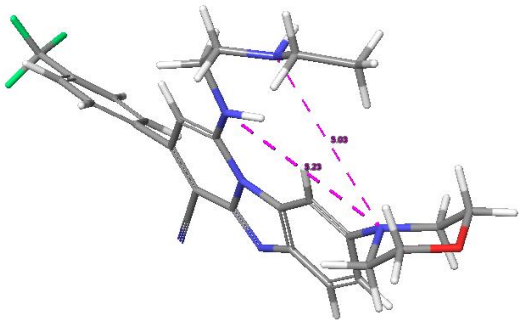 Solubility = 105 µM IC_{50} NF54 = 0.250
28	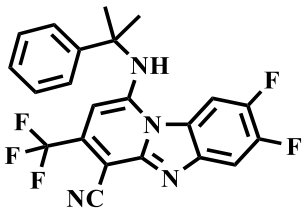	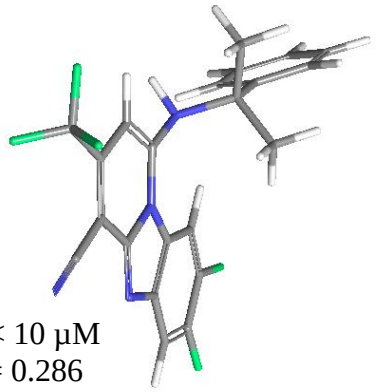 Solubility = < 10 µM IC_{50} NF54 = 0.286

Figure 3.12: Density functional theory (DFT)-optimized structure conformations and observed solubilities for compounds **49**, **55**, and **28**

3.3.2 *In vitro* gametocytocidal activity evaluation of SAR 2 analogues

Although not all SAR 2 compounds were preliminarily screened for dual-point inhibition against the early and late stages of parasite gametocytogenesis, a few compounds demonstrated activity at 1.0 and 5.0 µM test concentrations. Details of these compounds and their gametocytocidal inhibitory effects at various concentrations are shown in figure 3.13.

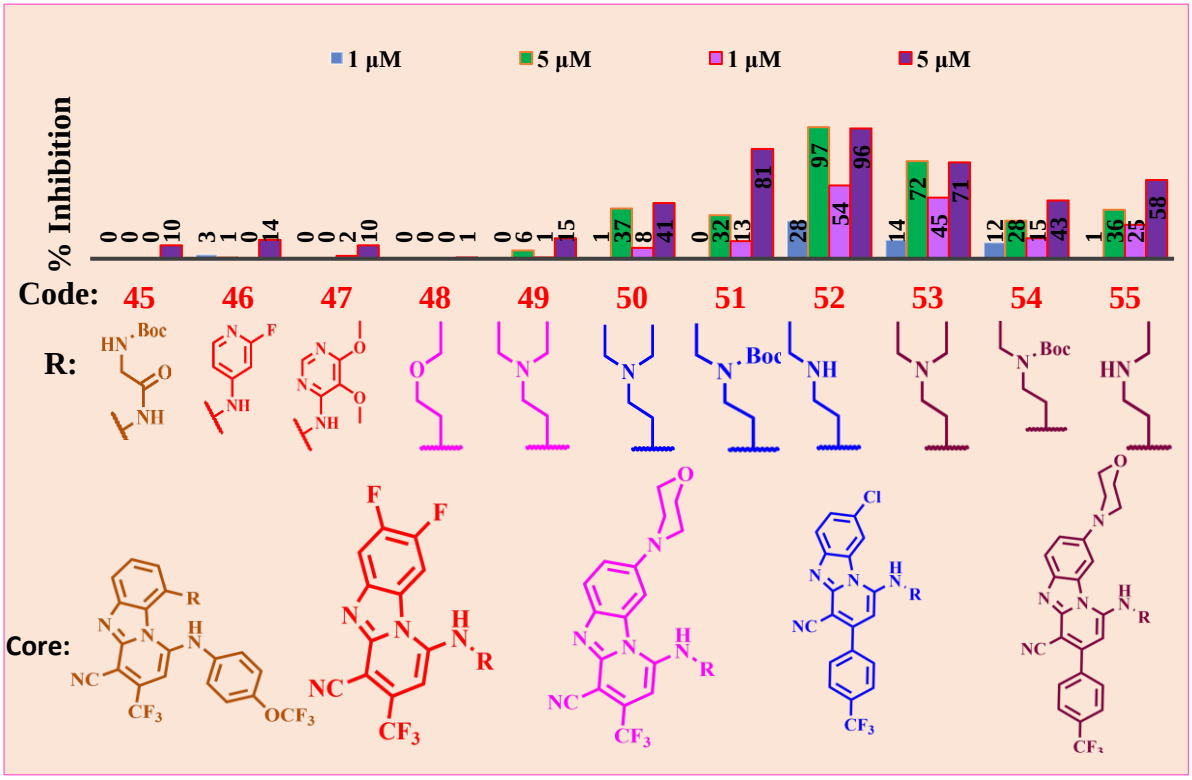

	Reference drugs (1.0 µM)	Early gametocytes	Late gametocytes
1	**Methylene blue**	93% (luc)	90% (luc), 50% (ATP)
2	**Dihydroartemisinin**	75% (luc)	70% (luc), 15% (ATP)
3	**MMV048**	77% (n=3)	92% (n=3)

Figure 3.13: *In vitro* gametocytogenesis inhibitory effects of SAR 2.2 to 2.5 compounds against early- and late-stage P*f*NF54 gametocytes

luc**,** parasite viability measured via luciferase reporter assay; ATP**,** parasite viability measured via ATP bioluminescence assay[6]

Although analogues with polar functionalities such as the amide-substituted compound **45**, the heterocyclic aromatic amine-substituted analogues **46** and **47,** and the double-aminated analogues **48** and **50** demonstrated negligible activity, the lipophilic analogues derived from the 4-CF_3Ph-substituted core scaffold demonstrated higher activity (compounds **51** to **55)**. Compound **52** demonstrated the highest potency.

3.3.3 *In vitro* antischistosomal evaluation of SAR 2 analogues

The *in vitro* antischistosomal activities of SAR 2.1 and 2.2 analogues against adult schistosomes were evaluated. The analogues in this SAR study were obtained by modifying the LHS of compound **35**. Although the analogues in this series demonstrated potent antischistosomal effects, reduced potency was observed for all compounds, including the resynthesized control sample compound **36,** compared to the previously reported activity of front-runner compound **35** (data not shown). Details of these compounds and their antischistosomal activities (IC_{50} values) are presented in figure 3.14 below.

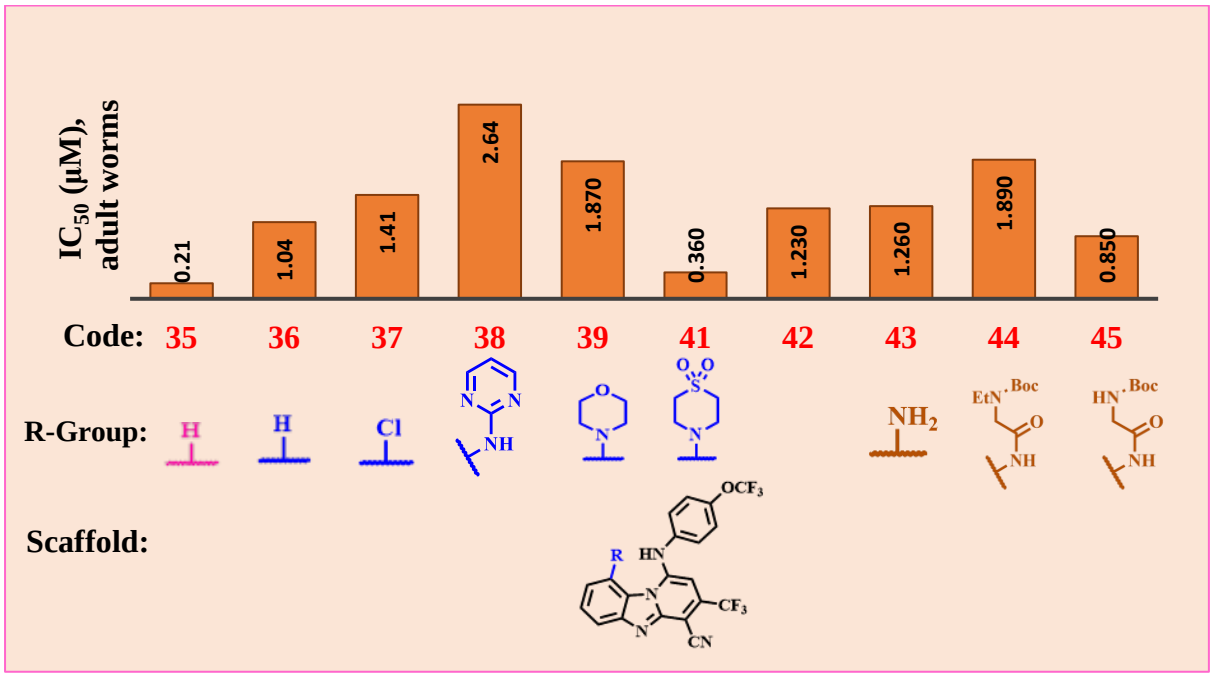

Figure 3.14: *In vitro* antischistosomal activity of SAR 2.1 to 2.2 compounds against adult *Schistosoma mansoni* worms

SAR 2.1, blue; SAR 2.2, brown
Control: praziquantel, IC_{50} = 0.21 μM

An unexpected significant difference in antischistosomal activities between the previously reported result for the front-runner **GMP-19** (compound **35**, IC_{50} = 0.210 μM) and the resynthesized sample (compound **36**, IC_{50} = 1.04 μM), corresponding to a 5-fold difference in antischistosomal activity against the adult worms, was observed. However, these results were reconciled after a repeat analysis of the front-runner sample **35** alongside the resynthesized sample **36**. In this controlled analysis, compound **35** demonstrated lower antischistosomal activity (IC_{50} = 1.24 μM) than originally reported (IC_{50} = 0.210 μM).

A modification that involved incorporating an electron-withdrawing group on the phenyl ring produced the less active intermediate compound **37** (IC_{50} = 1.41 μM). Similarly, reduced antischistosomal activity was observed when a nitro group was incorporated to produce compound **42** (IC_{50} = 1.23 μM). Furthermore, incorporating an electron-donating group such as an amino group, as demonstrated by compound **43**, also resulted in lower potency (IC_{50} = 1.26 μM). Despite the difference in the electronic nature of compounds **42** and **43**, no significant difference in antischistosomal activity was observed. Thus, the nitro-substituted analogue **42** and its reduced form **43** showed similar activities against adult *S. mansoni* worms. Although the final aminated and amidated analogues did not show clear SARs, 1,1-dioxidothiomorpholinyl-substituted analogue **41** exhibited the strongest antischistosomal activity (IC_{50} = 0.36 μM) compared to the morpholinyl-substituted analogue **39** (IC_{50} = 1.87 μM). Similarly, the analogue **45** (IC_{50} = 0.850 μM) demonstrated a 2-fold increase in activity against adult worms compared to the analogue **44** (IC_{50} = 1.89 μM).

The antiplasmodium and antischistosomal SARs of PBI analogues were explored and analogues displaying high antiplasmodium and antischistosomal activities were identified. Additionally, compound **52** was identified as an analogue with strong *in vitro* asexual blood-stage antiplasmodium activity (IC_{50} < 0.012 μM) and dual activity at both the early and late stages of gametocytogenesis (>96% inhibition at 5.0 μM). Additionally, stage-specific activity against early-stage gametocytes (77% inhibition at 1.0 μM) was identified in compound **30**. Moreover, the same compound showed potent sub-micromolar dual antiparasitic *in vitro* activity (**30**: IC_{50} = 0.045 μM in P*f*NF54, 72% early-stage gametocyte inhibition at 1.0 μM, and 69% schistosomal inhibition of *S. mansoni* NTS at 0.370 μM). Furthermore, compounds displaying sub-micromolar *in vitro* antischistosomal activity (**41**: IC_{50} = 0.360 μM) were identified, as well as compounds also showing highly improved kinetic solubility between 30 and 85 μM **(**such as compound **45**, IC_{50} = 0.270 in P*f*NF54, IC_{50} = 0.850 μM in adult *S. mansoni*). Additional details of the physicochemical properties and the exploration of certain factors affecting the solubility of PBI compounds are presented in the next chapter.

References:

(1) Lovering, F.; Bikker, J.; Humblet, C. Escape from Flatland: Increasing Saturation as an Approach to Improving Clinical Success. *J. Med. Chem.* **2009**, (52), 6752–6756.

(2) Veber, D. F.; Johnson, S. R.; Cheng, H.-Y.; Smith, B. R.; Ward, K. W.; Kopple, K. D. Molecular Properties That Influence the Oral Bioavailability of Drug Candidates. *J. Med. Chem.* **2002**, *45* (12), 2615–2623.

(3) Zhang, Y.-Y.; Liu, Y.; Mehboob, S.; Song, J.-H.; Boci, T.; Johnson, M. E.; Ghosh, A. K.; Jeong, H. Metabolism-Directed Structure Optimization of Benzimidazole-Based Francisella Tularensis Enoyl-Reductase (FabI) Inhibitors. *Xenobiotica* **2014**, *44* (5), 404–416.

(4) Pearson, J.; Dahal, U. P.; Rock, D.; Peng, C.-C.; Schenk, J. O.; Joswig-Jones, C.; Jones, J. P. The Kinetic Mechanism for Cytochrome P450 Metabolism of Type II Binding Compounds: Evidence Supporting Direct Reduction. *Arch. Biochem. Biophys.* **2011**, *511* (1–2), 69–79.

(5) Hill, A. P.; Young, R. J. Getting Physical in Drug Discovery: A Contemporary Perspective on Solubility and Hydrophobicity. *Drug Discov. Today* **2010**, *15*, 648–655.

(6) Reader, J.; Botha, M.; Theron, A.; Lauterbach, S. B.; Rossouw, C.; Engelbrecht, D.; Wepener, M.; Smit, A.; Leroy, D.; Mancama, D.; Coetzer, T. L.; Birkholtz, L.-M. Nowhere to Hide: Interrogating Different Metabolic Parameters of Plasmodium Falciparum Gametocytes in a Transmission Blocking Drug Discovery Pipeline towards Malaria Elimination. *Malar. J.* **2015**, *14* (1), 213.

(7) Kamlet, M. J.; Doherty, R. M.; Abraham, M. H.; Marcus, Y.; Taft, R. W. Linear Solvation Energy Relationship. 46. An Improved Equation for Correlation and Prediction of Octanol/Water Partition Coefficients of Organic Nonelectrolytes (Including Strong Hydrogen Bond Donor Solutes). *J. Phys. Chem.* **1988**, *92* (18), 5244–5255.

(8) Why are the Nitro and Sulfone Groups Poor Hydrogen Bonders? https://docplayer.net/35923053-Why-are-the-nitro-and-sulfone-groups-poor-hydrogen-bonders.html (accessed Oct 9, **2018**).

4. PHYSICOCHEMICAL EVALUATION AND STRUCTURE-PROPERTY RELATIONSHIPS

4.1 Introduction

A drug's medical benefits depend entirely on its pharmacological effects and the duration of its action within the body. Specifically, the benefits of a drug are related to pharmacokinetic properties such as absorption, distribution, metabolism, and excretion (ADME). Ideally, the physicochemical properties of a drug-like molecule determine these ADME properties.[1,2] Most importantly, aqueous solubility and lipophilicity remain pivotal physicochemical properties in determining how much of the drug is dissolved, permeates the lipophilic biological membranes, and is absorbed.[1]

Lipinski's rule of five has been devised to provide guidelines on the suitable characteristic properties of drug-like compounds. This rule is based on a study of oral drug leads that progressed into the advanced stages of clinical development. Generally, the rule provides guidelines on the inherent properties of drug-like compounds, such as the physical count of the hydrogen-bond donors (HBD, ideally ≤ 5) and the hydrogen-bond acceptors (HBA, ideally ≤ 10). In addition, the rule emphasizes the importance of molecular weight (Mw, ideally ≤ 500 $g.mol^{-1}$), which, in addition to the number of HBDs and HBAs, affects lipophilicity. Lipophilicity is defined as the *in silico* calculated partition coefficient (cLogP), which should ideally be ≤ 5.[3]

However, certain properties that are not addressed by the rule of five but also have a significant effect on solubility, such as the topological polar surface area (tPSA) and saturation (increase in sp^3 character), have been evaluated and established. Although an increase in sp^3 character has previously been studied and associated with molecular conformations that influence crystallinity and thus improve solubility and permeability,[5] Veber *et al*. restricted the ideal total number of rotatable bonds to fewer than 10 and the optimal tPSA in the range 65 to 140 $Å^2$.[6] Similarly, the introduction of chirality leads to the disruption of molecular planarity and influences the crystal packing of the compound, which lowers the melting point (Mp) and leads to improved solubility.[4,7]

In this study, some of these intrinsic properties were evaluated to determine their effect on the solubility of PBI lead compounds. Parameters such as the Mp, cLogP, tPSA, and the high-pressure liquid chromatography (HPLC) retention times (t_R) were further evaluated.

4.2 Results and discussion

4.2.1 Physicochemical characterization

To minimize factors that may lead to uncertainties in the profiling of physicochemical properties, the purities of all the compounds used in this study were reassessed via HPLC in a single batch using the same HPLC buffer and solvent system, to ensure compounds were >95% pure. Results of the purity assessment for all compounds synthesized (n = 55) were found to be within 98.39 ± 2.58% at 95% confidence limit and are shown below in figure 4.1. The purity results were satisfactory, and all compounds displayed the minimum required purity.

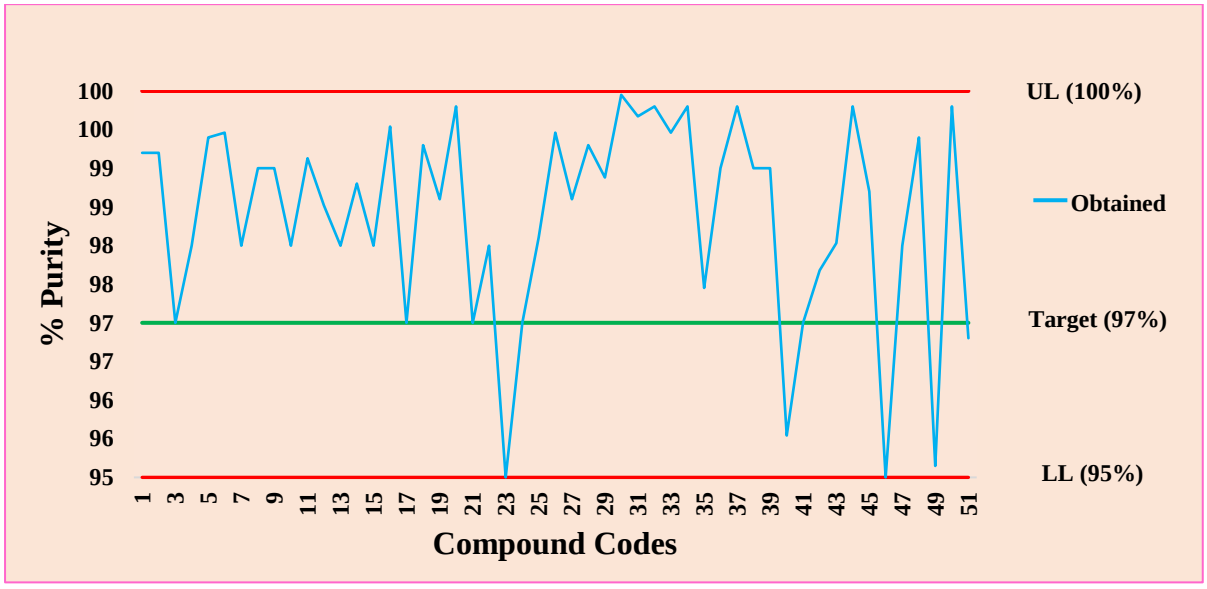

Figure 4.1: Purities of all compound synthesized (SAR 1.1 to 2.4) determined via high-performance liquid chromatography (HPLC)

This chart shows compliance with the 95% minimum purity requirement.
LL, lower limit; UL, the upper limit

4.2.2 Relationships between solubility, Mp, cLogP, and HPLC t_R

The solubilities and Mp were measured using appropriate techniques (outlined in Chapter 6), and the retention times were determined via HPLC. To ensure minimum uncertainties in the determination of the t_R, compounds were analyzed in a single sequence using the same buffer and solvent system. The cLogP and the tPSA values were generated *in silico* using ChemDraw professional 16.0 and StarDrop™ 64 softwares, respectively. Using Microsoft Excel 16.0, the statistical charts shown in figure 4.2 were produced to investigate the relationships between i) solubility and tPSA, ii) solubility and Mp, iii) solubility and cLogP, and iv) solubility and HPLC t_R.

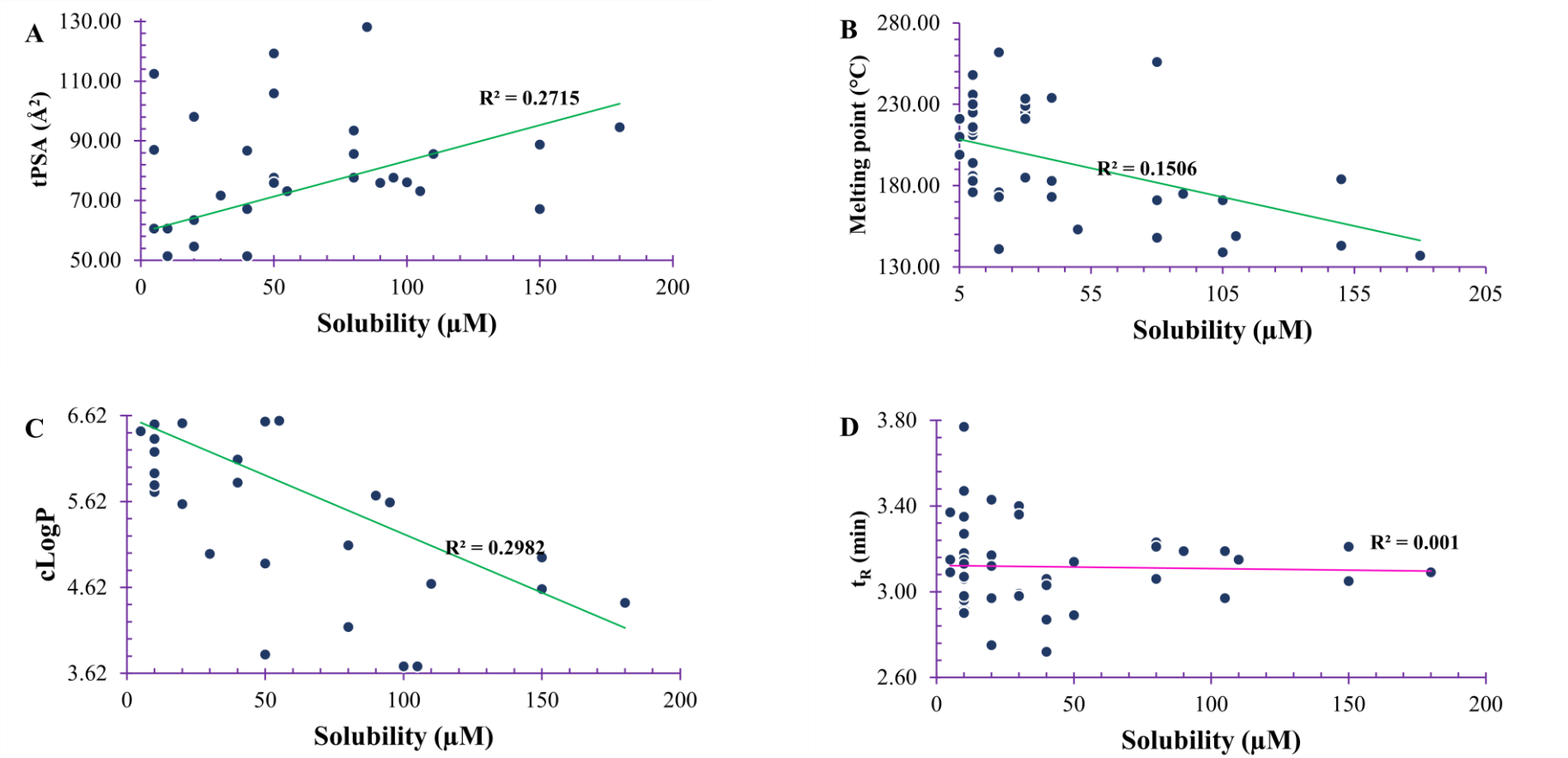

Figure 4.2: Relationships between selected physicochemical properties

A, solubility vs topological polar surface area (tPSA); **B,** solubility vs melting point; **C,** solubility vs calculated partition coefficient (cLogP); **D**, solubility vs high-performance liquid chromatography (HPLC) retention time (t_R)

Although a more accurate solubility determination method could have revealed clearer statistical correlations, the compound-specific inherent properties observed here appear to strongly influence the linear relationships shown in figure 4.2. An increase in tPSA is theoretically expected to improve hydrogen-bonding properties, and thus result in increased aqueous interactions and improved solubility. However, certain compounds such the nitro-substituted analogue **42** demonstrated poor solubility (20 µM) and high tPSA (112.46 $Å^2$). A similar result was observed with the sulfone-based analogue **41,** which exhibited poor solubility (< 20 µM) despite having a high tPSA (128.08 $Å^2$). Thus, the weak correlation (R^2 = 0.272) between solubility and the tPSA was attributed to the unusual behaviour of analogues such as compounds **42** and **41** (figure 4.3), which, despite showing favourably high tPSA, demonstrated low solubility. Inherent factors that limit the solubility of sulfone- and nitro-substituted analogues have been reported in the literature and are attributed to their weak hydrogen-bond interactions with water molecules. Despite having more hydrogen-bonding sites, the NO_2- and SO_2-substituted analogues show unfavourable hydration energies, thus leading to poor solvation.[8] The unusual relationship between tPSA and solubility displayed by such compounds are thought to have skewed the correlation observed in figure 4.2A.

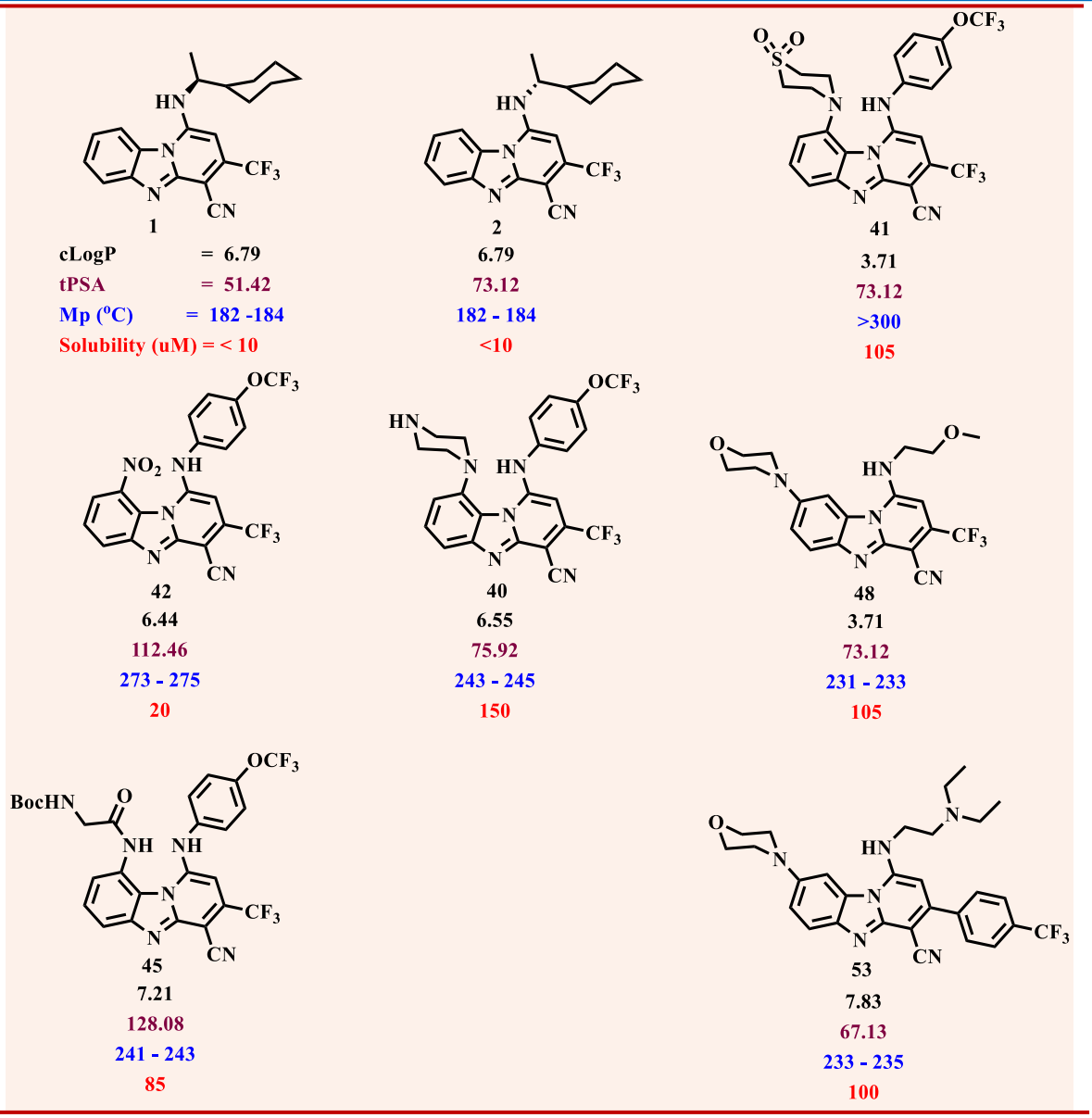

Figure 4.3: Selected PBI compound with their physicochemical properties

Additionally, although weak, a positive correlation (R^2 = 0.151) was observed between solubility and Mp, as demonstrated by the negative gradient shown in figure 4.2B. The negative slope observed is typical of the inverse linear relationship between solubility and Mp. Theoretically, the solubility of a chemical substance should increase as the Mp decreases. However, this theoretical expectation is limited by other factors that form part of the inherent properties of a compound. In addition to the number of rotatable bonds and saturation, which are thought to influence the Mp and in turn affect solubility, polar functionalities should increase optimally to facilitate hydrophilic interactions. In this regard, the saturated cyclohexyl-substituted analogues **1** and **2** demonstrated poor solubility (<10 µM) although complying with Veber's rules (<10 rotatable bonds) and demonstrating desirably low Mp (182 °C).

The positive trend between solubility and cLogP (figure 4.2C) was the strongest correlation observed (R^2 = 0.298) relative to that between other physicochemical parameters. Ideally, the solubility of a compound should vary inversely with cLogP, and a plot of solubility against cLogP is therefore expected to display a linear negative slope. Although this was observed in figure 4.2C, the inherent characteristics of different compounds will affect the *in silico*-predicted lipophilicities (cLogP) differently. Based on these *in silico*-generated cLogP values, the experimental solubilities may vary and depart from theoretical expectations. This may be because of the inherent properties of certain compounds that the software does not consider. Such properties may include inductive electronic effects, which mostly upsurge the basicity of some non-hydrogen-containing functional groups such as tertiary amines. In addition, the software may not recognize the effect of anti-coplanar structural conformations, although these may strongly impact crystal packing, Mp, and solubility. The piperazinyl- and linear amine-functionalized analogues **40** and **48** (cLogP = 6.55 and 4.96, solubility = 150 and 105 µM, for **40** and **48**, respectively, figure 4.3) are amongst the analogues that were thought to be affected by these software limitations.

Another aberrant experimental result that is thought to be functional group-specific concerns the sulfone- and the piperazinyl-substituted analogues **40** and **41** (cLogP = 6.55 and 5.59, solubility = 150 and 20 µM, for **40** and **41**, respectively). In these two cases, structures with lower cLogP values may theoretically be associated with higher solubilities, however, the opposite was observed here. These and other factors not discussed here are thought to have weakened these correlations.

Similarly, aberrant relationships between solubility and cLogP were demonstrated by compounds **45** (cLogP = 4.97, solubility = 150 µM) and **53** (cLogP = 5.69, solubility = 100 µM). Such compounds may have fewer hydrogen-bond donors but contain tertiary-substituted nitrogen atoms (3°) that are highly basic. The aberrant linear relationships between solubility and cLogP that are demonstrated by the nitro-, sulfonyl-, and tertiary nitrogen-substituted analogues[9] are attributable to the weak correlation observed (R^2 = 0.298). The fact that weak linear correlations were observed across all relationships indicates that several other factors including inductive effects, hydration, and crystal packing energies affect the solubility of these PBI compounds.

References

(1) Rutkowska, E.; Pajak, K.; Jóźwiak, K. Lipophilicity--Methods of Determination and Its Role in Medicinal Chemistry. *Acta Pol. Pharm.* **2013**, (1), 3–18.

(2) Lin, J. H.; Lu, A. Y. H. Role of Pharmacokinetics and Metabolism in Drug Discovery and Development. *Pharmacol. Rev.* **1997**, (4), 403–449.

(3) Lipinski, C. A.; Lombardo, F.; Dominy, B. W.; Feeney, P. J. Experimental and Computational Approaches to Estimate Solubility and Permeability in Drug Discovery and Development Settings. *Adv. Drug Deliv. Rev.* **1997**, *23* (1–3), 3–25.

(4) Lovering, F.; Bikker, J.; Humblet, C. Escape from Flatland: Increasing Saturation as an Approach to Improving Clinical Success. *J. Med. Chem.* **2009**, (52), 6752–6756.

(5) Williams, H. D.; Trevaskis, N. L.; Charman, S. A.; Shanker, R. M.; Charman, W. N.; Pouton, C. W.; Porter, C. J. H. Strategies to Address Low Drug Solubility in Discovery and Development. *Pharmacol. Rev. Pharmacol Rev* **2013**, *65* (January), 315–499.

(6) Veber, D. F.; Johnson, S. R.; Cheng, H.-Y.; Smith, B. R.; Ward, K. W.; Kopple, K. D. Molecular Properties That Influence the Oral Bioavailability of Drug Candidates. *J. Med. Chem.* **2002**, *45* (12), 2615–2623.

(7) Feng, K.; Wang, S.; Ma, H.; Chen, Y. Chirality Plays Critical Roles in Enhancing the Aqueous Solubility of Nocathiacin I by Block Copolymer Micelles. *J. Pharm. Pharmacol.* **2013**, *65* (1), 64–71.

(8) Why are the Nitro and Sulfone Groups Poor Hydrogen Bonders? https://docplayer.net/35923053-Why-are-the-nitro-and-sulfone-groups-poor-hydrogen-bonders.html (accessed Oct 9, **2018**).

(9) Kamlet, M. J.; Doherty, R. M.; Abraham, M. H.; Marcus, Y.; Taft, R. W. Linear Solvation Energy Relationship. 46. An Improved Equation for Correlation and Prediction of Octanol/Water Partition Coefficients of Organic Nonelectrolytes (Including Strong Hydrogen Bond Donor Solutes). *J. Phys. Chem.* **1988**, *92* (18), 5244–5255.

5. GENERAL SUMMARY

The synthesis, solubility, and pharmacological profiling of PBI compounds were successfully conducted. As a result, a new series of *N*-benzyl-3-trifluoromethylpyrido[1,2-*a*]benzimidazole analogues was identified and widely explored, leading to the successful expansion of SAR and SPR studies. Established synthetic protocols were employed to synthesize target analogues, which were characterized using nuclear magnetic resonance spectroscopy [^{1}H- and ^{13}C-NMR] and HPLC coupled to mass spectrometry (HPLC-MS), and subjected to Mp determination.

5.1 Summary of antiparasitic activities *against P*fNF54, PfK1, NTS, and *adult S. mansoni* worms

In vitro antiplasmodium activities were assessed against the chloroquine-sensitive *P. falciparum* strain NF54 and the chloroquine-resistant strain K1. SAR 1.1 to 1.4 and SAR 2.1 to 2.5 analogues were tested *in vitro* against asexual and sexual blood-stage *Pf*NF54 malaria parasites. In addition to this evaluation, SAR 2.1 to 2.4 analogues were screened against the chloroquine-resistant *P. falciparum* strain K1. SAR 2.1 to 2.4 compounds demonstrated similar activities against both the *Pf*NF54 and *Pf*K1 strains. Furthermore, the *in vitro* antischistosomal activities of the analogues were evaluated against both NTS and adult *S. mansoni*. Except for compound **18**, which showed dual activity against the juvenile and the adult schistosomes, all compounds in this series demonstrated variable activity against the two stages of parasite development (figure 5.1). Moreover, the solubility of the **55** analogues synthesized in SAR 1.1 to 1.4 and 2.1 to 2.5 was assessed using the turbidimetric and HPLC-based kinetic solubility protocols.

5.2 Summary of *in vitro* antiplasmodium and antischistosomal activities of SAR 1 analogues

i. Analogues possessing an unsubstituted phenyl ring in the core scaffold demonstrated poor antiplasmodium activity and showed a 2- to 14-fold decrease in potency relative to that of **GMP-19**. Similarly, these analogues also demonstrated weak inhibition of the early and late stages of gametocytogenesis. Moreover, the compounds exhibited weak inhibition of the growth of both NTS and the adult worms (10 to 55% inhibition at 1.0 µM).

ii. Compounds containing the monosubstituted 8-chloro core PBI scaffold demonstrated poor activity with a 7- to >14-fold decrease in antiplasmodium activity compared to that of **GMP-19**. Similarly, the monosubstituted analogues also exhibited negligible gametocytocidal effects against both early- and late-stage parasites. Low antischistosomal activity was also observed (0 to 55% inhibition at 1.0 µM).

iii. Analogues derived from a 7,8-dichlorinated core PBI scaffold demonstrated significant improvement in both antiplasmodium and antischistosomal activities and showed a 2-, 4-, and 14-fold increase in potency relative to that of **GMP-19**. Analogues **7** (a most active compound from SAR 1.1) and **14** (a most active analogue from SAR 1.2) also exhibited improved gametocytocidal effects (78 and 85% inhibition in early- and late-stage gametocytes at 5.0 µM, respectively).

iv. The 7,8-difluorinated core PBI scaffold (SAR 1.4) conferred the greatest antiplasmodium potency relative to that of **GMP-19**. In this regard, 15 of the 19 analogues from SAR 1.1 to 1.3 showed sub-micromolar asexual blood stage antiplasmodium activities ranging between 0.022 and 0.940 µM. The following is noteworthy:

- They exhibited 2- to 20-fold increases in asexual blood-stage antiplasmodium activity relative to that of the front-runner compound **GMP-19**
- One compound **30** exhibited early-stage gametocytocidal activity, which was comparable to that of **MMV048** (72 and 77% inhibition at 1.0 µM for **30** and **MMV048**, respectively)
- Compound **30** demonstrated antischistosomal activity with a 69% NTS inhibition at 0.37 µM

5.2.1 Summary of structure-activity relationship

i. Lipophilicity was identified as a key determinant of activity in this part of the SAR study.

ii. Compounds containing benzylamine moieties with electron-rich hydrophilic groups exhibited poor antischistosomal and antiplasmodium activities against both the asexual and sexual stages.

iii. Sulfonyl substitution and ring contraction compromised antischistosomal and antiplasmodium activities against both the asexual and sexual stages of parasite development.

iv. Although further investigations may be required, *R*-enantiomers displayed stronger activities than their *S*-counterparts against both parasites.

v. *Para*-substituted compounds demonstrated superior antiplasmodium activity, with 3-fold increases in potency relative to their *ortho*-substituted counterparts.

Various substitutions and their relative effects on antiplasmodium and antischistosomal activities are summarized below in figure 5.1 while the distribution of antiplasmodium activity for all the 55 compounds is shown in figure 5.3.

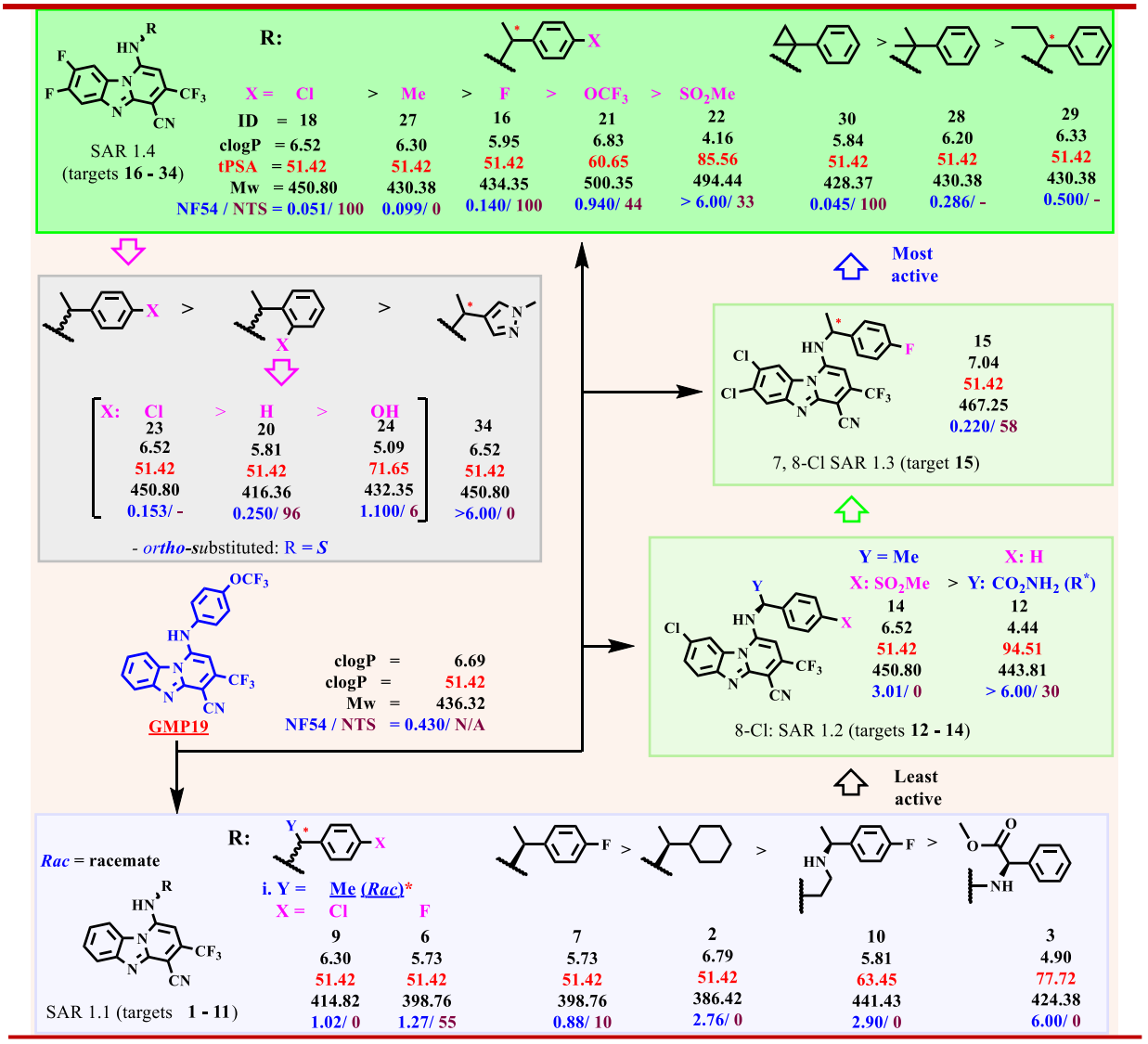

Figure 5.1: Antiplasmodium (IC_{50} (µM)) and antischistosomal (% inhibition at 1.00 µM) of the current PBI leads

5.2.2 Summary of solubility studies

Solubility studies were conducted using HPLC-based and turbidimetric kinetic solubility protocols. The melting points (Mp) were determined while predicted cLogP and the tPSA values were generated *in silico* for all analogues (figure 5.1) and compared to solubility. Findings were as follows:

i. As expected all analogues bearing a lipophilic substituent, such as the saturated lipophilic hexylamine, analogues **1** and **2**, and those containing chloro, fluoro, and methyl groups on the benzylamine ring, generally exhibited poor solubility (<10 µM).

ii. Chiral esters and their amide derivatives, analogues bearing a 2-carbon spacer (**10** and **11**), and the 5-membered heterocyclic-substituted analogue **34** demonstrated moderate to high solubility with 4- to 36-fold increases in solubility relative to that of **GMP-19**.

5.3 Summary of antiparasitic activity and solubility studies for SAR 2 analogues

Generally, the *in vitro* antiplasmodium and antischistosomal activities of SAR 2 analogues were improved. Analogues demonstrated up to a 36-fold increase in antiplasmodium potency relative to that of **GMP-19**. The following deductions were made:

5.3.1 Summary of antiparasitic activity

i. Antiplasmodium activity increased with lipophilicity as demonstrated by compound **53**;
   - The presence of electron-rich hydrophilic groups led to a decrease in activity against both the asexual and sexual blood-stage.
   - Replacing the 4-OCF_3Ph with hydrophilic amino moieties reduced the activity of C-3 CF_3-substituted analogues as exemplified by compound **48**.

ii. The introduction of partially acidic substituent moieties such as the sulfonyl and amide groups (**41** and **45**: figure 5.2) increased antischistosomal activity.

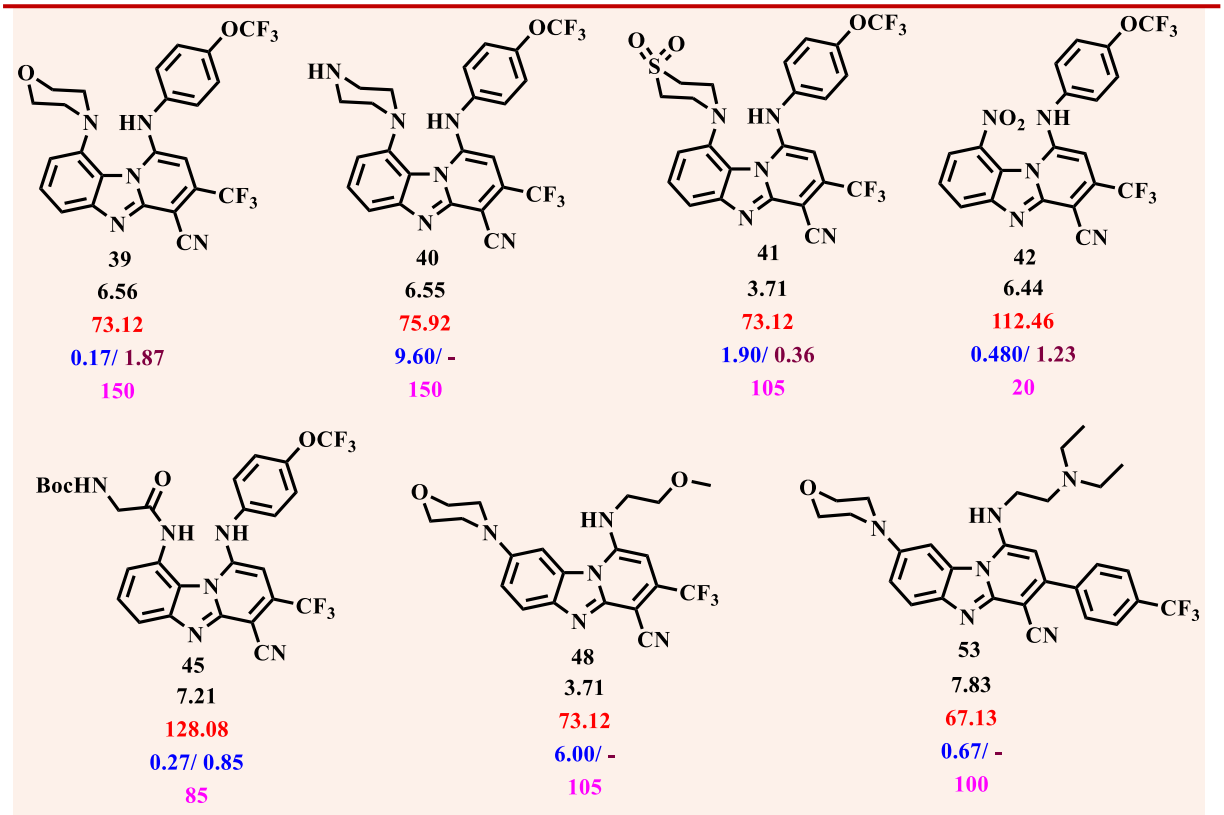

Figure 5.2: Antiparasitic activity and physicochemical profiles of selected SAR 2 analogues: cLogP (Black); tPSA (Red); NF54 (Blue); *S. mansoni* IC_{50} (µM: Brown); solubility (µM: Pink)

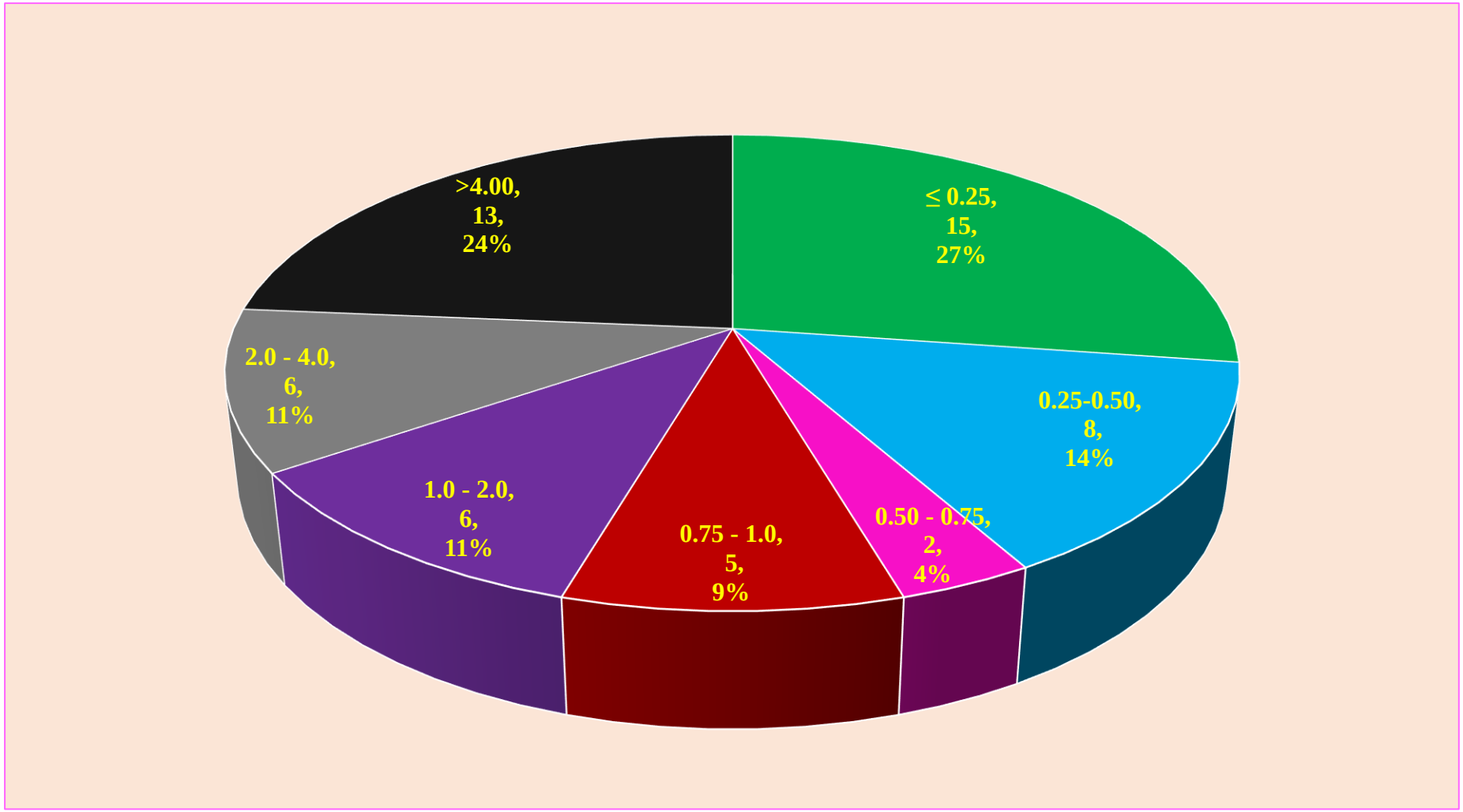

Figure 5.3: Statistical summary and distribution of antiplasmodium activities for all synthesized compounds (n = 55)
Activity ranges are in IC_{50} (µM) values against NF54 parasites

5.3.2 Summary of solubility studies

i. Generally, all analogues possessing a morpholino group on the phenyl ring and an acyclic amino moiety on the pyridyl ring of the core scaffold demonstrated a >30-fold increase in solubility relative to that of **GMP-19**.

ii. The introduction of amide functionalities on the phenyl ring of the core scaffold resulted in a >10-fold improvement in solubility relative to that of **GMP-19**.

iii. Compounds containing the sulfonyl group exhibited poor solubility, with approximately 4- and 7-fold reductions in aqueous solubility relative to that of analogous compounds **39** and **40**, respectively.

5.3.3 General summary of the physicochemical property profiling

i. In this study, cLogP, tPSA, and Mp were moderately correlated (R^2 = 0.298, 0.272, and 0.151, respectively), and were identified as suitable predictive parameters for solubility.

ii. No correlation was observed between solubility and HPLC t_R.

5.4 Future work and recommendations

5.4.1 Pharmacological profiling of SAR 1 and SAR 2 analogues

Considering the high sub-micromolar antiplasmodium activity exhibited by the newly explored *N*-benzyl-3-trifluoromethylpyrido[1,2-*a*]benzimidazole compounds, the following should be investigated:

i. Antischistosomal *in vitro* dose-response profiles (IC_{50})
ii. Cytotoxicity and metabolic stability profiles
iii. *In vivo* PK and efficacy profiles in appropriate animal models
iv. *Pf*K1 and cross-resistance profiles
v. Mechanism of action studies through target identification

5.4.2 Physicochemical profiling of SAR 1 and SAR 2 analogues

Poor solubility was observed in the most potent analogues, thus requiring medicinal chemistry optimization studies. The proposed SAR 1 and SAR 2 analogues were designed to improve the tPSA while maintaining some degree of lipophilicity.

5.4.3 Proposed SAR for physicochemical optimization of the α-methylbenzyl-PBI series

The recommendations are based on front-runner compounds **16**, **17**, **18**, **27,** and **30** as shown in figure 5.4.

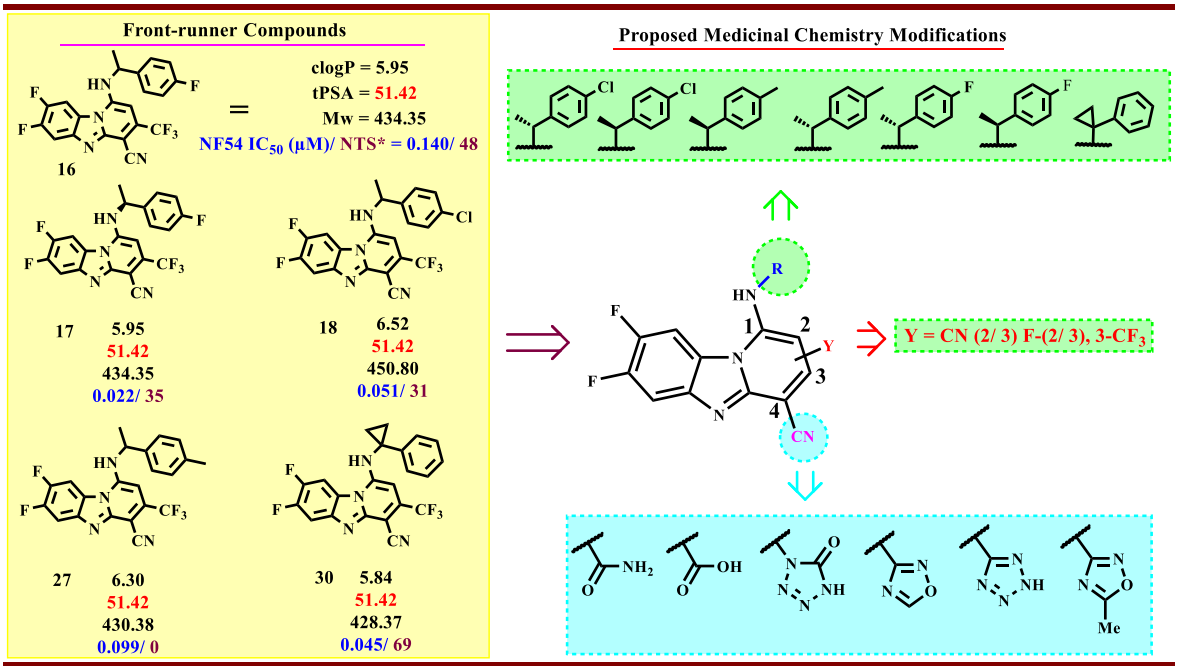

Figure 5.4: Proposed compounds for physicochemical property optimization

*Activity was determined as % inhibition at 0.37 µM, with 100% inhibition shown at 1.0 µM
Compound **27** exhibited no activity at both 0.37 and 1.0 µM.

5.4.4 Proposed SAR for physicochemical optimization of the SAR 2 series

Recommendations are based on front-runner compound **52** as shown in figure 5.5.

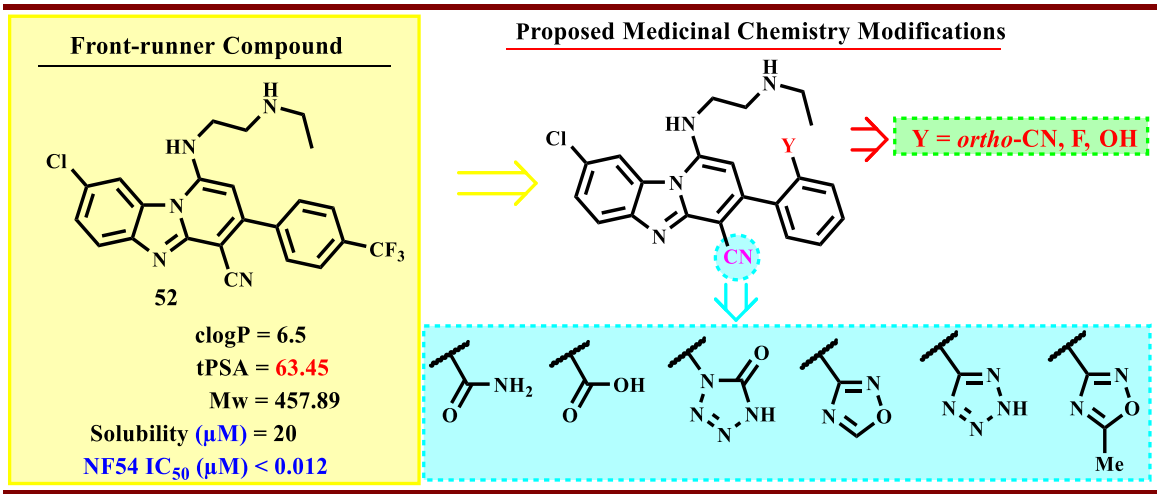

Figure 5.5: Proposed compounds for physicochemical properties optimization

5.4.5 *In silico* prediction of the physicochemical properties of proposed analogues

From this study, cLogP and tPSA were positively correlated with solubility. Therefore, the design of the new analogues aimed to maintain lipophilicity while increasing the tPSA. The details of the predicted physicochemical parameters including the tPSA (Å), cLogP, and calculated molar weights of the proposed new analogues for SAR 1 and SAR 2 are shown in figures 5.6 and 5.7, respectively.

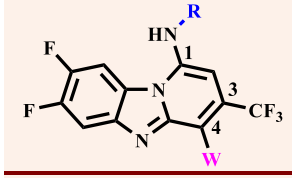

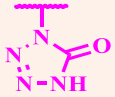

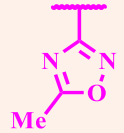

R	Parameter/target							
	65 ≤ tPSA ≤ 140	**51.42**	**70.72**	**64.93**	**81.45**	**61.58**	**76.74**	**61.58**
	cLogP ≤ 5	5.84	4.02	5.48	5.29	5.74	5.79	6.01
	Mol. Wt. ≤ 500	428.37	446.38	447.37	486.41	471.39	471.40	485.42
30	NF54 / NTS*	0.045/ 69	- -	- -	- -	- -	- -	- -
	cLogP ≤ 5	6.52	4.70	6.16	6.15	6.42	6.47	6.69
	Mol. Wt. ≤ 500	450.80	468.81	469.81	508.84	493.82	493.83	507.85
18	NF54 / NTS*	0.051/ 31	- -	- -	- -	- -	- -	- -
	R	- -	- -	- -	- -	- -	- -	- -
	S	- -	- -	- -	- -	- -	- -	- -
	cLogP ≤ 5	6.30	4.48	5.94	5.94	6.21	6.26	6.48
	Mol. Wt. ≤ 500	430.38	448.40	449.38	488.42	473.41	473.41	487.43
27	NF54 / NTS*	0.099/ 0	- -	- -	- -	- -	- -	- -
	R	- -	- -	- -	- -	- -	- -	- -
	S	- -	- -	- -	- -	- -	- -	- -
	cLogP ≤ 5	5.95	4.13	5.59	5.58	5.85	5.90	6.12
	Mol. Wt. ≤ 500	434.35	452.36	453.34	492.35	477.37	477.37	491.40
16	NF54 / NTS*	0.140/ 48	- -	- -	- -	- -	- -	- -
	R	0.022/ 35	- -	- -	- -	- -	- -	- -
	S	- -	- -	- -	- -	- -	- -	- -

Figure 5.6: Future work and recommendations for SAR 1

*Activity is expressed as % inhibition at 0.37 µM, with 100% inhibition shown at 1.0 µM; *% inhibition at both 0.37 and 1.0 µM;

- - recommended assays for future work

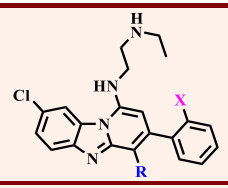

X	Parameter/target	CN	$CONH_2$	COOH	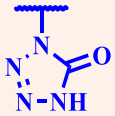			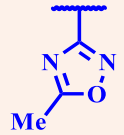
	**65 ≤ tPSA ≤ 140**	**63.45**	**82.75**	**76.96**	**93.48**	**73.61**	**88.77**	**76.61**
	clogP ≤ 5	5.79	4.66	3.11	5.04	5.02	5.06	5.29
	clogP ≤ 500	407.88	425.89	426.88	465.92	450.90	450.91	464.93
	**65 ≤ tPSA ≤ 140**	**87.24**	**106.54**	**100.75**	**117.27**	**97.4**	**112.56**	**97.40**
	clogP ≤ 5	5.08	3.95	2.40	4.33	4.31	4.35	4.58
	clogP ≤ 500	419.90	432.91	433.90	472.94	457.92	457.93	471.95
	**65 ≤ tPSA ≤ 140**	**83.68**	**102.98**	**97.19**	**113.71**	**93.84**	**109.00**	**93.84**
	clogP ≤ 5	4.69	3.56	2.01	3.93	3.91	3.95	4.18
	clogP ≤ 500	405.89	423.90	424.89	463.93	448.91	448.92	462.94
	**65 ≤ tPSA ≤ 140**	**72.68**	**91.98**	**86.90**	**102.71**	**82.84**	**98.00**	**82.84**
	clogP ≤ 5	5.00	3.88	2.32	4.25	4.23	4.28	4.50
	clogP ≤ 500	419.91	437.93	438.91	477.95	462.94	462.94	476.97
	**65 ≤ tPSA ≤ 140**	**80.52**	**99.82**	**94.03**	**110.55**	**90.68**	**105.84**	**90.68**
	clogP ≤ 5	4.06	2.93	1.38	3.31	3.28	3.33	3.55
	clogP ≤ 500	451.97	469.99	470.97	486.41	510.01	495.00	509.03

Figure 5.7: Future work and recommendations for SAR 2

6. EXPERIMENTAL

6.1 Chapter Overview

In Chapter six, supplementary experimental protocols and spectroscopic data for Chapters 2, 3, and 4 are described. The Chapter starts with a description of chemical materials used, the instrumental and technical requirements for the testing after which a detailed spectroscopic characterization of all the synthesized intermediate and target molecules is covered. The chapter ends with the description of biological assay protocols used to generate biological data reported in this dissertation.

6.2 Chemistry

6.2.1 Reagents and Solvents

All the commercially available chemicals and reagents were purchased from either Sigma-Aldrich in South Africa or Combi-Blocks Limited in the United States of America (USA) and were used without further purification. All the anhydrous solvents such as 1,4-dioxane, dimethyl sulfoxide (DMSO), acetonitrile (CH_3CN) and dimethylformamide (DMF) were purchased as such from Sigma Aldrich (South Africa). However, only tetrahydrofuran (THF) and ethanol which were purchased and used as analytical reagent (AR) grade and absolute (99.9%), respectively. HPLC grade solvents such as CH_3CN and methanol (MeOH) for HPLC-MS mobile phase preparation were purchased from Romil Ltd (Cambridge, UK).

6.2.2 Chromatography

The progress of reactions was monitored by a combination of analytical thin layer chromatography (TLC) and HPLC-MS. The TLC plates employed were sourced from Merck (TLC Silica gel 60 F254 coated on aluminium sheets). The TLC plates were visualized under ultraviolet light (UV 254 and 366 nm). An Agilent LC-MS instrument with the following components was used to monitor the progress of reactions including per cent purity determinations: Agilent 1260® Infinity Binary Pump, Agilent 1260® Infinity Diode Array Detector, Agilent 1290® Infinity Column Compartment, Agilent 1260® Infinity Autosampler, Agilent 6120® Quadrupole LC/MS, and Peak Scientific® Genius 1050 Nitrogen Generator. An X-bridge® (C18, 2.5 µm, 3.0 mm (ID) x 50 mm length) column maintained at 35 °C was used. The chromatographic mobile phases composed of 10 mM aqueous ammonium acetate (NH_4OAc) spiked with 0.4% acetic acid and 10 mM NH_4OAc in methanol spiked with 0.4% acetic acid (figure 6.1). The mass spectra were acquired using electrospray ionisation (ESI) or atmospheric pressure chemical ionization (APCI) in the positive or negative ionisation modes, respectively depending on the nature of the compound.

Time (min)	% A	% B	Composition	
			A	B
0.00-1.00	90	10	10.0 mM NH_4OAc (0.40% acetic acid buffer)	10.0 mM NH4OAc (0.40% acetic acid buffer) in 90% HPLC grade CH_3OH in H_2O
1.00-3.00	5	95		
3.00-5.00	5	95		
5.00-6.50	90	10		
6.50-7.00	90	10		

Figure 6.1: HPLC gradient conditions summary

Biotage grade silica gel was employed for column chromatographic purifications on the Biotage Isolera One Flash Chromatography system. The manual glass tube columns employed *Fluka* high purity grade silica gel (pore size 60 Å, 70 – 230 mesh, 63 – 200 µm). Additionally, Analtech Uniplate preparative TLC (prep-TLC) plates (20 × 20 cm, 2000 microns) were used for prep-TLC purifications. The solvents used as mobile phases were AR grade and were used without further distillation.

6.2.3 Spectroscopic characterization

^{1}H NMR and ^{13}C NMR spectra were recorded on a Ultrashield-Plus Bruker or Varian Mercury 300 (^{1}H 300.1, ^{13}C 75.5 MHz) or a Bruker (600 MHz) spectrometers. All ^{1}H NMR and ^{13}C NMR spectra were acquired at 30 °C in deuterated solvents ($CDCl_3$, CD_3OD, CD_3CN, or DMSO-d_6). The one-dimensional ^{1}H NMR and ^{13}C NMR spectra were processed using MestReNova 6.2.1-7569. Multiplicity patterns are reported using the following abbreviations br s = broad singlet, d = doublet, t = triplet, q = quartet, m = multiplet, dd = doublet of doublets, ddd = doublet of doublet of doublets, dt = doublet of triplets. Coupling constants (*J* values) are reported in Hertz (Hz).

6.2.4 Physical characterization

Melting points were measured using a digital thermometer Reichert Jung THERMONOVAR. The 4-chlorophenyl boronic acid (m.p = 284 – 289 °C) was used as a melting point control sample and was read every ten measurements. An average melting point 285 – 291 °C (n = 6) was obtained. The recorded melting points were measured in duplicate and are an average of the clear point which is a temperature at which all solid material on the slides turns to liquid. All the final compounds were subjected to purity check experiments using HPLC-MS to ensure an acceptable level of purity (≥ 95%).

6.3 Synthesis and Characterization

6.3.1 General procedure for the synthesis of benzimidazole acetonitrile intermediate compounds 1.1*a* – 2.2*a*

A suitably substituted 1,2-diaminobenzene (1.0 equiv), ethyl cyanoacetate (3.0 equiv) and DMF (1.0 mL/ 0.100g sample) were stirred at 160°C for 3 hours. At the completion of the reaction, the reaction mixture was cooled to room temperature, diluted with ethyl acetate, washed with 20mL portions of 5% lithium chloride (20 mL x 3), distilled water (20 mL x 3) and brine (10 mL x 3) in a separatory funnel. The treated organic layer was dried on anhydrous $MgSO_4$, concentrated and finally dried *in vacuo*. For the nitro-substituted benzimidazole, the product was purified by trituration using toluene at 40-45 °C filtered and solid **2.1.2*a*** was washed with diethyl ether and dried at ambient conditions. The toluene mixture was concentrated and solid was triturated using diethyl ether to obtain **2.1.1*a***.

2-(6-chloro-1H-benzo[d]imidazol-2-yl)acetonitrile,* 1.2*a

Compound **1.2*a*** was obtained from 4-chloro-1,2-diaminobenzene (**1.2**) (2.5 g, 17.53 mmol, 1.0 equiv), ethyl cyanoacetate (5.6 mL, 0.053 Mol., 3.0equiv) as a brown solid (2.82 g, 84%); Rf (MeOH : DCM, 0.5 : 9.5) 0.26; ^{1}H NMR (400 MHz, Acetonitrile-d_3) δ 12.9 (s, 1H, H^5), 7.6 (d, J = 1.9 Hz, 1H, H^4), 7.5 (d, J = 8.6 Hz, 1H, H^2), 7.2 (dd, J = 8.6, 1.9 Hz, 1H, H^3), 4.17 (s, 2H, H^1). ^{13}C NMR (101 MHz, Acetonitrile-d_3) δ 145.9, 127.8, 122.9 (3C), 115.5, 18.7 (3C). HPLC-MS (ACI/ ESI): Purity =86%, t_R = 0.74 min, m/z $[M-H]^-$ = 190.0.

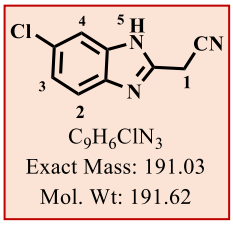

$C_9H_6ClN_3$
Exact Mass: 191.03
Mol. Wt: 191.62

2-(5,6-dichloro-1H-benzo[d]imidazol-2-yl)acetonitrile*, 1.3*a

Compound **1.3*a*** was obtained from 4,5-dichlorobenzene-1,2-diamine (**1.3**) (0.088 g, 0.50 mmol, 1.0 equiv) and ethyl cyanoacetate (0.170 g, 1.50 mmol, 3.0 equiv) as brown solid (0.073 g, 65 %); Rf (MeOH : DCM, 0.5 : 9.5) 0.30; ^{1}H NMR (400 MHz, DMSO-*d6*) δ 12.9 (s, 1H, H^4), 7.9 (s, 2H, $H^{2,3}$), 4.4 (s, 2H, H^1); ^{13}C NMR (101 MHz, DMSO-*d6*) δ 148.4, 145.2, 143.4, 120.4, 116.7, 116.0, 113.5, 110.2, 18.9; HPLC-MS (APCI/ESI): Purity = 90%, t_R = 4.01 min, *m/z* $[M+H]^+$ = 226.0.

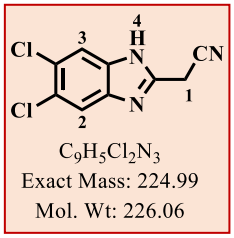

$C_9H_5Cl_2N_3$
Exact Mass: 224.99
Mol. Wt: 226.06

2-(5,6-difluoro-1H-indol-2-yl)acetonitrile*, 1.4*a

Compound **1.4*a*** was obtained from 4,5-difluorobenzene-1,2-diamine (**1.4**) (3.48 g, 23.84 mmol, 1.0 equiv) and ethyl cyanoacetate (8.09 g, 71.49 mmol ml 3.0 equiv) as a deep red solid (2.98 g, 65%); Rf (MeOH : DCM, 1 : 9) 0.32; ^{1}H NMR (300 MHz, DMSO-d_6) δ 12.8 (s, 1H, H^{4}), 7.6 (s, 2H, H$^{2, 3}$), 4.4 (s, 2H, H^{1}). ^{13}C NMR (101 MHz, DMSO-d_6) δ 148.4, 147.4, 146.0, 116.8, 106.5 (2C), 100.1 (2C), 18.9. HPLC-MS (ACI/ ESI): Purity = 90%, t_R = 2.24 min, m/z [M-H]$^-$ = 192.1.

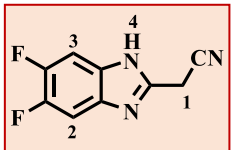

$C_{10}H_6F_2N_2$
Exact Mass: 192.05
Mol.Wt: 192.17

2-(7-Chloro-1H-benzo[d]imidazole-2-yl)acetonitrile*, 2.1.2*a

Compound **2.1.2*a*** was obtained from 3-nitro-1,2-diaminobenzene (**2.1**) (5.0 g, 32.65 mol, 1.0 equiv) and ethyl cyanoacetate (11.1 g, 97.45 mmol 3.0 equiv) as a yellowish solid (5.4 g, 82%); Rf (EtOAc : Hexane, 7 : 3) 0.43; ^{1}H NMR (300 MHz, DMSO-d_6) δ 8.2 (dd, J = 8.2, 1.0 Hz, 1H, H^{4}), 8.1 (dd, J = 8.0, 1.0 Hz, 1H, H^{2}), 7.4 (t, J = 8.1 Hz, 1H, H^{3}), 4.3 (s, 2H, H^{1}); ^{13}C NMR (151 MHz, DMSO-d_6) δ 149.2, 146.3, 133.4, 128.9, 127.3, 122.0, 119.5, 116.5, 18.8. HPLC-MS (ACI/ ESI): Purity = 99%, t_R = 3.06 min, m/z [M-H]$^-$ = 200.9.

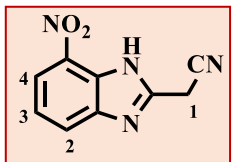

$C_9H_6N_4O_2$
Exact Mass: 202.05
Mol. Wt: 202.17

2-(7-Chloro-1H-benzo[d]imidazole-2-yl)acetonitrile*, 2.2*a

Compound **2.2*a*** was obtained from 3-chloro-1,2-diaminobenzene (**2.2**) (2.6 g, 18.23 mol, 1.0equiv) and ethyl cyanoacetate (6.20 g, 54.70 mmol, 3.0 equiv) as a brown solid (2.8 g, 80%); Rf (EtOAc : Hexane, 7 : 3) 0.33; ^{1}H NMR (300 MHz, DMSO-d_6) δ 13.0 (s, 1 H, H^{5}), 7.5 (dd, J = 7.5, 1.1 Hz, 1H, H^{4}), 7.3 (dd, J = 7.8, 1.1 Hz, 1H, H^{2}), 7.2 (t, J = 7.8 Hz, 1H, H^{3}), 4.4 (s, 2H, H^{1}). ^{13}C NMR (151 MHz, DMSO-d_6) δ 149.2, 146.3, 133.4, 128.9, 127.3, 122.0, 119.5, 116.5, 18.8. HPLC-MS (ACI/ ESI): Purity = 96%, t_R = 1.71 min, m/z [M+H]$^+$ = 191.9.

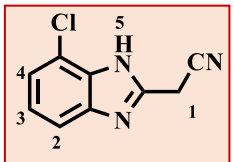

$C_9H_6ClN_3$
Exact Mass: 191.03
Mol Wt: 191.62

6.3.2 General procedure for the synthesis of hydroxy intermediates compounds (1.1*b* – 2.4*b*)

An appropriate benzimidazole acetonitrile (1.0 equiv), a suitably substituted β-keto ester (1.2 equiv) and ammonium acetate (2.0 equiv) were stirred under reflux conditions at 145 °C for 2 hours. Following completion of the reaction, the mixture was cooled to 70°C, followed by addition of 10 mL acetonitrile and stirring reaction product mixture stirred for a further 10 minutes at that temperature. The treated reaction mixture was cooled to room temperature. The cooled reaction mixture was filtered, the resulting solid product was washed with cold acetonitrile (2-3 mL x 3), dry ether (3-5mL x 3) and finally, the product was dried at ambient conditions. The product was used in subsequent step without further purification.

1-hydroxy-3-(trifluoromethyl)benzo[4,5]imidazo[1,2-a]pyridine-4-carbonitrile,* 1.1*b

Compound **1.1*b*** was obtained from **1.1*a*** (1.25 g, 7.95 mmol, 1.0 equiv) and ethyl 4,4,4-trifluoro-3-oxobutanoate (1.76 g, 9.54 mmol, 1.2 equiv) and ammonium acetate (1.23 g, 15.90 mmol, 2.0 equiv) as a brown solid (0.88 g, 40%); Rf (EtOAc : Hexane, 3 : 7) 0.22; ^{1}H NMR (300 MHz, DMSO-d_6) δ 8.6 (dd, J = 7.8, 1.6 Hz, 1H, H^{5}), 7.6 (dd, J = 7.8, 1.6 Hz, 1H, H^{2}), 7.6 – 7.5 (dt, J = 7.8, 1.6 Hz, 1H, H^{3}), 7.3 (dt, J = 7.7, 1.7 Hz, 1H, H^{4}), 6.23 (s, 1H, H^{1}). ^{13}C NMR (101 MHz, DMSO-d_6) δ 158.3 (3C), 148.3, 132.4, 127.8, 123.5, 116.8, 114.6, 112.3, 111.2, 103.3 (2C). HPLC-MS (ACI/ ESI): Purity = 98%, t_R = 2.57 min, m/z $[M+H]^+$ = 278.0.

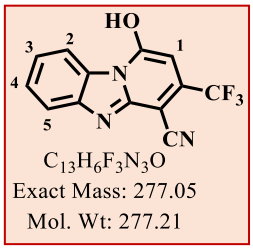

$C_{13}H_6F_3N_3O$
Exact Mass: 277.05
Mol. Wt: 277.21

8-chloro-1-hydroxy-3-(trifluoromethyl)benzo[4,5]imidazo[1,2-a]pyridine-4-carbonitrile,* 1.2*b

Compound **1.2*b*** was obtained from **1.2*a*** (1.90 g, 9.92 mmol, 1.0 equiv) and ethyl 4,4,4-trifluoro-3-oxobutanoate (2.19 g, 11.90 mmol, 1.2 Eq) as yellow solid (2.16 g, 70%); Rf (MeOH : DCM, 0.5 : 9.5) 0.20. ^{1}H NMR (300 MHz, DMSO-d_6) δ 8.5 (d, J = 2.2 Hz, 1H, H^{4}), 7.7 (d, J = 8.6 Hz, 1H, H^{2}), 7.5 (dd, J = 8.4, 2.2 Hz, 1H, H^{3}), 6.4 (s, 1H, H^{1}). ^{13}C NMR (101 MHz, DMSO-d_6) δ 158.0, 127.7, 123.4 (2C), 117.9 (2C), 116.4 (2C), 114.2, 112.4 (2C), 103.1 (2C). HPLC-MS (ACI/ ESI): Purity = 96%, t_R = 2.95 min, m/z $[M+H]^+$ = 309.9.

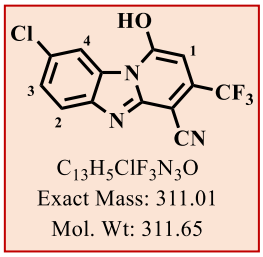

$C_{13}H_5ClF_3N_3O$
Exact Mass: 311.01
Mol. Wt: 311.65

7,8-dichloro-1-hydroxy-3-(trifluoromethyl)benzo[4,5]imidazo[1,2-a]pyridine-4-carbonitrile:* 1.3*b

Compound **1.3*b*** was obtained from **1.3*a*** (0.113 g, 0.50 mmol, 1.0equiv) and ethyl 4,4,4-trifluoro-3-oxobutanoate (0.110 g, 0.60 mmol, 1.2 equiv) and as grey solid (0.142 g, 82 %) Rf (EtOAc : Hexane 7 : 3) 0.36; ^{1}H NMR (300 MHz, DMSO-*d6*) δ 8.7 (s, 1H, H^{2}), 7.7 (s, 1H, H^{1}), 6.5 (s, 2H, $H^{2, 3}$). ^{13}C NMR (101 MHz, DMSO) δ 170.9, 168.0, 158.0, 155.2, 145.2, 130.2, 128.5, 124.0, 121.3, 116.7, 118.0, 117.7, 95.4. HPLC-MS (APCI/ESI): Purity = 96%, t_R = 2.98 min, *m/z* $[M+H]^+$ = 346.0.

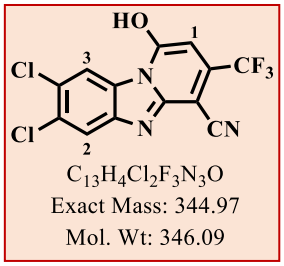

$C_{13}H_4Cl_2F_3N_3O$
Exact Mass: 344.97
Mol. Wt: 346.09

***7,8-difluoro-1-hydroxy-3-(trifluoromethyl)benzo[4,5]imidazo[1,2-a]pyridine-4-carbonitrile,* 1.4*b*.**

Compound **1.4*b*** was obtained from **1.4*a*** (2.86 g, 14.80 mmol, 1.0 equiv), ethyl 4,4,4-trifluoro-3-oxobutanoate (3.26 g, 17.8 mmol, 1.2 equiv) as a brown solid (1.76 g, 86%); Rf (EtOAc : Hexane, 7 : 3) 0.25; ^{1}H NMR (300 MHz, DMSO-d_6) δ 8.5 (dd, *J* = 10.3, 7.4 Hz, 1H, H^{2}), 7.7 (dd, *J* = 10.0, 7.0 Hz, 1H, H^{3}), 6.4 (s, 1H, H^{1}). ^{13}C NMR (101 MHz, DMSO-d_6) δ 157.8, 149.4, 129.7, 123.7, 114.7, 105.6 (2C), 102.7 (3C), 101.5 (3C). HPLC-MS (ACI/ ESI): Purity = 99%, t_R = 2.69 min, m/z $[M-H]^-$ = 313.03.

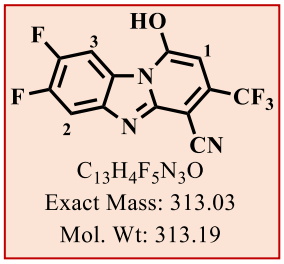

$C_{13}H_4F_5N_3O$
Exact Mass: 313.03
Mol. Wt: 313.19

1-hydroxy-9-Nitro-3-(trifluoromethyl)benzo[4,5]imidazo[1,2-a]pyridine-4-carbonitrile,* 2.1.2*b

Compound **2.1.2*b*** was obtained **2.1.2*a*** (5.0 g, 25 mmol, 1.0 equiv) and ethyl 4,4,4-trifluoro-3-oxobutanoate (0.29 g, 4.6 ml 1.2 equiv) and ammonium acetate (3.9 mg, 50 mmol, 2.0 equiv) as red solid (3.4 g, 42%); Rf (EtOAc : Hexane, 8 : 2) 0.25; ^{1}H NMR (300 MHz, DMSO-d_6) δ 9.0 (d, *J* = 8.0 Hz, 1H, H^{4}), 8.3 (d, *J* = 8.3 Hz, 1H, H^{2}), 7.5 (t, *J* = 8.2 Hz, 1H, H^{3}), 6.4 (s, 1H, H^{1}); ^{13}C NMR (151 MHz, DMSO-d_6) δ 158.5, 151.8, 139.7, 134.5, 132.3, 123.7, 122.3 (2C), 121.9, 121.5, 114.9, 102.2, 67.4. HPLC-MS (ACI/ ESI): purity = 99%, t_R = 1.23 min, m/z $[M+H]^+$ = 323.0.

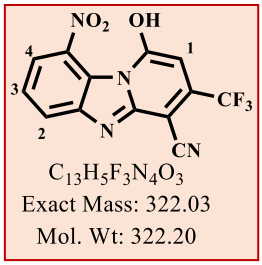

$C_{13}H_5F_3N_4O_3$
Exact Mass: 322.03
Mol. Wt: 322.20

9-chloro-1-hydroxy-3-(trifluoromethyl)benzo[4,5]imidazo[1,2-a]pyridine-4-carbonitrile,* 2.2*b

Compound **2.2*b*** was obtained from **2.2*a*** (1.1 g, 5.6 mmol, 1.0 equiv), ethyl 4,4,4-trifluoro-3-oxobutanoate (1.2 g, 6.8 mmol, 1.2 Eq) and ammonium acetate (0.97, 12.5 mmol, 2.0 equiv) as a beigy solid (1.4 g, 80%); Rf (EtOAc : Hexane, 7 : 3) 0.32; ^{1}H NMR (300 MHz, Chloroform-d_3) δ 8.6 (dd, J = 8.8, 1.2 Hz, 1H, H^{4}), 7.8 (dd, J = 7.8, 1.2 Hz, 1H, H^{2}), 7.5 (t, J = 7.9 Hz, 1H, H^{3}), 7.3 (s, 1H, H^{1}). ^{13}C NMR (101 MHz, DMSO-d_6) δ 166.0, 125.8 (2C), 122.3 (2C), 121.6, 121.4 (2C), 119.7, 118.3, 117.0, 96.6 (2C); HPLC-MS (ACI/ ESI): Purity = 99%, t_R = 2.63 min, m/z [M+H]$^{+}$ = 309.7.

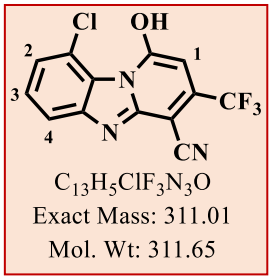

$C_{13}H_5ClF_3N_3O$
Exact Mass: 311.01
Mol. Wt: 311.65

8-chloro-1-hydroxy-3-(4-(trifluoromethyl)phenyl)benzo[4,5]imidazo[1,2-a]pyridine-4-carbonitrile*, 2.4*b

Compound **2.4*b*** was obtained from **1.2*a*** (1.47 g, 7.67 mmol, 1.0 equiv) and ethyl 3-oxo-3-(4-(trifluoromethyl)phenyl)propanoate (2.39 g, 9.20 mmol, 1.2 equiv) as brown solid (1.72 g, 58%; Rf (EtOAc : Hexane, 7 : 10) 0.27. ^{1}H NMR (600 MHz, DMSO-d_6) δ 8.6 (d, J = 2.0 Hz, 1H, H^{4}), 7.9 (d, J = 8.1 Hz, 2H, H^{6}), 7.9 (d, J = 8.0 Hz, 2H, H^{5}), 7.6 (d, J = 8.4 Hz, 1H, H^{2}), 7.4 (dd, J = 8.3, 2.1 Hz, 1H, H^{3}), 6.1 (s, 1H, H^{1}). ^{13}C NMR (151 MHz, DMSO-d_6) δ 158.2, 151.8, 148.5, 141.4, 131.6, 129.5 (3C), 127.2, 126.0 (3C), 123.2, 117.9, 116.4, 113.4, 111.8, 105.7, 105.5. HPLC-MS (ACI/ ESI): Purity = 98%, t_R = 3.02 min, m/z [M+H]$^{+}$ = 388.0.

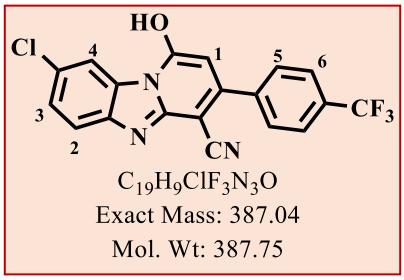

$C_{19}H_9ClF_3N_3O$
Exact Mass: 387.04
Mol. Wt: 387.75

6.3.3 General procedure for the synthesis of the chlorinated intermediates (1.1*c* – 2.4*c*)

A mixture of an appropriate hydroxy intermediate compound (1.0 equiv) and phosphoryl oxychloride ($POCl_3$: 20.0 equiv) was stirred at 130°C for 3 hours. On completion of the reaction, the reaction mixture was cooled to room temperature. The excess $POCl_3$ was removed *in vacuo*. Ice cooled water (20 mL) was added to the treated reaction mixture with consistent stirring for 15 minutes. The mixture was neutralized using sodium bicarbonate, crude product filtered off, washed with water and dried at ambient conditions. The product was used in the subsequent step without further purification.

1-chloro-3-(trifluoromethyl)benzo[4,5]imidazo[1,2-a]pyridine-4-carbonitrile*, 1.1*c

Compound **1.1*c*** was obtained from **1.1*b*** (0.94 g, 3.39 mmol, 1.0 Eq) and $POCl_3$ (10.4 g, 67.82 mmol, 20 Eq) as a yelow solid (0.812 g, 81%); Rf (EtOAc : Hexane, 1 : 9) 0.35; ^{1}H NMR (300 MHz, chloroform-*d*) δ 8.7 (dd, *J* = 7.8, 1.2 Hz, 1H, H^2), 8.6 (dd, *J* = 7.8, 1.2 Hz, 1H, H^5), 7.8 (dt, *J* = 7.8, 1.3 Hz, 1H, H^3), 7.6 (dt, *J* = 8.1, 1.2 Hz, 1H, H^4), 7.2 (s, 1H, H^1). ^{13}C NMR (101 MHz, DMSO-d_6) δ 158.1, 148.0, 132.3, 127.8 (2C), 123.6 (2C), 116.8 (2C), 112.3 (2C), 103.3 (2C). HPLC-MS (ACI/ ESI): Purity = 99%, t_R = 3.25 min, m/z $[M+H]^+$ = 296.0.

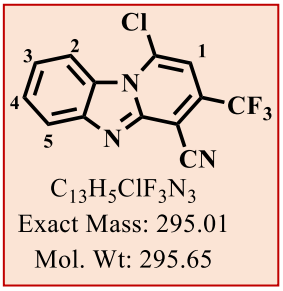

$C_{13}H_5ClF_3N_3$
Exact Mass: 295.01
Mol. Wt: 295.65

1,8-dichloro-3-(trifluoromethyl)benzo[4,5]imidazo[1,2-a]pyridine-4-carbonitrile*, 1.3*c

Compound **1.3*c*** was obtained from **1.3*b*** (1.2 g, 3.9 mmol, 1.0 equiv) and $POCl_3$ (1.3 g, 79 mmol, 1.5 equiv) as yellow solid (0.7 g, 85%); Rf (EtOAc : Hexane, 1.5 : 8.5) 0.21. ^{1}H NMR (600 MHz, DMSO-d_6) δ 8.7 (d, *J* = 1.1 Hz, 1H, H^4), 8.2 (d, *J* = 8.6 Hz, 1H, H^2), 7.9 (s, 1H, H^1), 7.7 – 7.6 (dd, *J* = 9.1, 1.1 Hz 1H, H^3). ^{13}C NMR (101 MHz, DMSO-d_6) δ 157.8, 148.6, 132.0, 127.9, 123.6, 117.9, 116.2, 114.3, 113.6, 112.0, 103.7 (3C). HPLC-MS (ACI/ ESI): Purity = 91%, t_R = 1.13 min, m/z $[M-H]^-$ = 329.90.

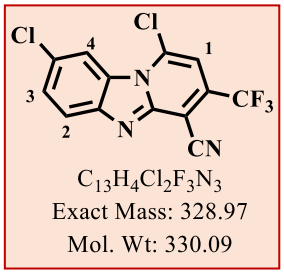

$C_{13}H_4Cl_2F_3N_3$
Exact Mass: 328.97
Mol. Wt: 330.09

1,7,8-trichloro-3-(trifluoromethyl)benzo[4,5]imidazo[1,2-a]pyridine-4-carbonitrile*, 1.3*c

Compound **1.3*c*** was obtained from **1.3*b*** (0.080 g, 0.23 mmol, 1.0 equiv) and $POCl_3$ (0.71 g, 4.6 mmol, 20.0 equiv) as yellow solid (0.080 g, 95 %) Rf (EtOAc : Hexane 1 : 9) 0.25; 1H NMR (300 MHz, DMSO-*d6*) δ 8.86 (s, 1H, H^3), 8.4 (s, 1H, H^1), 7.9 (s, 1H, H^2); 13C NMR (101 MHz, DMSO) δ 158.3 (2C), 150.2 (4C), 139.2, 132.7, 124.3 (2C), 120.3, 117.4. HPLC-MS (APCI/ESI): Purity = 99%, t_R = 5.04 min, m/z $[M-H]^-$ = 361.93.

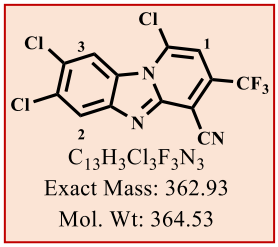

$C_{13}H_3Cl_3F_3N_3$
Exact Mass: 362.93
Mol. Wt: 364.53

1-chloro-7,8-difluoro-3-(trifluoromethyl)benzo[4,5]imidazo[1,2-a]pyridine-4-carbonitrile,* 1.4*c

Compound **1.4*c*** was obtained from **1.4*b*** (0.93 g, 3.0 mmol, 1.0 equiv) and phosphoryl oxychloride (9.11 g, 59.3 mmol, 20 equiv) as yellow solid (0.93 g, 95%); Rf (EtOAc : Hexane, 1.5 : 8.5) 0.17; ^{1}H NMR (300 MHz, DMSO-d_6) δ 8.8 (dd, J = 11.0, 7.4 Hz, 1H, H^{2}), 8.2 (dd, J = 10.7, 7.6 Hz, 1H, H^{3}), 7.9 (s, 1H, H^{1}). ^{13}C NMR (101 MHz, DMSO-d_6) δ 157.7, 136.8, 112.4, 108.3 (2C), 107.8, 107.6, 105.4, 105.1, 103.0 (2C), 101.5, 101.3. HPLC-MS (ACI/ ESI): Purity = 99%, t_R = 2.80 min, m/z $[M+H]^+$ = 332.0.

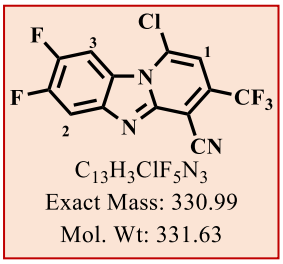

$C_{13}H_3ClF_5N_3$
Exact Mass: 330.99
Mol. Wt: 331.63

1-chloro-9-nitro-3-(trifluoromethyl)benzo[4,5]imidazo[1,2-a]pyridine-4-carbonitrile,* 2.1.2*c

Compound **2.1.2*c*** was obtained from **2.1.2*b*** (0.40 g, 1.4 mmol, 1.0 equiv) and $POCl_3$ (2.6 g, 28.0 mmol, 20.0 equiv) as a yellow solid (0.37 g, 78%); Rf (MeOH : DCM, 0.5 : 9.5) 0.25. ^{1}H NMR (400 MHz, DMSO-d_6) δ 7.8 (d, J = 8.1 Hz, 1H, H^{4}), 7.1 (t, J = 7.9 Hz, 1H, H^{3}), 6.8 (d, J = 7.9 Hz, 1H, H^{2}), 6.2 (s, 1H, H^{1}). ^{13}C NMR (101 MHz, DMSO-d_6) δ 158.7, 148.0, 13.0, 129.3, 123.7 (2C), 115.8, 111.1 (2C), 104.7 (2C), 100.3 (2C). HPLC-MS (ACI/ ESI): Purity = 96%, t_R = 1.04 min, m/z $[M+H]^+$ = 341.0.

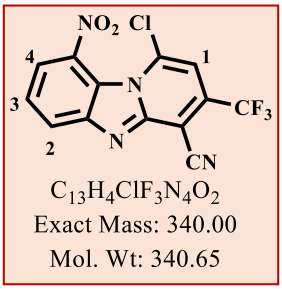

$C_{13}H_4ClF_3N_4O_2$
Exact Mass: 340.00
Mol. Wt: 340.65

9-chloro-1((4-(trifluoromethoxy)phenyl)amino)-3-(trifluoromethyl)benzo[4,5]-imidazo-[1,2-a] pyridine-4-carbonitrile*, 2.2*c

Compound **2.2*c*** was obtained from **2.2*b***, (0.85 g, 5.2 mmol, 1.0 equiv), and 4-(trifluoromethoxy)aniline (0.92 g, 5.2 mmol, 2.0 equiv) as a yellow solid (0.80 g, 94%); Rf (DCM) 0.25; ^{1}H NMR (300 MHz, chloroform-d_3) δ 8.6 (dd, J = 8.7, 0.9 Hz, 1H, H^{2}), 7.8 (dd, J = 7.8, 0.9 Hz, 1H, H^{4}), 7.5 (t, J = 8.7 Hz, 1H, H^{3}), 7.3 (s, 1H, H^{1}). ^{13}C NMR (101 MHz, DMSO-d_6) δ 158.9, 148.6, 133.2 (2C), 127.9, 123.6, 119.6, 116.2, 114.3, 115.6, 111.0, 104.7 (2C). HPLC-MS (ACI/ ESI): Purity = 99%, t_R = 1.19 min, m/z $[M+H]^+$ = 330.1.

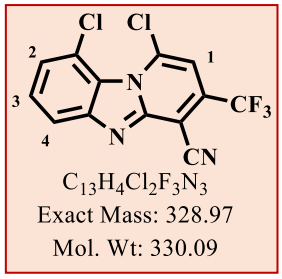

$C_{13}H_4Cl_2F_3N_3$
Exact Mass: 328.97
Mol. Wt: 330.09

1,8-dichloro-3-(4-(trifluoromethyl)phenyl)benzo[4,5]imidazo[1,2-a]pyridine-4-carbonitrile*, 2.4*c

Compound **2.4*c*** was obtained from **2.4*b*** (1.30 g, 6.78 mmol, 1.0 equiv) and $POCL_3$ (0.100 g, 67.1 mmol, 20 equiv) as yellow solid (0.79 g, 58%); Rf (EtOAc : Hexane, 3 : 7) 0.22. ^{1}H NMR (600 MHz, DMSO-d_6) δ 8.7 (d, J = 1.9 Hz, 1H, H^4), 8.0 (d, J = 8.2 Hz, 2H, H^6), 8.0 (d, J = 8.3 Hz, 2H, H^5), 8.0 (d, J = 8.7 Hz, 1H, H^2), 7.7 (dd, J = 8.8, 2.0 Hz, 1H, H^3), 7.5 (s, 1H, H^1). ^{13}C NMR (151 MHz, DMSO-d_6) δ 148.8, 139.4, 135.1, 130.3 (3C), 127.3, 127.9, 126.3 (3C), 123.2, 121.6, 119.5, 117.6, 115.8, 114.9, 113.4 (2C). HPLC-MS (ACI/ ESI): Purity = 99%, t_R = 3.08 min, m/z $[M+H]^+$ = 406.0.

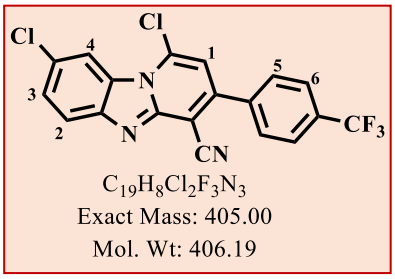

$C_{19}H_8Cl_2F_3N_3$
Exact Mass: 405.00
Mol. Wt: 406.19

6.3.4 General procedure for the aromatic nucleophilic amine coupling: synthesis of the final compounds 1-34

A mixture of a chloro intermediate (**1.1*c*** – **2.4*c***: 1.0 equiv), an appropriate amine (2.0 equiv) and triethylamine (2.0 equiv) in tetrahydrofuran (THF) (2 mL/ 100mg sample) was reacted with continuous stirring in a microwave set at 150W, 80°C for 25 minutes. The cooled reaction mixture was transferred to a round bottom flask and concentrated *in vacuo*. The product was recrystallised in a minimum volume of acetone (or ethanol). Where purification was required, a column with a 25-30% ethyl acetate (EtOAc) in hexane eluent system was used to purify the compound. The appropriate fractions were reconstituted, concentrated and dried *in vacuo*.

***(R)-1-((1-cyclohexylethyl)amino)-3-(trifluoromethyl)benzo[4,5]imidazo[1,2-a]pyridine-4-carbonitrile*, 1**

Compound **1** was obtained from **1.1*c*** (0.124 g, 0.42 mmol, 1.0 equiv) and *S*-1-cyclohexylethan-1-amine (0.107 g, 0.84 mmol, 2.0 equiv) as yellow solid (0.109 g, 67%), m.p 182 - 184 °C; Rf (EtOAc : Hexane, 3 : 7) 0.33. ^{1}H NMR (400 MHz, DMSO-d_6) δ 8.4 (dd, J = 7.8, 1.4 Hz, 1H, H^5), 7.9 (dd, J = 7.8, 1.4 Hz, 1H, H^2), 7.6 (m, 2H, $H^{3, 6}$), 7.5 (dt, J = 7.8, 1.4 Hz, 1H, H^4), 6.5 (s, 1H, H^1), 3.9 (m, 1H, H^8), 2.0 – 1.6 (m, 6H, $H^{9, 10a, 11a, 12a}$), 1.3 (d, J = 6.4 Hz, 3H, H^7), 1.3 – 1.0 (m, 5H, $H^{10e, 11e, 12e}$). ^{13}C NMR (101 MHz, DMSO-d_6) δ 150.2, 145.5, 128.4, 127.0 (2C), 121.5, 119.3, 115.9, 86.6, 55.2, 42.6, 29.9, 29.2 (2C), 26.4 (2C), 26.3 (3C), 17.6 (2C). HPLC-MS (ACI/ ESI): Purity = 99%, t_R = 3.27 min, m/z $[M+H]^+$ = 387.1.

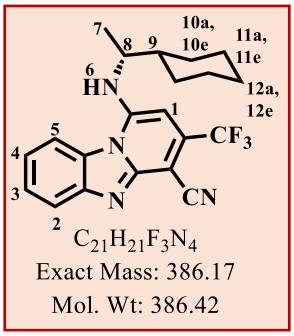

$C_{21}H_{21}F_3N_4$
Exact Mass: 386.17
Mol. Wt: 386.42

***(S)-1-((1-cyclohexylethyl)amino)-3-(trifluoromethyl)benzo[4,5]imidazo[1,2-a]pyridine-4-carbonitrile*, 2**

Compound **2** was obtained from **1.1*c*** (0.124 g, 0.42 mmol, 1.0 equiv) and *R*-1-cyclohexylethan-1-amine (0.107 g, 0.84 mmol, 2.0 equiv) as yellow solid (0.117 g, 72%), m.p 182 - 184 °C; Rf (EtOAc : Hexane, 3 : 7) 0.30. ^{1}H NMR (400 MHz, DMSO-d_6) δ 8.4 (d, J = 7.8, 1.4 Hz, 1H, H^{5}), 7.9 (dd, J = 7.8, 1.4 Hz, 1H, H^{2}), 7.6 (m, 2H, H$^{3, 6}$), 7.5 (dt, J = 7.8, 1.4 Hz, 1H, H^{4}), 6.5 (s, 1H, H^{1}), 3.9 (m, 1H, H^{8}), 2.0 – 1.6 (m, 6H, H$^{9, 10a, 11a, 12a}$), 1.3 (d, J = 6.4 Hz, 3H, H^{7}), 1.3 – 1.0 (m, 5H, H$^{10e, 11e 12e}$). ^{13}C NMR (101 MHz, DMSO-d_6) δ 150.2, 145.5, 128.4, 127.0 (2C), 121.5 (2C), 119.3, 115.9, 86.6, 55.2, 42.6, 29.6 (3C), 26.3 (4C), 17.6 (2C). HPLC-MS (ACI/ ESI): Purity = 99%, t_R = 3.47 min, m/z $[M+H]^+$ = 387.1.

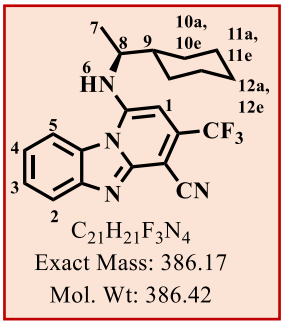

$C_{21}H_{21}F_3N_4$
Exact Mass: 386.17
Mol. Wt: 386.42

***Methyl (R)-2-((4-cyano-3-(trifluoromethyl)benzo[4,5]imidazo[1,2-a]pyridin-1-yl)amino)-2-phenylacetate*, 3**

Compound **3** was obtained from 1.1*c* (1.00 g, 3.38 mmol, 1.0 equiv) and methyl (R)-2-amino-2-phenylacetate (1.36 g, 6.76 mmol, 2.0 equiv) as yellow solid (0.520g, 36%), m.p 224 - 226 °C; Rf (MeOH : DCM, 0.2 : 9.8) 0.21. ^{1}H NMR (600 MHz, DMSO-d_6) δ 8.7 (dd, J = 8.4, 1.3 Hz, 1H, H^{2}), 7.9 (dd, J = 8.2, 1.3 Hz, 1H, H^{5}), 7.7 – 7.6 (m, 3H, H$^{4, 8}$), 7.6 (dt, J = 7.9, 1.3 Hz, 1H, H^{3}), 7.4 (t, J = 7.8 Hz, 2H, H^{9}), 7.4 (m, 1H, H^{10}), 6.3 (s, 1H, H^{1}), 5.9 (s, 1H, H^{7}), 3.8 (s, 3H, H^{6}). ^{13}C NMR (151 MHz, DMSO-d_6) δ 171.2, 149.0, 148.0, 136.5 (2C), 129.3 (3C), 128.9, 128.8, 128.1 (3C), 127.1 (2C), 122.4 (2C), 116.3 (2C), 114.4, 53.4 (2C). HPLC-MS (ACI/ ESI): Purity = 97%, t_R = 3.36 min, m/z $[M+H]^+$ = 425.1.

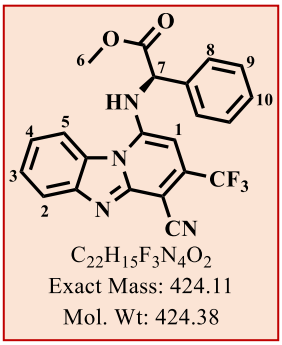

$C_{22}H_{15}F_3N_4O_2$
Exact Mass: 424.11
Mol. Wt: 424.38

***(R)-2-((4-cyano-3-(trifluoromethyl)benzo[4,5]imidazo[1,2-a]pyridin-1-yl)amino)-2-phenyl-acetic acid*, 4**[1]

A solution of compound **3** (0.45 g, 1.06 mmol, 1.0 equiv) in methanol (1.0 mL) was heated to 30 °C with continuous stirring. Potassium hydroxide (KOH: 0.12 mg, 2.12 mmol, 2.0 equiv) was added to the treated solution at that temperature and the reaction mixture was stirred for 10 minutes. The reaction mixture was cooled to room temperature, diluted with deionised water (10 mL) after which it was acidified using hydrochloric acid (HCl: 0.12 g, 3.20 mmol, 3.0 equiv). The organic residues were taken-up in ethyl EtOAc after which the aqueous phase was

removed using a separatory funnel. The EtOAc layer was washed with deionised water (20 mL x 3), brine (10 mL x 3), dried over Na_2SO_4 and was finally concentrated *in vacuo*. Compound

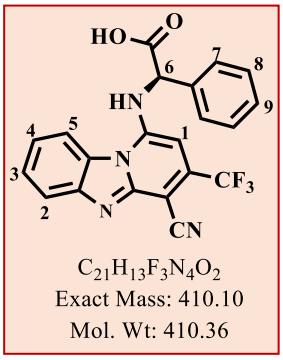

$C_{21}H_{13}F_3N_4O_2$
Exact Mass: 410.10
Mol. Wt: 410.36

4 was obtained as yellow solid (0.422 g, 97%), m.p 244 – 246 °C; Rf (MeOH : DCM, 1 : 9) 0.17. ^{1}H NMR (600 MHz, DMSO-d_6) δ 8.6 (dd, J = 8.2, 1.6 Hz, 1H, H^2), 8.0 (dd, J = 8.2, 1.7 Hz, 1H, H^5), 7.8 – 7.7 (m, 3H, $H^{4,7}$), 7.6 (dt, J = 7.8, 1.7 Hz, 1H, H^3), 7.4 (t, J = 7.8 Hz, 2H, H^8), 7.4 (m, 1H, H^9), 6.2 (s, 1H, H^1), 5.8 (s, 1H, H^6). ^{13}C NMR (151 MHz, DMSO-d_6) δ 171.6, 148.6, 136.8, 129.3 (3C), 128.9, 128.6, 128.0 (3C), 127.2 (2C), 122.4, 119.1, 115.5 (2C), 114.2, 88.7, 60.8 (2C). HPLC-MS (ACI/ ESI): Purity = 98%, t_R = 3.06 min, m/z $[M+H]^+$ = 411.0.

***1-((1-(4-fluorophenyl)ethyl)amino)-4-(trifluoromethyl)benzo[4,5]imidazo[1,2-a]pyridine-3-carbonitrile*, 6**

Compound **6** was obtained from 1.1*c* (0.087 g, 0.31 mmol, 1.0 equiv) and 1-(4-

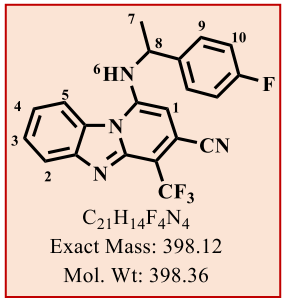

$C_{21}H_{14}F_4N_4$
Exact Mass: 398.12
Mol. Wt: 398.36

fluorophenyl)ethan-1-amine (0.087 g, 0.63 mmol, 2.0 Eq) as yellow solid (0.079 g, 64%), m.p 181 – 183 °C; Rf (EtOAc : Hexane, 3 : 7) 0.26. ^{1}H NMR (400 MHz, DMSO-*d6*) δ 8.6 (dd, J = 7.8, 2.1 Hz, 1H, H^2), 8.3 (s, 1H, H^6), 7.9 (dd, J = 7.8, 2.0 Hz, 1H, H^5), 7.7 (dt, J = 7.6, 2.1 Hz, 1H, H^4), 7.6 (dd, J = 8.3, 5.6 Hz, 2H, H^{10}), 7.5 (dt, J = 7.8, 2.1 Hz, 1H, H^3), 7.5 (d, J = 8.5 Hz, 2H, H^9), 6.2 (s, 1H, H^1), 5.3 (q, J = 6.9 Hz, 1H, H^8), 1.8 (d, J = 6.7 Hz, 3H, H^7). ^{13}C NMR (151 MHz, DMSO-d_6) δ 149.6, 145.6, 139.2, 128.7 (3C), 127.1, 121.8 (2C), 119.5, 116.3 (2C), 115.8 (3C), 87.8 (2C), 53.6 (2C), 23.4 (2C). HPLC-MS (ACI/ ESI): Purity = 99%, t_R = 3.05 min, m/z $[M+H]^+$ = 399.1.

***(R)-1-((1-(4-fluorophenyl)ethyl)amino)-4-(trifluoromethyl)benzo[4,5]imidazo[1,2-a]pyridine-3-carbonitrile*, 7**

Compound **7** was obtained from 1.1*c* (0.100 g, 0.36 mmol, 1.0 equiv) and *R*-1-(4-fluorophenyl)ethan-1-amine (0.100 g, 0.72 mmol, 2.0 Eq) as yellow solid (0.092 g, 64%), m.p 175 – 177 °C; Rf (MeOH : DCM, 1 : 9) 0.37. ^{1}H NMR (600 MHz, DMSO-d_6) δ 8.6 (dd, *J* = 7.8, 2.1 Hz, 1H, H^2), 8.0 (s, 1H, H^6), 7.9 (dd, *J* = 7.7, 1.8 Hz, 1H, H^5), 7.7 (dd, *J* = 7.7, 5.4 Hz, 2H, H^{10}), 7.7 (dd, *J* = 8.4, 0.9 Hz, 2H, H^9) 7.6 (dt, *J* = 7.8, 1.7 Hz, 1H, H^3), 7.5 (dt, *J* = 7.8, 1.7 Hz, 1H, H^4), 6.2 (s, 1H, H^1), 5.2 (q, *J* = 6.7 Hz, 1H, H^8), 1.8 (d, *J* = 6.7 Hz, 3H, H^7). ^{13}C NMR (151 MHz, DMSO-d_6) δ 149.6, 145.6, 139.2, 128.7 (3C), 127.1, 121.8 (2C), 119.4, 116.3 (2C), 115.8 (3C), 87.8 (2C), 53.6 (2C), 23.4 (2C). HPLC-MS (ACI/ ESI): Purity = 98%, t_R = 2.95 min, m/z $[M+H]^+$ = 399.1.

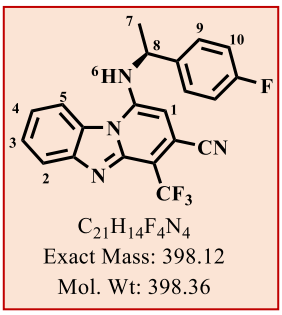

***(S)-1-((1-(4-fluorophenyl)ethyl)amino)-4-(trifluoromethyl)benzo[4,5]imidazo[1,2-a]pyridine-3-carbonitrile*, 8**

Compound **8** was obtained from **1.1*c*** (0.100 g, 0.36 mmol, 1.0 equiv) and (*S*)-1-(4-fluorophenyl)ethan-1-amine (0.100 g, 0.72 mmol, 2.0 equiv) as yellow solid (0.047 g, 33%), m.p 182 – 184 °C; Rf (EtOAc : Hexane, 3 : 7) 0.21. ^{1}H NMR (600 MHz, DMSO-d_6) δ 8.6 (dd, *J* = 7.7, 1.7 Hz, 1H, H^2), 8.1 (s, 1H, H^6), 7.9 (dd, *J* = 7.8, 1.8 Hz, 1H, H^5), 7.7 (dd, *J* = 7.7, 5.4 Hz, 2H, H^{10}), 7.7 (dd, *J* = 8.5, 0.9 Hz, 2H, H^9), 7.6 (dt, *J* = 7.8, 1.7 Hz, 1H, H^3), 7.5 (dt, *J* = 7.9, 1.7 Hz, 1H, H^4), 6.2 (s, 1H, H^1), 5.2 (q, *J* = 5.9 Hz, 1H, H^8), 1.8 (d, *J* = 6.8 Hz, 3H, H^7). ^{13}C NMR (151 MHz, DMSO-d_6) δ 149.6, 145.6, 139.2, 128.7 (3C), 127.1, 121.8 (2C), 119.4, 116.4 (2C), 115.8 (3C), 87.8 (2C), 53.6 (2C), 23.4 (2C). HPLC-MS (ACI/ ESI): Purity = 99%, t_R = 2.90 min, m/z $[M+H]^+$ = 399.1.

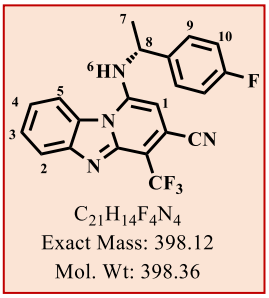

***1-((1-(4-chlorophenyl)ethyl)amino)-4-(trifluoromethyl)benzo[4,5]imidazo[1,2-a]pyridine-3-carbonitrile*, 9**

Compound **9** was obtained from **1.1*c*** (0.14 g, 0.42 mmol, 1.0 Eq) and 1-(4-chlorophenyl)ethan-1-amine (0.163 g, 0.85 mmol, 2.0 Eq) as yellow solid (0.119 g, 68%), m.p 185 – 187 °C; Rf (EtOAc : Hexane, 1 : 9) 0.27. ^{1}H NMR (400 MHz, DMSO-d_6) δ 8.6 (dd, J = 8.5, 1.9 Hz, 1H, H^2), 8.3 (d, J = 6.4 Hz, 1H, H^6), 7.9 (dd, J = 8.2, 1.7 Hz, 1H, H^5), 7.6 (m, 3H, $H^{4, 10}$), 7.5 (dt, J = 7.8, 1.8 Hz, 1H, H^3), 7.4 (d, J = 8.5 Hz, 2H, H^9), 6.2 (s, 1H, H^1), 5.2 (m, 1H, H^8), 1.8 (d, J = 6.7 Hz, 3H, H^7). ^{13}C NMR (101 MHz, DMSO-d_6) δ 149.6, 148.2, 145.4, 142.1 (3C), 132.4 (3C), 127.2 (2C), 121.7, 119.4 (2C), 116.5 (2C), 87.8, 53.4 (2C), 23.3 (2C). HPLC-MS (ACI/ ESI): Purity = 99%, t_R = 2.97 min, m/z $[M+H]^+$ = 415.1.

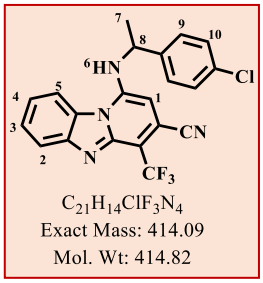

1-((2-hydroxyethyl)amino)-3-(trifluoromethyl)benzo[4,5]imidazo[1,2-a]pyridine-4-carbonitrile*, 1.1*d

Compound **1.1*d*** was obtained from **1.1*c*** (0.200 g, 0.70 mmol, 1.0 equiv) and 2-aminoethan-1-ol (0.083 g, 1.35 mmol, 2.0 equiv) as yellow solid (0.147 g, 68%); Rf (MeOH : DCM, 0.1 : 9.9) 0.47. ^{1}H NMR (600 MHz, DMSO-d_6) δ 8.6 (dd, J = 8.1, 1.5 Hz, 1H, H^2), 7.8 (dd, J = 8.0, 1.6 Hz, 1H, H^5), 7.6 (dt, J = 8.1, 1.5 Hz, 1H, H^3), 7.4 (dt, J = 8.2, 1.5 Hz, 1H, H^4), 6.4 (s, 1H, H^1), 3.8 (t, J = 5.8 Hz, 2H, H^7), 3.7 (t, J = 5.9 Hz, 2H, H^8). ^{13}C NMR (151 MHz, DMSO-d_6) δ 150.7, 126.4 (2C), 121.1 (2C), 118.7 (2C), 115.8 (2C), 86.6 (2C), 60.3 (2C), 47.3 (2C). HPLC-MS (ACI/ ESI): Purity = 98%, t_R = 2.97 min, m/z $[M+H]^+$ = 321.1.

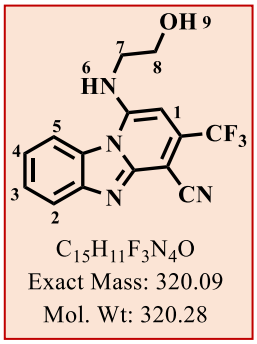

6.3.5 Synthesis of 1-((2-bromoethyl)amino)-3-(trifluoromethyl)benzo[4,5]imidazo[1,2-a]pyridine-4-carbonitrile, 1.1e[1]

A mixture of 1.1*d* (0.300 g, 0.94 mmol, 1.0 Eq) and triphenylphosphine (PPh_3) (0.370 g, 1.41 mmol, 1.5 Eq) in DMF (1.0 mL) was cooled to 0 °C with continuous stirring. Tetrabromomethane (CBr_4) (0.470 g, 1.41 mmol, 1.5 Eq) was added to the reaction mixture at that temperature. The treated reaction mixture was stirred at room temperature for 1.5 hours in a sealed tube. The product was purified by column chromatography using 15% EtOAc in hexane.

Compound **1.1*e*** was obtained as yellow solid (0.231 g, 64%); Rf (MeOH : DCM, 0.1 : 9.9) 0.47. ^{1}H NMR (600 MHz, DMSO-d_6) δ 8.6 (dd, J = 8.3, 1.5 Hz, 1H, H^5), 7.9 (dd, J = 8.1, 1.5 Hz, 1H, H^2), 7.6 (dt, J = 8.2, 1.4 Hz, 1H, H^3), 7.5 (dt, J = 8.1, 1.5 Hz, 1H, H^4), 6.6 (s, 1H, H^1), 4.1 (t, J = 6.4 Hz, 2H, H^6), 3.9 (t, J = 6.4 Hz, 2H, H^7). ^{13}C NMR (151 MHz, DMSO-d_6) δ 143.9, 134.5, 130.7, 128.1, 127.4, 122.1 (2C), 118.6 (2C), 115.8, 114.3, 87.9 (2C), 45.6, 31.6. HPLC-MS (ACI/ ESI): Purity = 85%, t_R = 3.29 min, m/z $[M+H]^+$ = 383.0/ 385.0.

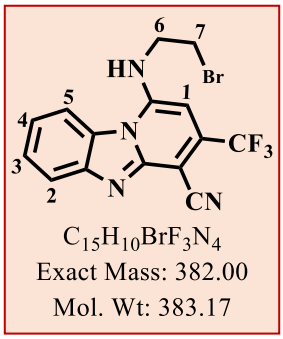

$C_{15}H_{10}BrF_3N_4$
Exact Mass: 382.00
Mol. Wt: 383.17

6.3.6 General procedure for the synthesis of the two-carbon spaced (2-C between the PBI core scaffold-linked N and the α-methylene carbon-linked N of the substituent benzylamine moiety) analogues- 10 and 11

A mixture of 1.1*e* (1.0 equiv), the appropriate amine (1.2 equiv) and anhydrous potassium carbonate (K_2CO_3: 2.0 equiv) in acetonitrile (1.0 mL per 100 mg of the sample) were heated to 79 °C with continuous stirring for 2.0 hours. The reaction mixture was cooled to room temperature, diluted with EtOAc and washed with deionized water (20 mL x 3), dried with brine and finally over Na_2SO_4. The organic layer was concentrated and dried *in vacuo.* The product was purified by trituration in DCM.

***(S)-1-((2-((1-(4-fluorophenyl)ethyl)amino)ethyl)amino)-3-(trifluoromethyl)benzo[4,5]imidazo[1,2-a]pyridine-4-carbonitrile,* 10**

Compound **10** was obtained from **1.1*d*** (0.100 g, 0.26 mmol, 1.0 equiv) and *R*-1-(4-fluorophenyl)ethan-1-amine (0.035 g, 0.25 mmol, 1.2 equiv) as yellow solid (0.054 g, 58%); Rf (MeOH : DCM, 0.2 : 9.8) 0.28. ^{1}H NMR (400 MHz, Methanol-d_4) δ 8.4 (dd, J = 8.3, 1.8 Hz, 1H, H^2), 7.9 (dd, J = 8.3, 1.8 Hz, 1H, H^5), 7.6 (dt, J = 8.2, 1.8 Hz, 1H, H^3), 7.5 (dt, J = 8.3, 1.8 Hz, 1H, H^4), 7.6 (d, J = 6.8 Hz, 1H, H^6), 7.7 (dd, J = 8.7, 5.5 Hz, 2H, H^{13}), 7.2 (dd, J = 8.5, 5.6 Hz, 2H, H^{12}), 6.3 (s, 1H, H^1), 4.5 (m, 1H, H^{11}), 3.9 (s, 1H, H^9), 3.3 (t, J = 5.7 Hz, 2H, H^7), 2.0 (t, J = 5.9 Hz, 2H, H^8), 1.7 (d, J = 6.9 Hz, 3H, H^{10}). ^{13}C NMR (101 MHz, Methanol-d_4) δ 132.5 (5C), 131.7 (5C), 129.7 (2C), 144.5 (4C), 143.2 (3C), 143.1, 142.6, 22.3 (2C). HPLC-MS (ACI/ ESI): Purity = 99%, t_R = 2.90 min, m/z $[M+H]^+$ = 442.1.

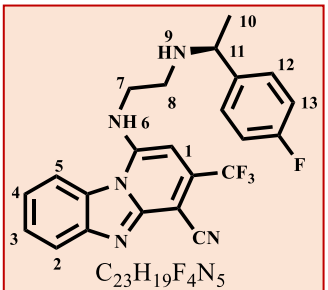

$C_{23}H_{19}F_4N_5$
Exact Mass: 441.16
Mol. Wt: 441.43

***(S)-1-((2-((1-(p-tolyl)ethyl)amino)ethyl)amino)-3-(trifluoromethyl)benzo[4,5]imidazo[1,2-a]pyridine-4-carbonitrile,* 11**

Compound **11** was obtained from **1.1*d*** (0.120 g, 0.31 mmol, 1.0 equiv) and (*R*)-1-(*p*-tolyl)ethan-1-amine (0.063 g, 0.37 mmol, 1.2 equiv) as yellow solid (0.087 g, 64%); Rf (MeOH : DCM, 0.1 : 9.9) 0.21. ^{1}H NMR (400 MHz, Methanol-d_4) δ 8.1 (dd, *J* = 7.6, 1.9 Hz, 1H, H^{2}), 7.6 (dd, *J* = 8.3, 1.8 Hz, 1H, H^{5}), 7.6 (dt, *J* = 8.2, 1.9 Hz, 1H, H^{3}), 7.5 (dt, *J* = 8.5, 1.9 Hz, 1H, H^{4}), 7.6 (s, 1H, H^{6}), 7.4 – 7.3 (d, *J* = 7.6 Hz, 2H, H^{12}), 7.1 (d, *J* = 7.7 Hz, 2H, H^{13}), 6.3 (s, 1H, H^{1}), 4.5 (q, *J* = 6.9 Hz, 1H, H^{11}), 3.9 (s, 1H, H^{9}), 3.3 (t, *J* = 5.7 Hz, 2H, H^{7}), 2.3 (s, 3H, H^{14}), 2.0 (t, *J* = 5.8 Hz, 2H, H^{8}), 1.7 (d, *J* = 6.8 Hz, 3H, H^{10}). ^{13}C NMR (101 MHz, Methanol-d_4) δ 132.4 (4C), 131.7 (7C), 129.7, 128.7 (8C), 127.5, 127.0, 122.2, 18.1. HPLC-MS (ACI/ ESI): Purity = 99.40%, t_R = 2.95 min, m/z $[M+H]^+$ = 438.1.

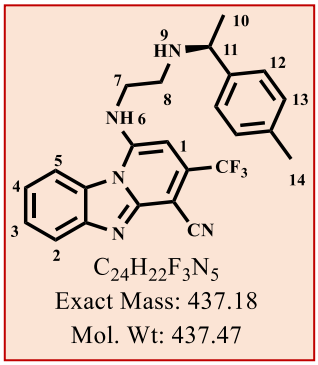

$C_{24}H_{22}F_3N_5$
Exact Mass: 437.18
Mol. Wt: 437.47

***(R)-2-((8-chloro-4-cyano-3-(trifluoromethyl)benzo[4,5]imidazo[1,2-a]pyridin-1-yl)amino)-2-phenylacetamide,* 12**

Compound **12** was obtained from **1.3*c*** (0.043 g, 0.13 mmol, 1.0 equiv) and 2-amino-2-phenylacetamide (0.039 g, 0.26 mmol, 2.0 equiv) as orange solid (0.098 g, 74%), m.p 147 – 149 °C; Rf (MeOH : DCM, 1 : 9) 0.12. ^{1}H NMR (600 MHz, DMSO-d_6) δ 8.6 (s, 1H, H^{5}), 8.5 (d, *J* = 2.5 Hz, 1H, H^{4}), 7.9 (d, *J* = 7.7 Hz, 1H, H^{2}), 7.7 (dd, *J* = 7.8, 2.6 Hz, 1H, H^{3}), 7.56 (dd, *J* = 7.0, 2.3 Hz, 2H, H^{8}), 7.5 (s, 2H, H^{6}), 7.4 (t, *J* = 7.5 Hz, 2H, H^{9}), 7.4 (dt, *J* = 7.5, 2.4 Hz, 1H, H^{10}), 6.1 (s, 1H, H^{1}), 5.5 (s, 1H, H^{7}). ^{13}C NMR (151 MHz, DMSO-d_6) δ 129.2 (5C), 128.7 (2C), 128.3, 127.7 (6C), 121.9 (2C), 116.5, 115.7, 88.1 (3C). HPLC-MS (ACI/ ESI): Purity = 98%, t_R = 3.23 min, m/z $[M+H]^+$ = 444.0.

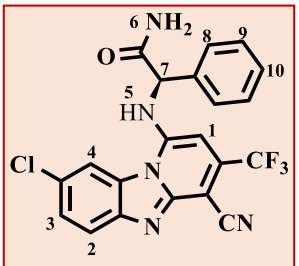

$C_{21}H_{13}ClF_3N_5O$
Exact Mass: 443.08
Mol. Wt: 443.81

***Methyl-(R)-2-((8-chloro-4-cyano-3-(trifluoromethyl)benzo[4,5]imidazo[1,2-a]pyridin-1-yl)amino)-2-phenylacetate*, 13**

Compound **13** was obtained from **1.3*c*** (0.100 g, 0.30 mmol, 1.0 equiv) and methyl (*R*)-2-amino-2-phenylacetate (0.100 g, 0.60 mmol, 2.0 equiv) as orange solid (0.121 g, 88%), m.p 183 – 187 °C; Rf (EtOAc : Hexane, 1 : 8) 0.25. ^{1}H NMR (600 MHz, DMSO-d_6) δ 8.59 (s, 1H, H^5), 7.9 (d, *J* = 2.3 Hz, 1H, H^4), 7.7 (d, *J* = 7.7 Hz, 1H, H^2), 7.6 (dd, *J* = 7.8, 2.4 Hz, 1H, H^3), 7.5 (dd, *J* = 7.2, 2.4 Hz, 2H, H^8), 7.4 (t, *J* = 7.5 Hz, 1H, H^9), 7.4 (dt, *J* = 7.5, 2.4 Hz, 1H, H^{10}), 6.3 (s, 1H, H^1), 6.0 (s, 1H, H^7), 3.8 (s, 3H, H^6). ^{13}C NMR (151 MHz, DMSO-d_6) δ 170.9, 148.9 (2C), 129.3 (6C), 128.2 (4C), 127.4, 122.4, 117.5, 114.1, 61.1 (3C), 53.5 (2C). HPLC-MS (ACI/ ESI): Purity = 99%, t_R = 3.40 min, m/z $[M+H]^+$ = 459.0.

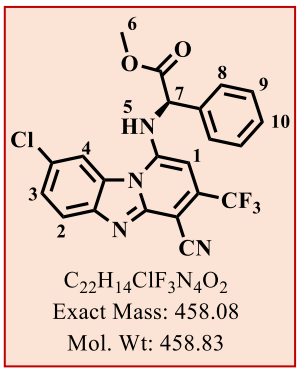

$C_{22}H_{14}ClF_3N_4O_2$
Exact Mass: 458.08
Mol. Wt: 458.83

***8-chloro-1-((1-(4-(methylsulfonyl)phenyl)ethyl)amino)-3-(trifluoromethyl)benzo[4,5]imidazo[1,2-a]pyridine-4-carbonitrile*, 14**

Compound **14** was obtained from **1.3*c*** (0.150 g, 0.46 mmol, 1.0 equiv) and 1-(4-(methylsulfonyl)phenyl)ethan-1-amine (0.182 g, 0.91 mmol, 2.0 equiv) as yellow solid (0.163 g, 72%), m.p 139 - 143 °C; Rf (MeOH : DCM, 0.2 : 9.8) 0.18. ^{1}H NMR (600 MHz, DMSO-d_6) δ 8.7 (s, 1H, H^5), 8.7 (d, *J* = 2.4 Hz, 1H, H^4), 8.0 (d, *J* = 8.4 Hz, 2H, H^9), 7.9 (d, *J* = 8.1 Hz, 2H, H^8), 7.6 (dd, *J* = 7.9, 2.4 Hz, 1H, H^3), 7.5 (d, *J* = 8.3 Hz, 1H, H^2), 6.2 (s, 1H, H^1), 5.3 (q, *J* = 6.0 Hz, 1H, H^7), 3.2 (s, 3H, H^{10}), 1.8 (d, *J* = 6.0 Hz, 3H, H^6). ^{13}C NMR (151 MHz, DMSO-d_6) δ 149.6, 140.5, 128.3, 127.7 (7C), 121.4, 117.4, 116.5, 88.9, 54.1 (2C), 50.2, 44.1 (3C), 23.4 (2C). HPLC-MS (ACI/ ESI): Purity = 99%, t_R = 2.75 min, m/z $[M+H]^+$ = 491.0.

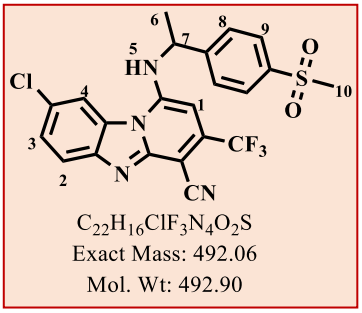

$C_{22}H_{16}ClF_3N_4O_2S$
Exact Mass: 492.06
Mol. Wt: 492.90

***7,8-dichloro-1-((1-(4-fluorophenyl)ethyl)amino)-3-(trifluoromethyl)benzo[4,5]imidazo[1,2-a]pyridine-4-carbonitrile,* 15**

Compound **15** was obtained from **1.3*c*** (0.070 g, 0.19 mmol, 1.0 equiv) and 1-(4-fluorophenyl)ethan-1-amine (0.053 g, 0.38 mmol, 2.0 equiv) as yellow solid (0.043 g, 48%), m.p 224 – 226 °C; Rf (EtOAc : Hexane, 3 : 7) 0.37. ^{1}H NMR (600 MHz, DMSO-d_6) δ 8.6 (s, 1H, H^2), 8.4 (s, 1H, H^4), 7.9 (s, 1H, H^3), 7.6 (dd, *J* = 8.5, 5.4 Hz, 2H, H^7), 7.2 (t, *J* = 8.9 Hz, 2H, H^8), 6.3 (s, 1H, H^1), 5.3 – 5.1 (m, 1H, H^6), 1.8 (d, *J* = 6.7 Hz, 3H, H^5). ^{13}C NMR (151 MHz, DMSO-d_6) δ 162.8, 149.9, 141.7, 138.9, 129.7, 128.8 (3C), 126.7 (2C), 125.5, 123.5, 115.7 (3C), 89.5 (2C), 53.9 (2C), 23.2 (2C). HPLC-MS (ACI/ ESI): Purity = 98%, t_R = 3.13 min, m/z $[M+H]^+$ = 467.0.

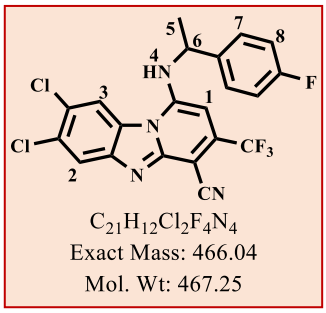

$C_{21}H_{12}Cl_2F_4N_4$
Exact Mass: 466.04
Mol. Wt: 467.25

***7,8-difluoro-1-((1-(4-fluorophenyl)ethyl)amino)-3-(trifluoromethyl)benzo[4,5]imidazo[1,2-a]pyridine-4-carbonitrile,* 16**

Compound **16** was obtained from **1.4*c*** (0.080 g, 0.26 mmol, 1.0 equiv) and 1-(4-fluorophenyl)ethan-1-amine (0.071 g, 0.51 mmol, 2.0 equiv) as yellow solid (0.064 g, 56.5%), m.p 182-185 °C; Rf (EtOAc : Hexane, 1 : 1) 0.25. ^{1}H NMR (400 MHz, DMSO-d_6) δ 8.7 (dd, *J* = 11.5, 7.2 Hz, 1H, H^2), 8.3 (d, *J* = 6.2 Hz, 1H, H^4), 8.0 (dd, *J* = 10.9, 7.6 Hz, 1H, H^3), 7.7 (dd, *J* = 8.6, 5.6 Hz, 2H, H^7), 7.2 (t, *J* = 8.9 Hz, 2H, H^8), 6.2 (s, 1H, H^1), 5.2 (m, 1H, H^6), 1.8 (d, *J* = 6.7 Hz, 3H, H^5). ^{13}C NMR (101 MHz, DMSO-d_6) δ 163.1, 149.2, 139.1, 128.8 (4C), 115.9 (4C), 106.2 (2C), 105.4 (2C), 88.4 (2C), 53.5 (2C), 23.4 (2C). HPLC-MS (ACI/ ESI): Purity = 98%, t_R = 2.95 min, m/z $[M+H]^+$ = 435.0.

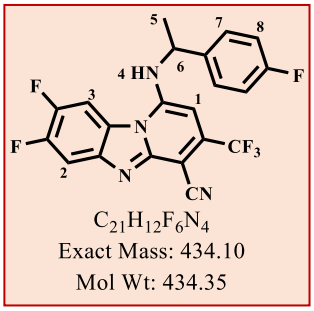

$C_{21}H_{12}F_6N_4$
Exact Mass: 434.10
Mol Wt: 434.35

***(R)-7,8-difluoro-1-((1-(4-fluorophenyl)ethyl)amino)-3-(trifluoromethyl)benzo[4,5]imidazo-[1,2-a]pyridine-4-carbonitrile*, 17**

Compound **17** was obtained from **1.4*c*** (0.046 g, 0.14 mmol, 1.0 equiv) and 1-(4-fluorophenyl)ethan-1-amine (0.039 g, 0.28 mmol, 2.0 equiv) as yellow solid (0.029 g, 48%), m.p 210 - 212 °C; Rf (EtOAc : Hexane, 1 : 1) 0.24. ^{1}H NMR (400 MHz, DMSO-d_6) δ 8.7 (dd, J = 11.2, 7.3 Hz, 1H, H^{2}), 8.3 (d, J = 6.2 Hz, 1H, H^{4}), 8.0 (dd, J = 11.0, 7.7 Hz, 1H, H^{3}), 7.6 (dd, J = 8.6, 5.6 Hz, 2H, H^{7}), 7.2 (t, J = 8.9 Hz, 2H, H^{8}), 6.2 (s, 1H, H^{1}), 5.2 (m, 1H, H^{6}), 1.8 (d, J = 6.9 Hz, 3H, H^{5}). ^{13}C NMR (101 MHz, DMSO-d_6) δ 163.1, 149.3, 139.1, 128.8 (4C), 115.9 (4C), 106.3 (2C), 105.4 (2C), 88.4 (2C), 53.6 (2C), 23.4 (2C). HPLC-MS (ACI/ ESI): Purity = 99%, t_R = 2.96 min, m/z $[M+H]^+$ = 435.0.

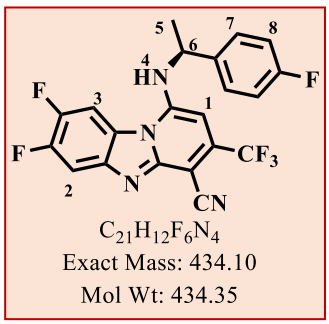

***1-((1-(4-chlorophenyl)ethyl)amino)-7,8-difluoro-3-(trifluoromethyl)benzo[4,5]imidazo[1,2-a]pyridine-4-carbonitrile*, 18**

Compound **18** was obtained from **1.4*c*** (0.080 g, 0.26 mmol, 1.0 equiv) and 1-(4-chlorophenyl)ethan-1-amine (0.098 g, 0.51 mmol, 2.0 equiv) as yellow solid (0.080 g, 68%), m.p 182 – 184 °C; Rf (EtOAc : Hexane, 1 : 1) 0.18. ^{1}H NMR (300 MHz, DMSO-d_6) δ 8.7 (dd, J = 11.4, 7.2 Hz, 1H, H^{2}), 8.3 (d, J = 6.4 Hz, 1H, H^{4}), 8.0 (dd, J = 11.0, 7.6 Hz, 1H, H^{3}), 7.6 (J = 8.5 Hz, 2H, H^{8}), 7.4 (d, J = 8.5 Hz, 2H, H^{7}), 6.2 (s, 1H, H^{1}), 5.3– 5.1 (m, 1H, H^{6}), 1.8 (d, J = 6.7 Hz, 3H, H^{5}). ^{13}C NMR (101 MHz, DMSO-d_6) δ 149.2, 141.9, 132.5, 129.1 (3C), 128.7 (4C), 114.2, 106.3 (2C), 105.4 (2C), 88.4 (2C), 53.5 (2C), 23.2 (2C). HPLC-MS (ACI/ ESI): Purity = 99%, t_R = 3.35 min, m/z $[M-H]^-$ = 449.0.

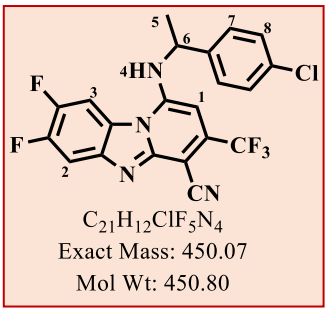

***(S)-7,8-difluoro-1-((1-phenylethyl)amino)-4-(trifluoromethyl)benzo[4,5]imidazo[1,2-a]pyridine-3-carbonitrile*, 19**

Compound **19** was obtained from **1.4*c*** (0.061 g, 0.18 mmol, 1.0 equiv) and 1-phenylethan-1-amine (0.045 g, 0.37 mmol, 2.0 equiv) as yellow solid (0.025 g, 34%), m.p 193 – 195 °C; Rf (EtOAc : Hexane, 3 : 7) 0.19. ^{1}H NMR (400 MHz, DMSO-d_6) δ 8.7 (dd, J = 11.3, 7.2 Hz, 1H, H^{2}), 8.3 (s, 1H, H^{4}), 8.0 (dd, J = 11.6, 7.7 Hz, 1H, H^{3}), 7.6 – 7.5 (dd, J = 7.5, 2.1 Hz, 2H, H^{7}), 7.4 (t, J = 7.3 Hz, 2H, H^{8}), 7.3 (dt, J = 7.3, 2.2 Hz, 1H, H^{9}), 6.2 (s, 1H, H^{1}), 5.2 (q, J = 6.6 Hz, 1H, H^{6}), 1.8 (d, J = 6.8 Hz, 3H, H^{5}). ^{13}C NMR (101 MHz, DMSO-d_6) δ 149.3, 143.0, 129.2 (3C), 127.9 (2C), 126.6 (4C), 123.7, 106.4, 105.4 (2C), 88.4 (2C), 54.3 (2C), 23.4 (2C). HPLC-MS (ACI/ ESI): Purity = 97%, t_R = 2.98 min, m/z $[M+H]^+$ = 417.19.

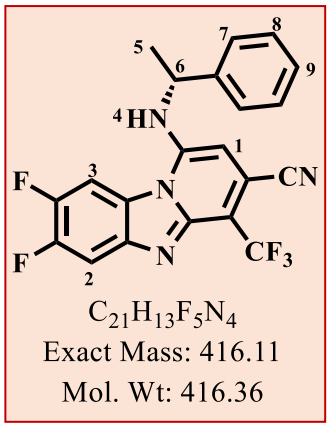

***(R)-7,8-difluoro-1-((1-phenylethyl)amino)-4-(trifluoromethyl)benzo[4,5]imidazo[1,2-a]pyridine-3-carbonitrile*, 20**

Compound **20** was obtained from **1.4*c*** (0.080 g, 0.24 mmol, 1.0 equiv) and 1-phenylethan-1-amine (0.059 g, 0.48 mmol, 2.0 equiv) as orange solid (0.052 g, 52%), m.p 210 – 212 °C; Rf (EtOAc : Hexane, 3 : 7) 0.20. ^{1}H NMR (400 MHz, DMSO-d_6) δ 8.7 (dd, J = 11.3, 7.2 Hz, 1H, H^{2}), 8.4 (d, J = 6.4 Hz, 1H, H^{4}), 8.0 (dd, J = 10.7, 7.7 Hz, 1H, H^{3}), 7.6 – 7.5 (dd, J = 7.5, 2.2 Hz, 2H, H^{7}), 7.4 (t, J = 7.3 Hz, 2H, H^{8}), 7.3 (dt, J = 7.4, 2.2 Hz, 1H, H^{9}), 6.2 (s, 1H, H^{1}), 5.2 (m, 1H, H^{6}), 1.8 (d, J = 6.7 Hz, 3H, H^{5}). ^{13}C NMR (101 MHz, DMSO-d_6) δ 149.8, 149.3, 143.0, 129.2 (3C), 127.9 (2C), 126.6 (3C), 114.3, 106.3 (2C), 105.4 (2C), 88.4 (2C), 54.3, 23.4 (2C). HPLC-MS (ACI/ ESI): Purity = 99%, t_R = 2.98 min, m/z $[M+H]^+$ = 417.19.

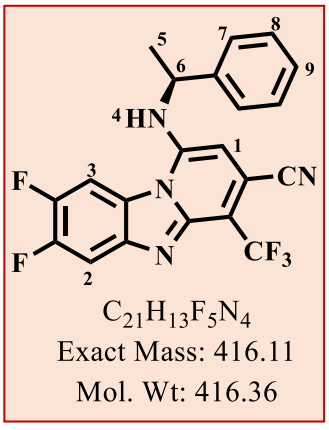

***7,8-difluoro-1-((1-(4-(trifluoromethoxy)phenyl)ethyl)amino)-3-(trifluoromethyl)benzo[4,5]-imidazo[1,2-a]pyridine-4-carbonitrile*, 21**

Compound **21** was obtained from **1.4*c*** (0.081 g, 0.24 mmol, 1.0 equiv) and 1-phenylcyclopropan-1-amine (0.100 g, 0.49 mmol, 2.0 equiv) as yellow solid (0.053 g, 44%), m.p 213 – 215 °C; Rf (EtOAc : Hexane, 3 : 7) 0.25. ^{1}H NMR (400 MHz, DMSO-d_6) δ 8.7 (dd, J = 11.3, 7.2 Hz, 1H, H^{2}), 8.3 (d, J = 6.2 Hz, 1H, H^{4}), 8.0 (dd, J = 10.7, 8.0 Hz, 1H, H^{3}), 7.7 (d, J = 7.7 Hz, 2H, H^{8}), 7.4 (d, J = 7.9 Hz, 2H, H^{7}), 6.2 (s, 1H, H^{1}), 5.3 (m, 1H, H^{6}), 1.8 (d, J = 6.7 Hz, 3H, H^{5}). ^{13}C NMR (101 MHz, DMSO-d_6) δ 149.2, 148.0, 142.4, 128.7 (4C), 121.7 (4C), 114.2, 106.3 (2C), 105.4 (2C), 88.4 (2C), 53.4 (2C), 23.2 (2C). HPLC-MS (ACI/ ESI): Purity = 99%, t_R = 3.06 min, m/z $[M+H]^+$ = 501.0.

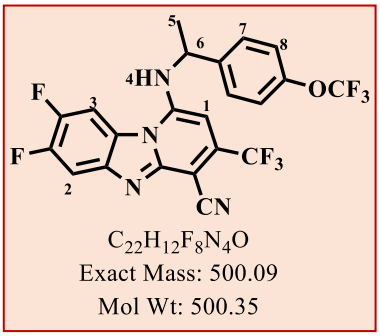

$C_{22}H_{12}F_8N_4O$
Exact Mass: 500.09
Mol Wt: 500.35

***7,8-difluoro-1-((1-(4-(methylsulfonyl)phenyl)ethyl)amino)-3-(trifluoromethyl)benzo[4,5]-imidazo[1,2-a]pyridine-4-carbonitrile*, 22**

Compound **22** was obtained from **1.4*c*** (0.084 g, 0.27 mmol, 1.0 equiv) and 1-(4-(methylsulfonyl)phenyl)ethan-1-amine (0.11 g, 0.54 mmol, 2.0 equiv) as yellow solid (0.063 g, 46%), m.p 261 – 263 °C; Rf (EtOAc : Hexane, 0.5 : 9.5) 0.18. ^{1}H NMR (400 MHz, DMSO-d_6) δ 8.7 (dd, J = 11.3, 7.1 Hz, 1H, H^{2}), 8.4 (s, 1H, H^{4}), 8.0 (dd, J = 10.9, 7.0 Hz, 1H, H^{3}), 8.0 (d = 8.8 Hz, 2H, H^{8}), 7.9 (d, J = 8.5 Hz, 2H, H^{7}), 6.3 (s, 1H, H^{1}), 5.4 (q, J = 7.5 Hz, 1H, H^{6}), 3.2 (s, 3H, H^{9}), 1.8 (d, J = 6.7 Hz, 3H, H^{5}). ^{13}C NMR (101 MHz, DMSO-d_6) δ 149.8, 149.2, 148.87, 141.8, 140.4, 127.8 (6C), 114.2, 106.4, 105.5 (2C), 88.3, 53.7 (2C), 43.9 (2C), 23.1 (2C). HPLC-MS (ACI/ ESI): Purity = 99%, t_R = 3.43 min, m/z $[M-H]^-$ = 493.0.

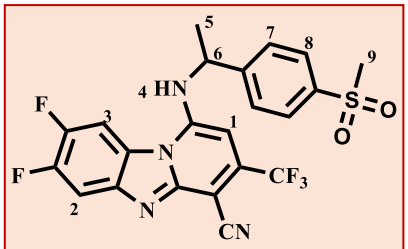

$C_{22}H_{15}F_5N_4O_2S$
Exact Mass: 494.08
Mol Wt: 494.44

***(R)-1-((1-(2-chlorophenyl)ethyl)amino)-7,8-difluoro-3-(trifluoromethyl)benzo[4,5]imidazo[1,2-a]pyridine-4-carbonitrile*, 23**

Compound **23** was obtained from **1.4*c*** (0.100 g, 0.30 mmol, 1.0 equiv) and (*S*)-1-(2-chlorophenyl)ethan-1-amine (0.094 g, 0.60 mmol, 2.0 equiv) as yellow solid (0.117 g, 86%), m.p 232 - 235 °C; Rf (DCM) 0.24. ^{1}H NMR (400 MHz, DMSO-d_6) δ 8.8 (dd, *J* = 11.3, 7.2 Hz, 1H, H^{2}), 8.4 (s, 1H, H^{4}), 8.0 (dd, *J* = 11.0, 7.0 Hz, 1H, H^{3}), 7.8 (dd, *J* = 8.3, 3.0 Hz, 1H, H^{10}), 7.6 (m, 1H, H^{9}), 7.5-7.3 (m, 2H, H$^{7, 8}$), 5.9 (s, 1H, H^{1}), 5.3 (q, *J* = 7.1 Hz, 1H, H^{6}), 1.8 (d, *J* = 6.7 Hz, 3H, H^{5}). ^{13}C NMR (101 MHz, DMSO-d_6) δ 149.6, 149.0, 139.8, 131.8, 129.9 (4C), 128.6 (2C), 128.2 (2C), 114.0, 105.5 (2C), 87.9 (2C), 51.8 (2C), 21.9 (2C). HPLC-MS (ACI/ ESI): Purity = 97%, t_R = 3.16 min, m/z $[M-H]^-$ = 451.0.

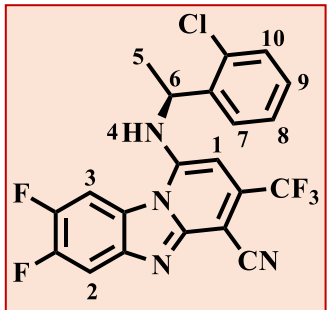

$C_{21}H_{12}ClF_5N_4$
Exact Mass: 450.07
Mol. Wt: 450.80

***7,8-difluoro-1-((1-(2-hydroxyphenyl)ethyl)amino)-3-(trifluoromethyl)benzo[4,5]imidzo[1,2-a]pyridine-4-carbonitrile*, 24**

Compound **24** was obtained from **1.4*c*** (0.089 g, 0.29 mmol, 1.0 equiv) and 2-(1-aminoethyl)phenol (0.100 g, 0.57 mmol, 2.0 equiv) as yellow solid (0.095 g, 76%), m.p 231 – 233 °C; Rf (MeOH : DCM, 3 : 7) 0.21. ^{1}H NMR (400 MHz, DMSO-d_6) δ 10.1 (s, 1H, H^{11}), 8.7 (dd, *J* = 11.3, 7.2 Hz, 1H, H^{2}), 8.3 (d, *J* = 6.7 Hz, 1H, H^{4}), 8.0 (dd, *J* = 11.0, 7.6 Hz, 1H, H^{3}), 7.5 (dd, *J* = 7.7, 1.7 Hz, 1H, H^{10}), 7.1 (dt, *J* = 7.8, 1.7 Hz, 1H, H^{9}), 6.9 (dt, *J* = 8.2, 1.7 Hz, 1H, H^{8}), 6.8 (dd, *J* = 7.5, 1.7 Hz, 1H, H^{7}), 6.4 (s, 1H, H^{1}), 5.3 (m, 1H, H^{6}), 1.7 (d, *J* = 6.7 Hz, 3H, H^{5}). ^{13}C NMR (101 MHz, DMSO-d_6) δ 154.5, 149.9, 149.1, 129.0 (2C), 128.4, 127.7, 123.5, 121.2, 120.1, 115.8, 114.4, 106.2 (2C), 104.9 (2C), 87.8 (2C), 49.3, 22.1 (2C). HPLC-MS (ACI/ ESI): Purity = 98%, t_R = 2.92 min, m/z $[M+H]^+$ = 433.1.

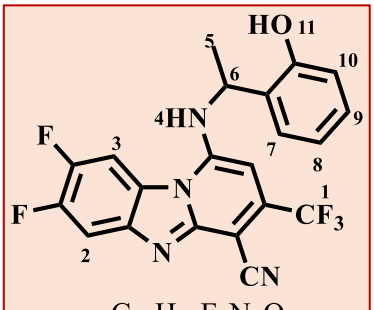

$C_{21}H_{13}F_5N_4O$
Exact Mass: 432.10
Mol Wt: 432.35

***(S)-1-((1-(2-chlorophenyl)ethyl)amino)-7,8-difluoro-3-(trifluoromethyl)benzo[4,5]imidazo[1,2-a]pyridine-4-carbonitrile*, 25**

Compound **25** was obtained from **1.4*c*** (0.100 g, 0.30 mmol, 1.0 equiv) and 1-(4-(methylsulfonyl)phenyl)ethan-1-amine (0.0.094 g, 0.60 mmol, 2.0 equiv) as yellow solid (0.101 g, 74%), m.p 231 - 233 °C; Rf (DCM) 0.23. ^{1}H NMR (400 MHz, DMSO-d_6) δ 8.8 (dd, *J* = 11.5, 7.4 Hz, 1H, H^{2}), 8.4 (s, 1H, H^{4}), 7.8 (dd, *J* = 11.0, 7.0 Hz, 1H, H^{3}), 7.8 (dd, *J* = 8.9, 3.3 Hz, 1H, H^{10}), 7.6 (m, 1H, H^{9}), 7.5-7.3 (m, 2H, $H^{7, 8}$), 5.9 (s, 1H, H^{1}), 5.2 (q, *J* = 6.7 Hz, 1H, H^{5}), 1.8 (d, *J* = 7.1 Hz, 3H, H^{6}). ^{13}C NMR (101 MHz, DMSO-d_6) δ 149.2 (2C), 131.8, 130.7, 129.8 (4C), 128.3 (3C), 105.4 (3C), 88.0 (3C), 52.0 (4C). HPLC-MS (ACI/ ESI): Purity = 97%, t_R = 3.15 min, m/z $[M-H]^-$ = 451.0.

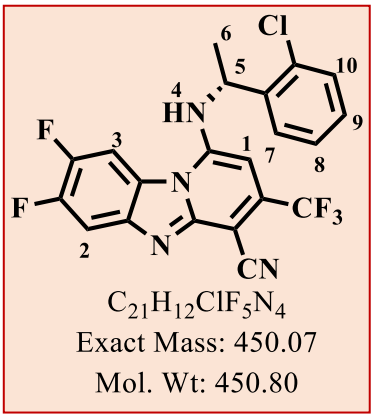

$C_{21}H_{12}ClF_5N_4$
Exact Mass: 450.07
Mol. Wt: 450.80

***1-((1-(2-chlorophenyl)ethyl)amino)-7,8-difluoro-3-(trifluoromethyl)benzo[4,5]imidazo[1,2-a]pyridine-4-carbonitrile*, 26**

Compound **26** was obtained from **1.4*c*** (0.20 g, 0.61 mmol, 1.0 equiv) and 1-(2-chlorophenyl)ethan-1-amine (0.19 g, 1.22 mmol, 2.0 equiv) as yellow solid (0.150 g, 55.0 %), m.p 231 - 233 °C; Rf (EtOAc : Hexane, 4 : 6) 0.26. ^{1}H NMR (400 MHz, DMSO-d_6) δ 8.7 (dd, *J* = 11.3, 7.2 Hz, 1H, H^{2}), 8.4 (d, *J* = 6.5 Hz, 1H, H^{4}), 7.8 (dd, *J* = 10.9, 7.0 Hz, 1H, H^{3}), 7.8 (dd, *J* = 8.3, 3.3 Hz, 1H, H^{10}), 7.5 (m, 1H, H^{9}), 7.4-7.3 (m, 1H, $H^{7, 8}$), 5.9 (s, 1H, H^{1}), 5.3 (m, 1H, H^{5}), 1.8 (d, *J* = 6.7 Hz, 3H, H^{6}). ^{13}C NMR (101 MHz, DMSO-d_6) δ 149.0, 139.7, 131.8, 129.9 (4C), 128.6 (2C), 128.2 (2C), 114.0, 106.4, 105.4 (2C), 87.8 (2C), 51.8 (2C), 21.8 (2C). HPLC-MS (ACI/ ESI): Purity = 97.0%, t_R = 3.18 min, m/z $[M-H]^-$ = 451.1.

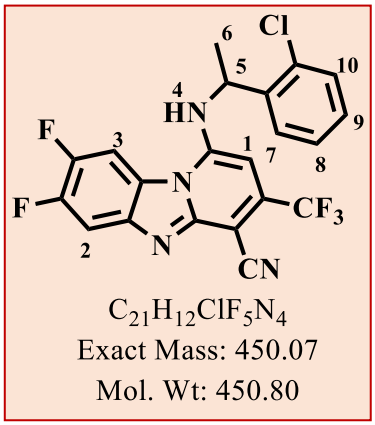

$C_{21}H_{12}ClF_5N_4$
Exact Mass: 450.07
Mol. Wt: 450.80

***7,8-difluoro-1-((1-(p-tolyl)ethyl)amino)-3-(trifluoromethyl)benzo[4,5]imidazo[1,2-a]pyridine-4-carbonitrile*, 27**

Compound **27** was obtained from **1.4*c*** (0.070 g, 0.21 mmol, 1.0 equiv) and 1-(*p*-tolyl)ethan-1-amine (0.057 g, 0.42 mmol, 2.0 equiv) as orange solid (0.074 g, 82%), m.p 215 – 217 °C; Rf (DCM) 0.27. ^{1}H NMR (400 MHz, DMSO-d_6) δ 8.68 (dd, J = 11.3, 7.2 Hz, 1H, H^{2}), 8.3 (d, J = 5.7 Hz, 1H, H^{4}), 8.0 (dd, J = 11.0, 7.6 Hz, 1H, H^{3}), 7.5 (d, J = 7.8 Hz, 2H, H^{7}), 7.2 (d, J = 7.8 Hz, 2H, H^{8}), 6.3 (s, 1H, H^{1}), 5.1 (m, 1H, H^{6}), 2.3 (s, 3H, H^{9}), 1.8 (d, J = 6.7 Hz, 3H, H^{5}). ^{13}C NMR (101 MHz, DMSO-d_6) δ 149.26, 139.9, 137.1, 129.7 (3), 126.6 (4C), 106.2 (2C), 105.3 (2C), 88.4 (2C), 54.1 (2C), 23.1 (2C), 21.1 (2C). HPLC-MS (ACI/ ESI): Purity = 98%, t_R = 3.07 min, m/z $[M+H]^+$ = 431.1.

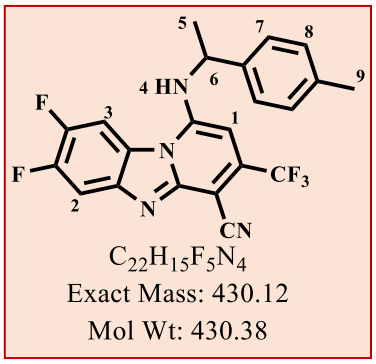

***7,8-difluoro-1-((2-phenylpropan-2-yl)amino)-3-(trifluoromethyl)benzo[4,5]imidazo[1,2-a]pyridine-4-carbonitrile*, 28**

Compound **28** was obtained from **1.4*c*** (0.10 g, 0.30 mmol, 1.0 equiv) and 2-phenylpropan-2-amine (0.81 g, 0.60 mmol, 2.0 equiv) as orange solid (0.11 g, 85%), m.p 197 – 199 °C; Rf (EtOAc : Hexane, 3 : 7) 0.36. ^{1}H NMR (400 MHz, DMSO-d_6) δ 8.5 (dd, J = 11.1, 7.3 Hz, 1H, H^{2}), 8.4 (s, 1H, H^{4}), 8.0 (dd, J = 11.0, 7.6 Hz, 1H, H^{3}), 7.6 (dd, J = 9.7, 1.3 Hz, 2H, H^{6}), 7.4 (t, J = 9.5 Hz, 2H, H^{7}), 7.4 (dt, J = 7.7, 1.3 Hz, 1H, H^{8}), 5.6 (s, 1H, H^{1}), 1.9 (s, 6H, H^{5}). ^{13}C NMR (101 MHz, DMSO-d6) δ 149.6, 129.2, 129.0 (5C), 127.8 (2C), 127.2 (5C), 105.1 (2C), 88.6 (3C), 11.5 (3C). HPLC-MS (ACI/ ESI): Purity = 99.0%, t_R = 3.77 min, m/z $[M-H]^-$ = 429.1.

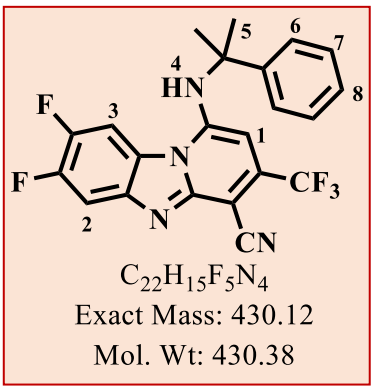

***7,8-difluoro-1-((1-phenylpropyl)amino)-3-(trifluoromethyl)benzo[4,5]imidazo[1,2-a]pyridine-4-carbonitrile*, 29**

Compound **29** was obtained from **1.4*c*** (0.10 g, 0.30 mmol, 1.0 equiv) and 1-phenylpropan-1-amine (0.81 g, 0.60 mmol, 2.0 equiv) as orange solid (0.11 g, 85%), m.p 185 – 187 C; Rf (MeOH : DCM, 0.4 : 9. 6) 0.25. ^{1}H NMR (400 MHz, DMSO-d_6) δ 8.7 (dd, *J* = 11.3, 7.3 Hz, 1H, H^{2}), 8.2 (s, 1H, H^{4}), 7.9 (dd, *J* = 10.8, 7.7 Hz, 1H, H^{3}), 7.6 (dd, *J* = 7.5, 1.3 Hz, 2H, H^{8}), 7.4 (t, *J* = 7.6 Hz, 2H, H^{9}), 7.3 (dt, *J* = 7.7, 1.4 Hz, 1H, H^{10}), 6.2 (s, 1H, H^{1}), 4.8 (t, *J* = 5.6 Hz, 1H, H^{7}), 2.3 – 1.9 (m, 2H, H^{6}), 0.8 (t, *J* = 7.4 Hz, 3H, H^{5}). ^{13}C NMR (101 MHz, DMSO-d6) δ 148.5, 145.1, 129.4 (3C), 127.8 (2C), 125.7 (4C), 114.1, 106.0 (3C), 90.5 (2C), 58.9, 29.6 (4C). HPLC-MS (ACI/ ESI): Purity = 99%, t_R = 3.13 min, m/z $[M-H]^-$ = 429.1.

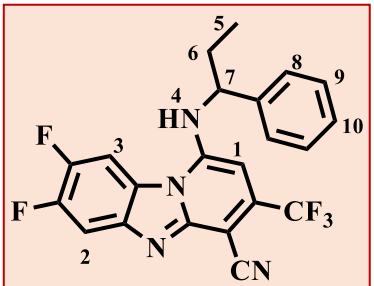

$C_{22}H_{15}F_5N_4$
Exact Mass: 430.12
Mol. Wt: 430.38

***7,8-difluoro-1-((1-phenylcyclopropyl)amino)-3-(trifluoromethyl)benzo[4,5]imidazo[1,2-a]pyridine-4-carbonitrile*, 30**

Compound **30** was obtained from **1.4*c*** (0.080 g, 0.24 mmol, 1.0 equiv) and 1-phenylcyclopropan- 1-amine (0.063 g, 0.48 mmol, 2.0 equiv) as yellow solid (0.066 g, 64%), m.p 182 – 184 °C; Rf (EtOAc : Hexane, 3 : 7) 0.17. ^{1}H NMR (400 MHz, DMSO-d_6) δ 9.0 (s, 1H, H^{4}), 8.9 (dd, *J* = 11.7, 7.3 Hz, 1H, H^{2}), 8.0 (dd, *J* = 11.0, 7.7 Hz, 1H, H^{3}), 7.3 (m, 4H, $H^{6,7}$), 7.3 (dt, *J* = 7.2, 1.6 Hz, 1H, H^{8}), 6.2 (s, 1H, H^{1}), 1.6 (s, 4H, H^{5}). ^{13}C NMR (101 MHz, DMSO-d_6) δ 150.0 (2C), 141.0, 129.0 (4C), 126.9, 124.9 (2C), 114.4, 106.2 (2C), 105.2 (2C), 88.9 (2C), 38.0 (2C), 20.4 (3C). HPLC-MS (ACI/ ESI): Purity = 99%, t_R = 2.99 min, m/z $[M+H]^+$ = 429.1.

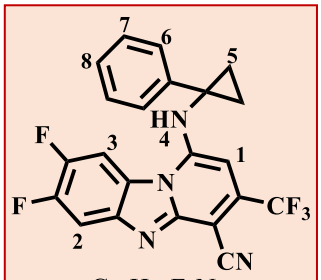

$C_{22}H_{13}F_5N_4$
Exact Mass: 428.11
Mol Wt: 428.37

***7,8-difluoro-1-((2-(4-fluorophenyl)propan-2-yl)amino)-3-(trifluoromethyl)benzo[4,5]imidazo[1,2-a]pyridine-4-carbonitrile*, 31**

Compound **31** was obtained from **1.4*c*** (0.045 g, 0.15 mmol, 1.0 equiv) and 1-phenylpropan-1-amine (0.045 g, 0.30 mmol, 2.0 equiv) as orange solid (0.037 g, 61 %), m.p 229 – 231 °C; Rf (MeOH : DCM, 4 : 6) 0.27. ^{1}H NMR (400 MHz, DMSO-d_6) δ 8.6 (dd, *J* = 11.2, 7.2 Hz, 1H, H^2), 8.4 (s, 1H, H^4), 8.1 (dd, *J* = 10.9, 7.6 Hz, 1H, H^3), 7.7 (dd, *J* = 8.7, 5.5 Hz, 2H, H^6), 7.3 (t, *J* = 8.8 Hz, 2H, H^7), 5.6 (s, 1H, H^1), 1.9 (s, 6H, H^5). ^{13}C NMR (101 MHz, DMSO-d_6) δ 148.4, 141.7, 141.3, 128.0 (4C), 123.9, 116.0 (4C), 114.0, 106.4, 105.8 (2C), 90.4 (2C), 58.5, 29.7 (3C). HPLC-MS (ACI/ ESI): Purity = 99%, t_R = 3.13 min, m/z $[M+H]^+$ = 449.0.

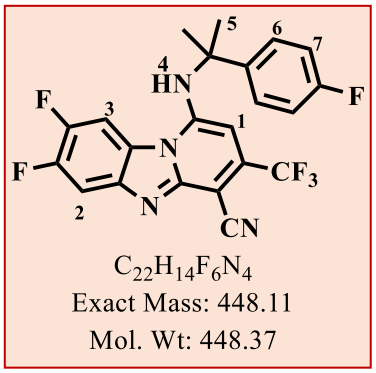

$C_{22}H_{14}F_6N_4$
Exact Mass: 448.11
Mol. Wt: 448.37

***Methyl (S)-2-((3-cyano-7,8-difluoro-4-(trifluoromethyl)benzo[4,5]imidazo[1,2-a]pyridin-1-yl)amino)-2-phenylacetate*, 32**

Compound **32** was obtained from **1.4*c*** (0.080 g, 0.26 mmol, 1.0 equiv) and methyl (S)-2-amino-2-phenylacetate (0.084 g, 0.51 mmol, 2.0 equiv) as yellow solid (0.033 g, 28%), m.p 228 – 230 °C; Rf (EtOAc : Hexane, 4 : 6) 0.24. ^{1}H NMR (400 MHz, DMSO-d_6) δ 8.6 (dd, *J* = 9.4, 7.3 Hz, 1H, H^2), 8.5 (dd, *J* = 8.8, 7.5 Hz, 1H, H^3), 8.0 (s, 1H, H^4), 7.7 (dd, *J* = 7.4, 1.6 Hz, 2H, H^7), 7.5 (t, *J* = 8.2 Hz, 2H, H^8), 7.4 (dt, *J* = 7.3, 1.7 Hz, 1H, H^9), 6.3 (s, 1H, H^1), 6.0 (s, 1H, H^5), 3.8 (s, 3H, H^6). ^{13}C NMR (101 MHz, DMSO-d_6) δ 149.3, 148.6 (3C), 129.3 (6C), 129.1 (2C), 128.3 (6C), 123.8, 53.6 (3C). HPLC-MS (ACI/ ESI): Purity = 99%, t_R = 2.98 min, m/z $[M-H]^-$ = 459.0.

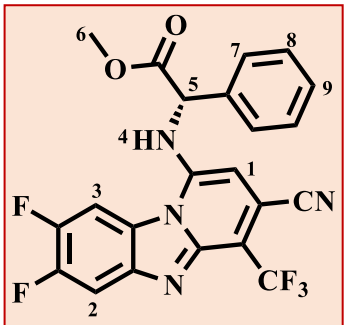

$C_{22}H_{13}F_5N_4O_2$
Exact Mass: 460.10
Mol. Wt: 460.36

***Methyl (R)-2-((3-cyano-7,8-difluoro-4-(trifluoromethyl)benzo[4,5]imidazo[1,2-a]pyridin-1-yl)amino)-2-phenylacetate,* 33**

Compound **33** was obtained from **1.4*c*** (0.12 g, 0.36 mmol, 1.0 equiv) and methyl (S)-2-amino-2-phenylacetate (0.12 g, 0.72 mmol, 2.0 equiv) as orange solid (0.070 g, 42%), m.p 232 – 235 °C; Rf (EtOAc : Hexane, 4 : 6) 0.24. ^{1}H NMR (400 MHz, DMSO-d_6) δ 8.6 (dd, J = 9.4, 7.2 Hz, 1H, H^{2}), 8.5 (dd, J = 8.8, 7.6 Hz, 1H, H^{3}), 8.0 (s, 1H, H^{4}), 7.7 (dd, J = 7.4, 1.4 Hz, 2H, H^{7}), 7.5 (t, J = 7.5 Hz, 2H, H^{8}), 7.32 (dt, J = 7.31, 1.63 Hz, 1H, H^{9}) 6.3 (s, 1H, H^{1}), 6.0 (s, 1H, H^{5}), 3.8 (s, 3H, H^{6}). ^{13}C NMR (101 MHz, DMSO-d_6) δ 149.4, 148.6 (2C), 129.3 (7C), 129.1 (2), 128.3 (7), 124.0, 53.6 (2). HPLC-MS (ACI/ ESI): Purity = 98%, t_R = 2.98 min, m/z [M-H]$^-$ = 459.0.

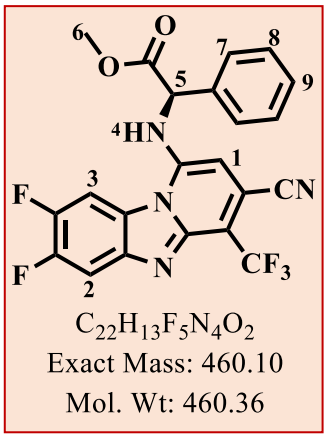

$C_{22}H_{13}F_5N_4O_2$
Exact Mass: 460.10
Mol. Wt: 460.36

***7,8-difluoro-1-((1-(1-methyl-1H-pyrazol-4-yl)ethyl)amino)-3-(trifluoromethyl)benzo[4,5]-imidazo[1,2-a]pyridine-4-carbonitrile,* 34**

Compound **34** was obtained from **1.4*c*** (0.10 g, 0.30 mmol, 1.0 equiv) and 1-(1-methyl-1H-pyrazol-4-yl)ethan-1-amine (0.075 g, 0.60 mmol, 2.0 equiv) as yellow solid (0.098 g, 78%), m.p 233 – 235 °C; Rf (EtOAc : Hexane, 3 : 7) 0.18. ^{1}H NMR (400 MHz, DMSO-d_6) δ 8.6 (dd, J = 11.4, 7.2 Hz, 1H, H^{2}), 8.3 – 8.2 (d, J = 7.0 Hz, 1H, H^{4}), 8.0 (dd, J = 11.0, 7.7 Hz, 1H, H^{3}), 7.8 (s, 1H, H^{8}), 7.5 (s, 1H, H^{7}), 6.5 (s, 1H, H^{1}), 5.2 (m, 1H, H^{6}), 3.8 (s, 3H, H^{9}), 1.7 (d, J = 6.7 Hz, 3H, H^{5}). ^{13}C NMR (101 MHz, DMSO-d_6) δ 150, 149.2, 137.3 (2C), 129.2 (2C), 123.6, 123.1, 114.4, 106.2 (2C), 105.2 (2C), 88.0 (2C), 46.5 (2C), 22.2 (2C). HPLC-MS (ACI/ ESI): Purity = 99%, t_R = 3.07 min, m/z [M-H]$^-$ = 419.1.

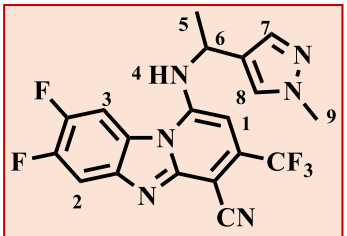

$C_{19}H_{13}F_5N_6$
Exact Mass: 420.11
Mol Wt: 420.35

***1-((4-(trifluoromethoxy)phenyl)amino)-(trifluoromethyl)benzo[4,5]imidazo[1,2-a]pyridine-4-carbonitrile,* GMP-19 (36)**

Compound **36** was obtained from **1.1*c*** (0.079 g, 0.27 mmol, 1.0 Eq) and 4-(trifluoromethoxy)aniline (0.054 g, 0.53 mmol, 2.0 Eq) as a yellow solid (0.091 g, 77%); Rf (EtOAc : Hexane, 1 : 1) 0.43; ^{1}H NMR (400 MHz, DMSO-d_6) δ 8.8 (dd, J = 7.7, 1.2 Hz, 1H, H^{5}), 7.7 (dd, J = 8.1, 1.1 Hz, 1H, H^{2}), 7.6 (dt, J = 7.7, 1.7 Hz, 1H, H^{3}), 7.4 (t, J = 8.8, 1.9 Hz, 1H, H^{4}), 7.3 (d, J = 8.3 Hz, 2H, H^{7}), 7.2 (d, J = 8.7 Hz, 2H, H^{6}), 6.2 (s, 1H, H^{1}). ^{13}C NMR (151 MHz, DMSO-d_6) δ 149.3, 145.8, 130.2, 126.7 (2C), 124.9 (4C), 122.8 (4C), 122.4 (2C), 116.0 (2C), 114.5, 92.7 (2C). HPLC-MS (ACI/ ESI): Purity = 99%, t_R = 3.06 min, m/z $[M+H]^+$ = 437.0.

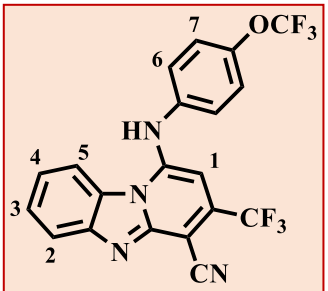

$C_{20}H_{10}F_6N_4O$
Exact Mass: 436.08
Mol. Wt: 436.32

***9-chloro-1-((4-(trifluoromethoxy)phenyl)amino)-3-(trifluoromethyl)benzo[4,5]imidazo-[1,2-a]pyridine-4-carbonitrile*, 37**

Compound **37** was obtained from **2.2*c*** (0.85 g, 2.58 mmol, 1.0 equiv) and 4-(trifluoromethoxy)aniline (0.91 g, 5.16 mmol, 3.0 equiv) as a yellow solid (0.57 g, 47%); Rf (EtOAc : Hexane, 7 : 3) 0.35; ^{1}H NMR (300 MHz, DMSO-d_6) δ 8.6 (d, J = 8.4 Hz, 1H, H^{4}), 7.7 (d, J = 8.0 Hz, 1H, H^{2}), 7.5 (d, J = 0.5 Hz, 4H, H$^{5, 6}$), 7.4 (t, J = 8.2 Hz, 1H, H^{3}), 6.4 (s, 1H, H^{1}). ^{13}C NMR (101 MHz, DMSO-d_6) δ 149.1 (2C), 145.8, 129.9 (2), 127.0 (2C), 124.9, 123.7, 123.1, 123.0, 122.7 (2C), 120.4, 119.7, 117.4 116.1 (3C), 114.0. HPLC-MS (ACI/ ESI): Purity = 99%, t_R = 3.37 min, m/z $[M+H]^+$ = 471.0.

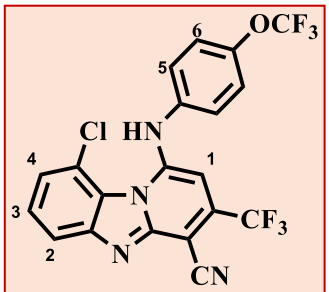

$C_{20}H_9ClF_6N_4O$
Exact Mass: 470.04
Mol Wt: 470.76

***9-nitro-1-((4-(trifluoromethoxy)phenyl)amino)-3-(trifluoromethyl)benzo[4,5]imidazo[1,2-a]pyridine-4-carbonitrile,* 42**

Compound **42** was obtained from **2.1.2*c*** (0.36 g, 1.07 mmol, 1.0 equiv) and 4-(trifluoromethoxy)aniline (0.38 g, 2.14 mmol, 2.0 equiv) as a yellow solid (0.24 g, 47%); Rf (EtOAc: Hexane, 4 : 6) 0.32; ^{1}H NMR (400 MHz, DMSO-d_6) δ 9.1 (d, J = 8.3 Hz, 1H, H^{4}), 8.4 (d, J = 8.2 Hz, 1H, H^{2}), 7.6 (t, J = 8.3 Hz, 1H, H^{3}), 7.5 – 7.4 (d, J = 8.5 Hz, 2H, H^{6}), 7.4 (d, J = 8.6 Hz, 2H, H^{5}), 6.4 (s, 1H, H^{1}). ^{13}C NMR (101 MHz, DMSO-d_6) δ 151.6, 149.2, 145.5, 132.1, 124.6 (4), 123.2 (2C), 123.0 (6C), 120.9, 114.7, 94.8 (2C). HPLC-MS (ACI/ ESI): Purity =99%, t_R = 3.31 min, m/z [M+H]$^{+}$ = 482.0.

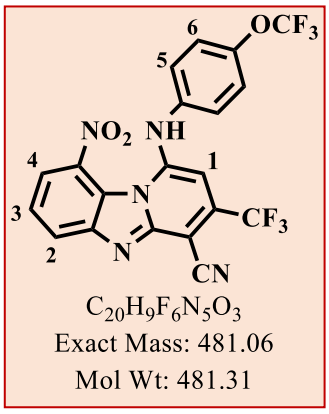

$C_{20}H_9F_6N_5O_3$
Exact Mass: 481.06
Mol Wt: 481.31

***9-amino-1-((4-(trifluoromethoxy)phenyl)amino)-3-(trifluoromethyl)benzo[4,5]imidazo[1,2-a]pyridine-4-carbonitrile,* 43**

A mixture of compound **42** (0.22 g, 0.46 mmol, 1.0 equiv) and ammonium chloride (0.26 g, 4.60 mmol 10.0 equiv) and iron (0.26 g, 4.60 mmol, 10.0 equiv) in a 1:1 methanol-water solution (2.0 mL) was stirred at 65 °C for 45 minutes. The reaction mixture was cooled to room temperature after which it was taken up in ethyl acetate (10.0 mL). The treated reaction mixture was filtered through celite, washed with deionised water (20 mL x 3), dried with brine (10 mL x2) and finally dried over $MgSO_4$. The organic layer was concentrated and dried *in vacuo*. The product was purified by flash-chromatography using EtOAc.

Compound **43** was obtained as a yellow solid (0.19 g, 90%); Rf (MeOH (NH_3): DCM, 1 : 9) 0.28; m.p 223 – 226 °C; ^{1}H NMR (400 MHz, Acetonitrile-d_3) δ 7.8 (dd, J = 8.4, 0.8 Hz, 1H, H^{2}), 7.4 (d, J = 0.5 Hz, 4H, H$^{7, 8}$), 7.2 (dd, J = 8.4, 7.7 Hz, 1H, H^{3}), 6.8 (dd, J = 7.7, 0.8 Hz, 1H, H^{4}), 6.2 (s, 1H, H^{1}), 5.5 (s, 1H, H^{6}), 3.3 (s, 2H, H^{5}). ^{13}C NMR (101 MHz, Acetonitrile-d_3) δ 138.6, 133.2, 128.4, 127.0, 125.2, 122.1 (2C), 122.5 (2C), 118.6, 108.9 (2C), 104.4 (2C), 90.0 (2C), 29.8 (4C). HPLC-MS (ACI/ ESI): Purity = 97%, t_R = 1.22 min, m/z [M+H]$^{+}$ = 452.0.

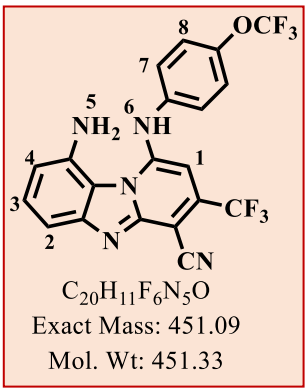

$C_{20}H_{11}F_6N_5O$
Exact Mass: 451.09
Mol. Wt: 451.33

6.3.7 General procedure for the synthesis of the amide derivatives - compounds 44 and 45[2]

A mixture of a suitable carboxylic acid (1.5 equiv), *N*,*N*-dimethylpyridin-4-amine (DMAP) (1.5 equiv) and *N*-Ethyl-*N*′-(3-dimethylaminopropyl)carbodiimide hydrochloride (EDCI) (1.5 equiv) in 0 °C cooled dichloromethane (1.0 mL per 100 mg of compound) was stirred at 0 °C for 5 minutes after which the temperature was increased to 17 – 25 °C (ambient temperature) for 15 minutes. The amine was added to the treated reaction mixture and stirring was continued at that temperature for 1.5 hours. The product was washed with three portions of 10 mL deionised water, filtered, washed using diethyl ether and finally dried on the filter paper at ambient conditions.

***(R)-1-((2-morpholino-2-oxo-1-phenylethyl)amino)-3-(trifluoromethyl)benzo[4,5]imidazo-[1,2-a]pyridine-4-carbonitrile,* 5**

Compound **5** was obtained from compound **4** (0.078 g, 0.19 mmol, 1.0 equiv) and 1, 1-dioxidothiomorpholine (0.039 g, 0.29 mmol, 1.5 equiv) as yellow solid (0.038 g, 38%), m.p 322 – 324 °C; Rf (EtOAc : Hexane, 0.1 : 9.9) 0.19. ^{1}H NMR (600 MHz, DMSO-d_6) δ 8.6 (dd, J = 7.9, 1.77 Hz, 1H, H^{2}), 8.5 (dd, J = 8.2, 1.4 Hz, 1H, H^{5}), 8.0 (s, 1H, H^{6}), 7.8 (dd, J = 7.4, 1.2 Hz, 2H, H^{10}), 7.7 (m, 2H, H$^{3, 4}$), 7.5 (t, J = 7.6 Hz, 2H, H^{11}), 7.4 (m, 1H, H^{12}), 6.5 (s, 1H, H^{1}), 6.4 (s, 1H, H^{7}), 4.3 - 3.8 (m, 4H, H^{9}), 3.4 – 2.9 (m, 4H, H^{8}). ^{13}C NMR (151 MHz, DMSO-d_6) δ 168.8, 147.9, 147.4, 145.7, 136.1, 129.6 (4C), 128.3 (3C), 127.3, 122.5, 120.1, 114.4 (2C), 86.9 (2C), 57.0 (2C), 43.8, 42.3 (3C). HPLC-MS (ACI/ ESI): Purity = 99%, t_R = 3.14 min, m/z $[M+H]^+$ = 528.1.

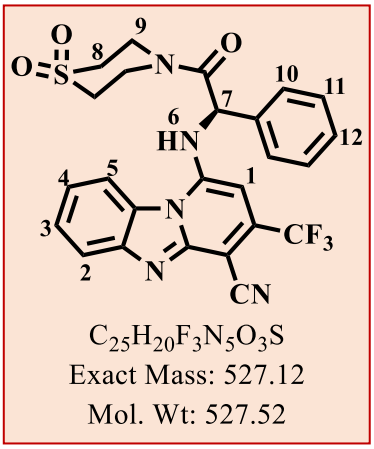

$C_{25}H_{20}F_3N_5O_3S$
Exact Mass: 527.12
Mol. Wt: 527.52

***9-(((((tert-butoxycarbonyl)oxy)glycyl)oxy)amino)-1-((4-(trifluoromethoxy)phenyl)amino)-3-(trifluoromethyl)benzo[4,5]imidazo[1,2-a]pyridine-4-carbonitrile*, 44**

Compound **44** was obtained from compound **43** (0.06 g, 0.13 mmol, 1.0 equiv) and *N*-(*tert*-butoxycarbonyl)-*N*-ethylglycine (0.040 g, 0.20 mmol, 1.5 equiv) as a beige solid (0.072 g, 81%), m.p 219 – 221 °C; Rf (EtOAc : Hexane, 6:4) 0.35. ^{1}H NMR (300 MHz, Acetonitrile-d_3) δ 9.0 (s, 1H, H^5), 8.4 (dd, 8.4, 1.1 Hz, 1H, H^2), 8.2 (dd, *J* = 8.0, 1.2 Hz, 1H, H^4), 7.3 (d, *J* = 7.9 Hz, 2H, H^{11}), 7.3 (t, *J* = 8.3 Hz, 1H, H^3), 7.2 (d, *J* = 7.6 Hz, 2H, H^{10}), 6.1 (s, 1H, H^1), 3.6 (s, 2H, H^6), 3.1 (q, *J* = 7.2 Hz, 2H, H^8), 1.5 (s, 9H, H^7), 1.2 (t, *J* = 6.5 Hz, 3H, H^9). ^{13}C NMR (101 MHz, Acetonitrile-d_3) δ 152.8, 150.4, 127.6, 123.8 (3C), 122.2 (3C), 120.0 (2C), 112.0, 110.9 (2C), 89.1 (3C), 80.0, 53.3, 31.1 (2C), 29.8 (3C), 27.6 (5C). HPLC-MS (ACI/ ESI): Purity = 99%, t_R = 3.37 min, m/z $[M-H]^-$ = 635.0.

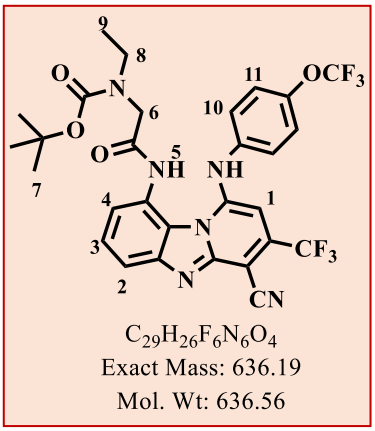

$C_{29}H_{26}F_6N_6O_4$
Exact Mass: 636.19
Mol. Wt: 636.56

***tert-butyl (2-((4-cyano-1-((4-(trifluoromethoxy)phenyl)amino)-3-(trifluoromethyl) benzo[4,-5]imidazo[1,2-a]pyridin-9-yl)amino)-2-oxoethyl)(ethyl) carbamate*, 45**

Compound **45** was obtained from compound **43** (0.06 g, 0.13 mmol, 1.0 equiv) and (*tert*-butoxycarbonyl)glycine (0.035 g, 0.20 mmol, 1.5 Eq) as an orange solid (0.029 g, 37%), m.p 215 – 218 °C; Rf (MeOH : DCM, 1 : 9) 0.18. ^{1}H NMR (300 MHz, Acetonitrile-d_3) δ 9.0 (s, 1H, H^5), 8.4 (dd, *J* = 8.3, 0.9 Hz, 1H, H^2), 8.3 (dd, *J* = 8.0, 1.2 Hz, 1H, H^4), 7.3 (d, *J* = 7.9 Hz, 2H, H^9), 7.3 (t, *J* = 8.1 Hz, 1H, H^3), 7.2 (d, *J* = 7.7 Hz, 2H, H^8), 6.1 (s, 1H, H^1), 4.1 (s, 2H, H^6), 1.5 (s, 9H, H^7). ^{13}C NMR (101 MHz, Acetonitrile-d_3) δ 168.5, 149.9, 127.2, 124.3 (3C), 122.3 (3C), 120.4, 114.2 (2C), 111.9, 89.8 (3C), 80.0, 51.5 (2C), 43.5 (3C), 30.8, 29.8, 27.6 (3C). HPLC-MS (ACI/ ESI): Purity = 99%, t_R = 3.35 min, m/z $[M-H]^-$ = 607.0.

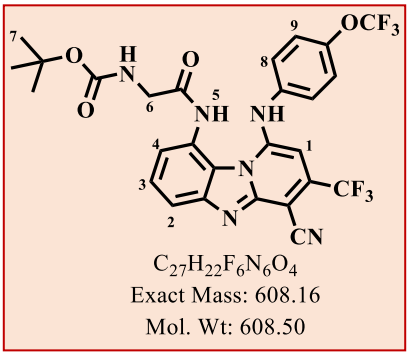

$C_{27}H_{22}F_6N_6O_4$
Exact Mass: 608.16
Mol. Wt: 608.50

***1-((5,6-dimethoxypyrimidin-4-yl)amino)-7,8-difluoro-3-(trifluoromethyl)benzo[4,5]imidazo[1,2-a]pyridine-4-carbonitrile*, 46**

Compound **46** was obtained from **1.4*c*** (0.15 g, 0.45 mmol, 1.0 equiv) and 5,6-dimethoxypyrimidin-4-amine (0.14 g, 0.90 mmol, 2.0 equiv) as yellow solid (0.093 g, 46%), m.p 299 – 302 °C; Rf (EtOAc : Hexane, 3 : 7) 0.18. ^{1}H NMR (400 MHz, DMSO-d_6) δ 8.4 (s, 1H, H^4), 8.3 (dd, J = 10.7, 7.5 Hz, 1H, H^2), 8.3 (dd, J = 8.7, 6.9 Hz, 1H, H^3), 6.1 (s, 1H, H^1), 4.2 (s, 3H, H^7), 4.0 (s, 3H, H^6). ^{13}C NMR (101 MHz, DMSO-d_6) δ 153.9, 145.2 (2C), 127.4, 119.2 (2C), 113.6, 111.1, 104.4, 106.2 (3C), 105.2 (3C), 88.0 (2C), 46.5 (2C). HPLC-MS (ACI/ ESI): Purity = 97%, t_R = 3.17 min, m/z $[M+H]^+$ = 451.1

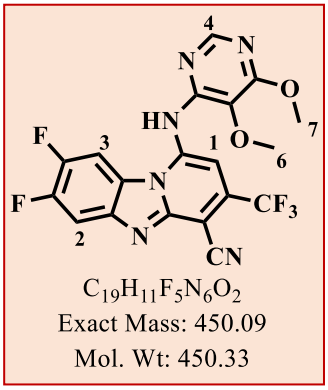

***7,8-difluoro-1-((2-fluoropyridin-4-yl)amino)-3-(trifluoromethyl)benzo[4,5]imidazo[1,2-a]pyridine-4-carbonitrile*, 47**

Compound **47** was obtained from **1.4*c*** (0.10 g, 0.30 mmol, 1.0 equiv) and 1-(1-methyl-1H-pyrazol-4-yl)ethan-1-amine (0.075 g, 0.60 mmol, 2.0 equiv) as yellow solid (0.098 g, 78%), m.p > 300 °C; Rf (EtOAc : Hexane, 3 : 7) 0.18. ^{1}H NMR (400 MHz, DMSO-d_6) δ 8.2 (d, J = 7.7 Hz, 1H, H^6), 8.4 (dd, J = 10.9, 7.4 Hz, 1H, H^2), 7.8 (dd, J = 7.8, 6.6 Hz, 1H, H^3), 6.8 (d, J = 7.6 Hz, 1H, H^5), 6.5 (d, J = 7.3 Hz, 1H, H^4), 6.2 (s, 1H, H^1). ^{13}C NMR (101 MHz, DMSO-d_6) δ 166.4, 165.3 (2C), 147.5 (3), 128.1, 121.2, 119.0, 113.9, 113.1, 106.2 (2C), 99.1 (2C), 88.0 (3C). HPLC-MS (ACI/ ESI): Purity = 96%, t_R = 3.03 min, m/z $[M-H]^-$ = 409.0

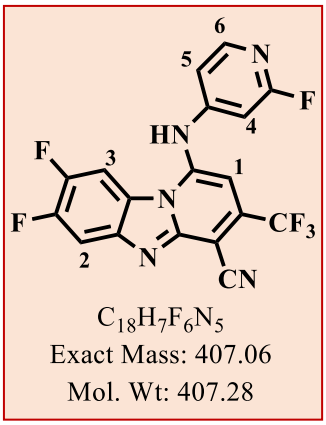

8-chloro-1-((2-methoxyethyl)amino)-3-(trifluoromethyl)benzo[4,5]imidazo[1,2-a]pyridine-4-carbonitrile,* 2.2*d

Compound **2.2*d*** was obtained from **2.2*c*** (0.11 g, 0.32 mmol, 1.0 equiv) and 2-methoxyethan-1-amine (0.048 mL, 0.64 mmol, 2.0 equiv) as yellow solid (0.063 g, 53%); Rf (EtOAc : Hexane, 4 : 6) 0.12. ^{1}H NMR (400 MHz, DMSO-d_6) δ 8.7 (d, J = 2.2 Hz, 1H, H^{4}), 8.6 (d, J = 8.8 Hz, 1H, H^{2}), 8.0 (dd, J = 8.9, 2.2 Hz, 1H, H^{3}), 6.6 (s, 1H, H^{1}), 3.9 (t, J = 5.4 Hz, 2H, H^{6}), 3.7 (t, J = 5.4 Hz, 2H, H^{5}), 3.4 (s, 3H, H^{7}). ^{13}C NMR (101 MHz, DMSO-d_6) δ 150.3, 127.2, 120.1, 118.3, 116.9 (2C), 115.2, 87.2 (2C), 70.9 (2C), 58.7 (2C), 44.0 (3C). HPLC-MS (ACI/ ESI): Purity = 97%, t_R = 3.11 min, m/z $[M+H]^+$ = 369.0.

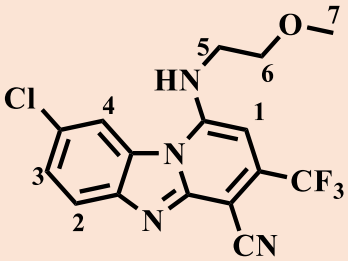

$C_{16}H_{12}ClF_3N_4O$
Exact Mass: 368.07
Mol. Wt: 368.74

***1-((2-(diethylamino)ethyl)amino)-8-morpholino-3-(trifluoromethyl)benzo[4,5]imidazo[1,2-a]pyridine-4-carbonitrile,* 49**

Compound **2.2*d*** was obtained from **2.2*c*** (0.088 g, 0.27 mmol, 1.0 equiv) and N^1, N^1-diethylethane-1,2-diamine (0.037.3 g, 0.32 mmol, 1.2 Eq) as an orange solid (0.062 g, 56%), m.p 238 – 240 °C; Rf (EtOAc : Hexane, 7 : 3) 0.22. ^{1}H NMR (400 MHz, DMSO-d_6) δ 7.9 (d, J = 2.3 Hz, 1H, H^{4}), 7.8 (s, 1H, H^{5}), 7.7 (d, J = 9.4 Hz, 1H, H^{2}), 7.3 (dd, J = 8.9, 2.3 Hz, 1H, H^{3}), 6.31 (s, 1H, H^{1}), 3.63 (t, J = 6.1 Hz, 2H, H^{6}), 2.98 (t, J = 6.33 Hz, 2H, H^{7}), 2.9 – 2.7 (q, J = 7.2 Hz, 4H, H^{8}), 1.1 (t, J = 7.2 Hz, 6H, H^{9}). ^{13}C NMR (101 MHz, DMSO-d_6) δ 155.9, 149.8, 141.7, 130.2, 119.8 (2C), 117.6, 102.2 (3C), 85.7, 73.8 (2C), 66.7 (2C), 51.1, 46.7, 11.4 (2C). HPLC-MS (ACI/ ESI): Purity = 96%, t_R = 2.56 min, m/z $[M-H]^-$ = 409.8/ 410.0.

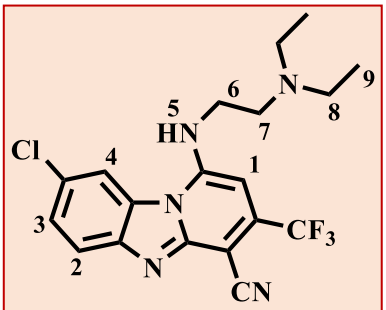

$C_{19}H_{19}ClF_3N_5$
Exact Mass: 409.13
Mol. Wt: 409.84

***8-chloro-1-((2-(diethylamino)ethyl)amino)-3-(4-(trifluoromethyl)phenyl)benzo[4,5]imidazo [1,2-a]pyridine-4-carbonitrile*, 50**

Compound **50** was obtained from **2.4*c*** (0.11 g, 0.27 mmol, 1.0 equiv) and N^1, N^1-diethylethane-1,2-diamine (0.063 g, 0.54 mmol, 2.0 equiv) as yellow solid (0.083 g, 63%); Rf (EtOAc : Hexane, 1 : 1) 0.20. ^{1}H NMR (600 MHz, DMSO-d_6) δ 8.7 (d, J = 2.1 Hz, 1H, H^4), 8.6 (dd, J = 8.9, 2.1 Hz, 1H, H^3), 8.0 (d, J = 8.2 Hz, 2H, H^{11}), 8.0 (d, J = 8.3 Hz, 2H, H^{10}), 7.8 (s, 1H, H^5), 7.6 (d, J = 8.9 Hz, 1H, H^2), 6.3 (s, 1H, H^1), 3.6 (t, J = 6.3 Hz, 2H, H^6), 2.9 (t, J = 6.3 Hz, 2H, H^7), 2.7 (q, J = 7.1 Hz, 4H, H^8), 1.0 (t, J = 7.1 Hz, 6H, H^9). ^{13}C NMR (151 MHz, DMSO-d_6) δ 149.4, 141.9, 130.0 (3), 129.0 (2), 126.0 (3), 121.6, 117.3, 114.1, 111.8, 91.7, 51.2 (2), 46.8 (3), 41.7 (2), 12.1 (3). HPLC-MS (ACI/ ESI): Purity = 92%, t_R = 2.85 min, m/z $[M+H]^+$ = 486.1.

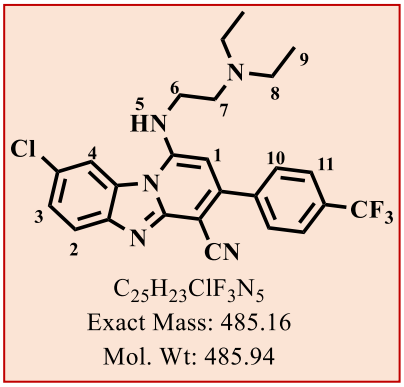

***tert-Butyl (2-((8-chloro-4-cyano-3-(4-(trifluoromethyl)phenyl)benzo[4,5]imidazo[1,2-a]pyridin-1-yl)amino)ethyl)(ethyl)carbamate*, 51**

Compound **51** was obtained from compound **2.4*c*** (0.110 g, 0.27 mmol, 1.0 equiv) and tert-butyl (2-aminoethyl)(ethyl)carbamate (0.102 g, 0.54 mmol, 2.0 equiv) as yellow solid (0.134 g, 89%), m.p 235 – 237 °C; Rf (EtOAc : Hexane, 3 : 7) 0.27. ^{1}H NMR (600 MHz, DMSO-d_6) δ 8.7 (d, J = 2.2 Hz, 1H, H^4), 8.6 (dd, J = 8.9, 2.1 Hz, 1H, H^3), 8.0 (d, J = 8.2 Hz, 2H, H^{12}), 7.9 (d, J = 8.3 Hz, 2H, H^{11}), 7.8 (s, 1H, H^5), 7.6 (d, J = 8.6 Hz, 1H, H^2), 6.4 (s, 1H, H^1), 3.7 (t, J = 6.2 Hz, 2H, H^6), 3.6 (t, J = 6.4 Hz, 2H, H^7), 3.3 (q, J = 6.97 Hz, 2H, H^9), 1.2 (s, 9H, H^8), 1.1 (t, J = 8.7 Hz, 3H, H^{10}). ^{13}C NMR (151 MHz, DMSO-d_6) δ 155.7, 151.1, 149.1, 130.0 (2C), 126.8, 126.0 (2C), 120.6, 120.0, 118.2, 116.2, 115.2, 91.2, 79.4, 46.4 (2C), 45.3, 42.6 (3C), 28.4 (4C), 13.9, 9.0 (2C). HPLC-MS (ACI/ ESI): Purity = 99%, t_R = 3.37 min, m/z $[M+H]^+$ = 558.1.

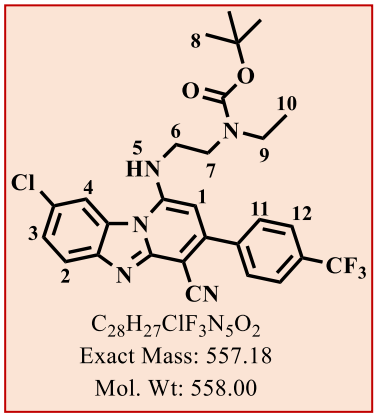

6.3.8 General procedure for the synthesis of the final compounds 38 – 41, 48, 49, 53 and 54 using the palladium (0) catalysed amine coupling (Buchwald-Hartwig reaction)[1]

A mixture of an aryl-halide (**2.3*d*, 2.3*e*, 37, 50 – 52**: 1.0 equiv), tris(dibenzylideneacetone) dipalladium (0) (Pd_2dba_3: 0.1 equiv), RuPhos (0.2 equiv), cesium carbonate (Cs_2CO_3: 3.0 equiv) and the appropriate amine (2.0 equiv) in anhydrous 1,4-dioxane in a sealed tube was flushed with nitrogen gas for 15 minutes. The treated reaction mixture was heated to 110 °C for aliphatic cyclic amines and at 120 °C for an aromatic amine for 8-16 hours at respective temperatures with continuous stirring. The excess solvent was removed *in vacuo* and the resulting residue taken up in ethyl acetate, washed with lithium chloride (20 mL x 3), deionized water (20 mL x 3), brine (10 mL x 3), dried over anhydrous magnesium sulphate ($MgSO_4$), filtered through celite, concentrated and dried *in vacuo* to obtain solid residues. A column was used where the compound needed further purification.

***9-(pyrimidin-2-ylamino)-1-((4-(trifluoromethoxy)phenyl)amino)-3-(trifluoromethyl)benzo-[4,5]imidazo[1,2-a]pyridine-4-carbonitrile,* 38**

Compound **38** was obtained from compound **37** (0.080 g, 0.17mmol, 1.0 equiv) and 2-amino pyrimidine (0.019 g, 0.20 mmol, 1.2 equiv) as a yellow solid (0.031 g, 34%); m.p 242 – 244 °C; Rf (EtOAc : Hexane, 3 : 7) 0.32; ^{1}H NMR (300 MHz, Acetonitrile-d_3) δ 9.0 (s, 1H, H^7), 8.8 (s, 1H, H^8), 8.6 (d, J = 5.04 Hz, 2H, H^6), 8.3 (dd, J = 8.0, 0.9 Hz, 1H, H^2), 8.2 (t, J = 8.7 Hz, 1H, H^3), 7.5 (d, J = 8.2 Hz, 2H, H^9), 7.4 (dd, J = 8.7, 0.8 Hz, 1H, H^4), 7.4 (d, J = 7.8 Hz, 2H, H^{10}), 7.0 (t, J = 4.9 Hz, 1H, H^5), 6.4 (s, 1H, H^1). ^{13}C NMR (151 MHz, DMSO-d_6) δ 158.8, 157.9 (3C), 152.2 (4C), 144.8, 143.5, 142.8 (2C), 138.7 (3C), 132.3, 132.3 (2C), 122.8, 118.2 (2C), 114.2, 98.5 (2C). HPLC-MS (ACI/ ESI): Purity = 98%, t_R = 3.27 min, m/z $[M+H]^+$ = 530.1.

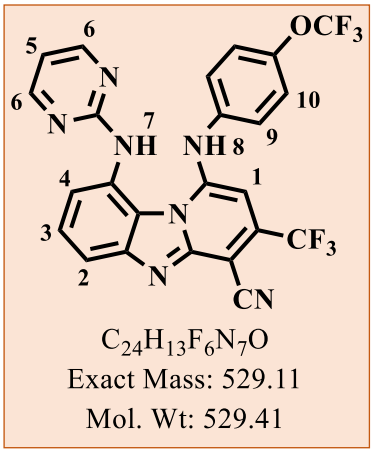

$C_{24}H_{13}F_6N_7O$
Exact Mass: 529.11
Mol. Wt: 529.41

***9-morpholine-1-((4-(trifluoromethoxy)phenyl)amino)-3-(trifluoromethyl)benzo [4,5]imidazo[1,2-a]pyridine-4-carbonitrile,* 1.7b**

Compound **39** was obtained from **37** (0.10 g, 0.21 mmol, 1.0 equiv) and morpholine (0.037 g, 0.42 mmol, 2.0 equiv) as a yellow solid (0.022 g, 20%), m.p 212 – 215 °C; Rf (EtOAc : Hexane, 7 : 3) 0.21; ^{1}H NMR (300 MHz, DMSO-d_6) δ 8.9 (s, 1H, H^7), 8.1 (dd, J = 7.3, 1.9 Hz, 1H, H^2), 7.5 (d, J = 8.7 Hz, 2H, H^8), 7.4 (d, J = 8.6 Hz, 2H, H^9), 7.4 (t, J = 8.2 Hz, 1H, H^3), 7.2 (dd, J = 8.1, 2.1 Hz, 1H, H^4), 6.4 (s, 1H, H^1), 3.9 (m, 4H, H^5), 3.5 (m, 4H, H^6). ^{13}C NMR (151 MHz, DMSO-d_6) δ 148.8, 148.6, 148.1, 147.7, 147.3, 145.9, 130.0, 124.8 (2C), 123.1, 122.8 (2C), 114.2, 66.7 (2C), 50.6 (2C). HPLC-MS (ACI/ ESI): Purity = 98%, t_R = 3.20 min, m/z $[M+H]^+$ = 522.0.

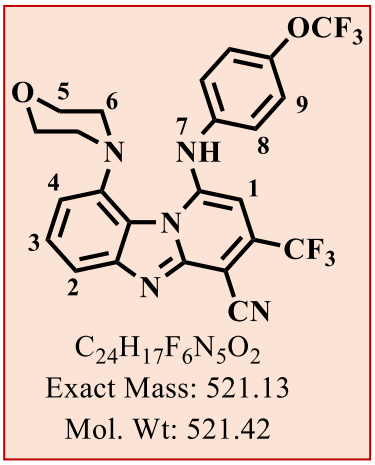

$C_{24}H_{17}F_6N_5O_2$
Exact Mass: 521.13
Mol. Wt: 521.42

tert-Butyl 4-(4-cyano-1-((4-(trifluoromethoxy)phenyl)amino)-3-(trifluoromethyl)benzo-[4,5]imidazo[1,2-a]pyridin-9-yl)piperazine-1-carboxylate,* 2.2*d

Compound **2.2*d*** was obtained from **37** (0.15 g, 0.32 mmol, 1.0 equiv) and *tert*-butyl piperazine-1-carboxylate (0.12 g, 0.64 mmol, 1.2 Eq) as a orange solid (0.070 g, 35%), m.p 185 – 187 °C; Rf (EtOAc : Hexane, 3 : 7) 0.29; ^{1}H NMR (300 MHz, DMSO-d_6) δ 8.8 (s, 1H, H^8), 8.5 (d, J = 8.9 Hz, 2H, H^9), 8.4 (dd, J = 8.6, 2.0 Hz, 1H, H^2), 8.2 (d, J = 8.9 Hz, 2H, H^{10}), 7.4 (t, J = 8.3 Hz, 1H, H^3), 6.8 (dd, J = 7.9, 2.0 Hz, 1H, H^4), 5.7 (s, 1H, H^1), 4.2 (m, 4H, H^7), 4.1 (m, 4H, H^6) 1.3 (s, 9H, H^5). ^{13}C NMR (101 MHz, DMSO-d_6) δ 163.7, 153.8, 143.3 (3C), 133.2 (3C), 127.5 (3C), 123.7, 122.6, 122.1, 121.8, 120.4 (4C), 105.5, 99.3 (2C), 77.9, 49.2 (2C), 26.7 (4C). HPLC-MS (ACI/ ESI): Purity = 98%, t_R = 3.19 min, m/z $[M-H]^-$ = 618.7.

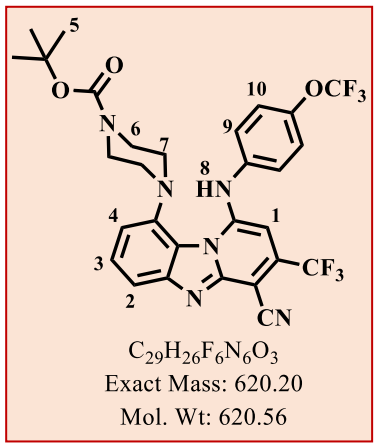

$C_{29}H_{26}F_6N_6O_3$
Exact Mass: 620.20
Mol. Wt: 620.56

***9-(1,1-dioxidothiomorpholino)-1-((4-(trifluoromethoxy)phenyl)amino)-3-trifluoromethyl)-benzo[4,5]imidazo[1,2-a]pyridine-4-carbonitrile,* 41**

Compound **41** was obtained from **37** (0.056 g, 0.12 mmol, 1.0 equiv) and thiomorpholine-1,1-dioxide (0.032 g, 0.24 mmol 2.0 equiv) as orange solid (0.021 g, 30%), m.p > 300 °C; Rf (EtOAc : Hexane, 1 : 1) 0.36; ^{1}H NMR (400 MHz, Acetonitrile-d_3) δ 8.0 (dd, J = 7.5, 2.2 Hz, 1H, H^2), 7.4 (d, J = 9.2 Hz, 2H, H^7), 7.4 (d, J = 9.4 Hz, 2H, H^8), 7.3 (t, J = 8.2 Hz, 1H, H^3), 7.1 (dd, J = 7.5, 2.2 Hz, 1H, H^4), 6.3 (s, 1H, H^1), 4.2 (t, J = 5.2 Hz, 4H, H^6), 3.2 (t, J = 5.2 Hz, 4H, H^5). ^{13}C NMR (151 MHz, Acetonitrile-d_3) δ 148.7, 146.6, 146.3, 140.0, 138.2, 136.9, 136.7, 129.8, 125.5 (2C), 123.3, 122.7 (3C), 121.4, 121.4, 113.8, 113.2, 108.6, 90.5, 51.0 (2C), 48.5 (2C). HPLC-MS (ACI/ ESI): Purity = 99%, t_R = 3.23 min, m/z $[M+H]^+$ = 570.0.

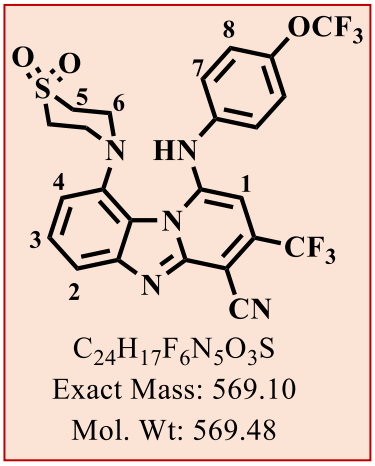

***1-((2-methoxyethyl)amino)-8-morpholino-3-(trifluoromethyl)benzo[4,5]imidazo[1,2-a]pyridine-4-carbonitrile,* 48**

Compound **48** was obtained from **2.2*d*** (0.060 g, 0.16 mmol, 1.0 equiv) and morpholine (0.043 g, 0.49 mmol, 3.0 equiv) as an orange solid (0.023 g, 35%), m.p 185 - 188; Rf (EtOAc : Hexane, 8 : 2) 0.36. ^{1}H NMR (400 MHz, Methanol-d_4) δ 8.2 (d, J = 9.2 Hz, 1H, H^2), 7.3 (d, J = 2.0 Hz, 1H, H^6), 6.8 (dd, J = 8.4, 2.0 Hz, 1H, H^3), 6.6 (s, 1H, H^1), 4.0 – 3.9 (m, 4H, H^4), 3.9 (t, J = 5.7 Hz, 2H, H^8), 3.6 (t, J = 5.7 Hz, 2H, H^7), 3.4 (s, 3H, H^9), 3.4 – 3.3 (m, 4H, H^5). ^{13}C NMR (101 MHz, Methanol-d_4) δ 130.1, 118.6, 113.8, 112.2, 107.9, 102.5, 85.8 (2C), 71.6, 69.9, 66.6 (3C), 57.9, 50.5 (2C), 49.3, 42.9 (2C), 36.8. HPLC-MS (ACI/ ESI): Purity = 99%, t_R = 2.95 min, m/z $[M+H]^+$ = 420.0.

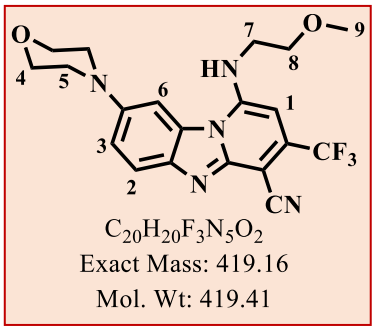

***1-((2-(diethylamino)ethyl)amino)-8-morpholino-3-(trifluoromethyl)benzo[4,5]imidazo[1,2-a]pyridine-4-carbonitrile*, 49**

Compound **49** was obtained from **2.2*d*** (0.058 g, 0.14 mmol, 1.0 equiv) and N^1, N^1-diethylethane-1,2-diamine (0.015 g, 0.17 mmol, 1.2 equiv) as an orange solid (0.022 g, 33%), m.p 232 – 235 °C; Rf (EtOAc : Hexane, 8 : 2) 0.17. ^{1}H NMR (400 MHz, DMSO-d_6) δ 7.9 (d, J = 2.1 Hz, 1H, H^6), 7.7 (d, J = 8.9 Hz, 1H, H^2), 7.3 (dd, J = 8.9, 2.1 Hz, 1H, H^3), 6.2 (s, 1H, H^1), 3.9 – 3.8 (m, 4H, H^4), 3.6 (t, J = 6.1 Hz, 2H, H^7), 3.2 – 3.1 (m, 4H, H^5), 3.0 (t, J = 5.9 Hz, 2H, H^8), 2.9 (q, J = 7.2 Hz, 4H, H^9), 1.1 (t, J = 7.0 Hz, 6H, H^{10}). ^{13}C NMR (101 MHz, DMSO-d_6) δ 150.6, 146.8, 139.9, 129.7, 118.8 (2C), 117.6, 102.2, 85.7, 66.7 (3C), 51.0 (5C), 46.6(3C), 11.2 (3C). HPLC-MS (ACI/ ESI): Purity = 99%, t_R = 2.94 min, m/z $[M-H]^-$ = 459.1.

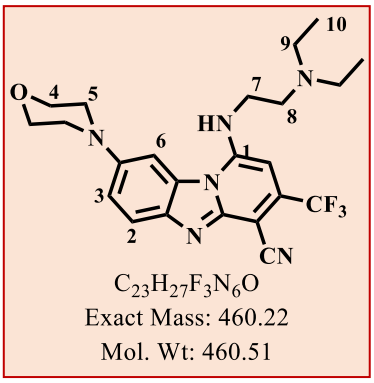

$C_{23}H_{27}F_3N_6O$
Exact Mass: 460.22
Mol. Wt: 460.51

***tert-Butyl (2-((4-cyano-8-morpholino-3-(4-(trifluoromethyl)phenyl)benzo[4,5]imidazo[1,2-a]pyridin-1-yl)amino)ethyl)(ethyl)carbamate*, 54**

Compound **54** was obtained from **51** (0.11 g, 0.20 mmol, 1.0 equiv) and morpholine (0.034 g, 0.39 mmol, 2.0 equiv) as orang solid (0.073 g, 60%), m.p 235 – 237 °C; Rf (EtOAc : Hexane, 3 : 7) 0.22. ^{1}H NMR (600 MHz, DMSO-d_6) δ 8.4 (s, 1H, H^7), 8.0 (d, J = 8.2 Hz, 2H, H^{14}), 7.9 (d, J = 8.3 Hz, 2H, H^{13}), 7.9 (d, J = 2.1 Hz, 1H, H^6), 7.7 (d, J = 8.9 Hz, 1H, H^2), 7.4 (dd, J = 9.0, 2.1 Hz, 1H, H^3), 6.5 (s, 1H, H^1), 3.8 (m, 4H, H^5), 3.8 (t, J = 6.2 Hz, 2H, H^8), 3.6 (t, J = 6.1 Hz, 2H, H^9), 3.1 (m, 4H, H^4), 3.2 (q, J = 10.0 Hz, 2H, H^{10}), 1.2 (s, 9H, H^{12}), 1.1 (t, J = 9.9 Hz, 3H, H^{11}). ^{13}C NMR (151 MHz, DMSO-d_6) δ 150.7, 141.3, 130.0 (3C), 126.0 (3C), 118.1, 117.5, 116.0, 111.7, 102.6, 100.7, 92.5, 79.4, 66.6 (3C), 50.7 (2C), 49.3, 45.3, 42.7 (3C), 28.4 (4C), 13.9 (2C). HPLC-MS (ACI/ ESI): Purity = 99%, t_R = 3.71 min, m/z $[M+H]^+$ = 609.2.

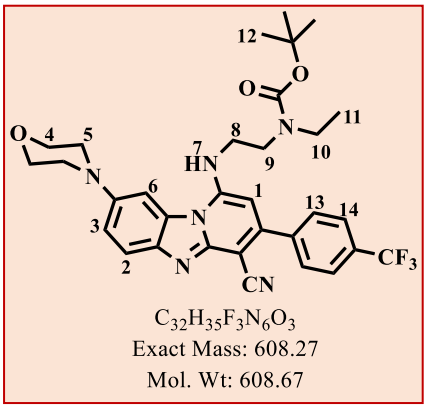

$C_{32}H_{35}F_3N_6O_3$
Exact Mass: 608.27
Mol. Wt: 608.67

6.3.9 General procedure for the amino-group deprotection: synthesis of compounds 40, 52 and 55[3]

A solution of 4 M HCl in 1,4-dioxane (1.0 mL per 100 mg sample) was added to a solution of an appropriate carbamate analogue. The reaction mixture was stirred for 1 hour from 0 °C to room temperature (17 - 25 °C). The completion of the reaction was confirmed by TLC and HPLC-MS after which excess 1, 4-dioxane and HCl were removed *in vacuo*. The compound residue was basified to pH 11 by a steady addition of saturated solution of sodium bicarbonate ($NaHCO_3$). The organic residues were taken up in ethyl acetate (EtOAc) after which the aqueous phase was removed using a separatory funnel. The EtOAc layer was washed with deionised water (20 mL x 3), brine (10 mL x 3), dried over $MgSO_4$ and was finally concentrated *in vacuo*.

***9-(piperan-1-yl)-1-((4-(trifluoromethoxy)phenyl)amino)-3-(trifluoromethyl)benzo [4,5]imidazo[1,2-a]pyridine-4-carbonitrile,* 40**

Compound **40** was obtained from **2.2*d*** (0.050 g, 0.080 mmol, 1.0 equiv) and HCl in dioxane (0.012 g, 0.096mmol, 1.2 equiv) as a brown solid (0.036 g, 87%), m.p: ND; Rf (MeOH : DCM, 0.5 : 9.5) 0.21; ^{1}H NMR (300 MHz, DMSO-d_6) δ 8.9 (s, 1H, H^8), 8.5 (d, J = 8.8 Hz, 2H, H^9), 8.4 (dd, J = 8.3, 2.0 Hz, 1H, H^2), 8.2 (d, J = 8.8 Hz, 2H, H^{10}), 7.4 (t, J = 8.1 Hz, 1H, H^3), 6.8 (d, J = 7.9, 2.0 Hz, 1H, H^4), 5.7 (s, 1H, H^1), 4.1 (m, 4H, H^7), 3.7 (m, 4H, H^6) 1.1 (s, 1H, H^5). ^{13}C NMR (101 MHz, DMSO-d_6) δ 163.7, 143.3 (2C), 133.2 (3C), 127.5 (3C), 123.7, 122.6, 122.1, 121.8, 120.4 (4C), 105.5, 99.3 (2C), 49.1 (2C), 45.9 (2C). HPLC-MS (ACI/ ESI): Purity = 98%, t_R = 2.95 min, m/z $[M+H]^+$ = 521.1.

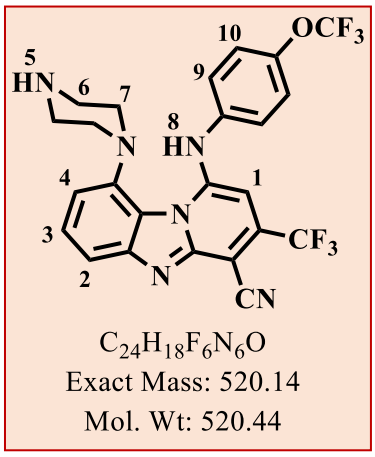

$C_{24}H_{18}F_6N_6O$
Exact Mass: 520.14
Mol. Wt: 520.44

***8-chloro-1-((2-(ethylamino)ethyl)amino)-3-(4-(trifluoromethyl)phenyl)benzo[4,5]imidazo-[1,2-a]pyridine-4-carbonitrile*, 52**

Compound **52** was obtained from compound **51** (0.070 g, 0.13 mmol, 1.0 equiv) and 4.0 M HCl in 1, 4-dioxane (0.70 mL) as yellow solid (0.057 g, 96%), m.p 226 - 228 °C; Rf (MeOH : DCM, 0.1 : 9.9) 0.17. ^{1}H NMR (600 MHz, DMSO-d_6) δ 8.6 (s, 1H, H^{5}), 8.4 (d, J = 2.2 Hz, 1H, H^{4}), 8.0 (d, J = 8.5 Hz, 2H, H^{11}), 8.0 (d, J = 8.6 Hz, 2H, H^{10}), 7.9 (dd, J = 8.6, 2.0 Hz, 1H, H^{3}), 7.6 (d, J = 8.6 Hz, 1H, H^{2}), 6.4 (s, 1H, H^{1}), 3.9 (t, J = 6.2 Hz, 2H, H^{6}), 3.4 (t, J = 6.0 Hz, 2H, H^{7}), 3.1 (q, J = 6.2 Hz, 2H, H^{8}), 1.3 (t, J = 6.2 Hz, 3H, H^{9}). ^{13}C NMR (151 MHz, DMSO-d_6) δ 151.2, 148.9, 141.6, 130.1 (3C), 127.0, 126.0 (2C), 125.4, 120.9, 120.0, 118.2, 117.1, 116.7, 115.7, 91.8, 91.6, 45.1, 45.0, 42.9, 42.9, 11.3. HPLC-MS (ACI/ ESI): Purity = 99%, t_R = 2.97 min, m/z [M-H]$^{-}$ = 458.1.

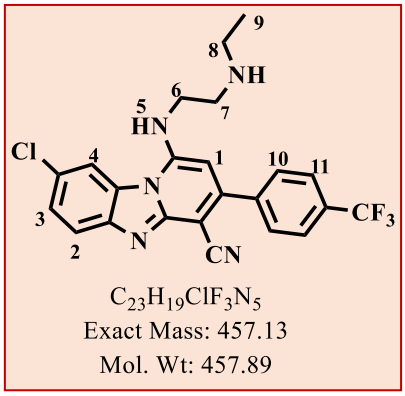

$C_{23}H_{19}ClF_3N_5$
Exact Mass: 457.13
Mol. Wt: 457.89

***1-((2-(ethylamino)ethyl)amino)-8-morpholino-3-(4-(trifluoromethyl)phenyl)benzo[4,5]imi-dazo[1,2-a]pyridine-4-carbonitrile*, 55**

Compound **55** was obtained from compound **54** (0.07 g, 0.12 mmol, 1.0 equiv) and 2.0m HCl in 1, 4-dioxane (0.5 mL) as orange solid (0.041 g, 70%), m.p 192 – 195 °C; Rf (MeOH : DCM, 0.4 : 9.6) 0.18. ^{1}H NMR (600 MHz, DMSO-d_6) δ 8.4 (s, 1H, H^{7}), 8.0 (d, J = 8.7 Hz, 2H, H^{14}), 7.9 (d, J = 8.7 Hz, 2H, H^{13}), 7.8 (d, J = 8.9 Hz, 1H, H^{2}), 7.4 (dd, J = 9.0, 2.1 Hz, 1H, H^{3}), 7.3 (d, J = 2.2 Hz, 1H, H^{6}), 6.3 (s, 1H, H^{1}), 3.9 (m, 4H, H^{4}), 3.8 (t, J = 6.3 Hz, 2H, H^{8}), 3.3 (t, J = 6.2 Hz, 2H, H^{9}), 3.3 – 3.2 (m, 4H, H^{5}), 3.1 (q, J = 7.2 Hz, 2H, H^{11}), 1.3 (s, 1H, H^{10}), 1.2 (t, J = 7.2 Hz, 3H, H^{12}). ^{13}C NMR (151 MHz, DMSO-d_6) δ 149.6, 142.0, 130.0 (3C), 126.0 (2C), 119.0, 117.4, 115.8, 103.4, 102.7, 90.6, 66.7 (3C), 50.9, 49.75, 45.4 (2C), 42.9 (2C), 26.5, 26.2, 22.2, 11.9 (2C). HPLC-MS (ACI/ ESI): Purity = 97%, t_R = 3.19 min, m/z [M+H]$^{+}$ = 509.2.

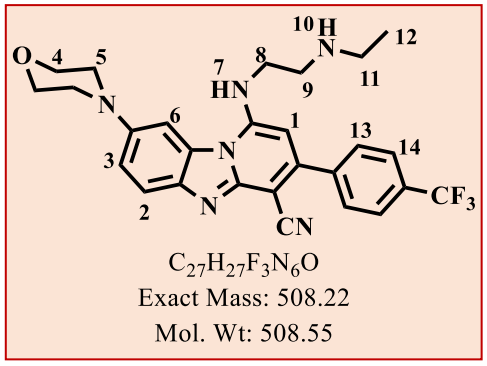

$C_{27}H_{27}F_3N_6O$
Exact Mass: 508.22
Mol. Wt: 508.55

6.4 Biological assays

6.4.1 *In vitro* asexual blood stage antiplasmodium assay

Compounds were screened against multidrug-resistant (K1) and sensitive (NF54) strains of *P. falciparum in vitro* using the modified [^{3}H]-hypoxanthine incorporation assay.[4] *P. falciparum* was cultivated in a variation of the medium previously described,[5,6] consisting of RPMI 1640 supplemented with 0.5% ALBUMAX® II, 25 mM Hepes, 25 mM $NaHCO_3$ (pH 7.3), 0.36 mM hypoxanthine and 100 µg/mL neomycin. Human erythrocytes served as host cells. Cultures were maintained at 37 °C in an atmosphere of 3% O_2, 4% CO_2 and 93% N_2 in humidified modular chambers. Compounds were dissolved by sonication in DMSO (10 mg/mL) and diluted in hypoxanthine-free culture medium. Infected erythrocytes (100 µL per well with 2.5% hematocrit and 0.3% parasitemia) were added to each drug titrated in 100 µL duplicates over a 64-fold range. After 48 hours incubation, 0.5 µCi of [^{3}H]hypoxanthine in 50 µL medium was added and plates were incubated for an additional 24 hours. Parasites were harvested onto glass-fibre filters and radioactivity was counted using a Betaplate liquid scintillation counter (Wallac, Zurich). The results were recorded as counts per minute (cpm) per well at each drug concentration and expressed as a percentage of the untreated controls. Fifty per cent inhibitory concentrations (IC_{50}) were estimated by linear interpolation.[7]

6.5.2 *In vitro* gametocytocidal assay

6.4.2.1 Luciferase Reporter Assay

Two transgenic parasite lines (NF54-PfS16-GFP-Luc and NF54-Mal8p1.16-GFP-Luc) were used in the luciferase assays which facilitated stage-specific determination of gametocytocidal activity. Gametocytes were produced according to Reader *et al.*[8] On days 5 and 10 which respectively represent > 90% of early stage (I – III) and > 90% of late stage (IV and V) gametocytes, drug assays were set up. In both cases, 2 – 3% gametocytaemia and 1.5% haematocrit culture were used with a 48-hour drug pressure in a gas chamber (90% N_2, 5% O_2 and 5% CO_2) at 37ºC. To 20 µL parasite lysates, 50 µL of luciferin substrate (Promega Luciferase Assay System) was added at room temperature. Luciferase activity was determined by detection of resulting bioluminescence at an integration constant of 10 seconds using the GloMax®-Multi+ Detection System with Instinct® Software. Methylene blue and dihydroartemisinin were used as controls.

6.4.2.2 ATP assay

In the ATP assay, late-stage gametocytes (IV and V, primarily stage V) were enriched using density gradient centrifugation and magnetic separation. Dilutions for the compounds were prepared in triplicate in 96-well plates. To each well, about 50,000 gametocytes in the glucose-rich complete medium were added to make a final volume of 100 µL where after the plates were incubated at 37 °C in a humidified gas chamber (90% N_2, 5% O_2 and 5% CO_2) for 24 hours. The BacTiter-Glo™ assay (Promega) was then carried out in accordance with the manufacturer's guidelines at room temperature in the dark with assay substrate incubated for 10 minutes to detect ATP levels. The GloMax®-Multi+ Detection System with Instinct® Software was used to detect bioluminescence at an integration constant of 0.5 seconds. Methylene blue and dihydroartemisinin were used controls.

6.5 Solubility Determination

6.5.1 Kinetic Solubility Employing HPLC

Using a miniaturised shake flask method,[10] solubility assays were obtained from a 10 mM stock solutions of the test compounds dissolved in DMSO, calibration standards (10 - 220 µM in DMSO) were prepared. The 10 mM stock solutions were also used to spike (1:50) duplicate aqueous samples in phosphate buffered saline (pH 6.5). The DMSO was dried off in a GeneVac (MiVac, 90 min, 37 °C) after which the samples were incubated while shaking for 20 hours at 25 °C. Thereafter, the solutions were filtered, and their absorbance measured using HPLC-DAD (Agilent 1200 Rapid Resolution HPLC with a diode array detector). The calibration standards were used to plot the calibration curves, which were used to determine the solubility of the aqueous samples.

6.5.2 Kinetic (Turbidimetric) Solubility[11]

A phosphate buffered saline (PBS) solution comprising 0.14 M NaCl, 0.003 M KCl and 0.01 M phosphate buffer (pH 7.4) was prepared by dissolving one intact PBS buffer tablet in 1 L of water. Particulate contaminants were removed by filtering the solution through a 0.22 µm nylon filter and the pH verified using a pH meter. Stock solutions (10 mM) of test compounds were prepared by dissolving in DMSO. Using a 96-well plate, serial dilutions of the compounds in DMSO were prepared in triplicate starting from 8 mM to 0.25 mM (predilution plate). Secondary serial dilutions (5 – 200 µM) in DMSO and PBS buffer, also in triplicate, were prepared by pipetting 4 µL aliquots from the predilution plate to corresponding wells in the

secondary plate containing 196 µL DMSO and PBS buffer (final volume of 200 µL in each well). The serial dilutions in DMSO acted as controls to make sure the test compounds in solution did not absorb electromagnetic radiation at the test wavelength. The plate was covered and incubated for 2 hours in an oven maintained at 37 °C. The absorbance values of the wells were then measured by a UV-Visible Multiskan Go 1510-05438 spectrometer (Thermo Scientific). The values were then corrected by subtracting the absorbance of the blank wells containing only DMSO and 2% DMSO in PBS. The corrected absorbance values were plotted as a function of concentration using excel. A constant absorbance value of 0 at all concentrations indicates the compound is soluble at all concentrations. Insoluble compounds will precipitate and cause turbidity the absorbance of which was measured by a UV-Visible spectrometer. Solubility was taken to be that concentration above which the test compound precipitates from solution causing a sustained upward deviation of absorbance values from zero.

References

(1) Paul, F.; Patt, J.; Hartwig, J. F. Palladium-Catalyzed Formation of Carbon-Nitrogen Bonds. Reaction Intermediates and Catalyst Improvements in the Hetero Cross-Coupling of Aryl Halides and Tin Amides. *J. Am. Chem. Soc.* **1994**, *116* (13), 5969–5970.

(2) Montalbetti, C. A. G. N.; Falque, V. Amide Bond Formation and Peptide Coupling. *Tetrahedron* **2005**, *61* (46), 10827–10852.

(3) Han, G.; Tamaki, M.; Hruby, V. J. Fast, Efficient and Selective Deprotection of the Tert-Butoxycarbonyl Group Using HCl/Dioxane (4 M). *J. Pept. Res.* **2001**, *58* (4), 338–341.

(4) Desjardins, R. E.; Canfield, C. J.; Haynes, J. D.; Chulay, J. D. Quantitative Assessment of Antimalarial Activity in Vitro by a Semiautomated Microdilution Technique. *Antimicrob. Agents Chemother.* **1979**, *16*, 710–718.

(5) Dorn, A.; Stoffel, R.; Matile, H.; Ridley, R. G. Malarial Haemozoin/β-Haematin Supports Haem Polymerization in the Absence of Protein. *Nature.* **1995**, *374*, 269–271.

(6) Trager, W.; Jensen, J. Human Malaria Parasites in Continuous Culture. *Science (80-.).* **1976**, *193*, 673–675.

(7) Huber, W.; Koella, J. C. A Comparison of Three Methods of Estimating EC50 in Studies of Drug Resistance of Malaria Parasites. *Acta Trop.* **1993**, *55*, 257–261.

(8) Reader, J.; Botha, M.; Theron, A.; Lauterbach, S. B.; Rossouw, C.; Engelbrecht, D.; Wepener, M.; Smit, A.; Leroy, D.; Mancama, D.; Coetzer, T. L.; Birkholtz, L.-M. Nowhere to Hide: Interrogating Different Metabolic Parameters of Plasmodium Falciparum Gametocytes in a Transmission Blocking Drug Discovery Pipeline towards Malaria Elimination. *Malar. J.* **2015**, *14* (1), 213.

(9) Ploemen, I. H. J.; Prudêncio, M.; Douradinha, B. G.; Ramesar, J.; Fonager, J.; van Gemert, G.-J.; Luty, A. J. F.; Hermsen, C. C.; Sauerwein, R. W.; Baptista, F. G.; Mota, M. M.; Waters, A. P.; Que, I.; Lowik, C. W. G. M.; Khan, S. M.; Janse, C. J.; Franke-Fayard, B. M. D. Visualisation and Quantitative Analysis of the Rodent Malaria Liver Stage by Real-Time Imaging. *PLoS ONE.* **2009**, *4*, e7881.

(10) Hill, A. P.; Young, R. J. Getting Physical in Drug Discovery: A Contemporary Perspective on Solubility and Hydrophobicity. *Drug Discov. Today* **2010**, *15*, 648–655.

(11) Bevan, C. D.; Lloyd, R. S. A High-Throughput Screening Method for the Determination of Aqueous Drug Solubility Using Laser Nephelometry in Microtiter Plates. *Anal. Chem.* **2000**, *72*, 1781–1787.